Technical University of Denmark

DTU

Optimisation of Combine Harvesters using Model-based Control

Hermann, Dan

Publication date:
2018

Document Version
Publisher's PDF, also known as Version of record

[Link back to DTU Orbit](#)

Citation (APA):
Hermann, D. (2018). Optimisation of Combine Harvesters using Model-based Control. DTU Elektro.

DTU Library
Technical Information Center of Denmark

Dan Hermann

Optimisation of Combine Harvesters using Model-based Control

Ph.D. dissertation, March 2018

AGCO
Your Agriculture Company

DAN HERMANN

Optimisation of Combine Harvesters using Model-based Control

Ph.D. dissertation, March 2017

Supervisors:

Ole Ravn,

Associate Professor at the Electrical Engineering Department of DTU

Nils Axel Andersen,

Associate Professor at the Electrical Engineering Department of DTU

Morten Leth Bilde,

Research and Advanced Engineering Manager at AGCO

DTU - Technical University of Denmark, Kgs. Lyngby - 2018

Optimisation of Combine Harvesters using Model-based Control

This report was prepared by:
Dan Hermann

Advisors:
Ole Ravn,
Associate Professor at the Electrical Engineering Department of DTU
Nils Axel Andersen,
Associate Professor at the Electrical Engineering Department of DTU
Morten Leth Bilde,
Research and Advanced Engineering Manager at AGCO

DTU Electrical Engineering
Automation and Control
Technical University of Denmark
Elektrovej, Building 326
2800 Kgs. Lyngby
Denmark
Tel: +45 4525 3576

studieadministration@elektro.dtu.dk

Project period: December 2014- March 2017

Education: Ph.D.

Field: Electrical Engineering

Remarks: This report is submitted as partial fulfillment of the require-
                  ments for graduation in the above education at the Technical
                  University of Denmark.

Summary

The world population is expected to grow by over one third between 2009 and 2050 according to the Food and Agriculture Organization of the United Nations. The arable areas are expected to decrease in the developed countries requiring an increase in yield on the available land meanwhile it gets increasingly harder to find qualified operators for combine harvesters.

The performance of the combine harvester is affected by a number of uncontrollable biological variables comprising both temporal and spatial field variations. The threshing, separation and cleaning processes can be optimised by adjusting a number of actuators, however this is not straight forward as the material flows are tightly coupled and the optimisation parameters are even conflicting. Integration of a closed-loop control system is highly challenging as most state of the art process sensors only offer a relative reading of the actual material flows in the combine.

The aim of the project is to design a closed-loop control system than can optimise the performance of the threshing, separation and cleaning processes in a combine harvester. Model development will be required to analyse, optimise and obtain transparency to the system states. The methods acknowledge that a high degree of model accuracy is not achievable as well as the complexity of observer and controller design is kept at a minimum.

Material flow models are generated for the threshing, separation and cleaning systems using acquired material samples from laboratory test stands and field test experiments. Material samples and sensor data are used to generate a virtual combine, which is utilised for initial testing of all controllers, greatly reducing the scarce field test time required for test and verification.

The material flow analysis revealed that the rotor speed had a dominating effect

on both separation grain losses as well as grain damage compared to the concave clearance, hence sole control of the rotor speed in the threshing and separation system is chosen. A Luenberger observer was designed to estimate grain damage from a grain quality sensor, which has a long settling time compared to impact loss sensors. This facilitate a fast response to changes in the separation grain loss in varying conditions. A closed-loop rotor speed controller was designed to balance rotor separation loss and grain damage using the grain damage observer. The controller was verified by means of simulation as well as during field test experiments.

The material flow analysis for the cleaning system showed degradation of cleaning performance is dominated by the MOG load and inclination angles as well as the effect from the fan speed and sieve actuators to material flows were tightly coupled, similar to the results from previous literature. It was shown that the fluidised phase characterising low grain losses could be identified using the tailings grain and MOG throughputs. The upper sieve primarily affected cleaning losses and tailings MOG throughout, and the lower sieve the cleanliness of the clean grain throughput and tailings grain throughput, hence these should be controlled using a distributed control scheme for optimisation, where each individual controller primarily will consider two balance parameters. An estimate of the tailings MOG throughput and tailings grain composition was obtained with reasonable good accuracy using sensor fusion of the tailings grain sensor and the non-linear tailings volume sensor. An on-line estimate of the tailings grain composition set-point characterising the fluidised phase was obtained, which facilitates a novel closed-loop fan speed control design. The fan speed controller was validated using a virtual combine, the cleaning system laboratory environment and during full scale field test. Implementation and verification of upper and lower sieve controllers is not addressed.

The average harvest grain loss in the industrialised countries is $4\,\%$ corresponding to the total cereal consumption of Germany. Hence reducing the grain loss by a fraction results in millions of tonnes of food as well as it can be the key to maintain a profitable business for the farmer, which is characterised by high revenues and small profit margins.

The contributions of this project enables integration of a control system for rotor speed, fan speed and sieve openings on the AGCO IDEAL series of combine harvesters. The developed controllers are planned to be included in the automation system and will be commercially available in 2019.

The dissertation is a summary of Ph.D. project and the methods developed during the project period. The results are disseminated in four conference articles, two submitted journal articles and one patent application.

Resume

Det forventes at verdens befolkning vil vokse med over en tredjedel mellem 2009 og 2050 ifølge Organisationen for Fødevarer og Landbrug (FAO) under de Forenede Nationer (FN). Det forventes at agerjorden i udviklingslandene mindskes, hvilket kræver et øget udbytte på den tilgængelige agerjord, mens det bliver stadig sværere at finde kvalificerede mejetærskeroperatører.

Mejetærskerens ydeevne er påvirket af adskillige ukontrollerbare biologiske variable omfattet af både sted- og tidsmæssige variationer. Tærske-, udskillelses- og renseprocessen kan optimeres ved at justere et antal aktuatorer, dog er det ikke ligetil da de forskellige materialestrømme er tæt koblede og optimeringsvariablerne er modstridende. Integration af et lukket-sløjfe kontrolsystem er yderst udfordrende, da de fleste moderne følere kun giver en relativ udlæsning af de aktuelle materialestrømme i mejetærskeren.

Målet med projektet er at designe et lukket-sløjfe kontrolsystem, der kan optimere ydeevnen for tærske-, udskillelses- og renseprocessen i en mejetærsker. Modeludvikling er nødvendigt for at analysere, optimere og opnå gennemsigtighed til de forskellige systemtilstande. Metoderne anerkender at en høj grad af modelnøjagtighed ikke er opnåelig samt at designkompleksiteten af systemer for tilstandsobservation og kontrol holdes på et minimum.

Materialestrømsmodeller er genereret for tærske-, udskillelses- og renseprocesserne ved brug fra udtagne materialeprøver under drift i laboratorieteststande og under markforsøg. Materialeprøver og følerdata er anvendt til at generere en virtuel mejetærsker, som benyttes til de indledende test af kontrolsystemerne, hvilket reducerer antallet af markforsøg.

Materialestrømsanalysen viste at rotorhastigheden havde den dominerende effekt

på både kerneudskillelsestabet samt kernebeskadigelsen sammenholdt med broåbningen, derfor er det valgt kun at styre rotorhastigheden. Til tilstandsobservation anvendes et Luenberger-design til at estimere kernebeskadigelsen fra en kernekvalitetsføler, som har en lang stabiliseringstid i forhold til spildføleren. Dette muliggør en kort stabiliseringstid for ændringer i kernespildet grundet varierende markforhold. En lukket-sløjfe rotorhastighedsstyring blev designet til at balancere kerneudskillelsestabet og kernebeskadigelse ved brug af et estimatet af kernebeskadigelsen med kort stabiliseringstid.

Materialestrømsanalysen for renseprocessen i soldkassen viste at forringelse af ydeevnen var domineret af belastningen fra ikke-kerne-bestandele (IKB) og hældningen samt af effekten fra underblæser- og soldaktuatorene er tæt koblet, lignende tidligere undersøgelser. Det blev eftervist af den fluiderede fase som karakteriserer lavt kernespild kunne identificeres ved brug af kerne- og IKB-returmaterialet. Oversoldet påvirkede primært spildet i soldkassen og IKB-returmaterialet, hvor undersoldet påvirkede returmaterialet af kerner og renheden af færdigvaren. Dermed bør disse styres ved brug af et distribueret kontrolsystem for optimering, hvor hver individuel styring primært betragter to balanceparametre. Et estimate af IKB-returmaterialestrømmen samt kernebestanddelen af returmaterialestrømmen blev opnået med en tilfredsstillende nøjagtighed ved at sammenholde flere følerudlæsninger fra returmaterialestrømmen for kerner samt en ulineær volumetrisk udlæsning. Et estimat af referenceindstillingen som karakteriserer den fluiderede fase blev opnået, hvilket muliggør en ny metode for lukket-sløjfe-styring af underblæserhastigheden. Underblæserstyringen blev valideret ved brug den virtuelle mejetærsker, soldkasselaboratoriet og under markforsøg. Implementering og verifikation af over- og undersoldstyring er ikke beskrevet.

Det gennemsnitlige korspild under høst i de industrialiserede lande er 4 %, svarende til Tysklands samlede forbrug af kornafgrøder. Derfor vil en reduktion af kornspildet på en brøkdel resultere i millioner af tons af fødevarer ligesom det kan være nøglen til at opreholde en profitabel forretning for landmanden, der er karakteriseret af høj omsætning og lave profitmargin.

Bidragene fra dette projekt muliggør integration af et kontrolsystem for rotorhastighed, underblæserhastighed og soldåbninger i AGCO's IDEAL-mejetærskerserie. Udviklingen at kontrolsystem er planlagt til at være kommercielt tilgængeligt i 2019.

Afhandlingen er udformet som et sammendrag af Ph.D.-afhandlingen samt de anvendt metoder under projektperioden. Resultaterne er formidlet i fire konferenceartikler, to indsendte journalartikler samt en patentansøgning.

Preface

This project was carried out as a collaboration between academia and industry, as part of the Industrial Ph.D. program founded by the Danish Agency for Science, Technology and Innovation, grant number 4135-00116B. The university partner was the Automation and Control Group, Department of Electrical Engineering, Technical University of Denmark. The industrial partner was AGCO, Research and Advanced Engineering Global Harvest, Randers, Denmark.

The dissertation was prepared in partial fulfilment of the requirements for acquiring the Ph.D. degree in engineering. The aim is to develop material flow models and utilise these to facilitate closed-loop control of the threshing, separation and cleaning systems in a combine harvester. Such a system increase the overall performance characterised by grain loss, grain damage and cleanliness of the clean grain product.

The dissertation consists of a summary report and a collection of research articles written during the period 2015-2018, which were published or submitted for publication.

Dan Hermann (s112423), March 2018

Acknowledgements

I would like to thank my main supervisors at DTU Ole Ravn and Nils Axel Andersen for great collaboration and advice throughout the project period, as well as I would like to thank all my colleagues and friends at DTU during my studies.

I would like to thank my supervisor at AGCO Morten Leth Bilde for giving me the opportunity of the industrial Ph.D. position, as well as my colleague throughput the project period Flemming Schøler for the great collaboration. I am grateful to my colleagues in the design engineering team for the threshing, separation and cleaning modules in Randers and the guys in the lab for the great support and for showing that a small dedicated team truly can accomplish something big.

Finally I would like to thank the engineering and field test teams in Europe, North America and South America for the collaboration and outstanding support.

Table of Contents

List of Symbols

Variable	Unit	Description
d_c	mm	Upper sieve spacing
d_p	mm	Concave clearance
d_s	mm	Lower sieve spacing
d_w	m	Header width
$\Gamma_{y,c}$	%	Cleanliness (MOG) in grain bin
$\Gamma_{p,b}$	%	Grain damage in grain bin
$\Gamma_{p,g}$	%	Threshing and separation input grain ratio
Γ_t	%	Tailings grain composition
M_t	ton/m^{2}10^{-4}	Local field crop density
$\dot{m}_{c,c}$	ton/h	Cleaning MOG throughput
$\dot{m}_{c,g}$	ton/h	Cleaning grain throughput
$\dot{m}_{c,l}$	ton/h	Cleaning grain loss
$\dot{m}_{c,r}$	ton/h	Cleaning MOG residue
$\dot{m}_f$	ton/h	Total throughput
$\dot{m}_{p,c}$	ton/h	Threshing and separation MOG sep. throughput
$\dot{m}_{p,g}$	ton/h	Threshing and separation grain sep. throughput
$\dot{m}_{p,l}$	ton/h	Separation grain loss
$\dot{m}_{p,r}$	ton/h	Threshing and separation MOG residue
$\dot{m}_{p,t}$	ton/h	Threshing grain loss
$\dot{m}_{t,g}$	ton/h	Tailings grain throughput
$\dot{m}_{t,c}$	ton/h	Tailings MOG throughput
$\dot{m}_{y,g}$	ton/h	Clean grain throughput
$\dot{m}_{y,c}$	ton/h	Clean grain throughput cleanliness
ω_f	RPM	Fan speed
ω_r	RPM	Rotor speed
ϕ	^{o}	Chassis longitudinal inclination angle (pitch)
ρ_g	%	Grain moisture content

ρ_c	%	Straw moisture content
θ	^{o}	Chassis lateral inclination angle (roll)
T_f	s	Delay from header cutting bar to feederhouse sensor
T_r	s	Cleaning system return loop delay
T_u	s	Header cutting table to threshing system delay
T_y	s	Delay from cleaning system to yield sensor reading
τ_c	s	Cleaning system time constant
τ_p	s	Threshing and separation system time constant
$u_{p,l}$		Optimisation weight for separation loss
$u_{\Gamma,b}$		Optimisation weight for grain damage
$u_{p,l}$		Optimisation weight for cleaning loss
$u_{\Gamma,c}$		Optimisation weight for yield cleanliness
v	m/s	Combine forward speed sensor
P_F		Probability of False detection
P_M		Probability of Missing detection
w_h	m^2/s	Header areal flow
y_α		Feederhouse throughput sensor reading
y_β	hPa	Rotor pressure sensor reading
$y_{c,g}$		Upper sieve distribution sensor reading
$y_{c,l}$		Cleaning grain loss sensor reading
$y_{\Gamma,b}$	%	Grain damage sensor reading
$y_{p,g}$		Threshing and separation distribution sensor reading
$y_{p,l}$		Separation loss sensor reading
$y_{t,g}$		Tailings grain throughput sensor reading
$y_{t,v}$	V	Tailings volume sensor reading
$y_{y,g}$	ton/h	Clean grain throughput (yield) sensor reading
$y_{\Gamma,c}$	%	Cleanliness (clean grain MOG throughput) sensor reading

Notation   Matrices are capital X, data vectors are bold $\mathbf{x}$ and parameters given by x. Vector are indexed primarily as p_1 for index number 1 in of the vector $\mathbf{p}$. If the index is used iterative it is given by bold a vector and index in squared parentheses $\mathbf{x}[1]$. Thus x_1 is index 1 of vector x and $\mathbf{x}_1$ is a vector. Multiple indices from e.g. 3 to 7 are given by $\mathbf{x}(3:7)$. The notation $1_{[1,3]}$ is the vector $[1,1,1]$ and $0_{[1,4]}$ is the vector $[0,0,0,0]$.

List of Abbreviations

AGCO   Allis-Gleaner Corporation
CFD   Computational Fluid Dynamics
CUSUM   CUmulative SUM control chart
DoE   Design Of Experiments
DEM   Discrete Element Method
DTU   Technical University of Denmark
GQS   Grain Quality Sensor
HIL   Hardware In the Loop
KFCV   K-Fold Cross Validation
KNN k Nearest Neighbours
LED   Light Emitting Diode
LOOCV   Leave One Out Cross Validation
MADS   Material And Distribution Sensor
MFS   Material Flow Sensor
MIMO   Multiple Inputs Multiple Outputs
MOG   Material Other than Grain
PSD   Power Spectral Density
R&AE   Research and Advanced Engineering
RGB   Red Green Blue
TVS   Tailings Volume Sensor
SISO   Single Input Single Output
SSD   Steady-State Detection

Introduction

1.1 Background

Due to an increasing world population the demand of agricultural products is estimated to annually increase by 1.5% towards 2030, equal a raise of one billion tonnes of cereals [37]. In the long term it is not possible to satisfy the demand only by increasing the production area. One of the key issues is therefore to increase the yield in the harvesting process, where the grain harvest loss is estimated to 4% and 14% in North America and Africa respectively [1]. With the increasing urbanisation and the ailing occupation in the agricultural profession it gets increasingly more difficult to attract qualified operators, while the complexity of the combine harvesters has grown in order to increase profitability. To comply with European legislation the total machine width has been restricted to 3.5 m in order to drive on public roads, hence machine capacity cannot continue to grow by physically increasing the combine harvester. This has procured a desire for automatic adjustment of the process actuators for the threshing, separation and cleaning systems in order to better utilise the available capacity, reduce grain loss and reduce operator fatigue.

1.1.1 Combine Harvester Process Modules and Sensors

The combine harvester consists of three crop processing modules, the threshing, separation and cleaning processes. The threshing process is done using a transverse (conventional) or longitudinal rotor with threshing elements to separate the grain kernels from the heads, stems or pods of the given crop. The purpose of the separation system is to segregate the threshed grain kernels through the crop mat from

the threshing system prior to leaving the machine as residue material in the field. The conventional separation system is constructed using straw walkers relying on gravity for kernel segregation or as a longitudinal rotor using the rotational force to increase the kernel segregation. The threshing and separation systems are constructed as one coherent system in modern combine harvesters. The conventional walker machines uses a transverse threshing rotor and a straw walker for separation, the an axial machines uses one or two parallel rotors with threshing elements in front and separation in the rear end, and the hybrid machines a transverse threshing rotor and a longitudinal separation rotor. The Ph.D. project was conducted in parallel with the development of the AGCO IDEAL combine harvester series using a single or dual axial rotor threshing and separation system depending on combine class grading, see Figure 1.1. It is possible to adjust rotor speed (ω_r) and concave

Figure 1.1: AGCO IDEAL series combine harvester.

clearance (d_p) in the threshing section to vary how hard the crop is threshed as well as the separation rate, see Figure 1.2. The concave facilitates an individual adjustment of the inside and outside clearances [14], however these were set identical for all tests, thus the clearance is denoted with one variable (d_p). The threshing and separation system is equipped with impact sensors longitudinally along the rotor to measure the separation curve and one transverse in the rear end to measure the separation loss. The total throughput ($\dot{m}_f$) can be measured using two different relative sensor readings, i.e. a mechanical sensor measuring the crop height in the

feederhouse and a measurement of the hydraulic oil pressure of the belt variator in the rotor drive train. The grain damage is measured with a grain quality sensor (GQS) located in the top of the clean grain elevator.

The threshing and separation system additionally separates a considerable amount
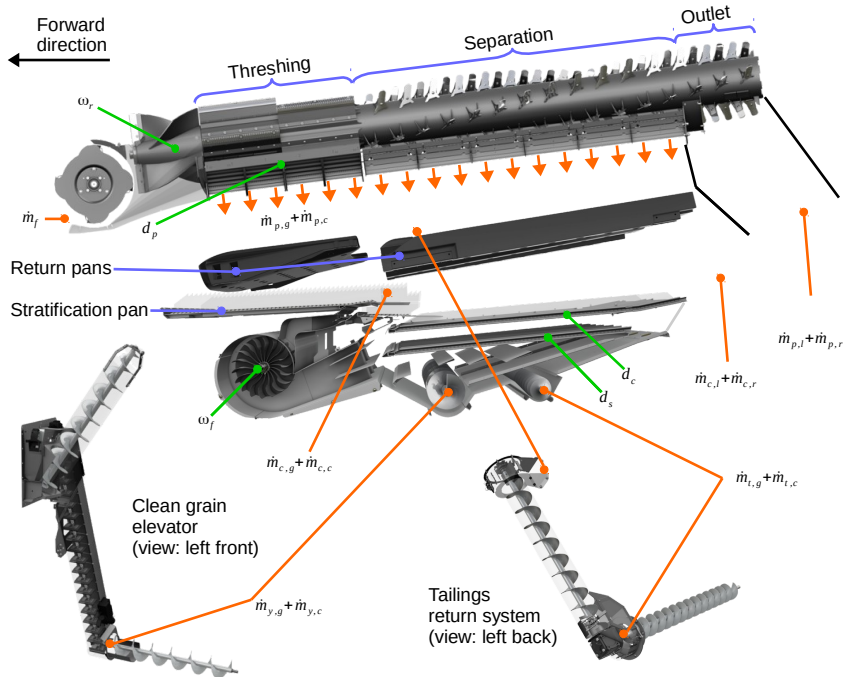
Figure 1.2: AGCO IDEAL threshing, separation and cleaning system material flows.

of chaff and straw pieces, generally characterised as material other than grain (MOG). The separated material flow of grain ($\dot{m}_{p,g}$) and MOG ($\dot{m}_{p,c}$) is collected using the front and rear return pans transporting the material in the forward direction. Both return pans deliver the material on the stratification pan which transport the material in the rearward direction where it enters the cleaning shoe ($\dot{m}_{c,g}$ and $\dot{m}_{c,c}$). The purpose of the cleaning system is to clean the grain ($\dot{m}_{c,g}$) from the MOG ($\dot{m}_{c,c}$) in the delivered material throughput from the threshing and separation system. All modern combine use a system with an adjustable fan (ω_f) and two sieves with adjustable openings (d_c and d_s). The purpose of the upper sieve is to separate the grain kernels before leaving the cleaning system as residue ($\dot{m}_{c,l}$ and $\dot{m}_{c,r}$), and for the lower sieve to avoid separation of MOG particles into the clean grain throughput ($\dot{m}_{y,g}$ and $\dot{m}_{y,c}$) to the grain bin. The material being segregated

through the upper sieve but not the lower sieve is denoted tailings ($\dot{m}_{t,g}$ and $\dot{m}_{t,c}$) and is returned into the cleaning system on the rear return as marked on Figure 1.2. The tailings return location depends on the overall design of the combine. The purpose on the cleaning fan is to maintain the MOG airborne where the grain can be segregated throughput the sieves. The cleaning system is equipped with longitudinal impact sensors under the upper sieve and transverse sensors for grain loss detection over the full width behind the upper sieve. Additionally a transverse impact sensor is used to measure the tailings grain throughput and a proximity sensor used to measure the volumetric tailings throughput. The amount of MOG in the clean grain throughput is measured with the GQS and the clean grain throughput is measured with the yield sensor in the top of the clean grain elevator. The $\dot{m}$ material flow sub-script notation refers the module before the comma and material type after the comma. Before the comma p notate threshing and separation system, c cleaning shoe, t tailings and y clean grain material flows, where after the comma g and c refers to grain and MOG that remains in the combine where l and r refers to grain (loss) and MOG (residue) leaving the combine.

1.1.2 Process Adjustment

The combine harvester has predefined default actuator settings for each crop type which are either set by selecting crop type in the operator terminal or obtained from the operators manual. In practice a number of biological parameters affect the performance of the threshing, separation and cleaning systems, hence the default settings are often sub-optimal. Variations in grain and straw moisture content as well as spatial varying soil conditions affect performance, which requires the operator to adjust the actuator settings multiple times during the harvest day to maintain high performance. However the operators do often have long working days reducing awareness for performance issues, thus variations in site specific conditions are often ignored. The performance is primarily characterised as the grain loss, grain damage, cleanliness and straw quality, where the weight on the different parameters depend of the utilisation of crop product. E.g. for malting barley grain damage and cleanliness are important factors, however for stock feeding grain loss is the dominating factor where grain damage and cleanliness have low priority. If the residue straw is being baled for bedding the straw quality is of high importance.

1.1.3 Process Optimisation

Increasing the performance of the combine harvester is assigned to a complex optimisation problem with a large number of parameters and tightly coupled non-linear interdependencies, where many of the parameters are even conflicting. The illustration in Figure 1.3 shows an example of a cost function with the primary parameters of interest for process optimisation. The total throughput is conflicting
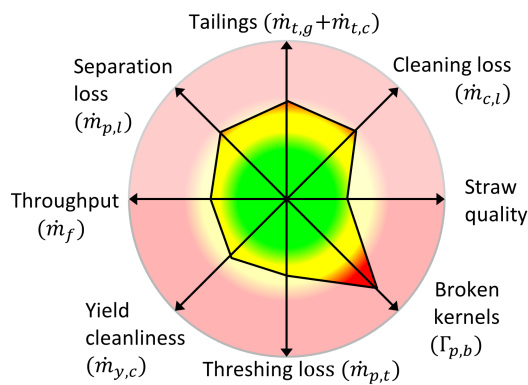
Figure 1.3: Overall parameters impact for combine harvester optimisation.

with grain loss, hence this is often the dominating factor reducing the capacity of the machine. Of the listed primary process parameters of interest no commercial sensor technologies are available for measuring straw quality and unthreshed heads [91], as well as straw moisture content which is known be have a significant influence of the performance for the threshing, separation and cleaning systems [46]. The actuator impact is roughly known to the average operator, however the system interdependencies depend on local field conditions, thus it often takes several attempts to obtain acceptable performance. A control system will have a more holistic overview by continuously monitoring the process sensors. However all process sensors by default provide a relative reading, which requires a calibration for each sensor in each crop in order to obtain an approximate throughput in a verifiable unit, e.g. ton/h. Though the sensors are calibrated to each crop type the sensor readings are still assigned to a relative gain uncertainty and disturbances from unobservable parameters.

1.2   State of the Art

The basic principles of combine harvesters have not changed for the last century, however the size and complexity has increase notably in the continuous effort to increase the profitability of the harvesting process. Miu [71] has published the only comprehensive book covering mechanical design of the various combine harvester modules, crop processing analysis, sensor systems and simulation. The early literature primarily focused on modelling non-linear dependencies to single input variables for performance evaluation. Recent literature has focused towards the aim of automating the actuator settings by modelling the total material flow for development of a virtual combine, throughput estimation from sensor readings and closed-loop control design.

1.2.1   Modelling

Philips [89] gave an extensive overview of overall costs in the harvesting process including various effects from weather and machine utilisation, which is useful to optimise of the whole harvesting logistics process.

General grain loss characteristics for threshing, separation and cleaning systems were shown by Nyborg [85], Glasbey [40], Kutzbach [52] and Myhan [81].

The effect on grain losses originating from straw moisture were shown by Hubner [46] and Wacker [108]. Wacker [87] showed the effect on corn grain damage from grain moisture content. Trollope gave the first comprehensive theoretical model of the conventional threshing system [102]. Since primarily Miu gave an extensive treatment on the theoretical and practical aspects of both tangential and axial threshing and separation systems [75, 76, 70, 73, 77, 78, 79], where the theoretical models were fitted with high accuracy to the theoretical separation curves. Maertens [62] showed a comparison of several mathematical distribution models fitted to material samples. Kutzbach [54] presented a comprehensive review of modelling approaches for grain separation and grain loss characteristics for the threshing and separation system.

Kutzbach [53] showed the basic loss characteristics for the cleaning system. Freye [38] gave a comprehensive description of relationship from gravity and air pressure in the cleaning system and characterised the packed, fluidised and flight phases which today are considered basics theory in the understanding of cleaning system performance. Dahany [29] presented optimisation of the cleaning process by optimising the air distribution under the sieves.

Simpson [97] showed the effect from longitudinal inclination on cleaning system grain losses. Similar results were presented in [88, 36, 13] for both longitudinal and lateral inclination, showing a significantly larger performance degradation for lateral than longitudinal inclination. Böttinger [11] showed a significant reduction of grain loss originating of pre-separation in the cleaning system by varying throughput as well as frequency and amplitude of the grain pan oscillation.

Miu [72] showed that the grain separation curve for the cleaning system could be modelled using a Weibull distribution. Similar results for modelling of grain distribution was shown by Schreiber [94]. Kutzbach [54] presented a comprehensive review of modelling approaches for grain separation and grain loss characteristics for the cleaning system, showing a performance enhancement from pre-separation of the material to the cleaning system. The effect of pre-separation was shown by Bilde [7] for various grades of pre-separation.

Within the last decade the increase in computational power has facilitated simulation of the cleaning system down the level of single grain, chaff and straw particles using the method of computational fluid dynamics (CFD) with the discrete element method (DEM) [51, 50, 55, 57]. The method is still at an early stage, however there is a large potential to obtain a much larger degree of transparency into the cleaning process which is not possible using traditional laboratory test stands, as the simulation facilitate full control of all biological parameters as well as observability of material flow in all locations without affecting the process.

1.2.2 Sensors and Estimation

Reyns [91] gave a comprehensive review of state-of-the-art process sensor technologies as of 2002. Since the most significant advancements has been within camera based grain quality sensors.

Veal [103] showed a sensor in the feederhouse measuring the total throughput. Bormann [10] presented a method to monitor the total throughput of the threshing and separation system with the aim of power requirement supervision for early warning blockage detection.

Multiple studies have investigated performance of the yield sensors measuring the clean grain throughput [90, 101, 2], which showed a relative large error in the momentary yield reading and well as drift due to unobservable biological parameters. State-of-the-art sensor use either a volumetric, impact energy or force sensing method [71], which all requires calibration to obtain the standard acceptable error of approx. 2%. Approaches for forward looking crop density scanning showed un-

satisfactory results using ultrasonic sensor [68], however Saeys showed that using a laser scanner [93] it was possible to estimate the crop density with a coefficient of determination of $R^2 > 0.80$.

Various publications have addressed separation and cleaning grain losses as well as tailings grain throughput using impact sensors [60, 112, 59, 58, 84, 17, 24, 4, 66]. Craessaerts [24, 28] showed an improvement in the cleaning grain loss estimate using sensor fusion with impact grain loss sensors and a sensor reading of the differential air pressure through the sieves. Maertens [65] presented an application of model based signal processing relying on material flow models of the cleaning system. Recent literature have presented novel sensor technologies for distribution sensing [44, 17] which procures a potential for increase transparency to the separation performance. Schwarz [95] showed a method to continuously measure cleaning grain loss by cleaning a sub-sampled material flow in a vertical cleaning unit and measuring the grain output with a piezo sensor, where an accuracy of 3 % was obtained. Beckmann [5] showed an X-ray method to discriminate between grain and MOG particles in a static mixture.

Wallays [110] presented a study of wavelengths characterising grain quality parameters of interest as wells as experimental results [109] using af computer vision. Neu [35] presented the implementation and verification of a commercial grain quality camera for detection of grain damage and cleanliness. Momin [80] used RGB images of soy-beans from a low cost camera to detect splits, cracks, contamination, leaves and stems. Craessaerts [26, 27] successfully showed an estimation model for cleanliness using a sensor reading of the differential air pressure through the sieves, fan speed and the lower sieve opening.

Lenaerts [56] presented an method to charactering straw quality by measuring the lateral curvature of the swath. Wan [111] showed a method to measure straw moisture content, however the measure depend on the density and is only applicable of bales.

1.2.3   Simulation

Miu [74] presented one of the first attempts to simulate the full material flow of the combine harvester, i.e. a virtual combine.

The first full scale virtual combines were shown by Eggerl [34] and Maertens [67, 64], providing full material flow, actuators settings and sensor readings. The underlying model describing the interdependencies were not presented.

1.2.4 Control Systems

De Baerdemaeker [30] gave a review for state-of-the-art control systems for header high control, feedrate control as well as control of the threshing, separation and cleaning processes, concluding that model-based techniques were suitable to obtain state estimates of the many throughputs for close-loop control purposes.

Böttinger [12] presented a review of the electronics on the combine harvester, and Mertins [69] presented the required sub-system to facilitate an automated combine.

Coen [23, 20, 21, 19, 22] presented a number for results for constant throughput control. Berner [6] showed the first approach for closed-loop control of the cleaning fan speed using differential air pressure sensors to measure the pressure drop through the sieves. An acceptable performance was obtained, however the method was highly sensitive to varying field conditions, hence it would require tedious calibration routines to be conducted in the field. Craessaerts [25] demonstrated a closed-loop fan speed control system based on impact sensor readings and differential air pressure using Fuzzy logic, showing a decrease in grain loss compared to a sub-optimal static fan speed setting. Omid [86] demonstrated closed-loop control of the threshing and separations system as well as cleaning system by applying Fuzzy logic using only impact loss sensor readings, obtaining significant grain loss reduction on both sub-systems. Eggerl [33] compared various search techniques using expert knowledge and artificial intelligent for combine optimisation, achieving af performance improvement of 35 % - 68 % using af virtual combine.

The Cemos Automatic system from Claas utilise a closed-loop control system with a gray-box model approach and continuous optimisation which was presented in [83, 100, 105]. The system is the only proven commercial control system for the threshing, separation and cleaning processes, hence from a commercial stand point, this is state of the art.

1.3 Objectives

The present dissertation is a result of a research project financed by AGCO in collaboration with the Danish Agency of Science, Technology and Innovation within the industrial Ph.D. program. AGCO contributed with experience of the threshing, separation and cleaning systems as well as access to the test facilities in terms of laboratory test stands for threshing and separation system, and cleaning system. In addition various field tests were conducted for data collection as well as

test and verification of the closed-loop control algorithms. Collaboration with the Technical University of Denmark brought expertise on non-linear modelling, state estimation and close-loop control into the project.

The Ph.D. project was initiated simultaneously with the parenting automation project within AGCO. The project focus was to support the automation project with various tasks of modelling and evaluation for the automation project, in order to deliver an automatic adjustment system for the AGCO IDEAL combine series for the start of production. The project was conducted in close collaboration with the design engineer team for the threshing, separation and cleaning modules. The project was conducted in close collaboration with a system engineer for implementation in the combine computer system through the whole project period.

The main objectives for the project were to

- Analyse and generalise material flow interdependencies for threshing, separation and cleaning system, as well as sensor representation of material flow

- Develop material flow models and sensor models to be utilised for observer design, process optimisation, fault detection and employment a virtual combine harvester

- Obtain an overall control architecture using process parameters that are observable from commercial process sensors

- Validation of closed-loop control system by means of simulation (virtual combine), using the cleaning system laboratory test stand and full scale field test

1.4   Dissertation Outline

The dissertation is written as a collection of articles. Chapter 2 describes the experimental setups, analysis, material flow interdependencies, and chosen model structure. Chapter 3 outlines the design and implementation of the virtual combine and throughput estimation. Chapter 4 describes the background for the controller architecture as well as it outlines the design, implementation and validation of the individual actuator controllers. Chapter 5 summarises the results for the project and presents perspectives and possible future research within the field. Appendix A contains conference and journal articles as well as a patent application.

1.5 Summary of Main Contributions

The main contributions of the project have been disseminated in four conference articles, two journal articles and one patent application. At the time of thesis submission the four conference articles (Appendix A.1, A.2, A.3, A.4) have been published, the two journal articles (Appendix A.5, A.6) have been submitted and the patent application (Appendix A.7) has be filed.

1.5.1 Conference Articles

A.1   D. Hermann, M.L. Bilde, N.A. Andersen, O. Ravn. "A Framework for Semi-Automated Generation of a Virtual Combine Harvester". 5th *IFAC AgriControl Conference 2016, Seattle WA, USA.*

This article describes a generic data-driven model of the threshing, separation and cleaning process in a combine harvester. The aim is a model that describes the actual material flow and sensor readings for relevant actuator configurations and measured biological disturbances in order to facilitate throughput estimation, simulation and optimisation. A modular data-driven model structure is chosen as it maintains the actual steady-state values and facilitates verification and debugging using laboratory and field data. The overall model structure and model generation procedure with estimation of parameters obtained from field data are described, as well as simulation results are presented.

A.2   D. Hermann, M.L. Bilde, N.A. Andersen, O. Ravn. "On-the-go Throughput Prediction in a Combine Harvester using Sensor Fusion". 1st *IEEE Conference on Control Technology and Applications 2017, Kohala Coast HI, USA.*

The article addresses design of a grain throughput observer for a combine harvester in order to reduce the delay from instantaneous sensor readings. The aim is to predict grain throughput changes using the forward speed and a throughput sensor in the feederhouse in addition to the yield sensor. By utilising a grain flow model and sensor fusion an estimate of the current grain throughput is obtained, hence the effect from the lag in the momentary yield sensor reading due to material transport delays can be reduced. Statistical change detection is used

to detect feederhouse load condition as well as sensor discrepancies using the observer innovation signal. The system is able to predict changes originating from forward speed and local crop density variations. Additionally temporary sensor discrepancies are detected and compensated in the grain flow estimate.

A.3   D. Hermann, F. Schøler, M.L. Bilde, N.A. Andersen, O. Ravn. "Computer based Control of the Separation Process in a Combine Harvester". *EurAgEng VDI-MEG Conference 2017, Hanover, Germany.*

This article addresses the design of a control system for an axial threshing and separation system in a combine harvester. Utilising a distributed control architecture containing all observable crop flow parameters, the rotor speed is adjusted to maintain acceptable separation grain loss using distributed impact mass flow sensor (MFS) readings and a measure of grain damage from a grain quality sensor (GQS). The GQS settling time for rotor speed changes was significantly reduced using a model based observer facilitating faster adjustment for grain losses in varying conditions. The observer and control loop were validated using the virtual combine showing a reduction of maximum grain loss and grain damage. Additionally the controller was validated during field test experiments where the rotor speed was adjusting to the abrupt changes in separation grain loss due to varying field conditions.

A.4   D. Hermann, F. Schøler, M.L. Bilde, N.A. Andersen, O. Ravn. "Design of Laboratory Environment for Development of Cleaning System". *EurAgEng VDI-MEG Conference 2017, Hanover, Germany.*

This article addresses the design of a laboratory environment for research and development activities used for automating the cleaning process in a combine harvester. The aim is to facilitate closed-loop controller test runs with extended duration which has not been possible using previous laboratory environments. By utilising individual MOG and grain feeding units any combination of these occurring in an actual field can be reproduced in the laboratory. Additionally recirculating the crop material facilitate long duration tests runs for closed-loop controller verification. A coefficient of determination for the MOG and grain feeding units of respectively $R^2 = 0.99$ and $R^2 = 1.00$

were obtained as well as a reasonable good representation field performance was obtained.

1.5.2 Journal Articles

A.5 D. Hermann, M.L. Bilde, N.A. Andersen, O. Ravn. "Model-based Cleaning Fan Speed Control in a Combine Harvester - Part I: Identification and Optimisation". *Biosystems Engineering (2018)*. Submitted.

This article addresses the modelling process for the cleaning system oriented towards design of a closed-loop control system. The aim is to generate a mathematical model of the material flow in the cleaning system that can be utilised for closed-loop control of the fan speed and sieve openings in using state-of-the-art process sensor technologies. A material flow model is generated using material sample data from laboratory test stands, which showed a dominating effect on grain loss from the MOG throughput and the inclination. The modelling showed how the grain loss can be reduced using feed-forward from the available sensor reading of the longitudinal inclination angle. The procedure for generation of steady-state material flow models using prior knowledge was outlined. By means of simulation and optimisation it was possible to identify a regime characterising the fluidised phase of the cleaning system operation using the tailings throughput, which facilitate a novel closed-loop fan speed control system.

A.6 D. Hermann, M.L. Bilde, N.A. Andersen, O. Ravn. "Model-based Cleaning Fan Speed Control in a Combine Harvester - Part II: Implementation and Control". *Biosystems Engineering (2018)*. Submitted.

The material flow model generated using material sample data obtained from laboratory test stands was used to identify the fluidised phase characterising high cleaning system performance, i.e. low grain loss. It was shown that the MFS tailings sensor has a reasonable good representation of the tailings grain throughput as well as a mathematical model of the tailings volume sensor was shown from the tailings grain and MOG throughputs. Using sensor fusion of the MFS tailings sensor and the tailings volume sensor the tailings grain composition could be estimated with $R^2 = 0.79$. The control scheme is implemented and tested by means of simulation using a virtual combine, in

a laboratory cleaning system test stand and during full scale field test, showing a significant reduction of grain loss in varying conditions.

1.5.3   Patents

A.7   D. Hermann, M.L. Bilde. "Volume Sensor for Combine Harvester Tailings Return System". Filed.

The patent application covers the tailings volume sensor used for the closed-loop fan speed controller in Article A.6.

The tailings volume sensor comprises a proximity sensor located in the ejection channel of the tailings return conveying system. The material is delivered from a paddle in a circular housing where it is thrown into the ejection channel where it travels along the back side-wall of the ejection channel due to the initial force originating from the paddle rotation. The proximity sensor is located at the front side-wall measuring the distance to the back side-wall, where the decrease in distance from the back side-wall corresponds to the volumetric throughput of the tailings return flow.

Modelling

This chapter describes the experimental setup, the model structure and the modelled steady-state material flows for the threshing, separation and cleaning systems as well as the process sensors. The framework for the semi-automated modelling process was published in Article A.1. The design of the continuous cleaning system laboratory environment was published in Article A.4. The cleaning system material flow models for the fan speed controller were presented in Article A.5. The sensor models for tailings throughput estimation were published in Article A.6 using the tailings volume sensor filed in Patent A.7.

The steady-state material flow models are essential to the control design in this project. A number of steady-state material flow models have been adapted from existing literature, however most models are generated without prior references. All steady-state models are generated from material samples. The models serve as a bias for the development of a virtual combine simulation environment, observer design, process optimisation and fault detection. The aim is to capture the dominating non-linear trends as the characteristics are known to depend on temporal and spatial varying unobservable biological parameters.

2.1 Data Acquisition

The utilised model data were acquired from both laboratory test stands and during field test experiments. The majority of the material samples have been acquired from laboratory tests, where the field tests data primarily has been utilised for validation. However some crops are not practical to bring to the laboratory, whereas data acquisition from field test experiments were the only option. Data was collected in wheat, barley, soy beans and corn in order to design individual controllers

for each crop type. The presented data will primarily be shown for the most relevant crop type, i.e. all four crops will not be included in all of the analyses.

2.1.1   Threshing and Separation Laboratory

The laboratory test stand for the threshing and separation process facilitate collection of material in separation boxes under the threshing and separation sections, as well as collection of the residue. Material is fed using a conveyor belt to a header mounted on the feederhouse, see Figure 2.1. The total throughput ($\dot{m}_f$) can
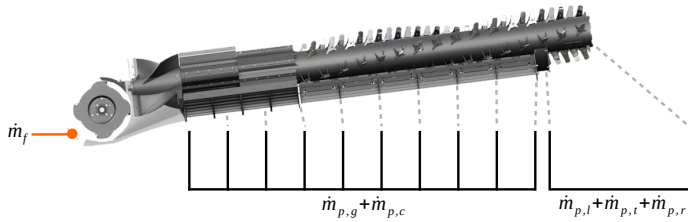

Figure 2.1: Threshing and separation system test stand with material collection boxes.

be varied by the material density (kg/m^2) on the conveyor belt combined with the conveyor belt speed, as well as the rotor speed (ω_r) and concave clearance (d_p) are adjustable, see Table 2.1. The separated material is cleaned for separation into grain ($\dot{m}_{p,g}$) and MOG ($\dot{m}_{p,c}$) components. The collected residue is likewise separated into grain separation loss ($\dot{m}_{p,l}$) and MOG residue ($\dot{m}_{p,r}$). The MOG is thoroughly re-threshed to obtain the threshing loss ($\dot{m}_{p,t}$), i.e. grain loss from kernels still attached to the head or cop of the crop when leaving the combine. The total loss include threshing and separation loss ($\dot{m}_{p,l} + \dot{m}_{p,t}$), however only the separation loss ($\dot{m}_{p,l}$) is observable using state of the art sensor technologies [91].

Table 2.1: Configurable and sampled variables for the threshing and separation system test stand.

Configurable	Sampled
Rotor speed (ω_r)	Separation grain loss ($\dot{m}_{p,l}$)
Concave clearance (d_p)	Threshing grain loss ($\dot{m}_{p,t}$)
Total throughput ($\dot{m}_f$)	MOG residue ($\dot{m}_{p,r}$)
	Separated grain ($\dot{m}_{p,g}$)
	Separated MOG ($\dot{m}_{p,c}$)
	Grain damage ($\Gamma_{p,g}$)

The threshing and separation system test stand run time is limited by the length of the conveyor belt and the availability of stored unthreshed crop, hence it is only used for data collection as it is not possible to conduct longer test sequences for closed-loop controller verification.

2.1.2 Cleaning System Laboratory

The cleaning system laboratory environment consistent of a hill-side cleaning system test stand as well as a system for continuous feeding of grain and MOG with material recirculation. Additionally smaller test stands have been utilised for test and verification of impact sensors and the tailings volume sensor.

Hill-side Cleaning System Test Stand

The test stand contain a full scale cleaning system from the AGCO IDEAL combine, which facilitate adjustment of fan speed (ω_f), upper sieve opening (d_c) and lower sieve spacing (d_s), see Table 2.2. The cleaning system is mounted in a frame facilitating excitation of lateral (θ) and longitudinal (ϕ) inclination angles using a single pivot point in the front end and two vertical actuated points in the left and right rear end. The test stand is additionally equipped with a yield sensor, moisture sensor, grain quality sensor, infra-red tailings volume sensor as well as impact type sensors [17] for loss, tailings and upper sieve distribution. Material flow samples can be acquired from the residue ($\dot{m}_{c,l} + \dot{m}_{c,r}$), tailings ($\dot{m}_{t,g} + \dot{m}_{t,c}$) and clean grain throughput ($\dot{m}_{y,g} + \dot{m}_{y,c}$). The samples are subsequently cleaned to obtain the individual grain and MOG throughputs. It is optional to return the tailings throughput into the cleaning system, which is enabled during controller testing and disabled when acquiring tailing materiel samples for modelling and validation purposes.

Continuous Crop Material Feeding

The development of a closed-loop control system for fan speed and sieve openings requires extensive testing with material collection for modelling of material flows, sensor characteristics and control scheme verification. The limiting factor for previous laboratory environments have been the time consuming manual layout of material as well as total duration of the individual tests. The largest single challenge in the overall laboratory configuration is to provide continuous MOG feeding, as the MOG material is challenging to handle due to slow varying fluctu-

Table 2.2: Configurable and sampled variables for the continuous cleaning system laboratory environment.

Configurable	Sampled
Fan speed (ω_f)	Grain loss $(\dot{m}_{c,l})$
Upper sieve (d_c)	MOG residue $(\dot{m}_{c,r})$
Lower sieve (d_s)	Tailings grain $(\dot{m}_{t,g})$
Grain feedrate $(\dot{m}_{p,g})$	Tailings MOG $(\dot{m}_{t,c})$
MOG feedrate $(\dot{m}_{p,c})$	Clean grain $(\dot{m}_{y,g})$
Longitudinal inclination angle (ϕ)	MOG in clean grain $(\dot{m}_{y,c})$
Lateral inclination angle (θ)	

ations where the MOG material easily can build up in lumps at various locations causing material blockage. A novel concept for MOG feeding [96] did show good performance, however it was limited by the size of the MOG reservoir. In order to further extent the individual test duration a material recirculation system was constructed, thus the controller test duration can be extended from less than a minute to several hours, Figure 2.2. MOG materiel is fed from the *MOG reservoir* to the
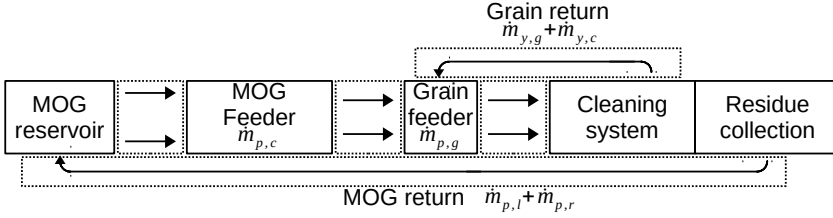

Figure 2.2: Overall continuous laboratory material flow with material recirculation.

MOG feeding unit, which delivers MOG $(\dot{m}_{p,c})$ to a conveyor belt. The *grain feeding* unit feeds grain $(\dot{m}_{p,g})$ on top of the MOG material, which is transported to the *cleaning system* $(\dot{m}_{p,g}+\dot{m}_{p,c})$. The *residue collection* unit collects all residue material $(\dot{m}_{p,l}+\dot{m}_{p,r})$ which is recirculated to the MOG reservoir. The clean grain throughput $(\dot{m}_{y,g}+\dot{m}_{y,g})$ is transported to the buffer on the grain feeding unit.

The overall setup will operate in two modes

- **Single run:** cleaning system performance evaluation and modelling with out material recirculation

- **Continuous run:** long duration runs for closed-loop controller testing with material recirculation

For single test runs the grain and MOG reservoir contains sufficient MOG and grain material to complete a 2 minute test. For longer controller test runs the crop material will be re-circulated to extend the test duration. Chopped straw is used to represent MOG as it is difficult to obtain sufficient quantities of separated MOG from the field.

2.1.3 Field Test

Field test experiments facilitate capturing of the threshing and separation system residue ($\dot{m}_{p,l} + \dot{m}_{p,t} + \dot{m}_{p,r}$), cleaning system residue ($\dot{m}_{c,l} + \dot{m}_{c,r}$), tailings throughput ($\dot{m}_{t,c} + \dot{m}_{t,c}$) and clean grain throughputs ($\dot{m}_{y,g} + \dot{m}_{y,c}$) using different means for each sample position, see Figure 2.3. The residue from threshing, cleaning and separation systems are captured using bags or tarps. The tailings and clean grain throughputs are captured from the cross augers using a bag system, similar to [4]. The material is subsequently cleaned in mobile cleaning units.
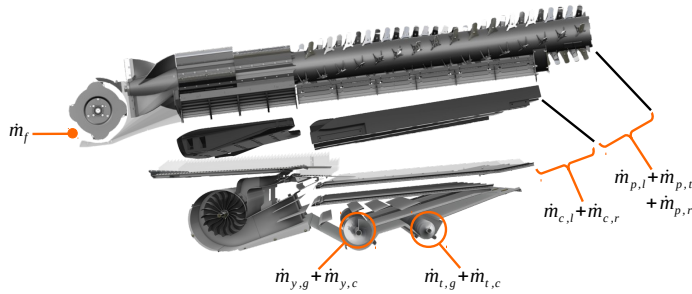

Figure 2.3: Sample position for field test experiments.

2.2 Threshing and Separation System

The axial threshing and separation system of the IDEAL combine is shown in Figure 2.3 and facilitate adjustment of rotor speed ω_r and concave clearance d_p. The input material flow $\dot{m}_f$ is delivered from the feederhouse to the transverse mounted beater that feeds the material into the axial single rotor or dual rotors depending on machine size classification. A short auger section squeezes the material from the beater into the threshing section where large longitudinal mounted threshing elements separate grain kernels from heads/stems/pods and delivers the separated material to the front return pan. The majority of the grain kernels are separated in the threshing section, however a significant ratio of kernels are still en-

capsulated in the straw material after the threshing section. Fingers on the last two thirds of the rotor are used to segregate free kernels to the rear return pan before the MOG ends as residue on the field.

2.2.1   Actuator and Throughput Impact

A number of actuator curves exciting throughput, rotor speed and concave clearance obtained in barley and soy beans are shown in Figure 2.4.
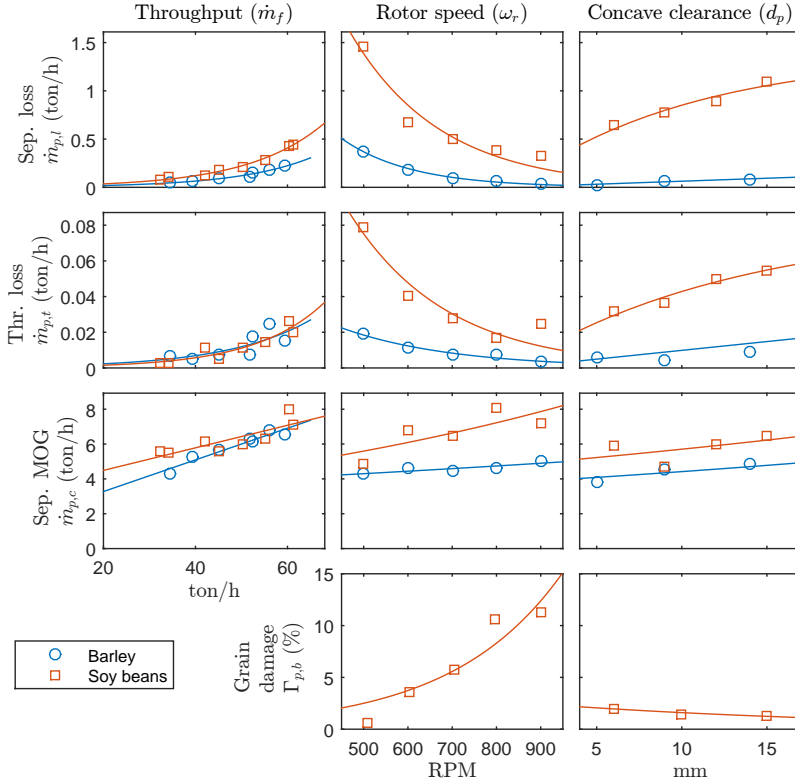
Figure 2.4: Threshing and separation system performance.

The normalised version of the relative gain array (RGA) [98] is shown for the same data points in Table 2.3, where the normalised relative gain g_{ij} from material flow or actuator input u in column j till material flow impact state x in row i is given by

$$g_{ij} = \frac{\sum_{k=1}^{n}(\mathbf{u_i}[k] - \bar{\mathbf{u}}_\mathbf{i})(\mathbf{x_i}[k] - \bar{\mathbf{x}}_\mathbf{i})}{\sum_{k=1}^{n}(\mathbf{u_i}[k] - \bar{\mathbf{u}}_\mathbf{i})^2} \cdot \frac{max(\mathbf{u_j}) - min(\mathbf{u_j})}{max(\mathbf{x_i}) - min(\mathbf{x_i})}. \qquad (2.1)$$

Table 2.3: Threshing and separation system normalised relative gain matrix.

Crop		$\dot{m}_f$	ω_r	d_p
Barley	$\dot{m}_{p,l}$	0.26	−0.21	0.04
	$\dot{m}_{p,t}$	0.44	−0.17	0.16
	$\dot{m}_{p,c}$	0.68	0.07	0.09
Soy beans	$\dot{m}_{p,l}$	0.49	−0.68	0.32
	$\dot{m}_{p,t}$	0.52	−0.66	0.35
	$\dot{m}_{p,c}$	0.49	0.30	0.12
	$\dot{m}_{\Gamma,b}$		1.15	−0.08

The columns are excited by total throughput $\dot{m}_f$, rotor speed ω_r and concave clearance d_p, where the rows show the response for separation grain loss $\dot{m}_{p,l}$, threshing grain loss $\dot{m}_{p,t}$, separated MOG $\dot{m}_{p,c}$ and grain damage $\Gamma_{p,b}$. The grain loss increases exponentially with throughput as shown in [66, 63, 72, 71]. In the presented data the unobservable threshing loss is approximately twenty times lower than the observable separation grain loss as well as it follows the same trends, thus the uncertainties from threshing loss in most cases will be negligible. However it is know that the threshing loss can be considerable in some crop conditions which has to be supervised by the operator. The separated MOG increase with the total throughput, however it is not proportional, thus a reduction in total throughput will not yield a corresponding reduction in the MOG load for the cleaning system. The rotor speed generally has a larger effect on separation losses than the concave spacing, where the effect on grain damage is somehow similar. The total throughput and rotor speed has a dominating effect on MOG separation in the shown sequences. However this is also known to depend on the conditions, e.g. i very dry conditions a substantial MOG separation throughput ($\dot{m}_{p,c}$) can occur when the concave clearance is set tight in order to reduce threshing loss ($\dot{m}_{p,t}$).

2.3 Cleaning System

The IDEAL combine series use a cleaning system with adjustable fan speed (ω_f) as well as adjustable opening of the upper (d_c) and lower (d_s) sieves, see Figure 2.5.

The cleaning system consists of three mechanical modules. First the material from the threshing and separation system in Figure 2.1 is collected with the front and rear return pans, both conveying the grain and MOG material in the forward direction, delivering the material in the front and rear end of the stratification pan.
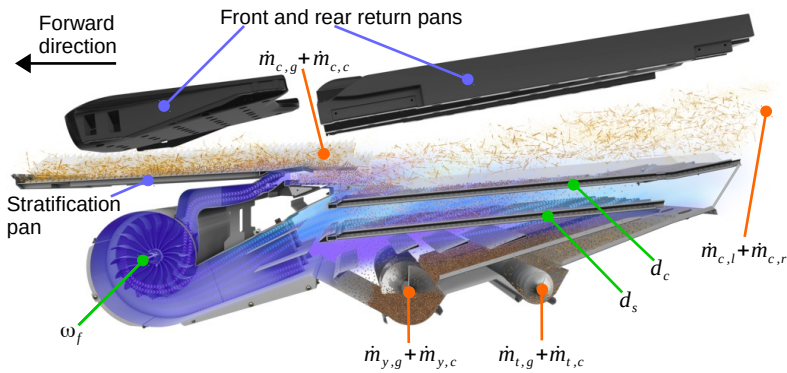
Figure 2.5: Cleaning system.

The stratification pan convey the material in rearwards direction and delivers the material via a pre-sieve cascade to the front end of the upper sieve. Second, in the cleaning shoe the fan speed should be adjusted such that the MOG material is airborne and the grain is segregated through the sieves. The purpose of the upper sieve is to segregate all grain kernels while reducing the segregation of MOG, where the purpose of the lower sieve is to avoid segregation of MOG while separating as many grain kernels as possible. Third the grain and MOG material segregating only the upper sieve (tailings) is transported to the rear return pan using the tailings return system.

2.3.1   Actuator and Throughput Impact

A large number of data sets have been obtained in various crop types both in the laboratory and during field tests, however this section will focus on the performance in wheat which generally is the crop providing the highest MOG throughput for the cleaning system. A series of designed experiments were conducted in the continuous cleaning system laboratory test stand using various combinations of throughput and MOG composition while exciting fan speed as well as upper and lower sieve openings. During each sequence material samples were acquired for 10 s after the system had reached steady-state. The tailings throughput was not returned into the system in order reduce test time and allow material sampling of the tailings throughput. The obtained data sets are useful to investigate interdependencies from actuators (inputs) to the various material flows (states), and from the material flows to the sensor readings (observations).

In Figure 2.6 a sub-set of the raw sample data is presented, where the nor-

malised version of the relative gain array (RGA) [98] is shown for all data points in Table 2.4, using Eq. (2.1).

The columns are excited by cleaning MOG throughput $\dot{m}_{c,c}$, fan speed ω_f, upper sieve opening d_c and lower sieve opening d_s, and the rows represent cleaning grain loss $\dot{m}_{c,l}$, tailings grain $\dot{m}_{t,g}$, tailing MOG $\dot{m}_{t,c}$ and clean grain MOG throughput (cleanliness) $\dot{m}_{y,c}$.

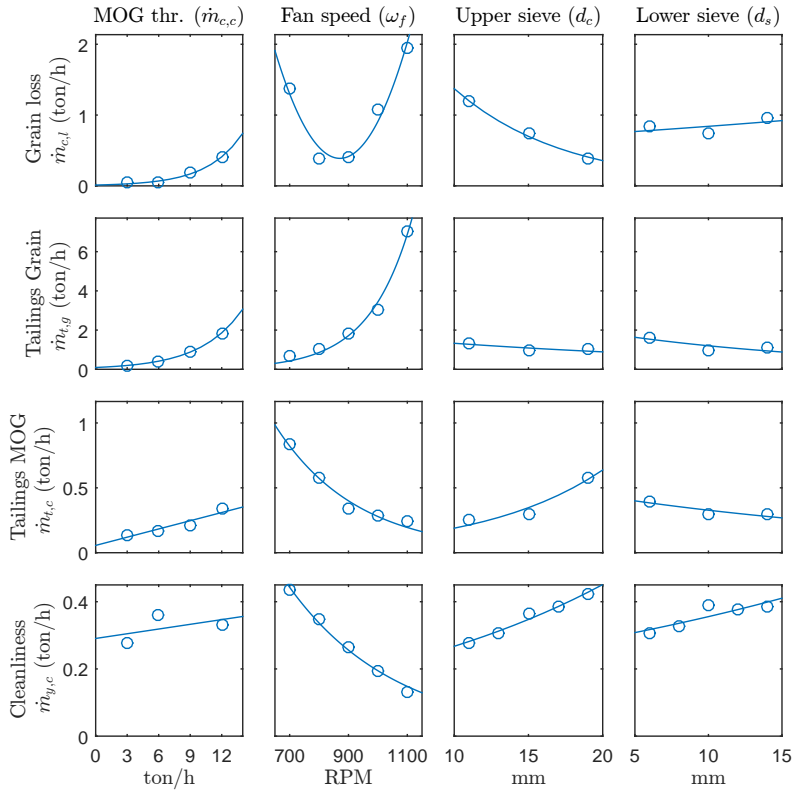Figure 2.6: Cleaning system performance in wheat.

Table 2.4: Cleaning system material normalised relative gain matrix.

	$\dot{m}_{c,c}$	ω_f	d_c	d_s
$\dot{m}_{c,l}$	0.22	0.18	-0.13	-0.03
$\dot{m}_{t,g}$	0.13	0.48	-0.09	-0.18
$\dot{m}_{t,c}$	0.36	-0.31	0.19	-0.00
$\dot{m}_{y,c}$	-0.04	-0.99	0.49	0.28

The grain loss and tailing throughputs all have a monotonic response to the excitation variables, except for grain loss $\dot{m}_{c,l}$ from fan speed ω_f, hence the direction of change to improve performance (reduce the grain loss) is not known in advance. The MOG throughput clearly has the largest negative effect on both grain loss and tailings, hence reducing the MOG throughput (forward speed) is the easiest way to increase performance, though maintaining a high total throughput is often the main priority. In order to reduce the grain loss adjusting the fan speed and upper sieve opening are the two dominating effects. The tailings grain throughput primarily affected by adjusting fan speed and lower sieve opening, where the tailings MOG throughput is primarily is affected by fan speed and upper sieve opening. The fan speed has the largest effect on cleanliness considering the laboratory data set, where the MOG consist of fine chopped straw pieces. However, during field test large straw pieces and weed particles are often present which are difficult to separate from the clean grain flow. Thus in practice the lower sieve is often used to reduce the amount of heavy MOG particles as it has less negative impact on grain loss compared to the fan speed and upper sieve opening. From Figure 2.6 it is clear that the vast majority of the impact relationships does have a non-linear response as well as the rate of the response varies with the MOG throughput and other unobservable variables. Especially it is challenging to adjust the fan speed as multiple loss samples are required to ensure that the combine is operating in the region with low grain loss.

2.3.2 Separation Performance

The separation performance rely on the difference in density of the grain and MOG material. The cleaning separation performance was characterised in [38], by dividing the process into three phases, see Figure 2.7.

- **Flight phase**: both grain and MOG particles are airborne due to high air pressure causing high grain losses (high fan speed)

- **Fluidised phase**: MOG particles are airborne and grain kernels are segregated through the upper sieve

- **Packed phase**: air pressure is not sufficient to maintain the MOG particles airborne, hence it is conveyed on the upper sieve, blocking the segregation of grain kernels causing high grain losses (low fan speed)
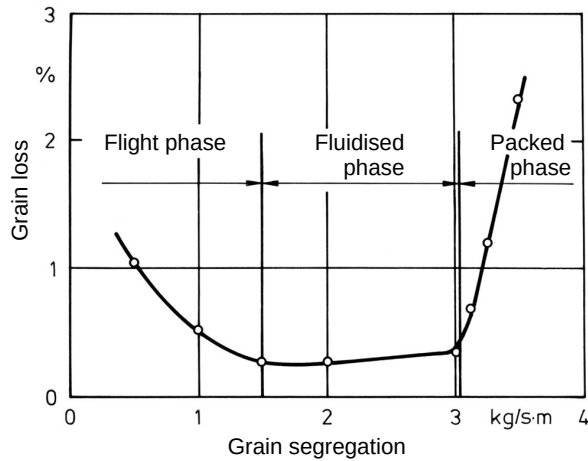
Figure 2.7: Cleaning sieve segregation model by Freye [38]

Both the flight phase and the packed phase can cause a substantial grain loss. The fan speed required to maintain operation in the fluidised phase depends on the physical size and weight of grain and MOG particles where moisture content is an important factor. Additionally the MOG characterises straw, chaff, cops and weed among others which have individual densities depending on local conditions. Hence the performance is charactered by the physical dimension of the MOG particles when the density is similar or higher than grain, thus the upper sieve opening obtain a large effect on the MOG segregation. During high MOG loads reaching the packed phase often causes a collapse where the cleaning system cannot recover to the fluidised phase without reducing the MOG load, i.e. reducing forward speed.

The impact on the cleaning loss and tailing throughputs are shown in Figure 2.8 for a five point fan speed curve from 700 RPM to 1100 RPM. The data points originate from the data-set used to obtain the results in Table 2.4. The curvature for the cleaning loss ($\dot{m}_{c,l}$) is similar to that on the three operational phases shown in Figure 2.7, except that the fan speed on the horizontal axes is shown in Figure 2.8, and Figure 2.7 shows the grain segregation, where the effect on the cleaning process is increasing in the opposition direction. The trend of the tailings grain throughput ($\dot{m}_{t,g}$) clearly follows the cleaning loss ($\dot{m}_{c,l}$) in the high fan speed range corresponding to the flight phase. The fan speed affects the tailings MOG throughput ($\dot{m}_{t,c}$) in the opposite direction causing a higher throughput in the low fan speed range, corresponding to the packed phase. However the slope of the tailings MOG throughput is not as steep compared to the cleaning loss. The aim
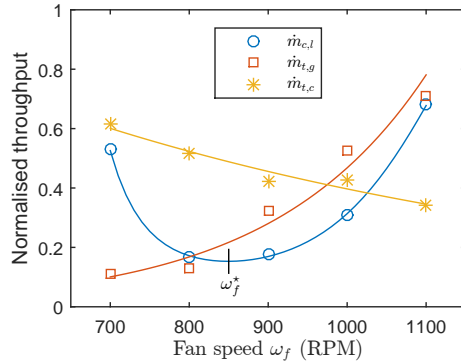
Figure 2.8: Fan speed dependency curve for cleaning loss and tailings return throughputs.

is to utilise the two tailing throughput components to obtain a satisfactory balance characterising the fluidised phase, indicated on Figure 2.8 as the fan speed $\omega_r^\star$ at the minima on the grain loss curve. Estimation of the tailings grain composition characterising the fluidised phase is treated in Section 3.3.5.

Fan speed curves at three different MOG feedrates are shown in Figure 2.9, where three plots show cleaning grain loss ($\dot{m}_{c,l}$), tailings grain throughput ($\dot{m}_{t,g}$) and tailings MOG throughput ($\dot{m}_{t,c}$). The trends for the tailings grain and MOG
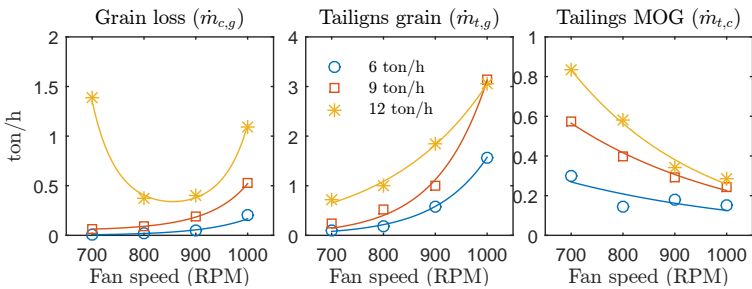
Figure 2.9: Fan speed curve with different MOG ($\dot{m}_{c,g}$) throughputs.

throughputs respectively shows a consistent increase and decrease from the fan speed. However the packed phase is only visible at the MOG feedrate of 12 ton/h from the cleaning grain loss curve in the given fan speed range. The packed phase will be present at even lower fan speeds for the lower rates of cleaning MOG throughput, however the potential performance gain by reducing the fan speed further is negligible compared to the risk of instantaneously collapse for varying MOG

throughputs in practice. The challenges relies in the fact that the packed phase is not always present, however it can instantly occur for an increase in the MOG throughput. Hence in can be an advantage to maintain sub-optimal (higher) fan speed in order to reduce the risk of a collapse originating from throughput variations, i.e. increase the robustness of the control loop.

2.3.3 Inclination Impact

In order to obtain high performance from the cleaning system it is vital to adjust the fan speed to operate in the fluidised phase, where the MOG is airborne and the grain is segregated through the sieves. This process is very sensitive to the effect from lateral (θ) and longitudinal (ϕ) inclination which has previously been addressed in [97, 36, 13], however the effect from the fan speed has not been been thoroughly investigated. Both longitudinal and lateral inclination variations in on the cleaning system has a significant effect on the cleaning losses, however the largest effect originate from the lateral inclination [36, 13].

The fan speed cannot not compensate for the performance decrease imposed by the lateral inclination angle (θ) [36], for this reason an number of mechanical solutions have been developed to compensate for lateral inclination [32, 92, 10, 9, 16, 7].

The fan speed is known to potentially reduce the effect from longitudinal inclination (ϕ) using feed-forward from the measured longitudinal inclination angle to the fan speed. In Figure 2.10 the cleaning loss is mapped with excitation of fan speed (ω_r) and longitudinal inclination angle (ϕ), where the lower and upper limit for the lateral inclination angle (ϕ) are $-6.1°$ (down hill) and $6.1°$ (up hill) respectively. All data-set were obtained with identical grain and MOG throughputs.

The loss mesh is fitted to the measured data points marked with blue circles, where the largest contribution to grain loss exist in the corners either with low fan speed and negative longitudinal inclination, or with high fan speed and positive longitudinal inclination, which can be linked to the packed and flight cleaning phases in Figure 2.7. At a large down-hill inclination angle the conveying capability decreases due to gravity, hence grain loss increases at lower fan speeds. During large up-hill inclination angles the conveying capacity is increased, hence high fan speeds significantly increases the grain loss.

It is clear that an acceptable loss can be maintained on-line using linear feed-
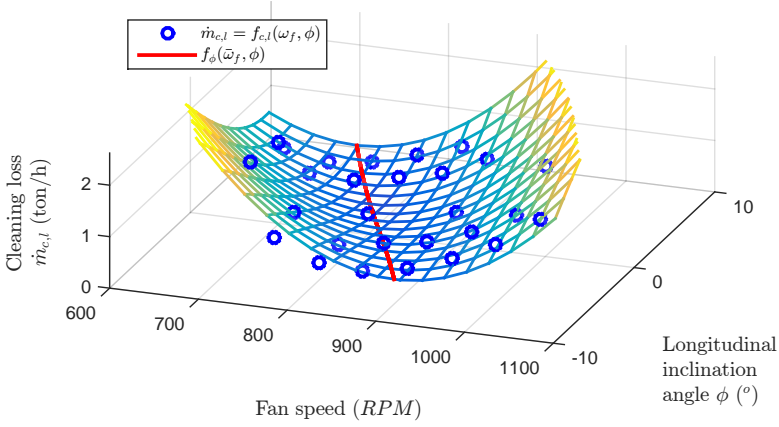
Figure 2.10: Cleaning grain loss for fan speed (ω_f) versus chassis longitudinal inclination angle (ϕ).

forward term from the longitudinal inclination angle (ϕ) to the fan speed (ω_f),

$$\omega_f = f_\phi(\bar{\omega}_f, \phi) = \bar{\omega}_f + c\phi, \tag{2.2}$$

where $\bar{\omega}_f$ is the initial fan speed set-point on flat land from the operator or a control system and c the feed-forward rate from the longitudinal inclination angle. The c parameter can be obtained by solving the general optimisation problem off-line,

$$\underset{\bar{\omega}_f, c}{\arg\min} \quad f_{c,l}(\omega_f = f_\phi(\bar{\omega}_f, \phi), \phi) \quad \forall \quad \omega_f \in \mathbb{N}[\omega_{f,min} : \omega_{f,max}]. \tag{2.3}$$

Here $\bar{\omega}_f$ is the fan speed setting characterising the fluidised phase in flat land conditions, which is required as a prerequisite to compensate for the varying longitudinal inclination angle using Eq. (2.2).

2.4   Plant Modelling

The modelling work is based on a desire to apply closed-loop control using the actuators in the threshing, separation and cleaning systems. This requires knowledge of the actuators affect on the material throughputs (controllability) and how the process sensors representation the actual material flows (observability). Additionally the threshing, separation and cleaning processes as well as the sensor readings are known to be affected by a number biological variables (disturbances), where only a sub-set is observable. The aim is to capture the dominating non-linear

trends knowing that the relative effect of a given system throughput or actuator setting is affected by the various disturbances.

The models should have a flexible modular based structure where individually obtained datasets from the threshing and separation system, and the cleaning system can be combined, or a new sensor can be added from a dataset obtained later. Material samples acquired from combine harvesters during field test experiments are known to have a high variance and a relatively low number of samples, hence it is required that the model generation process include evaluation of data and model validity, i.e. cross validation.

2.4.1 Model Structure

The combine harvester contains four mechanical crop processing modules, where the grain pans and tailings return system are considered solely as transport delays, see Figure 2.11. All the material flows are modelled from a single point of delivery indicated by the lines between the modules. This facilitate a modular structure where data can be acquired from individual data sources and the total material flow model can be validated from material samples obtained at a single point of delivery.

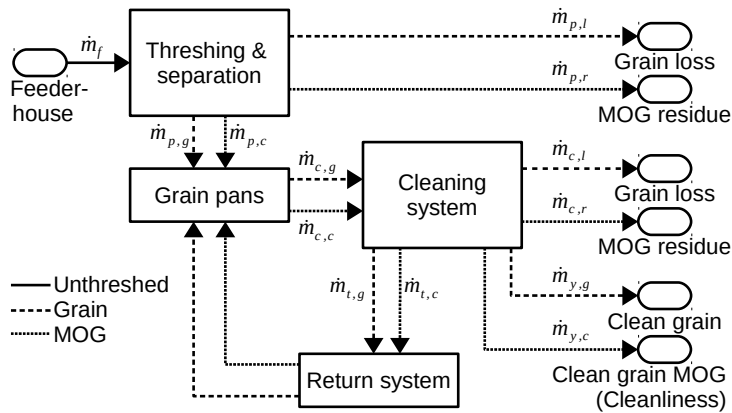Figure 2.11: Combine material flow model block diagram.

The acquired material samples represent the various non-linear steady-state trends of the combine harvester, where the dynamics are captured from the sensor readings during field test experiments using standard ARX modelling methods [104]. The steady-state periods are captured semi-automatically using the steady-state detection methods presented in [49, 15].

A Weiner model structure is chosen where the dynamics is modelled using first order moving average filters and the non-linear interdependencies are modelled individually for each material flow or sensor reading [82], see Figure 2.12.
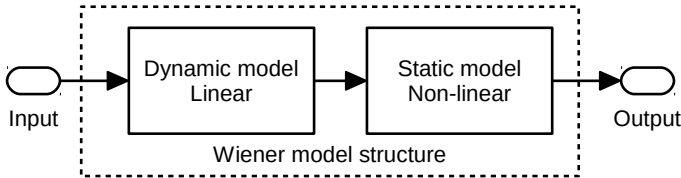

Figure 2.12: Wiener model structure

Previous modelling efforts have used a variety of model functions to describe the various material flows in the threshing, separation and cleaning systems.

Different black-box approaches exist where models can be generated with-out any prior knowledge of the actual internal model structure, e.g. Fuzzy systems or neural networks. Fuzzy models were used to describe the static material flow by [18, 86, 25, 27], as it provide an intuitive representation of the process by character-ing the process in to a number different regimes (discrete states) [82], however the models are generated using hidden states which are very difficult to troubleshoot and has a tendency of over-fitting for a low number of measurements.

Non-parametric methods such as K-Nearest Neighbours (KNN) provide a rep-resentation of the system that maintains the static characteristics with a relatively low bias-error. The KNN utilise a weighted average of the nearest k observations from a measurement database, hence it does not require a fitting procedure as well as it is flexible to any non-linear trend, however it is know to be outperformed by polynomial based models for low number of samples [39].

A number of analytical non-linear gray-box models and probability density functions were used by [102, 75, 72, 99, 106, 107] to model material flow de-pendencies and separation curves for a single variable input. The models generally have a low bias error, however expansion to multiple inputs is arduous.

Polynomial based models were used in [100, 83, 105] and provide a high de-gree of transparency and flexibility for multiple regression models. However many trends of physical system are not well represented by low order polynomial models increasing the bias-error.

A polynomial based model structure is chosen as it facilitate a number of sta-tistical tools for evaluation of model uncertainties and statistical parameters of the acquired data sets. Additionally it allows to update parameters fully or partially

online [105, 45], if the data-set fulfils some predetermined criteria depending on the model structure, actuator excitation and sensor readings.

2.4.2   Modelled Material Flows

Based on the trends from actuators and disturbances to material flows shown in Section 2.2 and Section 2.3 a sub-set of the material flows are modelled. The vectors containing the model input variables for the threshing and separation system are given in Eq. (2.4) and for the cleaning system in Eq. (2.5), where $\Gamma_{p,g}$ is the ratio of grain in the total throughput ($\dot{m}_f$) in the feederhouse, and ρ_g and ρ_c respectively are the grain and straw moisture content.

$$\mathbf{\Theta_p} = \begin{pmatrix} \omega_r & d_p & \dot{m}_f & \Gamma_{p,g} & \phi & \theta & \rho_g & \rho_c & \dots \end{pmatrix}^T \qquad (2.4)$$

$$\mathbf{\Theta_c} = \begin{pmatrix} \omega_f & d_c & d_s & \dot{m}_{c,g} & \dot{m}_{c,c} & \phi & \theta & \rho_g & \rho_c & \dots \end{pmatrix}^T \qquad (2.5)$$

The model variable vectors contain actuator settings, material throughputs and disturbances from inclination angles and moisture content.

The material flows at a single point of delivery are shown in Figure 2.11. In steady-state the material flow constraints for the threshing and separation system are given by

$$\Gamma_{p,g}\dot{m}_f \quad = \dot{m}_{p,g} + \dot{m}_{p,l} \qquad (2.6)$$

$$(1 - \Gamma_{p,g})\dot{m}_f \quad = \dot{m}_{p,c} + \dot{m}_{p,r}, \qquad (2.7)$$

where the threshing grain loss ($\dot{m}_{p,t}$) is neglected, and for the cleaning system by

$$\dot{m}_{c,g} \quad = \dot{m}_{t,g} + \dot{m}_{p,g} = \dot{m}_{t,g} + \dot{m}_{y,g} + \dot{m}_{c,l} \qquad (2.8)$$

$$\dot{m}_{c,c} \quad = \dot{m}_{t,c} + \dot{m}_{p,c} = \dot{m}_{t,c} + \dot{m}_{y,g} + \dot{m}_{c,r}. \qquad (2.9)$$

In the model generation process it is necessary to ensure that a number of constraints are fulfilled, where some originates in the polynomial structure and some are given as inequality constraints in the optimisation problem. The material flows are modelled using a relative gain function $f(p, \mathbf{\Theta})$ which yield the ratio of the input flow u going to the output flow y, for the vector $\mathbf{\Theta}$ containing actuator settings and sensor readings,

$$y = f(\mathbf{p}, \mathbf{\Theta})u. \qquad (2.10)$$

All material flows in Eq. (2.6-2.9) are modelled except one, which is obtained as the remaining material flow in Eq. (2.6-2.9). The modelled material flows are selected

based on the priority for optimisation of the overall performance, see Figure 1.3 on page 5. Thus the separation loss ($\dot{m}_{p,l}$), separated MOG ($\dot{m}_{p,c}$) and grain damage ($\Gamma_{p,b}$) are modelled as

$$\dot{m}_{p,l} = f_{p,l}(\mathbf{p_{p,l}}, \mathbf{\Theta_p})\Gamma_{p,g}\dot{m}_f \tag{2.11}$$

$$\dot{m}_{p,c} = f_{p,c}(\mathbf{p_{p,c}}, \mathbf{\Theta_p})(1 - \Gamma_{p,g})\dot{m}_f \tag{2.12}$$

$$\Gamma_{p,b} = f_{p,b}(\mathbf{p_{p,b}}, \mathbf{\Theta_p}). \tag{2.13}$$

Given the material flow of grain ($\dot{m}_{p,g}$) and MOG ($\dot{m}_{p,c}$) from the threshing and separation system, the four material flows desirable to control in the cleaning system are the cleaning grain loss ($\dot{m}_{c,l}$), tailings grain throughput ($\dot{m}_{t,g}$), tailings MOG throughput ($\dot{m}_{t,c}$) and clean grain MOG throughput ($\dot{m}_{y,c}$),

$$\dot{m}_{c,l} = f_{c,l}(\mathbf{p_{c,l}}, \mathbf{\Theta_c})\dot{m}_{c,g} \tag{2.14}$$

$$\dot{m}_{t,g} = f_{t,g}(\mathbf{p_{t,g}}, \mathbf{\Theta_c})\dot{m}_{c,g} \tag{2.15}$$

$$\dot{m}_{t,c} = f_{t,c}(\mathbf{p_{t,c}}, \mathbf{\Theta_c})\dot{m}_{c,c} \tag{2.16}$$

$$\dot{m}_{y,c} = f_{y,c}(\mathbf{p_{y,c}}, \mathbf{\Theta_c})\dot{m}_{c,c}. \tag{2.17}$$

Hence the remaining material flows $\dot{m}_{p,g}$, $\dot{m}_{p,c}$, $\dot{m}_{y,g}$ and $\dot{m}_{c,r}$ are obtained by substituting the modelled material flows from Eq. (2.11-2.17) into Eq. (2.6-2.9).

2.4.3 Model Generation

The material flows in Eq. (2.11-2.17) are modelled using a polynomial regression with the model variable vectors in Eq. (2.4-2.5). The polynomial regression is often used in conjunction with an exponential function or a logistic sigmoid function, i.e.

$$f(\mathbf{p}, \mathbf{\Theta}) = \mathbf{p}X(\mathbf{\Theta}) \tag{2.18}$$

$$f(\mathbf{p}, \mathbf{\Theta}) = \exp(\mathbf{p}X(\mathbf{\Theta})) \tag{2.19}$$

$$f(\mathbf{p}, \mathbf{\Theta}) = \frac{1}{1 + \exp(\mathbf{p}X(\mathbf{\Theta}))}, \tag{2.20}$$

for the design matrix X being a function of $\mathbf{\Theta}$.

The observation matrices for Eq. (2.4-2.5) are given by $Y_{p,l} = \dot{m}_f/(\dot{m}_{p,g}\Gamma_{p,g})$, $Y_{p,c} = \dot{m}_{p,c}/(\dot{m}_f(1 - \Gamma_{p,g}))$, $Y_{c,l} = \dot{m}_{c,l}/\dot{m}_{c,g}$, $Y_{t,g} = \dot{m}_{t,g}/\dot{m}_{c,g}$, $Y_{t,c} = \dot{m}_{t,c}/\dot{m}_{c,c}$ and $Y_{y,c} = \dot{m}_{y,c}/\dot{m}_{c,c}$.

The material flow models have to fulfil a number of constraints in order to provide a useful representation of the actual material flow. First the model structure

given in Eq. (2.10) ensures zero output flow at zero input flow. The general feasible constraints are listed with a physical description and a mathematical interpretation in Table 2.5, in a similar fashion as shown in [63]. Constraint *1a* and *1b* addresses

Table 2.5: Definition of material flow model constraints and mathematical interpolation.

	Physical material flow constraint	Mathematical interpolation
1a	Negative material flows not possible	$f(\mathbf{p}, \mathbf{x}) \geq 0$
1b	Output flows cannot exceed input flows	$f(\mathbf{p}, \mathbf{x}) \leq 1$
2a	Output increases monotonically with input	$\dfrac{\partial f(\mathbf{p}, \mathbf{x})u}{\partial u} \geq 0$
2b	Output decreases monotonically with input	$\dfrac{\partial f(\mathbf{p}, \mathbf{x})u}{\partial u} \leq 0$
3a	Output flow increase more rapidly than increasing input	$\dfrac{\partial^2 f(\mathbf{p}, \mathbf{x})}{\partial^2 u} \geq 0$
3b	Output flow increase more rapidly than decreasing input	$\dfrac{\partial^2 f(\mathbf{p}, \mathbf{x})}{\partial^2 u} \leq 0$

physical model limits, where *1a* always will be satisfied using Eq. (2.19-2.20) and *1b* always will be satisfied using Eq. (2.20) due to the model function. The constraints *2* and *3* can be applied using parameter bounds, inequality constraints or a customised penalty function, depending on whether it is applied to a rate of the material flow ($f(\mathbf{p}, \mathbf{\Theta})$) or the actual throughput ($f(\mathbf{p}, \mathbf{\Theta})\dot{m}$). Given the constraints in Table 2.5 the general actuator and material flow interdependencies (operator experiences) can then be included in the polynomial based models.

From the obtained observation matrix Y and design matrix X the model parameters $\mathbf{p}$ can now be obtained by solving the optimisation problem

$$\arg\min_{\mathbf{p}}||Y - f(\mathbf{p}, X(\mathbf{\Theta}))|| \quad s.t. \quad \begin{cases} \mathbf{p_{min}} \leq \mathbf{p} \leq \mathbf{p_{max}} \\ A\mathbf{p} \leq \mathbf{b} \\ c(\mathbf{p}) \leq 0 \end{cases} . \quad (2.21)$$

The model order selection is crucial for the overall project as it is the foundation which all methods for process optimisation, material flow estimation and process simulation relies on. Numerous factors as observation uncertainties, system excitation, unobservable disturbances, collinearity, bias/variance trade-off as well as prior system knowledge have to be considered in the variable selection process. In addition the purpose of the model can determine the model order, e.g. a higher model

order can be suitable for a simulation in a virtual combine where model order re-
duction is relevant for adaptive observer design. The *forward selection* method [47]
is utilised for model order selection, where the model is initiated as a *null model*
and the number of parameters is increased as long it can be justified according to
a predetermined set of statistical evaluation parameters (ξ). The obtained models
are automatically checked for model input variable information criteria, parame-
ters uncertainty and collinearities as well as high leverage and outliers statistics are
computed for each data point.

Numerous unobservable biological variables (disturbances) are know to affect
the threshing, separation and cleaning processes, hence it is not realistic to validate
the material flow models using cross validation with data sets acquired in non-
uniform conditions. Thus only acquired data from the same field with a narrow
time frame are comparable as well as laboratory data with store crop from the same
batch (field) are comparable. The coefficient of determination R^2 has been applied
on the fitted data set (training data) for verification purposes in the vast majority
of the related literature. For multiple regression and higher degree polynomials
verification by means of R^2 alone easily results in over-fitted models [39], thus the
fitting procedure utilise measures for parameter uncertainty, outliers, high leverage
points, collinearities etc. As the datasets size in general is limited re-sampling
based methods can advantageously be used for cross-validation. Depending of the
size of the individual data sets *leave lone out cross validation* (LOOCV) is used for
small data sets and *k-fold cross validation* (KFCV) for larger data sets.

2.5   Sensor Modelling

The combine harvester has a number of sensors in order to measure the grain
and MOG components of the several material flows throughout the machine. The
individual sensor locations on the combine are marked with orange in Figure 2.13.

The sensors are listed in Table 2.6 in the order material impact occurs.

In the feederhouse a lever with a roller on the elevator chain is measuring the
height of the crop material using a potentiometer (y_α) which correspond to the to-
tal throughput ($\dot{m}_f$). The hydraulic oil pressure for the belt variation gear in the
drive train for the threshing and separation rotor is measured (y_β) which represents
the total throughput ($\dot{m}_f$) [3]. The grain throughput ($\dot{m}_{p,g}$) under the threshing
concave and separation grates are measured with impact mass flow sensors (MFS)
($y_{p,g}$), see Figure 2.14a. In the same manner the grain throughput is measured lon-
gitudinally under the upper sieve, lateral in the rear end under the upper sieve and
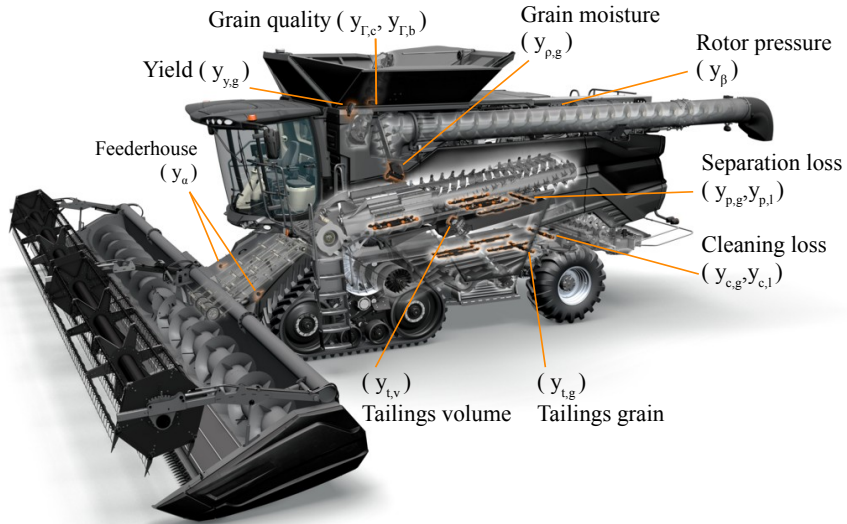
Figure 2.13: Combine harvester sensor location.

Table 2.6: Process sensors.

Measurement	Technology
Feeedehouse throughput (y_α)	Potentiometer
Rotor hydraulic oil pressure (y_β)	Oil pressure
Threshing and separation dist./loss $(y_{p,g}, y_{p,l})$	Impact type (MFS)
Cleaning system dist./loss $(y_{c,g}, y_{c,l})$	Impact type (MFS)
Tailings grain $(y_{t,g})$	Impact type (MFS)
Tailings volume sensor $(y_{t,v})$	Infra-red proximity (TVS)
Grain moisture (ρ_g)	Capacitive
Grain damage $(y_{\Gamma,b})$	Camera (GQS)
Cleanliness $(y_{\Gamma,c})$	Camera (GQS)
Clean grain throughput $(y_{y,g})$	Impact type

lateral in the discharge plate after the upper sieve using the MFS. The tailings grain throughput $(\dot{m}_{t,g})$ is measured using a MFS $(y_{t,g})$ mounted after the lower sieve in the tailings return pan. An infra-red proximity sensor is used to measure the material volume $(y_{t,v})$ after paddle throw in the tailings return system, see Figure 2.14b. The tailings volume sensor was develop during the Ph.D. project as the obtained knowledge showed the importance of the tailings MOG throughput $(\dot{m}_{t,c})$ to describe the cleaning process and the high correlation to the cleaning MOG through-

put ($\dot{m}_{p,c}$), see Table 2.4. A capacitive sensor measures the grain moisture content (ρ_g) in the cleaning grain elevator. The grain quality sensor (GQS) is located in the top of the clean grain elevator and provides a relative reading of broken kernels ($y_{\Gamma,b}$) and MOG ($y_{\Gamma,c} \approx \dot{m}_{y,c}/(\dot{m}_{y,g} + \dot{m}_{y,c})$) in the clean grain throughput, see Figure 2.14c. A impact type yield sensor ($y_{y,g}$) measures the cleaning grain throughput ($\dot{m}_{y,g}$) in the clean grain elevator head. The noise profile of the process sensors varies significantly between the employed sensor technologies, hence a variety of model approaches are used to reproduce realistic sensor readings, e.g. band-width limited white noise models for the feederhouse and yield sensors are obtained using the power spectral density (PSD) [41], where the Poisson, Chi and the Chi-squared distributions [48] are used to represent sensor noise for the MFS, TVS and GQS respectively.

(a) Mass Flow Sensor   (b) Tailings Volume Sensor   (c) Grain Quality Sensor

Figure 2.14: Primary Process Sensors

2.5.1   Mass Flow Sensor

The mass flow sensor [17] is utilised throughout the combine and provide an impact energy reading with a high throughput range as well as an impact count reading with higher accuracy for lower throughputs. The impact energy reading is intended for the location under the concave and sieves, where the impact count reading is more applicable for loss sensing. The MFS tailings sensor reading ($y_{t,g}$) reading of the absolute tailings grain flow ($\dot{m}_{t,g}$) obtained from material samples is shown in Figure 2.15a. The Poisson probability density function

$$\mathcal{P}(\lambda, x) = \frac{\lambda^x \exp(-\lambda)}{x!}, \tag{2.22}$$

is used to model the impact count sensor reading from the MFS sensor. The Poisson distribution and histogram ($\mathcal{H}$) is shown in Figure 2.15b for two steady-periods with an average reading ($\bar{y}_{t,g}$) of 0.67 and 10.22, showing a reasonably good representation.
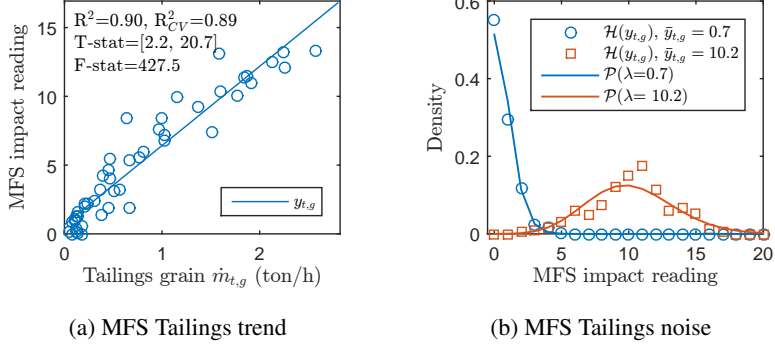
(a) MFS Tailings trend

(b) MFS Tailings noise

Figure 2.15: Mass Flow Sensor (MFS) model

2.5.2 Tailings Volume Sensor

The tailings return system utilise an auger to elevate the tailings material, where a paddle is mounted on top of the auger to spread the material on the rear return pan before re-entering the cleaning shoe. The tailings volume sensor provide a voltage reading corresponding the observed distance. A series of designed experiments exciting tailings grain ($\dot{m}_{t,g}$) and MOG ($\dot{m}_{t,c}$) throughputs using a dedicated sensor test stand is shown in Figure 2.16a.

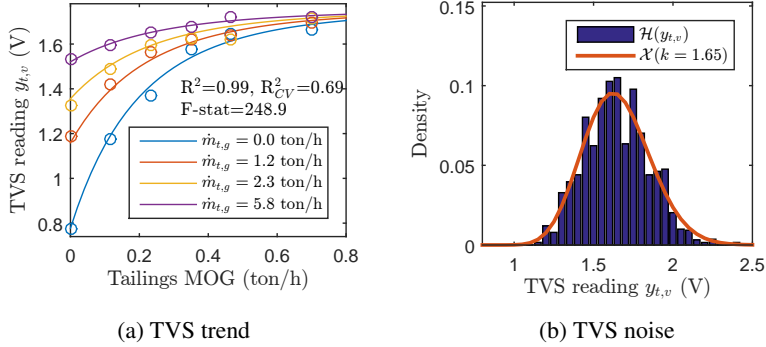(a) TVS trend

(b) TVS noise

Figure 2.16: Tailings volume sensor (TVS) model

The material flow is modelled by

$$y_{t,v} = h_{t,v}(\mathbf{q_{t,v}}, \dot{m}_{c,g}, \dot{m}_{c,c}) \tag{2.23}$$

$$\Updownarrow$$

$$y_{t,v} = q_{t,v1} + q_{t,v2}\left(1 - \exp(q_{t,v3}\dot{m}_{c,g} + q_{t,v4}\dot{m}_{c,g}^3 + q_{t,v5}\dot{m}_{c,c} + q_{t,v6}\dot{m}_{c,c}^3)\right),$$

from the tailings throughputs of grain ($\dot{m}_{t,g}$) and MOG ($\dot{m}_{t,c}$), using the parameter vector $\mathbf{p_{t,v}}$. The sensor noise is modelled using a modified *Chi* distribution

$$\mathcal{X}(k,x) = \frac{1}{2^{(k/2)-1}\Gamma(k/2)}v^{k-1}\exp(-v^2/2) \quad \wedge \quad v = \frac{x-q_{x1}}{q_{x2}}, \qquad (2.24)$$

where $y_{t,v}$ is scales to x using an affine model parameters $\mathbf{q_x}$, see Figure 2.16b.

2.5.3 Grain Quality Sensor

The grain quality sensor is located in the top of the clean grain elevator where the captured images are synchronised with the paddle throw from the elevator. The captured images are used to compute are measure of broken grain ($y_{\Gamma,b}$) and MOG particles (cleanliness) ($y_{\Gamma,c}$). Material samples of broken kernels versus the GQS broken grain reading ($y_{\Gamma,b}$) are shown in Figure 2.17a for soy-beans, with a good representation of the actual grain damage.

(a) GQS trend   (b) GQS noise
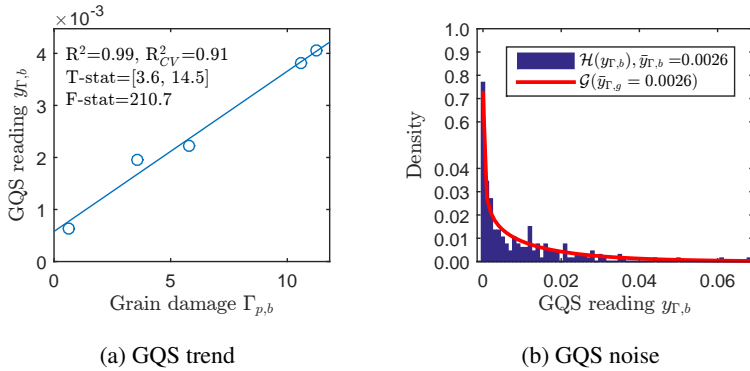
Figure 2.17: Grain quality sensor (GQS) model

The distribution of the samples are shown in Figure 2.17b, which show a large number of zero readings indicating that the sensor readings could be modelled with a uniform distribution, i.e. $\mathcal{N}(0,1) \leq \Gamma_{p,b}$. Note that the scale on the vertical axes changes to show the zero reading bar. However each of the non-zero readings are characterised by a *Chi-squared* distribution,

$$\mathcal{X}^2(k,x) = \frac{1}{2^{k/2}\Gamma(k/2)}x^{k/2-1}\exp(-x/2). \qquad (2.25)$$

By joining the *uniform* and *Chi squared* distribution a reasonable approximation of

the observations can be obtained,

$$\mathcal{G}(k, x) = \begin{cases} \dfrac{\mathcal{X}^2(k, x)}{kc_\lambda} & \text{if} & \mathcal{U}(0, 1) > c_\lambda x \\ 0 & \text{else} \end{cases}. \tag{2.26}$$

The *uniform* distribution represents if material is visible in the captured frame, which enables the *Chi squared* distribution normalised by k, as $k = E\{\mathcal{X}^2(k, x)\}$. The *Chi-squared* distribution is scaled with c_λ to the range of the GQS readings.

2.6 Control Strategy Analysis

The actuator impact plots in Figure 2.4 and Figure 2.6 showed a tightly coupled MIMO system which yield a large number of potential configurations of the closed-loop control system in order to reduce the overall optimisation problem, see visualisation in Figure 1.3 on page 5. The aim of this section is to enlighten the possible pairings of actuator inputs to material flows, and material flows to sensor readings.

Classical closed-loop control systems are aimed towards a given reference set point, however aiming for a specific throughput is undesirable in order to solve the overall optimisation problem as

- The actual impact from each actuator varies with crop conditions, thus it is often not possible to reach a certain reference set point

- In conditions where e.g. grain loss is below the reference set-point the controller will actively decrease performance

- Each controller will adjust one parameter though most actuators affect multiple optimisation parameters

In order to optimise performance the individual actuator setting will always be a compromise to obtain overall acceptable performance, where the following parameters will be considered the closed-loop control system

- Total throughput ($\dot{m}_f$)

- Grain loss ($\dot{m}_{p,l}$ and $\dot{m}_{c,l}$)

- Grain damage ($\Gamma_{p,b}$)

- Cleanliness ($\dot{m}_{y,c}$)

As shown in Figure 2.4 and Figure 2.6 each individual actuator had a dominating effect on multiple material flows, thus multiple material flows should be included in the resolution for each individual actuator change.

In order to facilitate a closed-loop control system it is essential to investigate the ability to control (controllability) the desirable material flows as well as observe (observability) the material flows desirable to control [42]. During the design process it is vital to pair of actuators with the material flows providing the highest relative gain from Table 2.4, i.e. with the actuators providing the dominating controllability [98].

A summary is shown in Table 2.7 of the general mapping of controllability based on Figure 2.4, Figure 2.6 and the general operator experiences as well as the general mapping of observability based on the presented static sensor models in Section 2.5.

Table 2.7: Mapping of controllability (● dominant, ○ significant) and observability (▶ full, ▷ partial).

Parameter	Sym.	Obs.	v	ω_r	d_p	ω_f	d_c	d_s
Total throughput	$\dot{m}_f$	▶	●					
Separation loss	$\dot{m}_{p,l}$	▶	●	●	○			
Threshing loss	$\dot{m}_{p,t}$		●	●	●			
MOG separation	$\dot{m}_{p,c}$		●	●	●			
Grain damage	$\Gamma_{p,b}$	▶		●	○			
MOG throughput	$\dot{m}_{c,c}$		●					
Cleaning loss	$\dot{m}_{c,l}$	▷	●			●	●	
Tailings grain	$\dot{m}_{t,g}$	▶	○			●	○	●
Tailings MOG	$\dot{m}_{t,c}$	▶	○			●	●	
Clean grain	$\dot{m}_{y,g}$	▶	●					
Cleanliness	$\dot{m}_{y,c}$	▶	○			○	○	●

The first two columns shows material flow, third column (full ▶ or partial ▷) observability and the remaining columns (● dominating or ○ significant) controllability. The controllability indication is primarily based on the normalised RGA for the threshing and separation system in Table 2.3 and the cleaning system in Table 2.4, where the dominating controllability (●) is set for $|g_{ij}| > 0.15$ and significant controllability (○) is set for $|g_{ij}| > 0.05$. The actual gain depends on crop and the local conditions where the data is acquired, thus some indications are set based on general operator experience. Controllability from the threshing and separation sys-

tem to the cleaning system is not marked, e.g. as the effect from rotor speed (ω_r) to the MOG separation ($\dot{m}_{p,c}$) which has an affect on the cleaning grain loss ($\dot{m}_{c,g}$).

In general increasing throughput results in increased separation and threshing losses, thus reducing grain losses is normally the primary concern in order to maintain a high throughput. The rotor speed (ω_r) primarily affects separation loss ($\dot{m}_{p,l}$) and grain damage ($\Gamma_{p,b}$). The concave clearance (d_p) does in some conditions cause considerable threshing grain losses ($\dot{m}_{p,t}$) which are unobservable, thus it is not possible to facilitate closed-loop control.

The partial observability of $\dot{m}_{c,l}$ is primarily related to the packed phase of the cleaning system where grain kernels are encapsulated in the collapsed MOG travelling on the upper sieve, thus the grain kernels cannot cause an impact on the MFS impact sensor. In the transition phase between the fluidised and packed phases the same effect can cause the representation of the convex cleaning grain loss curve shown in Figure 2.8 to be skewed, causing a significant diversity in the observation off the desirable fan speed $\omega_f^\star$. The tailings volume sensors does only provide partial observability of the tailings MOG throughput $\dot{m}_{t,c}$, however using the sensor fusion with the MFS tailings grain sensor as shown in Figure 2.16a full observability is obtained.

Utilisation of the cleaning grain loss reading for fan speed control would require sensor fusion in order compensate for the partial observability in the packed phase. However the modelling effort showed a potential to identify the fluidised phase using the tailings grain composition for closed-loop control of the fan speed, which led the development of the tailings volume sensor in order to obtain full observability of the tailings MOG throughput. The upper sieve has a dominating effect on the tailings MOG throughput ($\dot{m}_{t,c}$) and the cleaning grain loss ($\dot{m}_{c,l}$) which is full observable while the fan speed controller can maintain the fluidised or airborne phase of the cleaning system. The lower sieve has the dominating effect on cleanliness ($\dot{m}_{y,c}$) and tailings grain ($\dot{m}_{t,g}$). The controllers for the two sieves should consider grain loss ($\dot{m}_{c,l}$), tailings throughputs ($\dot{m}_{t,g}$ and $\dot{m}_{t,c}$) and cleanliness ($\dot{m}_{y,c}$) as the material flow impact from both actuators are tightly coupled.

2.7 Conclusion

The experimental setup for laboratory tests of threshing, separation and cleaning systems as well as field tests were presented. An analysis of the threshing and separation system showed that the rotor speed (ω_r) had the dominating effect of separation loss ($\dot{m}_{p,l}$) and grain damage ($\Gamma_{p,b}$) compared to the concave clearance

(d_p). The cleaning system analysis showed that the fan speed (ω_f) and upper sieve opening (d_c) had the dominating actuator effect on grain losses as well as the cleanliness ($\dot{m}_{y,c}$) primarily should be adjusted using the lower sieve opening (d_s).

The modular model structure was outlined with a description of the specific modelled material flow rates. It was shown how the prior knowledge of material flow interdependencies could be included in the static models. The material flow representation and noise characteristics were shown for the three primary process sensors used for closed-loop control.

Simulation and Estimation

This chapter describes the design and implementation of the virtual combine and applied throughput estimation methods. The framework for the semi-automated modelling process was published in Article A.1. Throughput prediction using a dynamic model and fault detection was published in Article A.2. Design of the grain damage observer was published in Article A.3, identification of the fluidised phase was shown in Article A.5, and the tailings throughput estimate was shown in Article A.6.

The verification of a closed-loop control system for a combine harvester requires substantial test activities to be conducted in order to test observers and control loops. Some tests can partially be conducted using stored data sets, however the closed-loop verification requires the system feedback. The utilisation of a virtual combine will facilitate closed-loop control testing at an early stage for sensor fusion, material flow estimation and fault detection as well as it can be incorporated in HIL unit test procedures to verify the integration. All process sensors provide a relative throughput measurement which requires some interpretation in order to obtain the necessary understanding of the actual material flow. By means of sensor fusion using the MFS tailings sensor and the tailings volume sensor it is shown how to estimate the tailings MOG material flow.

3.1 Virtual Combine

The virtual combine should resemble the actual combine sufficiently to conduct closed-loop control testing, i.e. provide realistic actuator inputs, material flows and sensor readings. The implementation will utilise the generated models for material flow and sensor readings presented in Section 2.

3.1.1   Architecture

The virtual combine is based on the overall material flow diagram shown in Figure 2.11. The block diagram of the virtual combine is shown in Figure 3.1, where the four modules represent plant models for material flow followed by sensor models for both the threshing and separation system as well as the cleaning system. Input vectors are denoted with $\mathbf{u}$, state vectors $\mathbf{x}$, output vectors $\mathbf{y}$ and disturbance vectors $\mathbf{\Delta}$, where subscript p represent threshing and separation system, and c represents cleaning system. The miscellaneous dynamic parameters and disturbances ($\mathbf{\Delta}$) are generally not shown in the model diagrams to maintain simplicity, however they do cover various offsets, gains, biological parameters and parameter changes for individual components.
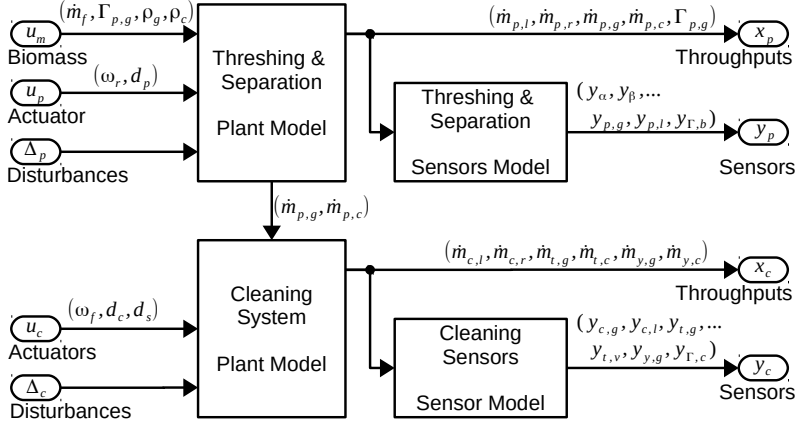

Figure 3.1: Virtual combine block diagram.

The plant model for the threshing and separation system is shown in Figure 3.2. The model is provided with a total throughput $\dot{m}_f$ and grain ratio $\Gamma_{p,g}$. The grain and MOG throughputs are computed using the model for separation loss $f_{p,l}(\mathbf{p_{p,l}}, \mathbf{\Theta_p})$ and MOG separation $f_{p,c}(\mathbf{p_{p,c}}, \mathbf{\Theta_p})$. The ratio of damaged grain is obtained using $f_{p,b}(\mathbf{p_{p,b}}, \mathbf{\Theta_p})$. The unobservable threshing grain loss ($\dot{m}_{p,t}$) is not modelled.

A sub-set of the material flows from the threshing and separation plant model in Figure 3.2 are used as inputs to the sensor models in Figure 3.3. The feederhouse sensor y_α and rotor pressure sensor y_β uses a *Gaussian distribution*, i.e. zero mean band-width limited white noise. The MFS distribution and loss sensor readings uses the *Poission* distribution shown in Figure 2.15b.
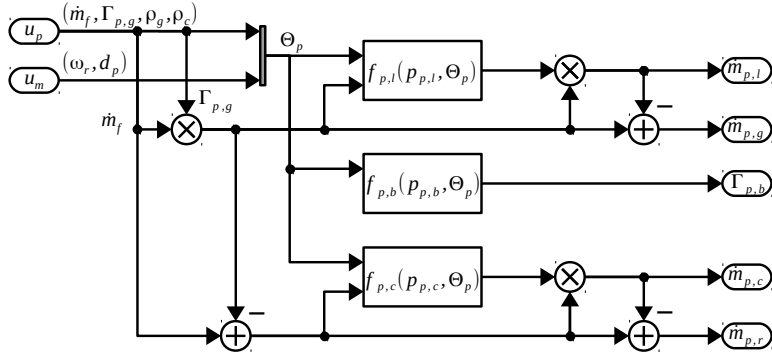
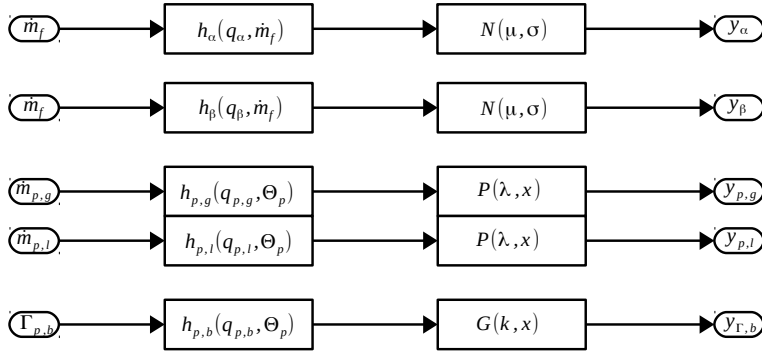Figure 3.2: Virtual threshing and separation system plant model.

Figure 3.3: Virtual threshing and separation system sensor model.

The cleaning system plant model is shown in Figure 3.4 consisting of the return and stratification pans, the cleaning shoe with fan and sieve as well as the tailings return system. The stratification and return pans receive its material flow of grain $\dot{m}_{p,g}$ and MOG $\dot{m}_{p,c}$ from the threshing and separation system and delivers it to the cleaning shoe characterised $\dot{m}_{c,g}$ and $\dot{m}_{c,c}$ in Figure 2.11. The delay from the return and stratification pans are modelled solely as time delays by dividing the rotor into n_z zones and modelling the delay of $\mathbf{n_m}[i]$ samples for zone i. The delays are found by the distance to travel $\mathbf{d_t}[i]$ from each zone to the cleaning shoe, the material conveying velocity $\mathbf{v_m}[i]$ and the sample rate T_s,

$$\mathbf{n_m}[i] = \frac{\mathbf{d_t}[i]\mathbf{v_m}[i]}{T_s}. \tag{3.1}$$

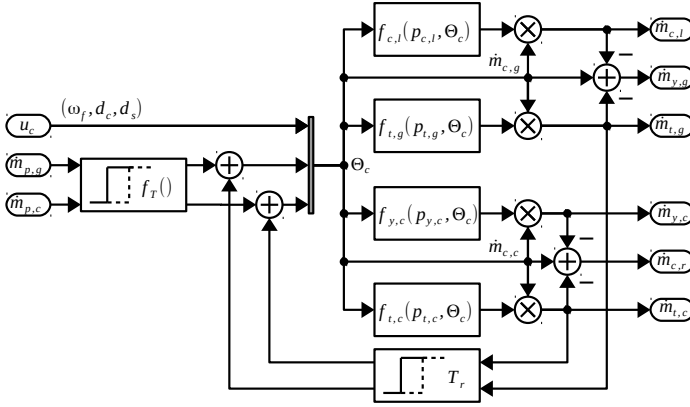The throughput delivered from the threshing and separation system to the cleaning

Figure 3.4: Virtual cleaning system plant model.

system is then given by

$$\dot{m}_c = f_T(\mathbf{\dot{m}_p}) = \sum_{i=1}^{n_z} \mathbf{\dot{m}_p}\left[i, k - \mathbf{n_m}[i]\right], \tag{3.2}$$

where the first index in $\mathbf{\dot{m}_p}$ refers zone i under the threshing and separation system and second index to the discrete time index k.

From the cleaning shoe material throughput of grain ($\dot{m}_{c,g}$) and MOG ($\dot{m}_{c,c}$), the grain loss ($\dot{m}_{c,l}$), tailings throughputs ($\dot{m}_{t,g}$ and $\dot{m}_{t,c}$) and cleanliness ($\dot{m}_{y,c}$) are computed according to Eq. (2.14-2.17) whereupon the clean grain throughput ($\dot{m}_{y,g}$) and MOG residue ($\dot{m}_{c,r}$) are found according to Eq. (2.8-2.9). The tailings system is modelled as a time delay T_r charactering the time from the material entering the cleaning shoe till it has been transported through tailings return system re-entering the cleaning shoe.

All modelled material flows in the cleaning system are observable except for the MOG throughput $\dot{m}_{c,c}$, see Figure 3.5. The MFS measurements ($y_{c,g}$) under the upper sieve is modelled in a similar fashion as MFS under the threshing and separation rotor. The MFS tailings sensor is modelled purely from the tailings grain throughput ($\dot{m}_{t,g}$) using a *Poisson* distribution, see Figure 2.15b. The tailings volume sensor is modelling from the tailings grain ($\dot{m}_{t,g}$) and MOG ($\dot{m}_{t,c}$) material flows shown in Figure 2.16a using a modified *Chi* distribution, see Figure 2.16b.

3.1.2 Implementation and Simulation

The virtual combine is built using data acquired from a large number of data sets obtained from both laboratory and field experiments. The model basically
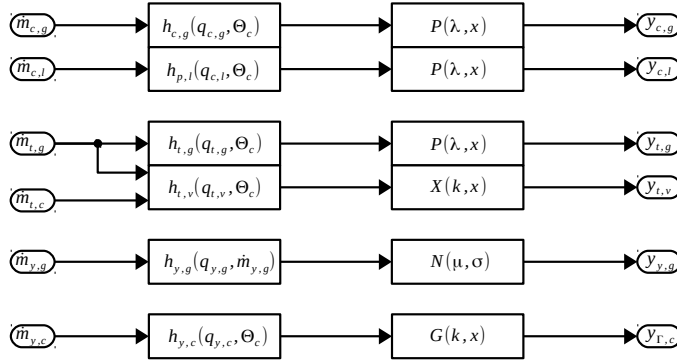
Figure 3.5: Virtual cleaning system sensor model.

comprises a skeleton structure that is parametrised. The overall steps in the model generation procedure are as follows

- Data acquisition of material samples and sensor data

- Obtain features from data-sets (Article A.1)

    Time delays

    Time constants

    Average sensor reading during steady-state

    Stochastic sensor parameters during steady-state

- Generate steady-state models (Section 2.4)

- Compile models for all sub-modules

- Compile virtual combine from sub-modules

3.2   Validation of Test Environments

All sub-processes in the combine harvester are affected by unobservable disturbances. Thus validation in absolute terms of given throughputs or sensor readings is not realistic, as the actual e.g. grain loss or tailing throughputs does vary significantly due to local crop conditions. The non-linearity of the steady-state trends is more consistent, thus the primary aim is to compare the trends from the material flows for a given change in throughput or actuator setting.

During field test data sets were acquired using design of experiments (DoE), exciting forwards speed (v), rotor speed (ω_f), concave clearance (d_p), fan speed (ω_f), upper (d_c) and lower (d_s) sieve spacings. Similar sequences were obtained in the continuous cleaning system laboratory and using the virtual combine for comparison. As the actual throughputs were not available for field DoE sequences, the evaluation is based on the raw sensor readings.

In Figure 3.6 three random fan speed actuator curves for the MFS tailings sensor are shown, obtained respectively from the virtual combine, laboratory and field. The data sets are fitted using the exponential model
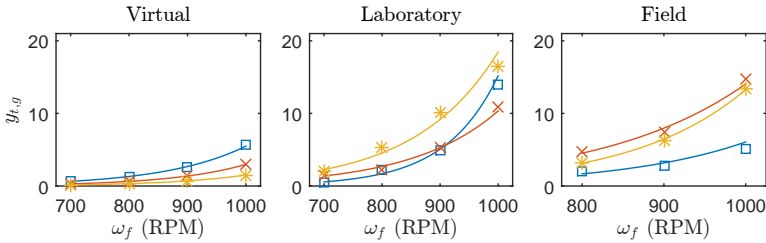

Figure 3.6: Steady-state actuator curve for tailings MFS ($y_{t,g}$) versus fan speed (ω_f).

$$y = a \exp(bx), \tag{3.3}$$

similar to the fitted actuator curves in Figure 2.4 on page 20 and Figure 2.6 on page 23, except the fan speed (ω_f) to grain loss reading ($\dot{m}_{c,l}$) which is not monotonic. Using the fitted b parameters the range of the non-linearity is mapped for the virtual, laboratory and field data sets.

In Figure 3.7 the trend analysis for corn is shown for the threshing and separation system with same plot division as in Figure 2.4, and in Figure 3.8 the cleaning system trend analysis for wheat is shown with same plot division as in Figure 2.6. Each plot contains a number of statistical box plots [31] of the obtained b parameters, where the virtual combine data is marked with V, laboratory test stands marked L and field test data marked F with a number for each field test data set. The vertical axis is normalised, however zero is marked with a grey line in all plots to clearly indicate if the trend is increasing or decreasing. Mappings from actuators to sensor readings that are not marked as controllable and observable in Table 2.7 on page 40 is intentionally left blank. The feederhouse sensor y_α response from total throughput $v \sim \dot{m}_f$ has comparable response from the virtual combine to the second field test data set, however the first field test shows large variations which
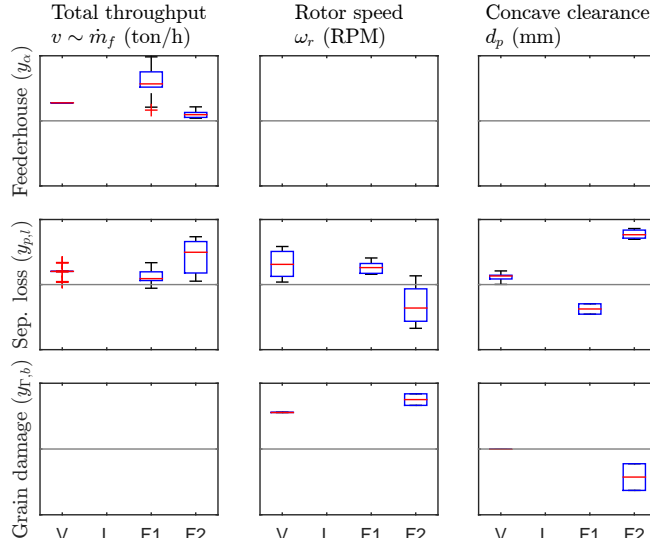
Figure 3.7: Threshing and separation process sensor trend analysis using the virtual, laboratory and field test data.

could originate from large variations the crop density. The separation loss reading $y_{p,l}$ is generally increasing with the total throughput $\dot{m}_f$ with some variations in the non-linearity of the field data. In general increasing the rotor speed ω_r causes a decrease in the separation grain loss reading $y_{p,l}$ and an increase in grain damage reading $y_{\Gamma,b}$, where the concave clearance d_p has the opposite effect on $y_{p,l}$ and $y_{\Gamma,b}$. The trends are shown in Figure 2.4 and are valid for wheat, barley and soy beans. However, for corn the trends are not well defined which is visualised for the two field test data sets.

In Figure 3.8 the MFS cleaning grain loss sensor $y_{c,l}$ does show a similar response from total throughput $v \sim \dot{m}_f$, fan speed ω_f and upper sieve opening d_c for the virtual, laboratory and field tests. The MFS tailings grain sensor $y_{t,g}$ response is also similar from fan speed ω_f, upper and lower sieve openings d_c and d_s. However the total throughput $\dot{m}_f$ has an approximately affine relationship for the virtual combine and the laboratory, where the first and second field test data sets respectively did not show a consistent trend and did show a larger non-linearity. The TVS reading $y_{t,v}$ also show a comparable response from total throughput $\dot{m}_f$, fan speed ω_f and upper sieve opening d_c. The reading depends on both the tailing grain $\dot{m}_{t,g}$ and MOG $\dot{m}_{t,c}$ throughputs which does increase the uncertainty. No field data DoE sequences are available as the sensor was not available early in the project.
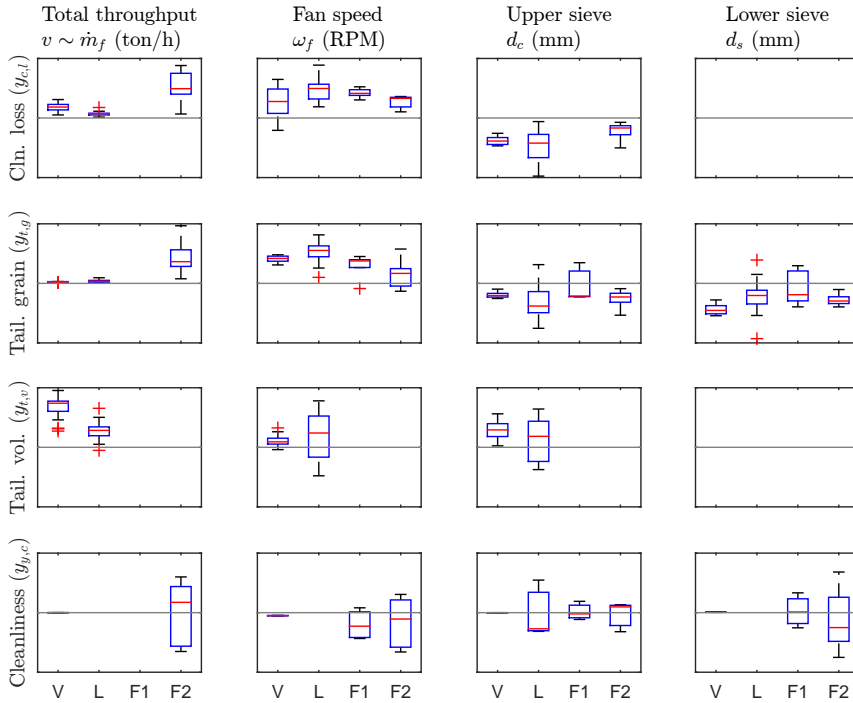
Figure 3.8: Cleaning process sensor trend analysis using virtual, laboratory and field test data.

The cleanliness reading $y_{\Gamma,c}$ is generally more scattered than the remaining sensor readings due to the short sample time for each data point, which does not allow a sufficient number frames to be captured to generate low variance average reading.

3.3 Throughput Estimation

The estimated throughputs originate from a variety of sensors comprising a number of challenges due to multiplicative uncertainties, low sample rate, time delays and indirect measurements. In order to reduce complexity a full state observer is undesirable, hence a number of primarily reduced order observers are designed. Thus model reduction is applied to the full state models generated in Section 2.4.

3.3.1 Feederhouse Total Throughput

In the feederhouse a lever with a roller on the elevator chain is measuring the height of the crop material using a potentiometer reading, see Figure 2.13. A total of 27 samples were collected to verify the relationship from total throughput $(\dot{m}_f)$ to the feederhouse sensor reading (y_α), see Figure 3.9. A coefficient of determination at $R^2 = 0.61$ was obtained using the affine model,

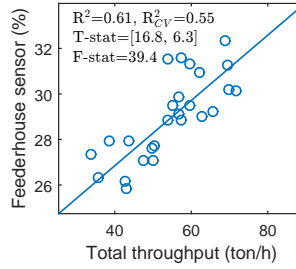$$y_\alpha \approx h_\alpha(\dot{m}_f, \mathbf{q}_\alpha) = q_{\alpha,1} + q_{\alpha,2}\dot{m}_f. \tag{3.4}$$

Figure 3.9: Steady-state relationship from total throughput $(\dot{m}_f)$ to feederhouse throughput sensor reading (y_α).

3.3.2 Impact Grain Throughput

The MFS sensors in the threshing and separation system as well as cleaning system each provide a vector containing sensor data from each individual sensor membrane from MFS sensor strips, respectively $\mathbf{y_{p,gl}} = (\mathbf{y_{p,g}}^T \quad \mathbf{y_{p,l}}^T)^T$ and $\mathbf{y_{c,gl}} = (\mathbf{y_{c,g}}^T \quad \mathbf{y_{c,l}}^T)^T$. The grain loss estimates $\dot{m}_{p,l}$ and $\dot{m}_{c,l}$ are computed using an affine model

$$\hat{\dot{m}}_l = \sum_{i=1}^{n} = (\mathbf{y_{gl}}[i]) - \mathbf{q_{gl1}}[i])\mathbf{q_{gl2}}[i] \tag{3.5}$$

for the offset and scaling parameters $\mathbf{q_{gl1}}$ and $\mathbf{q_{gl2}}$ respectively.

3.3.3 Grain Quality

The grain quality sensor captures information of approximately 100 grain kernels per frame in wheat. The actual grain damage is often significantly below 1% as well as a considerable computational effort is required to process each captured

frame resulting in a low update rate. Due to the measurement noise characteristics for the sensor signal ($y_{\Gamma,b}$) shown in Figure 2.17b, a large number of samples are required to reduce the standard error of the averaged reading, which significantly increases the settling time compared to the MFS separation grain loss estimate ($\hat{m}_{p,l}$). Thus the GQS is the limiting factor in order to obtain fast response to grain loss changes under varying field conditions.

The primary object is to reduce the settling time for the grain damage estimate $\hat{\Gamma}_{p,b}$ while maintaining an acceptable standard error of the estimate using a non-linear observer. A Luenberger [61, 43] observer structure was chosen due to its simplicity combined with the ability to suppress measurement noise, see Figure 3.10. In order to ensure robustness and facilitate manual tuning a constant feedback
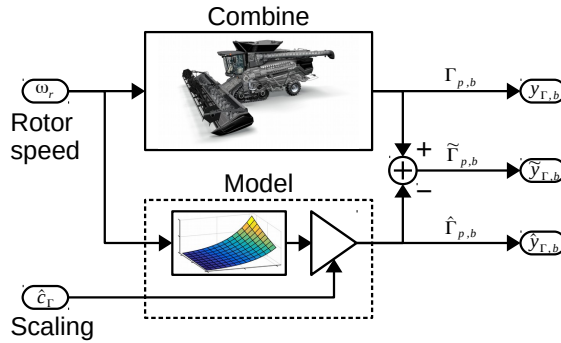

Figure 3.10: Grain damage observer.

gain is chosen.

The state-space vector $\mathbf{x} = \begin{pmatrix} c_\Gamma & \omega_p \end{pmatrix}^T$ is given by the model scaling parameter c_Γ and ω_p, the filtered state of the input vector $u = \omega_r$. The state ω_p is filtered with the time constant τ_p characterising the threshing and separation system dynamics. The continuous time state-space model and output function are respectively given by

$$\dot{\mathbf{x}} = f(\mathbf{x}) = \begin{bmatrix} \dot{c}_\Gamma \\ \dot{\omega}_p \end{bmatrix} = \begin{bmatrix} \sigma_c^2 \\ a_p\omega_p + b_p\omega_r \end{bmatrix} \quad \text{and} \quad \Gamma_{p,g} = y = h(\mathbf{x}) = c_\Gamma \exp(p_\Gamma \omega_p)$$

for the zero-mean white noise variance σ_c^2, threshing and separation system dynamics a_p and b_p as well as the grain damage loss model parameter p_Γ. As the capturing functionality relies on material flow in the clean grain elevator, synchronisation of the paddle throw and a considerable processing time the sample time (T_{GQS}) of the GQS is not constant. For each GQS measurement update the estimate is updated

using

$$\hat{\mathbf{x}}(k+1) = F\hat{\mathbf{x}}(k) + Gu(k) + K(y(k) - \hat{y}(k)), \qquad (3.6)$$

else the estimate is predicted according to

$$\hat{\mathbf{x}}(k+1) = F\hat{\mathbf{x}}(k) + Gu(k), \qquad (3.7)$$

where F and G are the discrete matrices for the state-space model.

The observer is preliminary validated using the virtual combine, see Figure 3.11. The first plot shows the filtered average sensor reading ($\bar{\Gamma}_{p,b}$), the observer estimate ($\hat{\Gamma}_{p,b}$) and the true ($\Gamma_{p,b}$) percentage of broken kernels, second plot the separation loss ($\dot{m}_{p,l}$) and yield sensor reading ($y_{y,g}$), and third plot the rotor speed ω_r.
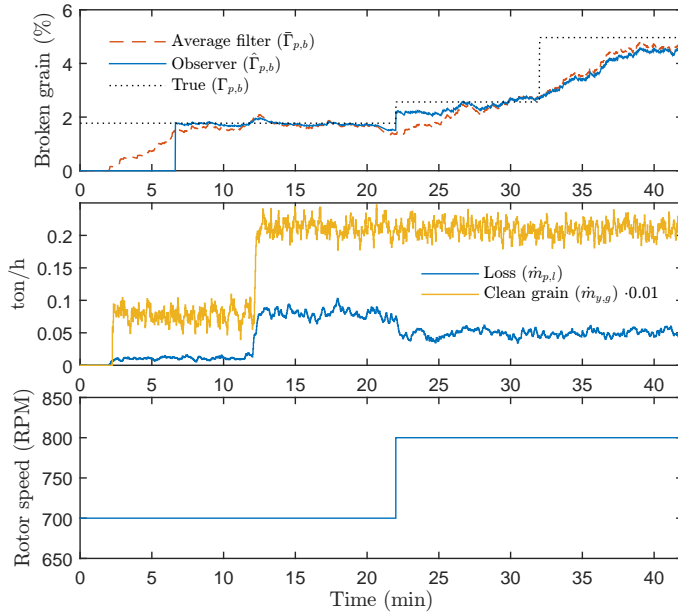
Figure 3.11: Simulated grain damage observer response.

The combine enters crop after 2 minutes and after 7 minutes the grain damage estimate is fully initialised. After 12 minutes the throughput increases causing a corresponding increase in the separation loss, where the observer estimate follows the average filter. The rotor speed is increased after 22 minutes which reduces separation loss and increases grain damage. Notice the rapid response from the model based observer compared to the average filter. After 32 minutes a change (disturbance) in the field conditions increases the grain damage significantly. Generally

the model based observer shows a similar response as the average filter, however the response to rotor speed changes is significantly faster allowing faster control loop.

3.3.4 Tailings Throughput

The aim is to estimate the tailings grain ratio with a reasonable accuracy in order to facilitate closed-loop control of the fan speed. The individual throughput estimates of grain ($\dot{m}_{t,g}$) and MOG ($\dot{m}_{t,c}$) are given in the state-space vector $\mathbf{x} = (\dot{m}_{t,g} \quad \dot{m}_{t,c})^T$. The output vector $\mathbf{y} = (y_{t,g} \quad y_{t,v})^T$ consists of the measurements of tailings grain $y_{t,g}$ and tailings volume $y_{t,v}$ for the output function

$$\hat{\mathbf{y}} = h(\hat{\mathbf{x}}) = \begin{pmatrix} q_{t,g1} + q_{t,g2}\dot{m}_{t,g} \\ h_{t,v}(\mathbf{q}_{t,v}, \dot{m}_{c,g}, \dot{m}_{c,c}) \end{pmatrix}, \tag{3.8}$$

where $h_{t,v}()$ is given in Eq. (2.23). The throughput estimate update equation is given by,

$$\hat{\mathbf{x}}(k) = K(\mathbf{y}(k) - \hat{\mathbf{y}}(k)) = K(\mathbf{y}(k) - h(\hat{\mathbf{x}}(k))), \tag{3.9}$$

for the discrete time index k.

In Figure 3.12 the validation results are shown for the tailings grain composition estimate $\hat{\Gamma}_t$, where the actual tailings grain composition Γ_t for cross validation is sampled from the laboratory cleaning system. The model parameters were obtained from the data sets shown in Figure 2.15a and Figure 2.16a. A coefficient of determination at $R^2 = 0.79$ is obtained which is acceptable.
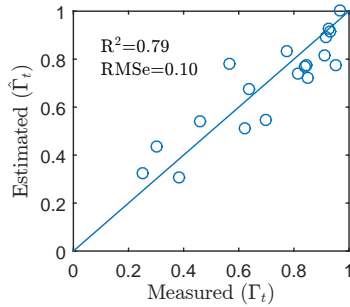

Figure 3.12: Estimated tailings throughput.

3.3.5 Identification of the Fluidised Phase

In Section 2.3 it was shown that the packed, fluidised and airborne phases of the cleaning system to some extend could be decomposed to a combination of the tailings grain and MOG throughputs representing the airborne and packed phases respectively. It is desirable to obtain a model characterising the fluidised phase from the tailings grain composition, which is obtained from a set of fan speed curves.

In order to obtain the fan speed $\omega_f^\star$ characterising the minima on the loss curve, a number of fan speed curves with material samples are acquired with various excitation of the parameters in the input vector $\mathbf{\Theta_c}$. The material samples are acquired without tailings return and with a spacing of 50 or 100 RPM, however a lower resolution is desirable for the identification.

The general procedure to generate the set-point model has four steps. First fan speed curves with material samples are acquired whereupon reduced order material flow models are generated for each curve as shown in Section 2.4 and in Figure 2.8 on page 26. Second step is to apply closed-loop simulation for each fan speed setting ($\omega_f \in \mathbb{N}[\omega_{f,min} : \omega_{f,max}]$) using the Algorithm 1 from Article A.5 in order to obtain the closed-loop performance $f_{CLT}(\dot{m}_{p,g}, \dot{m}_{p,c}, \mathbf{\Theta_c}, \omega_f)$. Third step is to obtain $\omega_f^\star$ by solving Eq. (3.10) for each fan speed curve, where the corresponding tailings throughputs $\dot{m}_{t,g}^\star$ and $\dot{m}_{t,c}^\star$ are extracted.

$$\arg\min_{\omega_f} \; f_{CLT}(\dot{m}_{p,g}, \dot{m}_{p,c}, \mathbf{\Theta_c}, \omega_f) \quad \forall \quad \omega_f \in \mathbb{N}[\omega_{f,min} : \omega_{f,max}] \quad (3.10)$$

The fourth step is fitting of the obtained tailing throughput sets $\dot{\mathbf{m}}_{\mathbf{t,g}}^\star$ and $\dot{\mathbf{m}}_{\mathbf{t,c}}^\star$ characterising the fluidised phase from the model vector $\mathbf{\Theta}_c$,

$$\Gamma_t^\star = \frac{\dot{m}_{t,g}^\star}{\dot{m}_{t,g}^\star + \dot{m}_{t,c}^\star} \approx \hat{\Gamma}_t^\star = f_t^\star(\mathbf{p_t}^\star, \mathbf{\Theta_c}). \quad (3.11)$$

The measured $\Gamma_t^\star$ and predicted $\hat{\Gamma}_t^\star$ values of the tailings grain composition are show in Figure 3.13 with a coefficient of determination at $R^2 = 0.88$. The high R^2 value show that it is realistic to predict the desirable fan speed setting without knowledge of the actual cleaning MOG load $\dot{m}_{c,c}$, as this information instead is mapped from the input model vector $\mathbf{\Theta_c}$ and the tailings throughput.
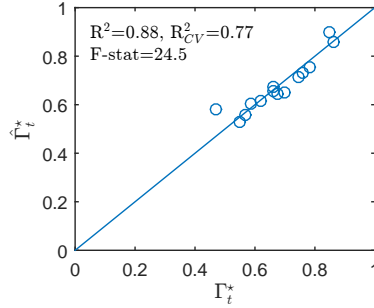
Figure 3.13: Estimated tailings grain composition $\Gamma_t^\star$ for fan speed controller.

3.4 Throughput Prediction

All sub-modules of the combine harvester comprise material transport, thus the momentary reading of the process sensors located throughout the machine are all affected by time delays. Hence the measured sensor signals are not directly comparable at a given time instance, thus an instrumentation system or closed-loop control system is required to postpone signals for comparison or average over longer time periods. This is in particular of interest for the grain loss observations which are normalised with the yield sensor reading ($y_{y,g}$) with a delay of $T_y \simeq$ 8.5 s, causing large deviations in the momentary normalised grain loss estimate at changing throughput.

The aim is to predict grain throughput changes using the forward speed (v) and a throughput sensor in the feederhouse (y_α), with the delay T_f from a change in forward speed to the feederhouse sensor. By utilising a grain flow model and sensor fusion an estimate of the current grain throughput in the threshing and separation system ($\dot{m}_{p,g}$) can be obtained, hence the effect from the lag in the momentary yield sensor reading due to material transport delays can be reduced.

3.4.1 Simplified Dynamic Throughput Model

In order to estimate the grain throughput in the threshing and separation system it is not required to model all the material flows indicated in Figure 2.11. A discrete reduced order model describing the dominating dynamics of the grain flow is given in Figure 3.14.
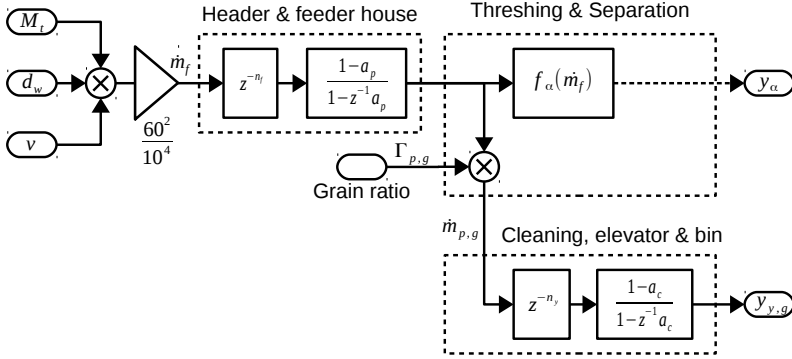
Figure 3.14: Discrete time simplified grain flow model block diagram.

The material grain flow is reduced to the following steady-state constraints

$$\dot{m}_{p,g} \simeq \dot{m}_f \Gamma_{p,g} \tag{3.12}$$

$$\dot{m}_{y,g} \simeq \dot{m}_{p,g} \tag{3.13}$$

$$w_h = v d_w \tag{3.14}$$

$$\dot{m}_f = M_t \frac{60^2}{10^4} w_h, \tag{3.15}$$

for the threshing and separation system grain mass flow ($\dot{m}_{p,g}$), clean grain throughput ($\dot{m}_{y,g}$), header areal flow (w_h) for given the header width (d_w), and the total throughput ($\dot{m}_f$). The total input mass flow ($\dot{m}_f$) equals the local crop density (M_t) times the covered areal flow of the header (w_h). In practice the full header width is not always utilised thus it would be beneficial to use a cutting with sensor [91], however no such a sensor was available thus full cutting width will be assumed at all times.

3.4.2 Observer Design

The aim is to estimate the grain throughput state in the threshing and separation system ($\dot{m}_{p,g}$) using the reduced order model shown in Figure 3.14. The model structure leverages the time delays T_f and T_y using the local field crop density state M_t and input from the forward speed v, where M_t is corrected using the feederhouse sensor reading y_α and the estimated grain ratio $\hat{\Gamma}_{p,g}$ is corrected using the yield sensor reading $y_{y,g}$.

The state vector of the discrete time state-space system is given by

$$\mathbf{x} = \begin{pmatrix} M_t & w_h & \Gamma_{p,g} & \dot{m}_{y,g-n_y} & \ldots & \dot{m}_{y,g} \end{pmatrix}^T, \tag{3.16}$$

where the $\dot{m}_{y,g}$ states specifies the delay of n_y samples. The input and output vectors for the state-space model are then given by

$$\mathbf{u} = v_{-n_f} \quad \text{and} \quad \mathbf{y} = \begin{pmatrix} y_\alpha & y_{y,g} & \dot{m}_{p,g} \end{pmatrix}^T, \tag{3.17}$$

where the input v_{-n_f} characterises the forward speed with a reading delay of n_f samples. The system transition and input matrices are given by

$$F(k) = \begin{bmatrix} \begin{bmatrix} F_D(k) & 0_{[n_x,n_y-1]} \end{bmatrix} \\ \begin{bmatrix} 0_{[n_y,n_x-1]} & I_{[n_y]} \end{bmatrix} \end{bmatrix} \quad \text{and} \quad G = \begin{bmatrix} 0 \\ d_w(1-a_p) \\ 0_{[n_y+2,1]} \end{bmatrix}. \tag{3.18}$$

The dynamic part of the system transition matrix (F) is

$$F_D(k) = \begin{bmatrix} 1 & 0 & 0 & 0 \\ 0 & a_p & 0 & 0 \\ 0 & 0 & 1 & 0 \\ 0 & 0 & \bar{M}_t \bar{w}_h \dfrac{60^2}{10^4}(1-a_c) & a_c \end{bmatrix}, \tag{3.19}$$

at the linearisation points $\bar{M}_t$ and $\bar{\omega}_h$, where n_x is the number of rows/columns of square matrix F_D, a_p and a_c are the first order time constants for threshing and separation system and cleaning system respectively.

The output matrix

$$H(k) = \begin{bmatrix} p_{\alpha,2}\bar{w}_h \dfrac{60^2}{10^4} & 0 & 0 & 0 & \ldots & 0 \\ 0 & 0 & 0 & 0 & \ldots & 1 \\ 0 & 0 & \bar{M}_t \bar{w}_h \dfrac{60^2}{10^4} & 0 & \ldots & 0 \end{bmatrix}, \tag{3.20}$$

provides estimates of the two sensor observations of y_α and $y_{y,g}$ as well as the unobservable material flow $\dot{m}_{p,g}$.

The prediction and estimation output update equations are given by

$$\hat{\mathbf{x}}(k+1) = F(k)\hat{\mathbf{x}}(k) + G\mathbf{u}(k) \tag{3.21}$$

$$\hat{\mathbf{y}}(k) = H(k)\hat{\mathbf{x}}(k), \tag{3.22}$$

and the measurement update by

$$\hat{\mathbf{x}}(k) = K(\mathbf{y}(k) - \hat{\mathbf{y}}(k)). \tag{3.23}$$

The observer gain K is tuned based on data acquired from laboratory and field experiments.

In order to avoid division by zero in Eq. (3.12) the measurement update Eq. (3.23) is be disabled by the flag H_{cor} when then combine is not loaded, as well as the one-step-ahead prediction without the input matrix (G) is enabled when the machine is detected empty by H_{est},

$$\hat{\mathbf{x}}(k+1) = F(k)\hat{\mathbf{x}}(k). \tag{3.24}$$

The detection of H_{cor} and H_{est} will be treated in Section 3.5.

The observer performance during field test in barley is shown in Figure 3.15. The first plots shows forward speed (v), second plot the feederhouse sensor (y_α
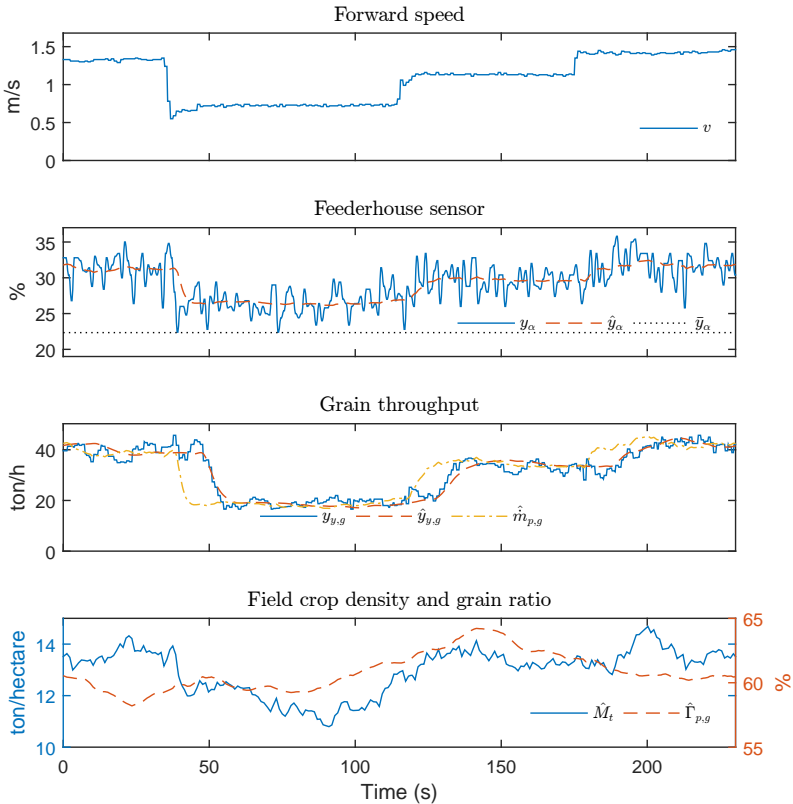

Figure 3.15: Field data with forward speed stairs and grain throughput estimation.

and $\hat{y}_\alpha$), third plot the grain throughputs ($y_{y,g}$, $\hat{y}_{y,g}$ and $\hat{m}_{p,g}$), and fourth plot the estimated local crop density $\hat{M}_t$ and grain ratio $\hat{\Gamma}_{p,g}$. The combine travels at four

different forward speeds (v) during the test sequence, which clearly corresponds
to the changes in the yield sensor reading $y_{y,g}$ with the combined delays from T_f
and T_y. The observer estimates the grain mass flow $\hat{m}_{p,g}$ reasonably well in the
threshing and separation system observed T_y seconds before the instantaneous yield
sensor reading $y_{y,g}$. Though the feederhouse sensor reading y_α has a considerable
noise level the representation of the grain mass flow from the step occurring after
176 s originates from y_α and not v in the estimated grain mass flow $\hat{m}_{p,g}$, providing
a reasonably good representation of the yield sensor reading $y_{y,g}$. The estimates $\hat{M}_t$
and $\hat{\Gamma}_{p,g}$ show no larger variations during the test sequence.

3.5   Change Detection

A combine harvester operates in steady-state the majority of the time, however
in periods when entering or leaving crop rows the threshing, separation and clean-
ing systems are only partially loaded which can cause undesirable behaviour from
the observers. Additionally combine harvesters are prone to material build up or
blockages causing sensor errors. Using a threshold value offers a simple method the
determine change detection, however it is prone to a large number of false detec-
tions (P_F) as well as missing detections (P_M). The cumulative sum control chart
(CUSUM) offers a simple method for change detection based on a log-likelihood
measure to monitor change detection between two states characterised by the aver-
age values μ_0 and μ_1, [8].

The methods assume a normal distributed signal

$$\mathcal{N}(\mu, \sigma) = \frac{1}{\sigma\sqrt{2\pi}} exp\left(-\frac{(x-\mu)^2}{2\sigma^2}\right), \tag{3.25}$$

requiring predefined knowledge of the standard deviations of the signal σ as well
as the two average values μ_0 and μ_1.

For each measurement the sequential CUSUM state $g(k)$ is updated using

$$g(k) = g[k-1] + \frac{\mu_0 - \mu_1}{\sigma^2}\left(r(k) - \frac{\mu_1 + \mu_0}{2}\right), \tag{3.26}$$

for the signal $r(k)$. When the CUSUM state reaches the threshold h_0 or h_1 the
change detection is generated, respectively H^- or H^+. The threshold can be de-
termined based on the design parameters P_F and P_M, which however affects the
mean time for detection τ. For further information please refer to Article A.2 or
[8].

The aim is to swiftly detect a change from an un-loaded to a loaded state and vice versa. Due to the large time delays the conditions should be tested on the first and last sensor observing crop flow, i.e. y_α and $y_{y,g}$ respectively. Thus H_{cor} will enable the measurement update in Eq. (3.23) when load is detected on the feederhouse sensor (y_α), and H_{est} will enable Eq. (3.21) where $\neg H_{est}$ enables Eq. (3.24).

The CUSUM will use a total of four residual signals, two observing load changes from the feederhouse sensor $r_{Y1} = y_\alpha - \bar{y}_\alpha$ and yield sensor $r_{Y2} = y_{y,g} - \bar{y}_{y,g}$ as well as the observer innovation signals $r_{E1} = \tilde{y}_\alpha = y_\alpha - \hat{y}_\alpha$ and $r_{E2} = \tilde{y}_{y,g} = y_{y,g} - \hat{y}_{y,g}$.

In Figure 3.16 the histogram ($\mathcal{H}$) is plotted using the fitted normal distribution in Eq. (3.25) for the residual signals r_{Y1}, r_{Y2}, r_{E1} and r_{E2}. The data is compiled from the steady-state periods in 27 data sets, compensated by subtracting the average from each period. The four signal histograms in Figure 3.16 are reasonably well represented by the normal distribution.
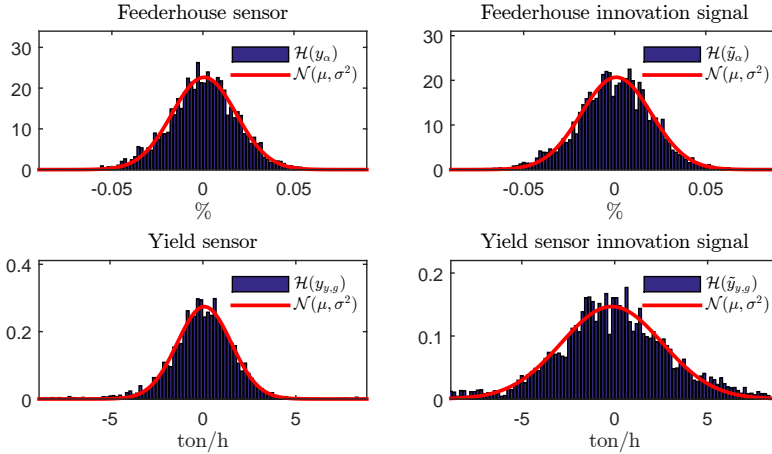
Figure 3.16: Histogram and normal distribution for CUSUM residuals signals.

For the residuals r_{Y1} and r_{Y2} the relative condition flags (H_{Y1}^+ and H_{Y2}^+) are set from g_{Y1}^+ and g_{Y2}^+. The innovation signal residuals r_{E1} and r_{E2} both have a positive and negative detection, hence H_{E1}^+, H_{E1}^-, H_{E2}^+ and H_{E2}^- are set from g_{E1}^+, g_{E1}^-, g_{E2}^+ and g_{E2}^- respectively. The observer correction flags are set from the

boolean equations

$$H_{cor} = H_{Y1}^+ \wedge H_{Y2}^+ \wedge \neg H_{ino} \tag{3.27}$$

$$H_{ino} = H_{E1}^+ \vee H_{E1}^- \vee H_{E2}^+ \vee H_{E2}^- \tag{3.28}$$

$$H_{est} = \neg H_{E1}^- \wedge H_{Y1}^+ \wedge H_{Y2}^+, \tag{3.29}$$

where H_{ino} is the condition flag for change detection in the innovation signals.

In Figure 3.17 a sequence of field data is shown, where first plots shows the feederhouse sensor (y_α, $\hat{y}_\alpha$ and $\bar{y}_\alpha$), second plots grain throughput ($y_{y,g}$, $\hat{y}_{y,g}$ and $\hat{\dot{m}}_{p,g}$), and third plots shows a normalised CUSUM condition detection. The CUSUM detectors are denoted g^+ and g^- for the positive and negative change detection of the normalised residuals between h_0 and h_1. The CUSUM value $g(k)$ is marked with $\square$ or $\bigcirc$ when reaching the upper h_1 or lower h_0 thresholds respectively.

After 42 s the yield sensor reading of $y_{y,g}$ rapidly increases from 40 ton/h to 62 ton/h. Considering the yield sensor reading only, it is not possible to clarify whether the increase is due to increasing grain throughput or a temporary error to the reading. When comparing with the estimated feederhouse sensor reading y_α the spike is uncorrelated. The two signals y_α and $y_{y,g}$ are not directly comparable due to the time delays and scaling. However when using the innovation signal r_{E2} the change is detected almost instantly, disabling the observer measurement update (H_{est}), hence the estimated yield sensor reading $\hat{y}_{y,g}$ remains unaffected. The feederhouse sensor reading starts decreasing after 176 s when leaving the crop row. Here g_{Y1}^+ and g_{E1}^- both detects the change to the un-loaded condition, hence disabling H_{cor}. Again the model based change detection g_{E1}^- provides a fast detection a few seconds before g_{Y1}^+ based on the static reference. The observer measurement update flag H_{cor} is enabled again after 215 s, when the load condition is detected on both H_{Y1}^+ and H_{Y2}^+.

3.6   Conclusion

The design and implementation of the virtual combine was outline using the material flow models from Chapter 2.

A plurality of state estimators were presented ranging from affine regression models, Luenberger grain damage observer, the non-linear constant gain tailings MOG throughput estimate as well as the grain throughput observer.
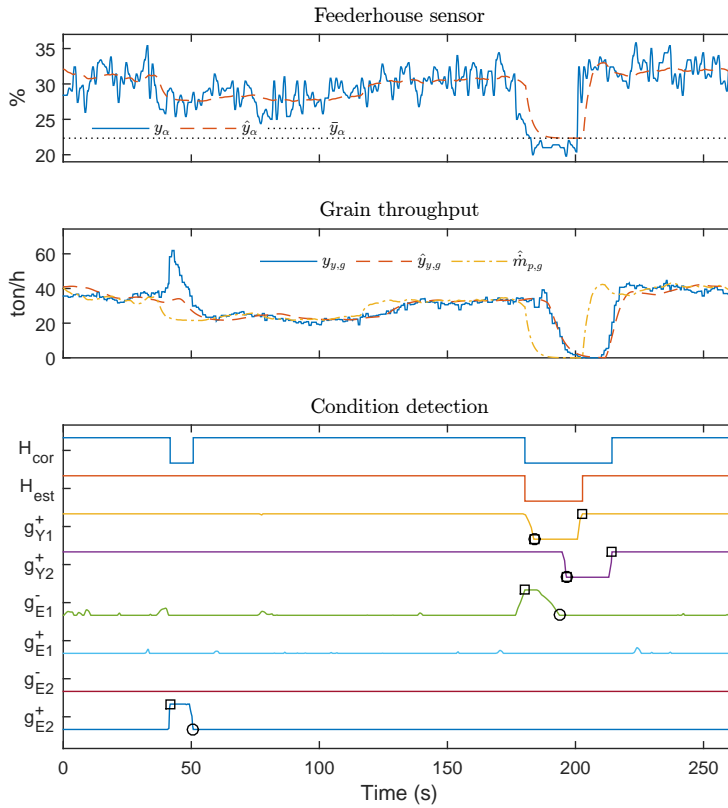
Figure 3.17: Field data with CUSUM sensor error detection and fast observer load detection.

It was shown that the fluidised phase could be identified using the tailings grain composition which facilitates closed-loop fan speed.

The design of change detection to fast detection of material load and sensor errors readings were presented, and showed swiftly load detection as well as detection and compensation for a temporary yield sensor error.

Control

This chapter describes the proposed overall control architecture for closed-loop control of the threshing, separation and cleaning systems. The design of the closed-loop controllers for rotor and fan speed adjustment are outlined including results obtained from simulation, laboratory and field tests. The design and results for the rotor and fan speed controllers were shown in Article A.3 and Article A.6 respectively.

This chapter outlines the motivation for the proposed hierarchical control architecture using distributed control schemes for the individual actuators.

The model-based grain damage observer is used to reduce the response time for separation grain loss variations in the rotor speed controller. The estimated tailing throughput components are used in the closed-loop fan speed controller to maintain the fluidised phase of the cleaning system. Design and implementation of the sieve controllers are not addressed.

4.1 Controller Architecture

The overall aim for the control system is to increase the profitability of the combine harvester, i.e. operating at a high throughput with acceptable performance. The performance is characterised by various parameters as shown in Figure 1.3 on page 5, however the primary performance parameters are grain losses, grain damage and cleanliness which directly affects the value of the clean grain product. No commercial sensor technologies are available for direct measurement of un-threshed heads or straw quality, hence the closed-loop control system cannot optimise performance based on these parameters. The system interdependency analysis in Chapter 2 revealed that the separation loss and grain damage primarily depended

on the rotor speed as well as the fan speed and sieve actuators each had a dominating effect on two of the observable throughputs in the cleaning system.

The overall optimisation problem can be formulated as one common cost function for all observable process parameters,

$$f_w = u_{p,l} \frac{\dot{m}_{p,l}}{\dot{m}_{p,l} + \dot{m}_{y,g}} + u_{\Gamma,b}\Gamma_{p,b} + u_{c,l} \frac{\dot{m}_{c,l}}{\dot{m}_{c,l} + \dot{m}_{y,g}} + u_{\Gamma,c}\Gamma_{y,c}, \qquad (4.1)$$

where four main criteria for performance each have an associated weight assigned for separation grain loss ($u_{p,l}$), grain damage ($u_{\Gamma,b}$), cleaning grain loss ($u_{c,l}$) and cleanliness ($u_{\Gamma,c}$). The complexity associated with the overall cost function of each term alone is substantial. Additionally the architecture should consider the dissimilarity in the available update rates from sensors and observers as well as the constraint to reduce sieve actuator wear, thus it is desirable to run the control system using different actuator update rates. In order to simplify the controller complexity a hierarchical architecture is proposed with distributed control schemes for each actuator, where the individual control-loops can be designed using standard methodologies preferably for single-input-single-output (SISO) systems. Note that no feedback exists from the cleaning system to the threshing and separation system, hence the these can be considered independent series connected systems. The chosen architecture is expected to reduce the implementation time as well as the required testing period. The overall hierarchical control architecture is shown in Figure 4.1. The hierarchy is divided into three layers where the top layer is the constant throughput controller maintaining a constant crop throughput at varying crop densities by adjusting the forward speed (v), the middle layer contains the closed-loop rotor speed and fan speed controllers, and the lower layer involve concave clearance and sieve spacings.

The constant throughput controller is a state-of-the-art controller adjusting the forward speed (v) in order to maintain a constant throughput using the feederhouse throughput sensor (y_α), which is known to increase the capacity of the combine [30, 20]. The constant throughput controller is not a part of the Ph.D. project. The rotor speed and fan speed controllers are designed using classic SISO closed-loop control methods. The rotor speed is actuated using a belt variator gear and the fan speed using a hydraulic motor allowing a high update rate, i.e. every 1 to 30 seconds. The lower layer is the control of concave clearance and sieve spacings, where the actuators will be updated at a lower rate than the rotor and fan speed controllers. Especially the sieve actuators does have a limited number of actuations, hence a high update rate from the controllers will wear out the actuators, as well
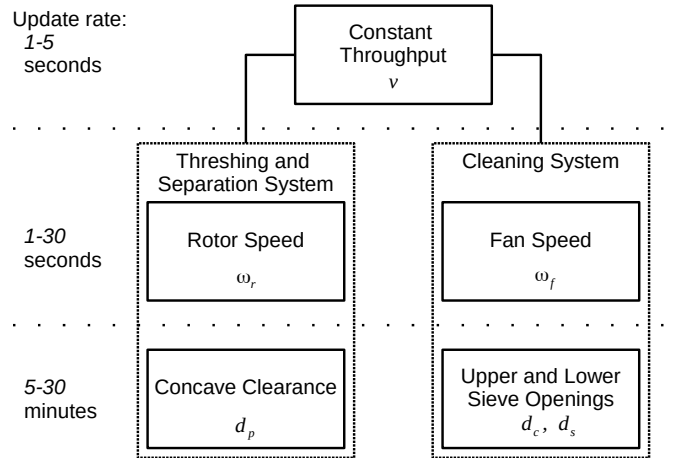
Figure 4.1: Control architecture.

as an actuator change can take several seconds as the controller deliberately under-shoots to reduce the effect from actuator backlash. The sieve actuators can be set in a range of integer values from 4 mm to 25 mm using small grain sieves, however the actual actuation range in a given crop is often less than 10 mm, thus the utilisation of classic closed-loop control design is not desirable due to the large actuator discrimination noise. The sieve control system design should utilise a model based optimisation method to estimate the best actuator setting. The concave clearance will not be adjusted automatically as vital information regarding unthreshed heads (threshing loss) is not observable.

4.1.1 User Interface

The user interface in Figure 4.2 allows the operator to prioritise the performance parameters as well as throughput versus performance. A triangular slider (bottom right) allows the operator to change priorities on grain losses, grain damage and cleanliness for the controllers. A second slider (top right) is used to select the priority of the performance parameters from the triangle versus the total throughput of the combine. The operator weights for separation loss $u_{p,l}$, cleaning loss $u_{c,l}$, grain damage $u_{\Gamma,b}$ and cleanliness $u_{\Gamma,c}$ are calculated from the position of the triangular slider and provided as input parameters to the closed-loop controllers.
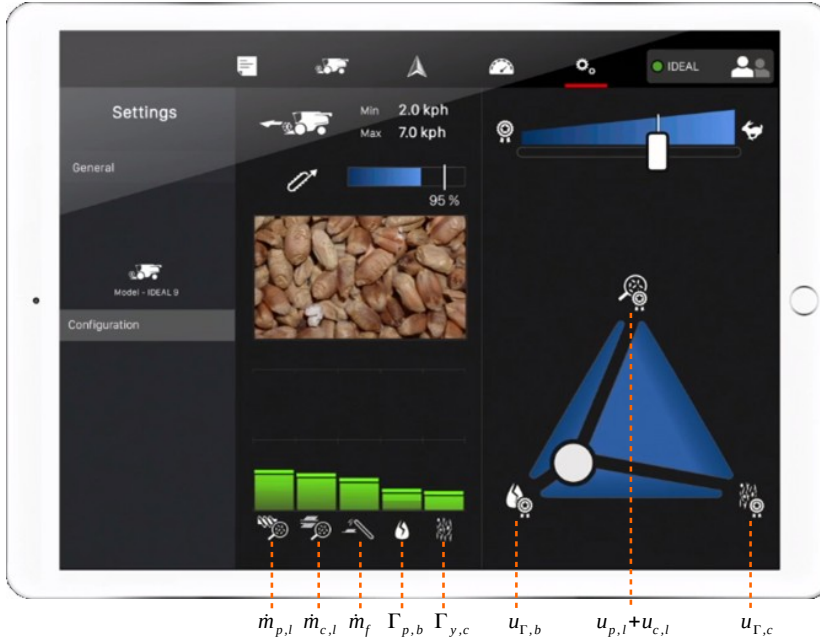
$$\dot{m}_{p,l} \quad \dot{m}_{c,l} \quad \dot{m}_f \quad \Gamma_{p,b} \quad \Gamma_{y,c} \qquad u_{\Gamma,b} \qquad\qquad u_{p,l}{+}u_{c,l} \qquad\qquad u_{\Gamma,c}$$

Figure 4.2: Operator user interface.

4.2   Rotor Speed

The rotor speed control uses the estimated separation loss $\hat{\dot{m}}_{p,l}$ and grain dam-age $\hat{\Gamma}_{p,b}$ obtained from the MFS and GQS respectively in the rotor speed control design. The controller is validated using the virtual combine as well as during field test experiments.

4.2.1   Controller Design

The aim of the controller is to adjust the performance based on the distributed convex cost function for the rotor speed,

$$f_{w,r}(\omega_r) = u_{\Gamma,b}f_{\Gamma,b}(\omega_r) + u_{p,l}f_{p,l}(\omega_r), \tag{4.2}$$

where $f_{\Gamma,b}(\omega_r)$ and $f_{p,l}(\omega_r)$ represents the actual ratio of grain damage and sepa-ration loss in percent. The trends for grain damage $\Gamma_{p,b}$ and separation loss $\dot{m}_{p,l}$ from collected material samples are shown in Figure 2.4 on page 20. As noted in Section 3.2 the sign of the impact from rotor speed (ω_r) to separation loss ($\dot{m}_{p,l}$)

does vary in corn, thus a modified version of the controller is required to facilitate closed-loop control in corn.

The controller is implemented as a SISO controller with a balanced feedback from grain damage and separation loss, see Figure 4.3. The grain damage and separation loss signals are normalised using the operator priority weights $u_{\Gamma,b}$ and $u_{p,l}$ respectively. The grain damage observer in Section 3.3.3 is used in the control loop in order to reduce the response time to variations in grain loss.
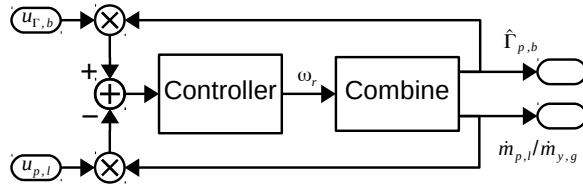

Figure 4.3: Control scheme for closed-loop rotor speed controller.

4.2.2 Results

The rotor speed controller is tested using the virtual combine presented in Section 3.1 to show transparency to the actual states which are not observable during field test experiments. The sequence shows excitation of total throughput ($\dot{m}_f$), operator weights ($u_{p,l}$ and $u_{\Gamma,b}$) and grain damage $\Gamma_{p,b}$. In Figure 4.4 the first plot shows the true percentage of broken kernels $\Gamma_{p,g}$, second plot the estimated separation loss $\hat{\dot{m}}_{p,l}$ and clean grain throughput $\dot{m}_{y,g}$, and third plot the rotor speed ω_r. Two simulations with identical excitation parameters are presented with the rotor speed controller enabled (blue sold line) and with the controller disabled using the static default rotor speed setting from the operators manual (dashed green line).

After 2 minutes the combine enters the crop row where all estimates are enabled. The total throughput is increase after 12 minutes causing an increase in the separation grain loss according to the exponential increase shown in Figure 2.4, thus the rotor speed controller increases the rotor speed in order to reduce grain loss. The user inputs ($u_{p,l}$ and $u_{\Gamma,b}$) in Figure 4.2 are changed after 22 minutes to increase focus on grain damage whereupon the rotor speed decreases. Local field conditions (disturbances) cause an increase in grain damage after 32 minutes where the rotor speed is decreased to maintain the control balance in Eq. (4.2). The rotor speed controller clearly responds to the increasing separation grain loss while reducing grain damage by reducing rotor speed in periods with lower grain losses.
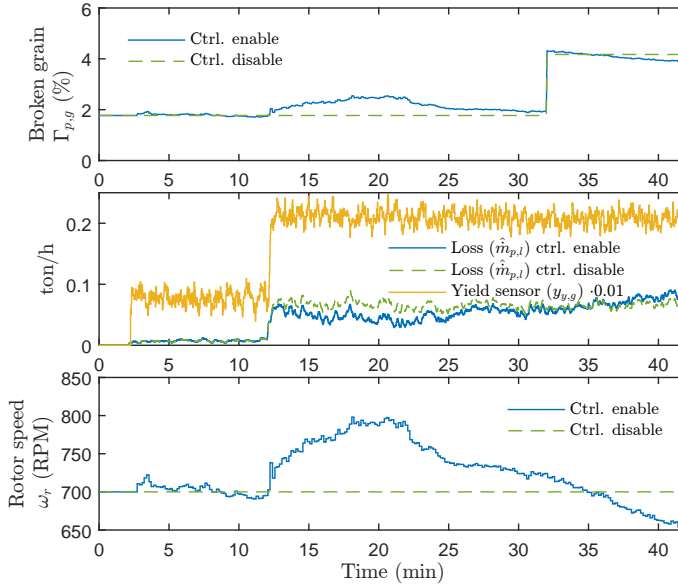
Figure 4.4: Simulation of the rotor speed closed-loop controller.

In Figure 4.5 a field test sequence from barley is shown with same row division as in Figure 4.4. The combine enters the crop row after 20 s, with a high initial rotor speed which is rapidly decreased. During the remainder of the sequence the throughput ($\dot{m}_{y,g}$) is relatively consistent, however the separation grain loss ($\dot{m}_{p,l}$) has large variations. This is most evident in the period from 2 till 6 minutes where the grain loss increases significantly and the controller responds swiftly by increasing the rotor speed while maintaining low grain damage. In a similar fashion the controller responds to smaller temporary changes in the grain loss estimate. The dataset clearly shows a rapid response to changes in separation loss without sacrificing grain damage.

Figure 4.5: Field test results for the rotor speed closed-loop controller in barley.
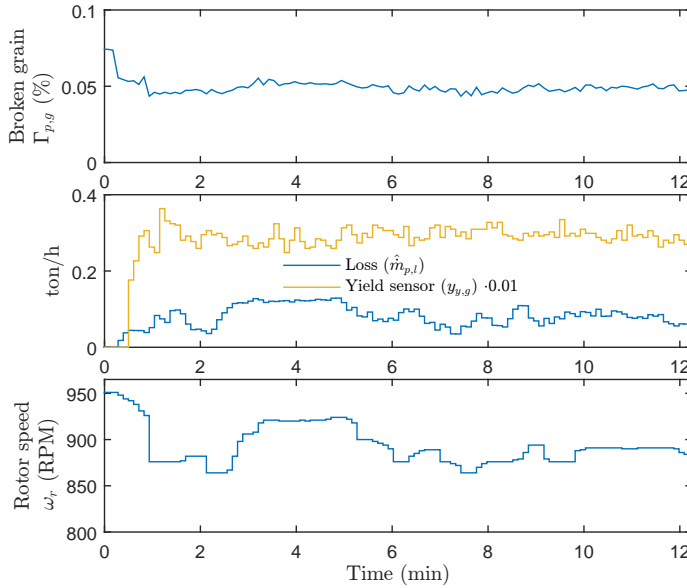
4.3 Fan Speed

The fan speed controller is based on the estimated tailing throughputs using the impact MFS tailings sensor and the proximity based volume reading from the TVS to estimate the tailings grain ($\dot{m}_{t,g}$) and MOG ($\dot{m}_{t,c}$) throughputs. The novel tailings grain set-point estimator for fan speed operation in the fluidised phase is used as reference to the closed-loop fan speed controller, see Figure 3.13 on page 56.

4.3.1 Controller Design

The closed-loop fan speed controller is shown in Figure 4.6. The fan speed is finally controlled using an error signal obtained from the estimated tailings grain ratio $\hat{\Gamma}_t$ presented in Section 3.3.4 and the estimated tailings grain ratio reference $\hat{\Gamma}_t^\star$ presented in Section 3.3.5. The actuator settings and sensor readings ($\mathbf{\Theta_c}$) are used by the set-point estimator to compute the tailings grain composition reference $\hat{\Gamma}_t^\star$ characterising the fluidised phase, i.e. low grain loss. The control error for the

fan speed controller is then given by

$$\epsilon_t = \hat{\Gamma}_t^\star - \hat{\Gamma}_t = f_t^\star(\mathbf{p_t^\star}, \mathbf{\Theta_c}) - \frac{\hat{\hat{m}}_{t,g}}{\hat{m}_{t,g} + \hat{m}_{t,c}}. \tag{4.3}$$
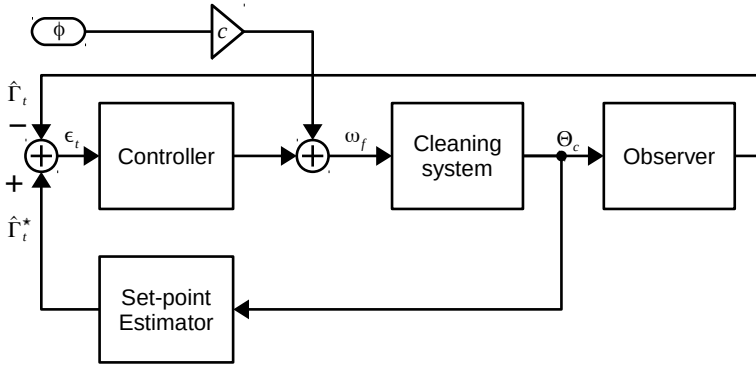

Figure 4.6: Control scheme for closed-loop fan speed controller.

The closed-loop fan speed controller should change the fan speed to variations in the longitudinal inclination angle. However by utilising the known effect from the longitudinal inclination angle (ϕ) to cleaning grain loss ($\dot{m}_{p,l}$) the control system can adjust the fan speed before the effect is observable on grain loss and tailing sensors, thus additionally reduce the cleaning grain loss.

4.3.2   Results

In order to verify the fan speed controller performance numerous tests have been conducted using the virtual combine, the continuous cleaning system laboratory and field test experiments. The initial tests are conducted using the virtual combine where a large number of tests conveniently can be obtained in order to verify response to various material and actuator variations. A sub-set of the tests conducted using the virtual combine will be repeated in the laboratory test environment where reference material samples are available for verification. The verification using the continuous cleaning system test environment facilitates verification representing one specific field condition. Numerous full scale field tests are required to verify the performance and robustness of the closed-loop fan speed controller in varying field conditions. However, acquiring material samples during field test experiments in a large scale is costly and often inadequate to capture

the variations from rapidly varying conditions due to low repeatability. Thus partial evaluation can be conducted verifying the response from a known effect to the controller response, i.e.

- The fan speed should increase with increasing MOG throughput by increasing forward speed as shown in Figure 2.9 on page 26

- The fan speed should increase at negative longitudinal inclination angles (ϕ) and vice versa, as shown in Eq. (2.2) and Figure 2.10 on page 28

Verification using the virtual combine in Article A.6, showed that the fan speed controller adjusted towards the fluidised phase when exposed to disturbances from the longitudinal inclination angle (ϕ), MOG throughput $\dot{m}_{p,c}$ and sieve changes (d_c and d_s).

Laboratory Test

A test sequence with increasing throughput ($\dot{m}_{p,g}$ and $\dot{m}_{p,c}$) is shown in Figure 4.7. First plot shows the increasing grain and MOG throughputs ($\dot{m}_{p,g}$ and $\dot{m}_{p,c}$), second plot the estimated tailings grain composition ($\hat{\Gamma}_g$) and third plot fan speed (ω_f). The last row shows fan speed curves with four sampled grain loss points ($\dot{m}_{c,l}$) using identical throughput and sieve openings for each of the three MOG throughputs stairs. The average fan speed from for the last 60 s in each throughput stair is marked $\bar{\omega}_f$ on the corresponding grain loss curve. The cleaning system throughput increases in a stair sequence with three steps, which is reflected in the tailings grain composition. The fan speed is relatively stable between 800 and 840 RPM during the first two periods, where the packed phase is not visible from the sampled fan speed curves. Note the controller does not decrease the fan speed to the 700 RPM where the grain loss is marginally lower compared to the average fan speed $\bar{\omega}_f$ from the closed-loop controller. The cleaning MOG throughput is increased to 12 ton/h in the third step causing high grain losses at 700 RPM. The fan speed $\bar{\omega}_f$ is clearly located in the fluidised phase reducing the grain loss for high MOG throughputs.

An overview of the results from the test sequence in Figure 4.7 is shown in Table 4.1. The table shows the grain loss in percent for the sampled reference fan speed curves and the estimated grain loss using the reduced order models for the trend curves for each stair in Figure 4.7. The controller does not necessarily obtain the optimum fan speed characterising the minimum grain loss for a given constant MOG throughput, however the obtained sub-optimal fan speed generally
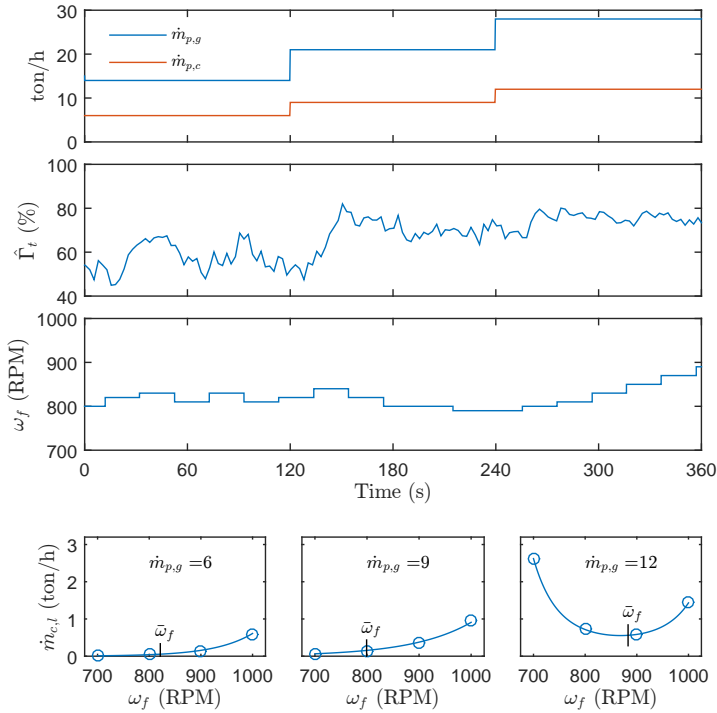
Figure 4.7: Closed-loop fan speed controller laboratory test with increasing throughput.

Table 4.1: Cleaning grain loss (%) for sampled fan speed curves and estimated grain loss for the closed-loop controller.

ω_f	700	800	900	1000	Ctrl.
$\dot{m}_{p,c} = 6$	0.06	0.37	1.05	4.17	0.39
$\dot{m}_{p,c} = 9$	0.34	0.64	1.73	4.65	0.74
$\dot{m}_{p,c} = 12$	9.29	2.61	2.04	5.15	2.14
Average	3.23	1.20	1.61	4.66	1.09

reduces the grain loss for varying MOG throughputs compared to one static setting by maintaining operation in the fluidised phase.

Field Test

In order to conduct partial field test verification of the closed-loop fan speed controller it was tested in hilly terrain in Scotland with longitudinal inclination,

and in hard threshing wheat in Australia causing a high MOG separation with large straw particles from the threshing and separation system.

Field test results with longitudinal inclination is shown in Figure 4.8, where left and right columns respectively show the controller enabled and disabled for two parallel crop rows in the same field providing comparable data sets. The first row shows the cleaning grain loss sensor reading $y_{c,l}$, second row the tailings grain composition estimate $\hat{\Gamma}_t$, third row the longitudinal inclination angle ϕ and last row the fan speed ω_f. The grain moisture (ρ_g) was 18 %.
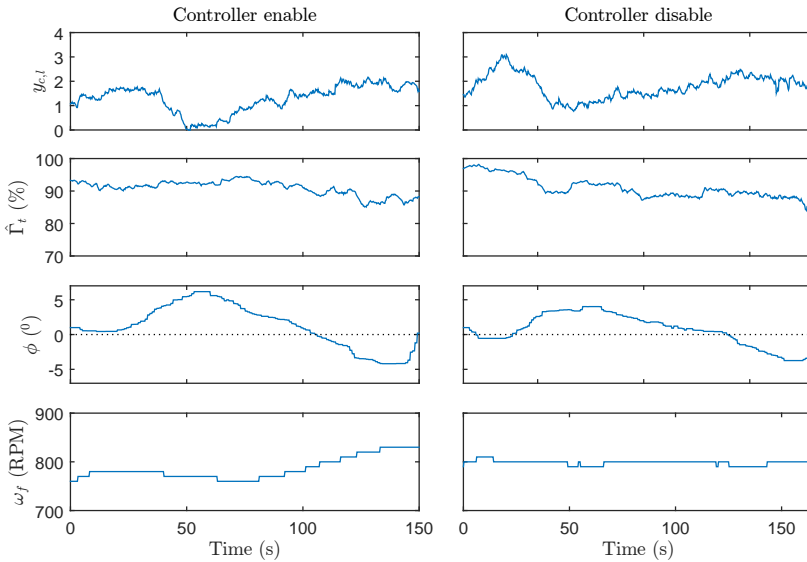
Figure 4.8: Closed-loop fan speed controller field test with longitudinal inclination.

The fan speed was manually adjusted by the operator from visual grain loss inspection of the residue swath prior to the test with the controller disabled. The feed forward compensation from the measured inclination angles in Eq. (2.2) was not applied in order to verify the anticipated effect using the tailing grain composition.

The combine starts at flat land where the fan speed is $\sim$30 RPM lower than the operator set-point. The fan speed is slightly reduced driving up-hill (40 s - 100 s), and increase the when driving down-hill (100 s - 150 s) by the closed-loop controller.

The average grain loss, inclination angle and inclination index are shown in Table 4.2, where the inclination index is given by $\phi_\angle = \|\phi\|$, indicating performance degradation due to longitudinal inclination angle. The reduction in grain losses is

Table 4.2: Evaluation parameters for field tests on sloped field.

Parameter	Enable	Disable
Grain loss $(y_{c,l})$	1.30	1.79
Min inclination	$-7.7°$	$-7.0°$
Max inclination	$8.9°$	$5.0°$
Inclination index $(\phi_\angle)$	1.18	0.53

found to be 34%, where the effect from both the maximum and minimum inclination angles as well as the inclination index $(\phi_\angle)$ indicate sub-optimal prerequisite conditions for the cleaning system when the controller was enabled compared to the sequence when the controller was disabled.

A fan speed controller test with increasing throughput was acquired in hard threshing wheat in Australia, see Figure 4.9. The first plot shows the grain loss reading $(y_{c,l})$, second plot the tailings grain composition $(\hat{\Gamma}_t)$, third plot the clean grain $(y_{y,g})$ and tailing throughputs $(\hat{\dot{m}}_{t,g}$ and $\hat{\dot{m}}_{t,c})$, and last plot the fan speed (ω_f). The grain moisture content (ρ_g) was $9\ \%$.
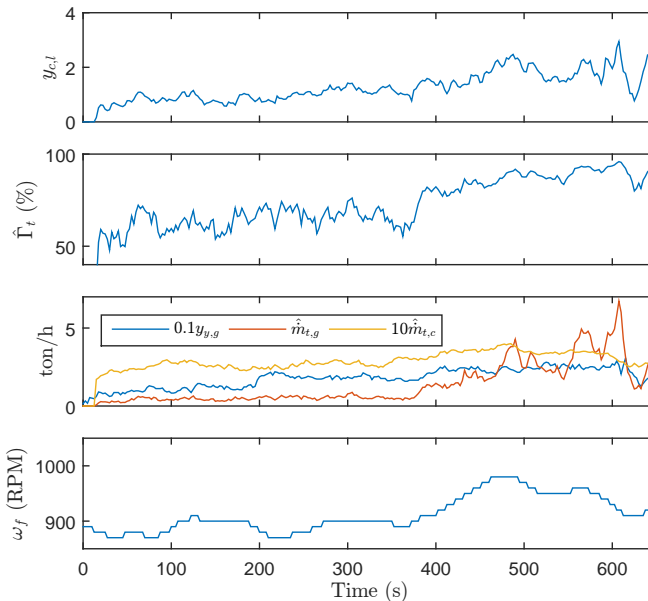

Figure 4.9: Closed-loop fan speed controller field test in hard threshing wheat.

Local crop conditions cause a significant increase in threshing loss (un-threshed

heads), which is referred to as hard threshing crop. The concave clearance is set tight to reduce the threshing loss which again causes a high MOG separation to the cleaning system, see Figure 2.4 on page 20. The tailings grain composition $\hat{\Gamma}_t$ is initially significantly lower than during the field test shown in Figure 4.8, though the fan speed initially start at 890 RPM, roughly 100 RPM higher than in Figure 4.8. A relatively high variance is visible in both the tailings grain and grain loss throughputs, however the fan speed clearly increase with the increasing throughput $y_{y,g}$ after 380 s, as well as the fan speed rapidly drops when the load is reduced after 600 s. No significant changes are observed during the increase in throughput after 180 s, where both tailing throughput components ($\dot{m}_{t,g}$ and $\dot{m}_{t,c}$) maintains roughly the same steady-state value corresponding to the loads of 6 and 9 ton/h in Figure 2.9 on page 26. However the changes in both $\dot{m}_{t,g}$ and $\dot{m}_{t,c}$ are significant as after the throughput step occurring after 380 s, similar to loads of 9 and 12 ton/h in Figure 2.9.

4.4 Sieve Spacing

The upper and lower sieve actuators does have a limited number of life time actuations as well as the range of valid settings for a given crop often is limited to roughly 10 different integer settings, thus the sieve actuator settings should be updated at a lower rate than the fan speed as indicated in Figure 4.1.

The overall optimisation function for the threshing, separation and cleaning systems is given in Eq. (4.1), where the sieve only affect the last two terms. The cleaning system sieves optimisation cost function is then given by,

$$f_{w,cs}(d_c, d_s) = u_{c,l} \frac{\dot{m}_{c,l}}{\dot{m}_{c,l} + \dot{m}_{y,g}} + u_{\Gamma,c} \Gamma_{y,c}. \tag{4.4}$$

A simplified sieve controller could be implemented as a balance controller like the rotor speed controller using standard SISO controller methodology, hence the upper and lower sieve controller errors are given by

$$\varepsilon_c = u_{c,l} \frac{\dot{m}_{c,l}}{\dot{m}_{c,l} + \dot{m}_{y,g}} - u_{t,c} \frac{\dot{m}_{t,g}}{\dot{m}_{t,g} + \dot{m}_{t,c}} \tag{4.5}$$

$$\varepsilon_s = u_{t,g} \frac{\dot{m}_{t,g}}{\dot{m}_{t,g} + \dot{m}_{y,g}} - u_{\Gamma,c} \Gamma_{y,c}, \tag{4.6}$$

where $u_{c,l}$, $u_{t,c}$, $u_{t,g}$ and $u_{\Gamma,c}$ are weights from the user interface in Figure 4.2. The actual implementation is relatively simple, however it does not consider actual impact variations due to environmental conditions.

In order to increase the performance it would be desirable to utilised the cost function in Eq. (4.4) directly. This requires a holistic overview of the impact from the sieve openings d_c and d_s to the primary optimisation parameters $\dot{m}_{c,l}$ and $(y_{\Gamma,c} \approx \dot{m}_{y,c}/(\dot{m}_{y,g} + \dot{m}_{y,c}))$, i.e. substituting reduced order models of Eq. (2.14) and Eq. (2.17) into Eq. (4.4),

$$f_{w,cs}(d_c, d_s) = u_{c,l} f_{c,l}(\mathbf{p_{c,l}}, \boldsymbol{\Theta_c}) + u_{\Gamma,c} f_{y,c}(\mathbf{p_{y,c}}, \boldsymbol{\Theta_c}), \qquad (4.7)$$

where online estimation of the model parameters for the reduced order models is desirable if not required. Scaling of the reduced order models $f_{c,l}(\mathbf{p_{c,l}}, \boldsymbol{\Theta_c})$ and $f_{y,c}(\mathbf{p_{y,c}}, \boldsymbol{\Theta_c})$ to the actual estimates of grain loss and cleanliness is required, whereupon the sieve settings d_c and d_s in theory can be obtained by solving the optimisation problem,

$$\underset{d_c, d_s}{\arg\min} \quad f_{w,cs}(d_c, d_s) \quad s.t. \quad \begin{cases} d_c \in \mathbb{N}[d_{c,min} : d_{c,max}] \\ d_s \in \mathbb{N}[d_{s,min} : d_{s,max}] \end{cases}. \qquad (4.8)$$

4.5 Conclusion

A general controller architecture was proposed, using a fast closed-loop controller for constant throughput, rotor speed and fan speed, and a model-based optimisation method for the concave clearance and sieve openings.

The simulation of the rotor speed controller showed a reduction in the maximum grain loss while maintaining acceptable grain damage. Results from full scale field test showed a fast response to large variations in local crop conditions temporarily causing high grain losses.

The fan speed controller showed to maintain the fluidised phase in the continuous cleaning system test environment for increasing MOG throughput. Additionally the fan speed controller was preliminary verified in hilly conditions with high grain moisture content and in hard threshing conditions with low moisture content.

Conclusions

5.1 Conclusions

The project demonstrated a novel closed-loop control system architecture for the threshing, separation and cleaning processes in a combine harvester. Furthermore the modelling approach using a semi-automated model generation framework as well as the design procedures for building a virtual combine were presented.

The dissertation showed how to acquire, analyse and process measurement data in order to generate steady-state (static) material flow models as well as dynamic models for material flow in a combine harvester. The generated models were validated using the virtual combine and by field test experiments where they were found to replicate the essential material flow and sensor characteristics in order to facilitate closed-loop control. A Luenberger observer was designed to estimate the amount of broken kernels for changes in rotor speed in order to compensate for the dominating settling time from the GQS. Using sensor fusion it was shown that it was possible to estimate the tailings MOG throughput and grain composition using an impact tailings sensor and a tailings volume sensor.

A virtual combine was developed to aid the design of the closed-loop control algorithms, which has provided a solid basis in the verification process of the rotor speed and fan speed closed-loop controllers.

Validation of the rotor and fan speed controllers were presented using a variety of experiments from the virtual combine, laboratory test stands and field tests. Simulation using the virtual combine showed the ability of the novel rotor speed controller to adapt to varying rates of separation loss while maintaining acceptable grain damage, where the field test verified the superior performance in varying conditions by swiftly adjusting to changes in the separation grain loss. A novel

approach describing the fluidised phase of the cleaning system using the tailings grain composition was presented. The generated set-point estimation model was verified using the virtual combine, continuous cleaning system test stand and field test experiments, showing a significant performance increase.

Farming is a business characterised by high revenues and small profit margins. With an estimated harvest loss of $4\,\%$ in the developed countries the superior performance of the rotor and fan speed controllers have the potential to beat the narrow but decisive margin changing deficits to profits for the farmer, as well as feeding an additional country the size of Germany with cereals by eliminating the annual harvest grain loss of 24 million tonnes of cereals in the industrialised countries alone.

5.2   Future Research

While the development of basic controllers to adjust rotor speed and fan speed have shown to improve the performance of the combine harvester, there are still plenty areas of interest for future research.

Immediate focus would be concave clearance and sieve openings. Numerous unobservable biological parameters are known to affect the behaviour of the processes, hence increasing the ability to adapt the online material flow models is of great interest.

The primary effort has been to model the steady-state characteristics of the combine harvester as it operates in steady-state the vast majority of the operational time. However due to the large process time delays there is a potential to utilise early process sensors to predict material flow throughout the combine and apply actuator settings for large throughput variations.

Material blockage of sensors is a common problem in combine harvesters, hence it is desirable to investigate methods for fault detection and predictive maintenance which for the most part relies on material flow models.

State of the art sensor technologies rely on relative readings as well as several process parameters of interest are unobservable, hence testing of new sensor technologies is a continuous research effort.

Appendices

Appendix I - Publications

A.1 Article 1: A Framework for Semi-Automated Generation of a Virtual Combine Harvester

Title:	A Framework for Semi-Automated Generation of a Virtual Combine Harvester
Publication type:	Conference Paper
Conference:	5th IFAC AgriControl Conference, Seattle WA, USA
Date:	August 2016
Authors:	Dan Hermann
	Morten Leth Bilde
	Nils Axel Andersen
	Ole Ravn

A Framework for Semi-Automated Generation of a Virtual Combine Harvester

D. Hermann[*,**] **M.L. Bilde**[**] **N.A. Andersen**[*] **O. Ravn**[*]

[*] *Automation and Control Group, Dept. of Electrical Engineering, Technical University Denmark, Lyngby, Denmark*
[**] *AGCO A/S, Research and Advanced Engineering, Randers, Denmark*

Abstract

This paper describes a generic data-driven model of the threshing, separation and cleaning process in a combine harvester. The aim is a model that describes the actual material flow and sensor values for relevant actuator configurations and measured environmental disturbances in order to facilitate Hardware In the Loop (HIL) simulation and sensor based material flow estimation. A modular data-driven model structure is chosen as it maintains the actual steady-state values and facilitates verification and debugging using laboratory and field data. The overall model structure, model generation procedure, and estimation of parameters from field data are described, as well as simulation results are presented.

1 Introduction

Combine harvesters are harvesting various crop types under varying environmental conditions all over the world. The threshing, separation and cleaning sub-processes should be adjusted continuously by the operator in order to optimise yield and crop quality. However actuator settings are often not accommodated due to lack of operator experience or information about the harvesting process. These processes are assigned to numerous uncontrollable biological variables and many of the optimisation parameters are even conflicting. Like loss, throughput, tailings, straw quality, grain cleanliness and power consumption. The aim is to obtain a total material flow model in order to increase the general process knowledge as well as facilitating HIL simulations and estimation of non-measurable process variables. The model inputs will be are material flows, biological parameters and actuators settings, and the outputs will be internal material flows, material residue flows and sensor readings.

Previous research has focused on an overall model structure with sub-models for threshing, separation, grain pans, cleaning shoe and return system, [5] and

[11]. In addition to this a variety of sub-models has been presented for material distribution, throughput estimation and simulation purposes.

Within the last decade advances within sensor technologies have been driven by the desire for increased process transparency for the operator and towards computer based systems for automatic adjustments of the machine settings for threshing, separation, and cleaning system. The focus is not to generate an advanced Computational Fluid Dynamics (CFD) model [7], but a material flow model that facilitates state estimation and simulations to the executed in real-time.

A generic procedure for mapping interdependencies between material flow, actuator excitation and sensor measurements on a combine harvester was presented by [1] and [2]. Literature summaries for material separation and loss models are found in [8] and [12].

Based on laboratory and field data from a threshing and separation unit [9] has compared mathematical separation models from literature and [10] has compared throughput-to-loss models from literature.

Based on 250 cleaning shoe laboratory experiments [12] has shown a coefficient of determination of $R^2 \geq 0.99$ using a Weibull separation model, [3] presented af Fuzzy model for MOG content in the grain bin, and [4] presented a Fuzzy model for prediction of sieve losses.

The paper is structured as follows. Model block diagram and component description are given in Section 2. Model variables and the model generation procedure is outlined in Section 3. Acquisition of dynamic, steady-state, and stochastic model parameters from field data is described in Section 4. Simulation results from the obtained model parameters are presented in Section 5.

2 Model Structure

The crop processing in a combine harvesters is divided into three processes: threshing, separation and cleaning, see Fig. 1. The threshing and separation process is combined mechanically into one unit whether is a traditional configuration of transverse threshing rotor with straw walker separation, a hybrid configuration with transverse threshing rotor and longitudinal separation rotor, or an axial configuration with threshing and separation on the same longitudinal rotor. The resisting blocks are a traditional cleaning system with two sieves and one fan, grain pans delivering material from the threshing and separation process to the cleaning system at one single point, and a tailings return system. The overall philosophy of the model design is to facilitate high modularity with

respect to the individual process modules and sensors, hence

- All modules can be built individually and compiled to the virtual combine

- Data obtained from laboratory and field can be combined

- New sensors can be included without re-acquiring all process data

The modelled state variables are actual material flows of grain or Material Others than Grain (MOG) in ton/h, which facilitate verification using obtained laboratory and field data. In between model inputs and outputs the steady-state (static) material flows are modelled with a grey-box model structure, where parameters are fitted to a mathematical description using experimental laboratory and field data, i.e. a data-driven model. The mathematical description is based on expressions from literature and findings from experimental data.
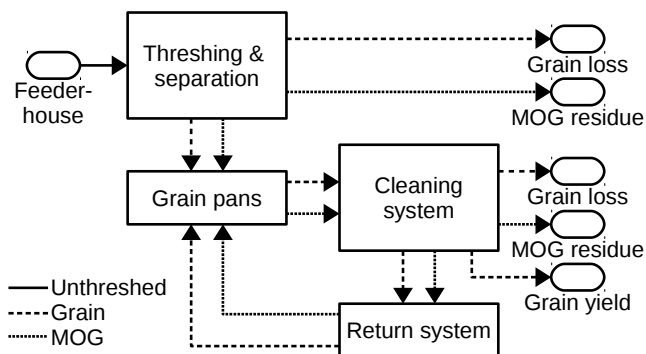

Figure 1: Generic combine model

The virtual combine harvester functions as a basic tool that facilitates design of a variety of functionalities as

- Sensor fusion and material flow estimation

- Model based control

- Actuator, system, and sensor fault detection

- HIL simulation and virtual sensors

- Operator training

The model is built from four basic building blocks, see Fig. 2. First order average filters are used to model the dynamic part of material flows, e.g. characterising cleaning shoe material flow dynamics, fan speed dynamic response and sensor response. Time delays are used to model material transport delays, e.g. in the tailings return system and grain elevator for the yield sensor. The dynamic parameters are assumed to be reasonably consistent through various crop types, as it primarily depends on the speed of rotors, augers, and elevators on the combine. The third block is the fitted trends for static material flow and
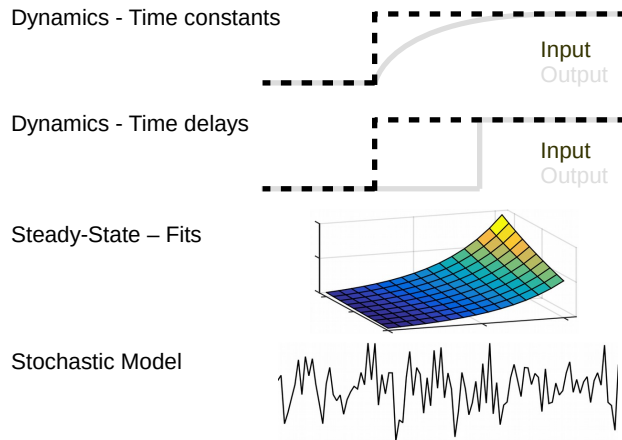

Figure 2: Building blocks for generic combine model

sensor response based on laboratory and field data, e.g characterising a relation from throughput to loss, fan speed to tailings flow or tailings flow to sensor reading. Together with the dynamic parameters the material flow is modelled using the Wiener model method [13], see Fig. 3. The fourth building block is the stochastic noise from crop flow variations and sensors readings. The noise is modelled as band-width limited white noise, e.g. characterising variations in material flow or noise in the yield sensor reading.

The relevant actuators, material flows and sensors for the model generation are given in Table 1. By using the modular structure of the presented model additional sensors can be added virtually to facilitate material flow estimation, e.g. of cleaning MOG or HIL simulation of a control system for loss reduction.
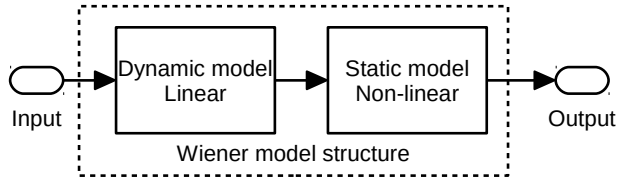
Figure 3: Wiener model structure

Table 1: List of actuators, material flows and sensors relevant for the virtual combine model.

Actuator	Material flow	Sensors
Rotor speed	Total throughput	Rotor torque
Concave spacing	Separation loss	Separation loss
	Threshing loss	
	Broken grain	
Fan speed	Grain throughput	Yield
Upper sieve spacing	Cleaning grain loss	Cleaning loss
Lower sieve spacing	Grain tailings	Tailings
	MOG throughput	Grain moisture
	MOG tailings	
	MOG in grain tank	

3 Model Generation

The virtual combine is built using data acquired from a large number of data sets obtained from both laboratory and field experiments. The dynamic parameters can be obtained from the standard machine sensors. Steady-state material flows collected in laboratory test stands are more consistent and repeatable than field data and provide more options for designed experiments. However laboratory experiments are more time consuming and requires large amounts of material to be stored.

The steps towards generation of the virtual combine model are as follows

- Data collection

- Obtaining time constants, time delays, steady-state values stochastic vari-

ables

- Generating individual trend fits

- Compile models for all sub-modules

- Compile virtual combine from sub-modules

The first step is acquisition of data sets from designed experiments or measurements acquired for other purposes that can be useful for modelling. The material flows to be obtained in order generate a material flow model are given in Table 1 for upper and lower block for threshing/separation and cleaning shoe respectively.

From the acquired data sets dynamic parameters and steady-state values are obtained as will be described in Section 4. From the obtained steady-state values fitted trends representing material flows and sensor readings are generated. This is the most time consuming and challenging part of the modelling process. Initially it requires mapping of the relationships between material flow, actuator excitation and sensor measurements.

Subsequently an evaluation of the interdependencies in order to obtain a mathematically description that provides an adequate representation of the chosen linear or non-linear relationship.

A model for each of the four main components (sub-modules) in the block diagram in Fig. 1 are generated from the obtained dynamic and stochastic parameters, as well as fitted trends obtained from laboratory and field data. The modular structure facilitates the individual system parameters and modelled trends to be utilised for online state estimators, model based control or fault detection.

The last step is compilation of the virtual combine which connects all the materials flows of the sub-modules to one model that describes the material flow throughout the machine.

4   Parameter Estimation

The parameter estimation process often requires analysis of several hundred data sets which each contain numerous sensor values. This calls for an automatic or semi-automatic routine for detecting steady-state periods, time constants, time delays and stochastic variables from the available data sets.

Fig. 4 shows collected field data from a Massey Ferguson 9540 driving from headland an into a crop row at constant forward speed. In the top plot the

89

forward speed is shown, the middle plot shows the hydraulic oil pressure from the rotor belt drive variator which is roughly proportional to the rotor torque and the yield sensor in the lower plot. The step response observed for the rotor pressure and yield sensor plot will be modelled using a first order average filter. The time delay between the rotor pressure and yield sensor impact is modelled by a delay chain. Steady-state values are obtained from 15 s - 60 s. Finally the stochastic variables will be obtained from the data in the steady-state period.

4.1   Steady-state

All data sets are evaluated using a Steady-State Detection (SSD) algorithm [6]. In order to obtain a steady-state set the relevant actuators and sensors for the relationship are all required to be in steady-state. E.g. for the rotor pressure sensor steady-state would be required for forward speed, rotor speed, concave spacing and rotor pressure sensor. The steady-state set is then obtained from the averages in the joint steady-state period.

4.2   Time constants

The first order time constants τ are obtained using a first order unit step function

$$
f(x) = \begin{cases} b + a(1 - e^{-(t-t_s)/\tau}) & \text{if } t \geq t_s \\ b & \text{else} \end{cases} ,
\tag{1}
$$

where the step response starts at t_s for the time t, with b as the steady-state value before the step occurs with step size a. The modelled time constants are obtained as an average of the observed time constants τ from several data sets, see Fig. 5.
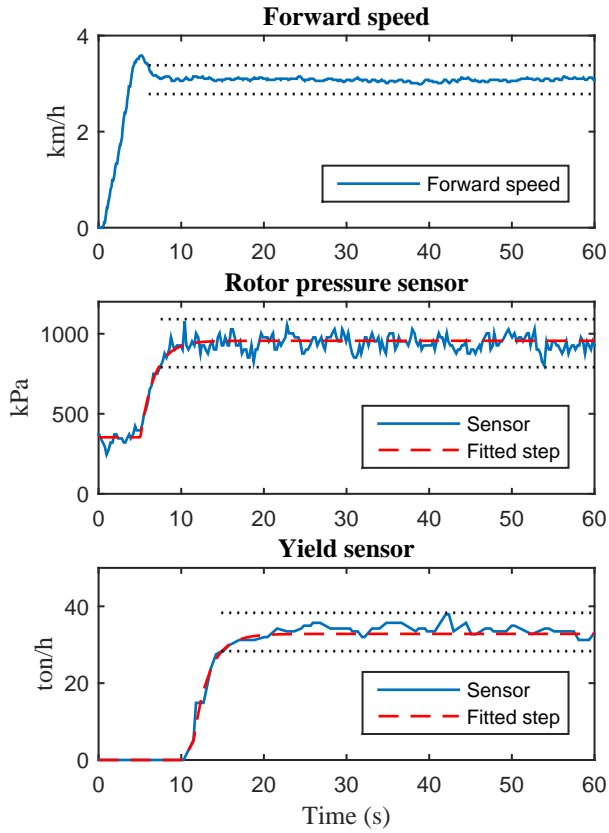
Figure 4: Automatic steady-state detection. Top plot shows forward speed, middle plot rotor pressure and bottom plot the yield sensor. Steady-state periods are marked with dashed black lines.
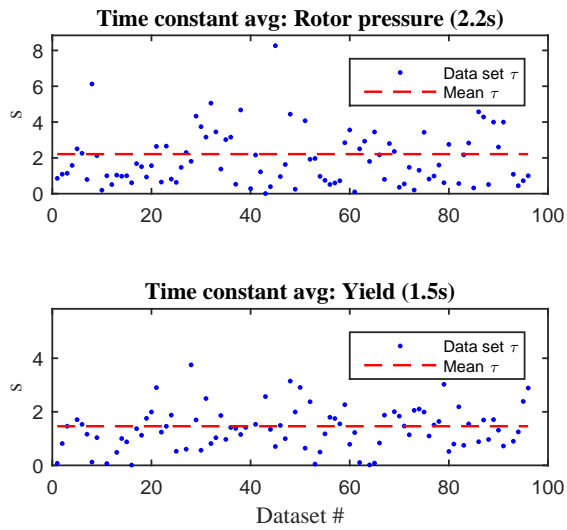
Figure 5: Combine first order time constant statistic for rotor pressure and yield sensor

4.3 Time delays

Transport time delays are occurring at several locations in the machine. The dominant time constants to be identified are

- Header to threshing and separation unit

- Threshing and separation unit to cleaning shoe (material pan delay)

- Tailings return system

- Elevator for yield sensor reading

In Fig. 4 the delay is evident from the rotor pressure step $(t_{s,r})$ after 5 s and yield step $(t_{s,y})$ after 11 s. The tailings return delay can be found by opening the upper sieve and closing the lower sieve in order to achieve a high tailings volume that is observable using the yield sensor, see Fig. 6. The figure shows the yield sensor reading where Eq. (1) is fitted to the first step for material impact in the cleaning system (black) and again to the second step caused by the tailings return material (red). The tailings delay is found to be 6 s.
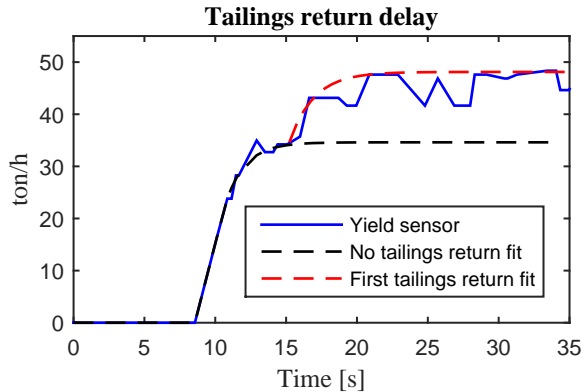

Figure 6: Combine tailings delay

4.4 Stochastic variables

In practical systems various noise sources contribute to the reading at the individual sensors located in the combine. E.g. for the rotor pressure sensor noise

are contributed from electrical magnetic noise are picked up in the cable, crop variations in hydraulic oil temperature, noise originating from variations in the field crop density, feeding variations to the rotor etc. Where the dynamic parameters and the steady-state fits represent the general trends in the machine, the stochastic model represents the real variations occurring in the machine in order to increase the realism of the simulated material flows and sensor output. For the simulation model the noise is modelled using data obtained during the steady-state period in Fig. 4. The noise is modelled as bandwidth limited white noise, see noise model in Fig. 7. The model is given by the white noise variance
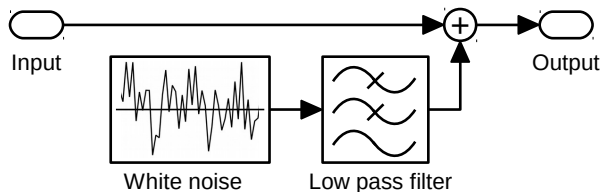
Figure 7: Stochastic noise model

σ_n^2 and bandwidth ω_n of the low-pass filter $H(\omega_n)$. For the rotor pressure sensor σ_n^2 is obtained from the variance of the steady-state period. In order to obtain the noise band-width parameter ω_n the Power Spectral Density function (PSD) S_{yy} is utilised, see Fig. 8. The parameter ω_n is obtained by solving the optimisation problem in Eq. (2) for the data set y obtained from the steady-state period.

$$\arg \min_{\omega_n} = ||S_{yy}(\mathbf{y})/\sigma_n^2 - |H(\omega_n)|^2|| \tag{2}$$

5   Simulation Results

When all the dynamic, steady-state and stochastic parameters are obtained for the four individual sub-models in Fig. 1, the full model for the virtual combine can be compiled. The interface between the individual sub-models is the material flow of grain and MOG in (ton/h). The simulation will provide the current state (material flow) and the associated sensor readings for the given throughput and actuator settings.

Figure 8: Rotor pressure power spectrum density

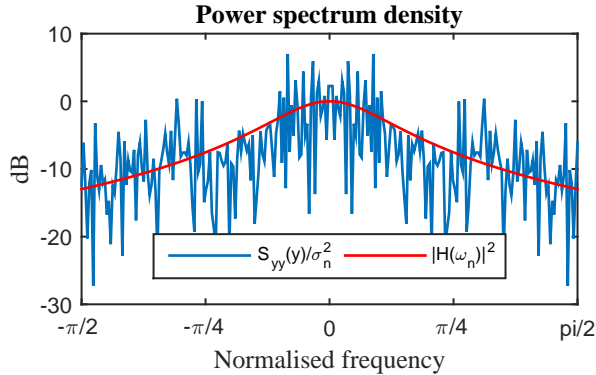The simulation results are shown in Fig. 9 for a step response occurring after 15 s.

The total throughput from the straw elevator is shown in the top plot. For a practical measurement the total throughput would also have a stochastic component, however it is disabled in the plot in order to clarify the difference between the actual material flows (state).

In the middle plot the rotor pressure is shown as the true value (dashed) and the stochastic component (solid) corresponding to the actual sensor reading from the machine.

As for the rotor pressure sensor the true yield sensor flow is shown with the dashed line and the sensor output with a solid line. For the lower plot the actual shoe load is added to the plot with yield sensor. The delay from the tailings return loop of 6 s is clearly visible in the extra contribution added to the grain load after 23 s. Compared to the field data in Fig. 4 a similar noise level and time response is observed, hence the model is considered to provide a reasonable good simulation result. However, as seen in Fig. 5 the time constant vary significantly between various runs in the same field.
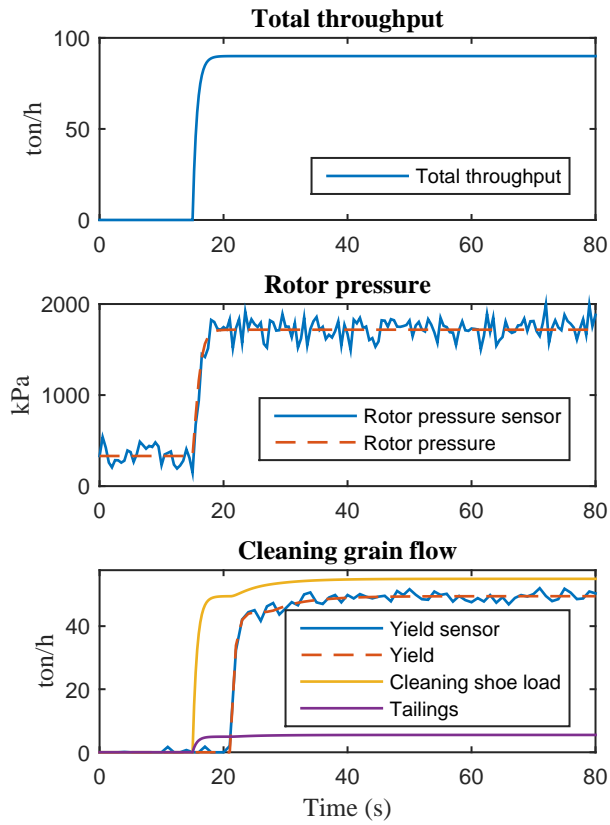
Figure 9: Simulation of rotor pressure and yield sensor value for step input

6   Conclusion

A generalised data-driven model structure for at combine harvester is presented, that models the actual material flow using a combination of average filters, time delays, fitted trends, and a bandwidth limited white noise stochastic model.

The model generation procedure is outlined with examples of how to obtain the model parameters from field data. The average filter time constants and time delays where found by fitting a first order step response, detection of steady-state periods using a SSD algorithm and stochastic model parameters using PSD from the steady-state period.

Simulation results were presented for the generated model with parameters obtained field data. Using the modular structure of the presented model additional sensors can be added virtually to facilitate material flow estimation, e.g. of cleaning MOG or HIL simulation of a control system for loss reduction.

Acknowledgements

References

[1] G. Craessaerts, W. Saeys, B. Missotten, and J. De Baerdemaeker. A genetic input selection methodology for identification of the cleaning process on a combine harvester, part i: Selection of relevant input variables for identification of the sieve losses. *Biosystems Engineering, Biosyst. Eng, Biosyst Eng, Biosystems Eng*, 98(2):166–175, 2007.

[2] Geert Craessaerts, Wouter Saeys, Bart Missotten, and Josse De Baerdemaeker. A genetic input selection methodology for identification of the cleaning process on a combine harvester, part ii: Selection of relevant input variables for identification of material other than grain (mog) content in the grain bin. *Biosystems Engineering*, 98(3):297–303, 2007.

[3] Geert Craessaerts, Wouter Saeys, Bart Missotten, and Josse De Baerdemaeker. Identification of the cleaning process on combine harvesters. Part I: A fuzzy model for prediction of the material other than grain (MOG) content in the grain bin. *Biosystems Engineering*, 101(1):42–49, 2008.

[4] Geert Craessaerts, Wouter Saeys, Bart Missotten, and Josse De Baerde-maeker. Identification of the cleaning process on combine harvesters, Part II: A fuzzy model for prediction of the sieve losses. *Biosystems Engineering*, 106(2):97–102, 2010.

[5] A. Eggerl, H. Bösch, A. Bruns, and S. Wöbcke. Model-based development of control algorithms for optimizing combine prococess. In *VDI-MEG Kolloquium Möhdrescher*, volume 40, 2010.

[6] Jeffrey D. Kelly and John D. Hedengren. A steady-state detection (ssd) algorithm to detect non-stationary drifts in processes. *Journal of Process Control*, 23(3):326–331, 2013.

[7] Christian Korn, Ralf Hübner, Thomas Herlitzius, Frank Rüdiger, and Jochen Fröhlich. Numerische untersuchung der luftströmung in der reinigungseinrichtung von mähdreschern. *Landtechnik*, 68(2):83–88, 2013.

[8] H.D. Kutzbach. Approaches for mathematical modelling of grain separation. *International Conference on Crop Harvesting and Processing*, 2003(701):9–11, 2003.

[9] K. Maertens and J. De Baerdemaeker. Flow rate based prediction of threshing process in combine harvesters. *Applied Engineering in Agriculture*, 19(4):383–388, 2003.

[10] K. Maertens, P. Calmeyn, H. D. Kutzbach, and J. De Baerdemaeker. Throughput-loss relation in conventional combine harvesters - a comparison between stationary and mobile units. In *Landtechnik AgEng Proceedings*, pages 591–597, 2003.

[11] K. Maertens, M. Reyniers, and J. De Baerdemaeker. Design and application of a dynamic separation model for combine harvesters. *Loboratory of Agro-Machinery and Processing*, 2001.

[12] P. I. Miu. Stochastic modeling of separation process on combine cleaning shoe. *International Conference on Crop Harvesting and Processing*, 2003(701):9–11, 2003.

[13] Oliver. Nelles. *Nonlinear system identification : From classical approaches to neural networks and fuzzy models*. Springer, 2001.

A.2   Article 2: On-the-go Throughput Prediction in a Combine Harvester using Sensor Fusion

Title:	On-the-go Throughput Prediction in a Combine Harvester using Sensor Fusion
Publication type:	Conference Paper
Conference:	1st IEEE Conference on Control Technology and Applications, Kohala Coast HI, USA
Date:	August 2017
Authors:	Dan Hermann
	Morten Leth Bilde
	Nils Axel Andersen
	Ole Ravn

On-the-go Throughput Prediction in a Combine Harvester using Sensor Fusion

D. Hermann[*,**] **M.L. Bilde**[**] **N.A. Andersen**[*] **O. Ravn**[*]

[*] *Automation and Control Group, Dept. of Electrical Engineering, Technical University Denmark, Lyngby, Denmark*
[**] *AGCO A/S, Research and Advanced Engineering, Randers, Denmark*

Abstract

The paper addresses design of a clean grain throughput observer for a combine harvester, i.e. delay free yield sensing. The aim is to predict grain throughput changes using the forward speed and a throughput sensor in the feederhouse. By utilising a grain flow model and sensor fusion an estimate of the current grain throughput is obtained, hence the effect from the lag in the momentary yield sensor reading due to material transport delays can be reduced. Statistical change detection is used to detect feederhouse load condition as well as sensor discrepancies using the observer innovation signal. The system is able to predict changes originating from forward speed and local crop density variations. Also temporary sensor discrepancies are detected and compensated in the grain flow estimate.

1   Introduction

The following paper describes the modelling process for a crop mass flow sensing system in a combine harvester. Commercial combine harvesters have a number of distributed mass flow sensors throughout the machine, however due to material transport on material pans, augers and elevators there are significant time delays between the sensor signals. Hence the measured sensor signals are not directly comparable at a given time instance, thus an instrumentation or control system is required to postpone signal comparison or average over longer time periods when estimating system load or grain loss. In a closed-loop fan speed control system a fast response is vital to system performance when operating near the maximum capacity for the cleaning system in order to avoid a collapse due to a sudden load change, i.e. causing substantial grain loss. The aim is to generate a delay free material flow estimate of the grain throughput in the threshing and separation system. The report will address the overall material flow of a combine harvester, assessment of model structure, extraction of model

parameters, detection of load condition using statistical change detection, and evaluation of the obtained model for grain throughput estimation.

Previous research has focused on post-processing yield sensor data for yield mapping [14], and estimation of momentary total throughput or grain loss [6, 7, 10]. This is state of the art for modern yield mapping tools and instrumentation systems in commercial combine harvesters.

Within the last decade focus has been on data-driven material flow models for combine harvesters [4, 8, 5]. These models have shown the ability to simulate the material flow through the machine.

It has been attempted to measure the incoming crop throughput with forward looking sensor technologies [13, 11], with the aim to perform corrective actions in an computer based control system. Using dynamic models [1] and [9] has shown that the yield sensor precision could be increased by post-processing yield sensor data with dynamic grain flow models. In [2] it was shown that a black-box model approach could be used to identify sensor faults on a combine harvester.

The paper is structured as follows. Section 2 presents an overall block diagram of the material flow in a combine harvester, derivation of a simplified grain flow model and observer design. Section 3 addresses system identification and parameter estimation. Section 4 concerns design of a scheme for detection of load condition and sensor faults using a statistical method. The results are discussed in Section 5.

2   Plant Model

In Fig. 1 the overall material flow block diagram is given, divided in the mechanical sub-systems of a combine harvester. The block diagram shows the material flow of unthreshed material, grian, and material other than grain (MOG).
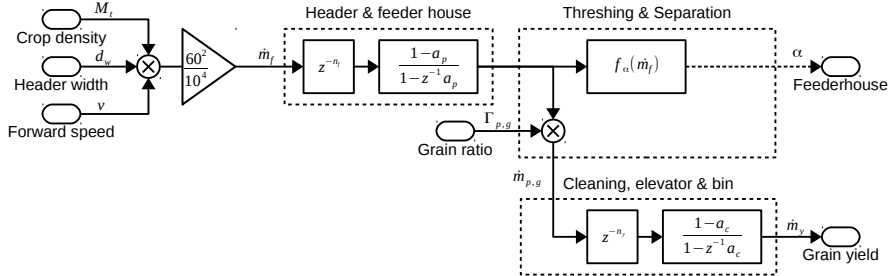
Figure 2: Discrete time simplified grain flow model block diagram.
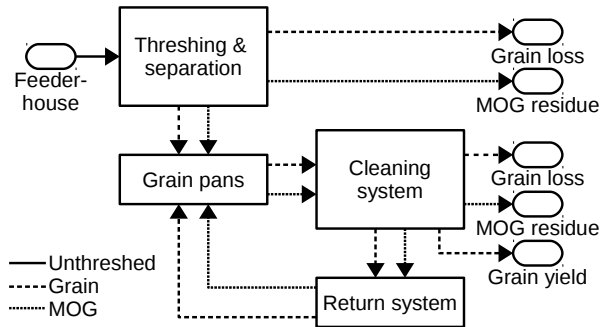
Figure 1: Combine material flow model block diagram.

The full model is generated from sub-components describing steady-state relationships and dynamics individually, [5].

As most of the available sensors only provide a relative reading of the material flow, all static models for material flow are based on experiments where material is sampled during steady-state. These steady-state models are used to describe material flow relationship from actuator changes or to sensor readings. The dynamics of the system are found from sensor readings, where the system is excited with a step responses and are primarily characterised by first order average filters or time delays.

Simplified model In order to estimate the grain throughput in the threshing and separation system it is not required to model all the material flows indicated

in Fig. 1. A simplified model describing the vast majority of the grain flow is given in Fig. 2. The material grain flow is reduced to the following steady-state constraints

$$\dot{m}_{p,g} \simeq \dot{m}_f \cdot \Gamma_{p,g} \tag{1}$$

$$\dot{m}_y \simeq \dot{m}_{p,g} \tag{2}$$

$$w_h = v \cdot d_w \tag{3}$$

$$\dot{m}_f = M_t \frac{60^2}{10^4} w_h, \tag{4}$$

where the total input grain mass flow in the threshing and separation system $(\dot{m}_{p,g})$ equals the grain ratio $(\Gamma_{p,g})$ of the total mass flow $(\dot{m}_f)$. Threshing, separation and cleaning losses are neglected in the simplified model. The average losses (1% to 3%) roughly corresponds to the inaccuracy of the yield sensor. The grain flow into the grain bin impacting the yield sensor $(\dot{m}_y)$ can then be approximated to the threshing and separation grain mass flow $(\dot{m}_{p,g})$. The total input mass flow $(\dot{m}_f)$ equals the local crop density (M_t) times the covered areal flow of the header (w_h), which is the product of the forward speed (v) and the header cutting width (d_w). In practice the full header width is not always utilised. However as no measurement is available, the header is assumed to use its full cutting width at all times.

Sensors The yield sensor measurement $\dot{m}_y$ is located at the top of the grain bin elevator. The transport time (T_y) for sliding down the grain pan under the lower sieve, through the cross auger and grain bin elevator causes the largest measurement delay in the machine. However the yield sensor is the only sensor providing an absolute reading of the material flow. The forward speed v is provided from a tachometer on the front wheel axis drive train. An experimental sensor mechanism using a potentiometer and a lever measures the height of the incoming material mat, referenced as the feederhouse throughput sensor α. The transport delay from the header cutting table to the threshing and separation system (T_f) is visible from an actuator change in v to a corresponding change in feederhouse sensor reading α.

State-space The grain flow model for the observer implementation in Fig. 2 is operating in the state-space domain. The main purpose is to estimate the grain throughput state in the threshing and separation system $(\dot{m}_{p,g})$. In order to leverage time delays T_f and T_y, using feed forward from the measurements

v and α, the knowledge of M_t and $\Gamma_{p,g}$ is required. Hence a change in forward speed v will be fed forward based on the local crop density M_t, where variations in M_t will be captured by the feederhouse sensor α. Changes in the grain ratio $\Gamma_{p,g}$ of the total throughput $\dot{m}_f$ are adjusted using the yield sensor. The value of $\Gamma_{p,g}$ does not vary significantly over the day and will in practice also compensate for inaccuracies originating from the measurements of α and $\dot{m}_y$. The state vector of the discrete time state-space system is given by

$$\mathbf{x} = \begin{pmatrix} M_t & w_h & \Gamma_{p,g} & \dot{m}_{y-n_y} & \dots & \dot{m}_y \end{pmatrix}^T, \tag{5}$$

where the $\dot{m}_y$ states specifies the delay of n_y samples. The input and output vectors for the state-space model is then given by

$$\mathbf{u} = v_{-n_f} \quad \text{and} \quad \mathbf{y} = \begin{pmatrix} \alpha & \dot{m}_y & \dot{m}_{p,g} \end{pmatrix}^T, \tag{6}$$

where the input v_{-n_f} characterises the forward speed sensor reading delay of n_f samples. The system transition and input matrices are given by

$$F(k) = \begin{bmatrix} [F_D(k) & 0_{[n_x, n_y-1]}] \\ [0_{[n_y, n_x-1]} & I_{[n_y]}] \end{bmatrix} \quad \text{and} \quad G = \begin{bmatrix} 0 \\ d_w(1 - a_p) \\ 0_{[n_y+2, 1]} \end{bmatrix}, \tag{7}$$

where the dynamic part of the system transition matrix (F) is

$$F_D(k) = \begin{bmatrix} 1 & 0 & 0 & 0 \\ 0 & a_p & 0 & 0 \\ 0 & 0 & 1 & 0 \\ 0 & 0 & \bar{M}_t \bar{w}_h \frac{60^2}{10^4}(1 - a_c) & a_c \end{bmatrix}, \tag{8}$$

at the linearisation points $\bar{M}_t$ and $\bar{\omega}_h$. The number of rows/columns of square matrix F_D is given by n_x. The output matrix

$$H(k) = \begin{bmatrix} p_{\alpha,2}\bar{w}_h \frac{60^2}{10^4} & 0 & 0 & 0 & \dots & 0 \\ 0 & 0 & 0 & 0 & \dots & 1 \\ 0 & 0 & \bar{M}_t \bar{w}_h \frac{60^2}{10^4} & 0 & \dots & 0 \end{bmatrix}, \tag{9}$$

provides estimates of two sensor observations of α and $\dot{m}_y$, and the non-observable internal state $\dot{m}_{p,g}$.

Observer design The prediction for time update and estimation output up-
date equations are given by

$$\hat{\mathbf{x}}(k+1) = F(k)\hat{\mathbf{x}}(k) + G\mathbf{u}(k) \tag{10}$$

$$\hat{\mathbf{y}}(k) = H(k)\hat{\mathbf{x}}(k), \tag{11}$$

and the measurement update by

$$\hat{\mathbf{x}}(k) = K(\mathbf{y}(k) - \hat{\mathbf{y}}(k)). \tag{12}$$

A reduced order observer is utilised for the sensor readings α and $\dot{m}_y$ only.
The observer gain K is tuned based on data acquired from laboratory and field
experiments. When the harvester is not fully loaded the measurement update
in (12) will be disabled according to the H_{cor} flag, as the grain ratio constraint
in (1), else implies dividing by zero. Likewise will the one-step-ahead prediction
be executed without the input matrix according to

$$\hat{\mathbf{x}}(k+1) = F(k)\hat{\mathbf{x}}(k), \tag{13}$$

when the machine is empty (H_{est}).

3   Parameter estimation

With the overall grain flow model structure in place the model parameters
can now be estimated. The data sets can originate from laboratory or field
experiments where material flow is sampled with relevant sensor data, or from
field data where all on the combine sensors are available. The feederhouse
throughput sensor parameters will be obtained using material samples, and the
dynamic parameters will be obtained from sensor data.

Throughput sensor The relation from actuator to the state (material flow),
and the relation from the state to the sensor reading is obtained from material
samples and the average of the sensor reading. A total of 27 data sets are
utilised for investigation of the relationship from total throughput ($\dot{m}_f$) to sensor
reading (α), see Fig. 3. The feederhouse throughput sensor (α) provides a
clear correlation to the total throughput ($\dot{m}_f$), with an obtained coefficient of
determination $R^2 = 0.72$ using the affine model

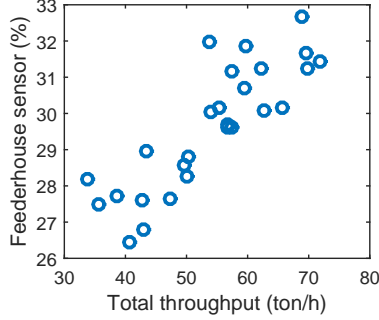$$f_\alpha(\dot{m}_f, p_\alpha) = p_{\alpha,1} + p_{\alpha,2} \cdot \dot{m}_f. \tag{14}$$

Figure 3: Steady-state relationship from total throughput ($\dot{m}_f$) to feederhouse throughput sensor reading (α).

Step response In Fig. 4 a sequence with a step in forward speed is shown. The first plot shows the forward speed (v) with step impact time of approx. 32 s, second plot the feederhouse sensor (α), and the third plot the yield sensor ($\dot{m}_y$). By fitting the step function

$$f(t, p_1, p_2, t_s, \tau) = \begin{cases} p_1 + p_2(1 - e^{-(t-t_s)/\tau}) & \text{if } t \geq t_s \\ p_1 & \text{else} \end{cases}, \qquad (15)$$

for each the steps in forward speed, feederhouse and yield sensor, the step response parameters are obtained. The step response starts at t_s for the time t, with the initial steady-state value p_1, step size p_2 and time constant τ. The sensor data is shown in blue and the fitted data in red.

System delays When the step impact time (t_s) for forward speed ($t_{s,v}$), feederhouse ($t_{s,\alpha}$) and yield sensor ($t_{s,y}$) are obtained the system material transport delays are given by

$$T_f = t_{s,\beta} - t_{s,v} \simeq 3.5s$$
$$T_y = t_{s,y} - t_{s,\beta} \simeq 8.5s.$$

System dynamics The filter time constants τ found using (15) are the response for a unit step input. For the grain flow model in Fig. 2 the relevant
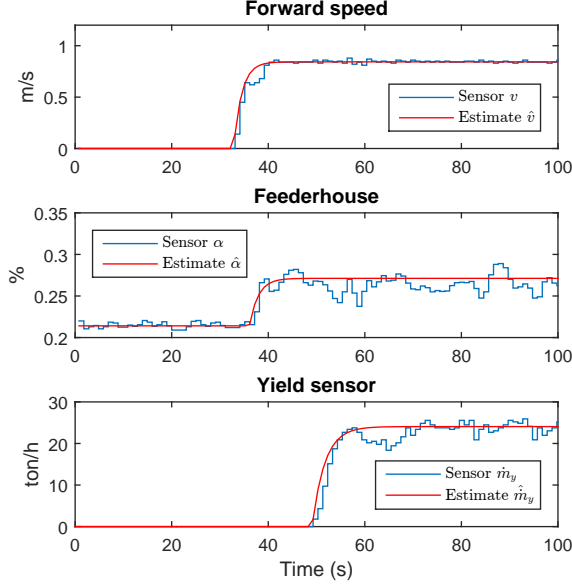
Figure 4: Field data with step input. First plot shows forward speed (v), second plot feederhouse sensor (α) and third plot the yield sensor ($\dot{m}_y$).

filter time constants to be obtained are a_p and a_c for the transfer functions,

$$G_p(z) = \frac{1 - a_p}{1 - z^{-1}a_p} \quad \text{and} \quad G_c(z) = \frac{1 - a_c}{1 - z^{-1}a_c}. \tag{16}$$

Given the system time delays T_f and T_y, the first order parameters for the dynamic model can be obtained by shifting the input time vectors n_f and n_y samples. The dynamic parameters (a_p and a_y) can be estimated using an ARX model with compensation for time delays

$$\begin{pmatrix} y(k) \\ y(k-1) \\ \vdots \\ y(k-n+1) \end{pmatrix} = - \begin{pmatrix} y(k-1) \\ y(k-2) \\ \vdots \\ y(k-n) \end{pmatrix} a + \begin{pmatrix} u(k-1-n_d) \\ u(k-2-n_d) \\ \vdots \\ u(k-n-n_d) \end{pmatrix} b, \tag{17}$$

given n samples and the time delay n_d between to input and output signal. In matrix form of (17) is given by $\mathbf{y} = \begin{bmatrix} -Y & U \end{bmatrix} \begin{pmatrix} a & b \end{pmatrix}^T$, where the parameters a and b can be found solving the least square representation,

$$\begin{pmatrix} a \\ b \end{pmatrix} = \begin{bmatrix} -Y & U \end{bmatrix}^{-1} \mathbf{y}. \tag{18}$$

As the steady-state gain parameters are already obtained for G_f and G_y in the model using $f_\alpha(\dot{m}_f)$ and $\Gamma_{p,g}$ respectively, only the dynamic parameters are of interest. Hence an unity gain in steady-state is desirable. In steady-state the gain in the ARX model from (17) is

$$\lim_{z \to 0} G(z) \frac{b}{1 - az^{-1}} = 1 \implies b = 1 - a,$$

which implies that the dynamics will be expressed using the a parameter only, using $y(k+1) = ay(k) + (1-a)u(k)$.

Results In Fig. 5 a sequence of field data with four steady-state periods of minimum 30 s is shown. The first plot shows the forward speed (v). Second plots shows the feederhouse sensor, where both the sensor reading and estimate follows the variations in forward speed, indicating an approximately uniform crop density.
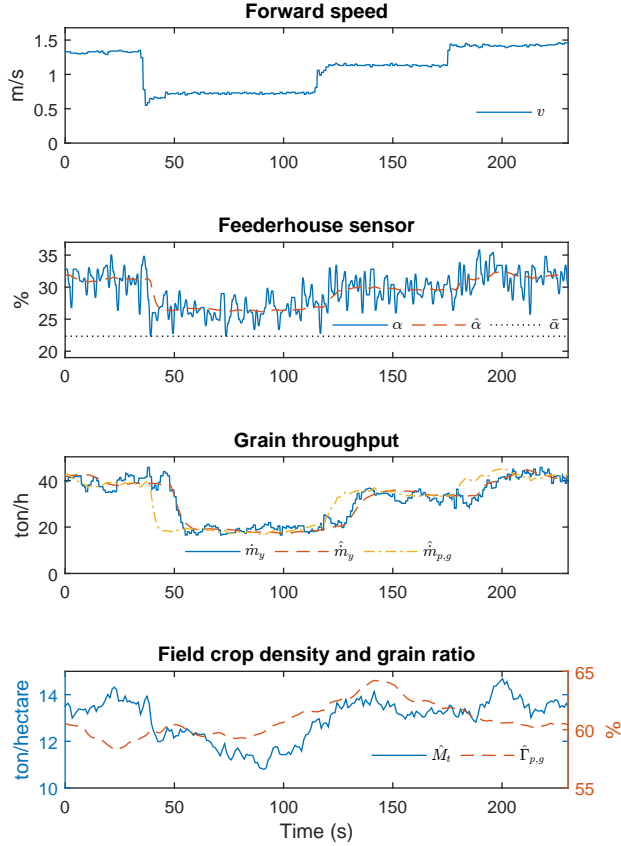
Figure 5: Field data with forward speed stairs and grain throughput estimation. First plots shows forward speed (v), second feederhouse sensor (α and $\hat{\alpha}$), third grain throughput ($\dot{m}_y$, $\hat{\dot{m}}_y$ and $\hat{\dot{m}}_{p,g}$), and fourth the estimate local crop density $\hat{M}_t$ and grain ratio $\hat{\Gamma}_{p,g}$.

The third plot shows the actual yield sensor reading of $\dot{m}_y$ and the estimates $\hat{\dot{m}}_y$ and $\hat{\dot{m}}_{p,g}$. The yield sensor reading $\dot{m}_y$ is tracked well in the estimate $\hat{\dot{m}}_y$, and the $\hat{\dot{m}}_{p,g}$ estimate provides a precise estimate of the grain flow T_y seconds in advance of the actual yield sensor reading. The local crop density estimate $\hat{M}_t$ is reduced after the second step at $\sim$140 s, which clearly matches forthcoming

decrease in the yield sensor reading $\dot{m}_y$. The same correlation is observed from feederhouse sensor to the grain flow estimates and yield sensor reading for the curved response to the last increase in forward speed after ~ 180 s. The fourth plot shows the internal observer states for local crop density $\hat{M}_t$ and grain ratio $\hat{\Gamma}_{p,g}$. No larger variations in the $\hat{M}_t$ and $\hat{\Gamma}_{p,g}$ estimates are observed during the sequence.

4   Load Detection

In order to enable and disable the observer measurement update in (12) and one-step-ahead prediction in (10) a fast and robust method is desirable. A change detection from un-loaded to a loaded condition can easily be tested using the tare sensor reading of the un-loaded state ($\bar{\alpha}$ and $\bar{\dot{m}}_y$) with appropriate thresholds. A fast detection from the loaded to an un-loaded condition, and detection of temporary inaccuracies in the sensor readings are more challenging due to the system dynamics. The cumulative sum control chart (CUSUM) is utilised to observe change detections of load on the feederhouse throughput sensor ($r_{Y1} = \alpha - \bar{\alpha}$), yield sensor ($r_{Y2} = \dot{m}_y - \bar{\dot{m}}_y$) as well as the observer innovation signals ($r_{E1} = \alpha - \hat{\alpha}$ and $r_{E2} = \dot{m}_y - \hat{\dot{m}}_y$). The CUSUM monitors change detection between two predefined signal levels (conditions) μ_0 and μ_1 using a statistical likelihood based measure for a signal with a normal distribution

$$N(\mu, \sigma) = \frac{1}{\sigma \sqrt{2\pi}} exp\left(-\frac{(x-\mu)^2}{2\sigma^2}\right). \qquad (19)$$

In Fig. 6 the histogram ($\mathcal{H}$) is plotted with a fitted normal distribution (19) for the residual signals r_{Y1}, r_{Y2}, r_{E1} and r_{E2}. The data is compiled from the steady-state periods in 27 data sets, compensated by subtracting the average from each period. The four signal histograms in Fig. 6 can be reasonable represented with the normal distribution.
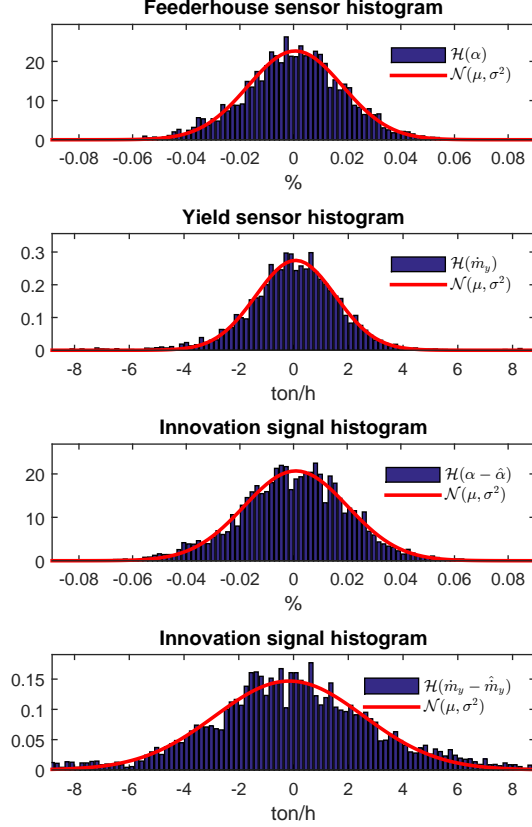
Figure 6: Histogram and normal distribution for CUSUM residuals signals. First plots shows feederhouse sensor (α), second yield sensor ($\dot{m}_y$), third feederhouse sensor innovation signal ($\alpha - \hat{\alpha}$), and fourth the yield sensor innovation signal ($\dot{m}_y - \hat{\dot{m}}_y$).

For each measurement cycle the sequential CUSUM state $g(k)$ is updated using

$$g(k) = g(k-1) + \frac{\mu_0 - \mu_1}{\sigma^2} - \left(r(k)\frac{\mu_0 + \mu_1}{2} \right), \tag{20}$$

for the residual signal $r(k)$ and standard deviation σ obtained from Fig. 6. The

average values μ_0 and μ_1 characterising the two conditions are obtained from experimental data. When (20) is updated, the condition flag H is set according to

$$
\begin{array}{lll}
\text{if } g(k) < h_0, & H = 0, & g(k) = h_0 \\
\text{if } g(k) > h_1, & H = 1, & g(k) = h_1 \\
\text{else,} & & \text{continue test.}
\end{array}
$$

For the residuals r_{Y1} and r_{Y2} the relative condition flags (H_{Y1}^+ and H_{Y2}^+) are set from g_{Y1}^+ and g_{Y2}^+. The innovation signal residuals r_{E1} and r_{E2} both have a positive and negative detection, hence H_{E1}^+, H_{E1}^-, H_{E2}^+ and H_{E2}^- are set from g_{E1}^+, g_{E1}^-, g_{E2}^+ and g_{E2}^- respectively. The observer correction flag is set from the boolean equation

$$H_{cor} = H_{Y1}^+ \wedge H_{Y2}^+ \wedge \neg H_{ino} \tag{21}$$

$$H_{ino} = H_{E1}^+ \vee H_{E1}^- \vee H_{E2}^+ \vee H_{E2}^- \tag{22}$$

$$H_{est} = \neg H_{E1}^- \wedge H_{Y1}^+ \wedge H_{Y2}^+, \tag{23}$$

where H_{ino} is the condition flag for change detection in the innovation signal. The detection threshold parameter h is computed from the two design parameters for probability of false detection P_F and probability of missing detection P_M, given in the equations

$$h_0 = \ln\left(\frac{P_M}{1 - P_F}\right), \qquad h_1 = \ln\left(\frac{1 - P_M}{P_F}\right). \tag{24}$$

Results In Fig. 7 a sequence of field data is shown, where a large deviation in the yield sensor reading occurs from 42 s till 50 s. Later the combine leaves and enters the crop row after 176 s and 201 s respectively.
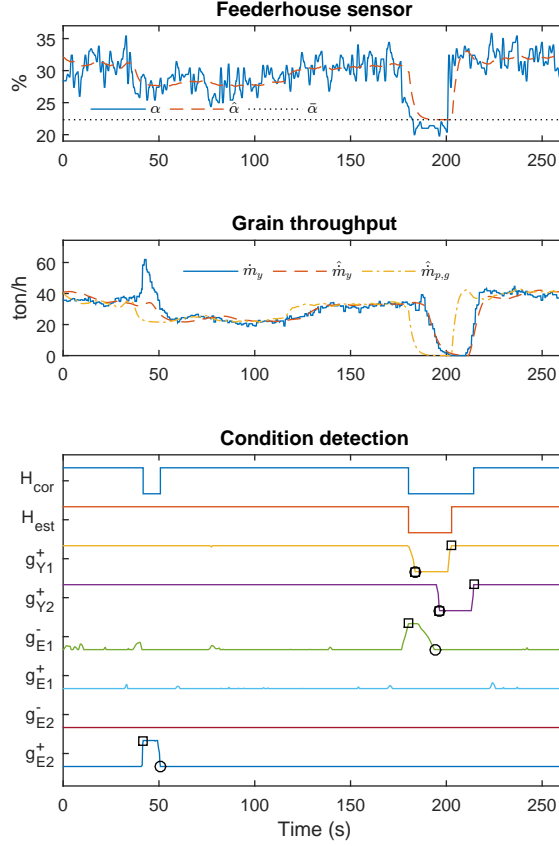
Figure 7: Field data with CUSUM sensor error detection and fast observer load detection. First plots shows the feederhouse sensor (α and $\hat{\alpha}$), second plots grain throughput ($\dot{m}_y$, $\hat{\dot{m}}_y$ and $\hat{\dot{m}}_{p,g}$), and third plots shows a normalised CUSUM condition detection.

The first plot shows the feederhouse sensor, where both the sensor reading α and estimate $\hat{\alpha}$ follow the variations in forward speed, indicating an approximately uniform crop density on the field. The second plot shows the actual yield sensor reading of $\dot{m}_y$ and the estimates $\hat{\dot{m}}_y$ and $\hat{\dot{m}}_{p,g}$. The third plot contains the CUSUM sequential change detection values and condition flags. The CUSUM detectors are denoted g^+ and g^- for the positive and negative change

detection of the normalised residuals between h_0 and h_1. The CUSUM value is marked with $g(k)$ □ or ○ when reaching the upper or lower thresholds respectively. After 42 s the yield sensor reading of $\dot{m}_y$ rapidly increases from 40 ton/h to 62 ton/h. Considering the yield sensor reading only, it is not possible to clarify whether the increase is due to increasing grain throughput or a temporary error to the reading. When comparing with the estimated feederhouse sensor reading α the spike is uncorrelated. The two signals α and $\dot{m}_y$ are not directly comparable due to the time delays and scaling. However when using the innovation signal r_{Y2} the change is detected almost instantly, disabling the observer measurement update (H_{est}), hence the estimated yield sensor reading $\hat{\dot{m}}_y$ remains unaffected. The feederhouse sensor reading starts decreasing after 176 s when leaving the crop row. Here g_{Y1}^+ and g_{E1}^- both detects the change to the un-loaded condition, hence disabling H_{cor}. Again the model based change detection g_{E1}^- provides a fast detection a few seconds before g_{Y1}^+ based on the static reference in the residual. The observer measurement update flag H_{cor} is enabled again after 215 s, when the load condition is detected on both H_{Y1}^+ and H_{Y2}^+.

5 Discussion

The observer results in Fig. 5 and Fig. 7 clearly showed the potential of utilising the experimental feederhouse throughput sensor in order to obtain a relative measurement of the incoming total throughput. The grain throughput estimate $\hat{\dot{m}}_{p,g}$ relies on the model to feed-forward the total throughput estimate in the observer, hence a good sensor is prerequisite for the precision of the grain throughput estimate.

Prospectively it would be of interest to predict other material flows using the throughput dependency, which would be advantageous for throughput control, whether it is an operator or a computer based system [3]. A prediction of the cleaning system load could also be utilised to ramp the fan speed up and down when entering and leaving a crop row respectively.

The current sensor configuration facilitates prediction of throughput changes as a function of forward speed, before the first actual measurement (α) of the throughput, due to the transport delay T_f. With some adjustment the grain throughput model in Fig. 2 could also leverage on forward looking sensor technologies for relative local crop density measurements, e.g. as presented in [13] and [11]. Hence the incoming crop mass could be measured before a change in the forward speed.

In the presented model the cutting width d_w was considered constant using the full width of the header. The assumption is true during the vast majority of the harvesting time. However during preparation of head land as well as entering and leaving crop rows in the field, the deviation from the full header assumption will affect the system as a disturbance. A measurement of the actual utilised header width is expected to increase the performance, e.g. an ultrasonic cutting width measurement of d_w was shown in [12].

6   Conclusion

The paper described an on-the-go model based method for throughput estimation in a combine harvester using sensor fusion. A grain flow model was given and the identification procedure for parameter estimation of steady-state relationship, time constants and time delays were outlined.

The observer showed good results predicting the grain throughput reading in advance of actual reading, using forward speed and an experimental feederhouse sensor design as additional inputs for sensor fusion. By estimating the local crop density it is possible to estimate grain throughput changes from the forward speed sensor faster and more precise than only using the feederhouse sensor.

A design using CUSUM change detection to fast and reliably detect system load condition and sensor errors was presented. It showed a faster detection of the feederhouse load reduction when leaving a crop row using the observer innovation signal rather than using the tare value obtained from the un-loaded condition. The CUSUM change detection also detected a temporary sensor error using the grain flow model and sensor fusion.

Acknowledgement

References

[1] Selcuk Arslan. A grain flow model to simulate grain yield sensor response. *Sensors*, 8(2):952–962, 2008.

[2] G. Craessaerts, T. Coen, and J. De Baerdemaeker. Identification of sensor faults on combine harvesters using intelligent methods. *IFAC Proceedings Volumes*, 38(1):75–79, 2005.

[3] J. De Baerdemaeker and W. Saeys. Advanced control of combine harvesters. *IFAC Proceedings Volumes*, 46(18):1 – 5, 2013. 4th IFAC Conference on Modelling and Control in Agriculture, Horticulture and Post Harvest Industry.

[4] A. Eggerl, H. Bösch, A. Bruns, and S. Wöbcke. Model-based development of control algorithms for optimizing combine prococess. In *VDI-MEG Kolloquium Möhdrescher*, volume 40, 2010.

[5] D. Hermann, M. L. Bilde, N. A. Andersen, and O. Ravn. A framework for semi-automated generation of a virtual combine harvester. *IFAC-papersonline*, 49(16):55–60, 2016.

[6] K. Maertens and J. De Baerdemaeker. Flow rate based prediction of threshing process in combine harvesters. *Applied Engineering in Agriculture*, 19(4):383–388, 2003.

[7] K. Maertens, P. Calmeyn, H. D. Kutzbach, and J. De Baerdemaeker. Throughput-loss relation in conventional combine harvesters - a comparison between stationary and mobile units. In *Landtechnik AgEng Proceedings*, pages 591–597, 2003.

[8] K. Maertens and J. De Baerdemaeker. Design of a virtual combine harvester. *Mathematics and Computers in Simulation*, 65(1-2):49–57, 2004.

[9] K. Maertens, J. De Baerdemaeker, and H. Ramon. Modelbased signal processing of a combine harvester. In *Proceedings of the 25th International Conference on Noise and Vibration Engineering, ISMA*, pages 1641–1646, 2000.

[10] K. Maertens, H. Ramon, and J. De Baerdemaeker. An on-the-go monitoring algorithm for separation processes in combine harvesters. *Computers and Electronics in Agriculture*, 43(3):197–207, 2004.

[11] K. Maertens, P. Reyns, J. De Clippel, and J. De Baerdemaeker. First experiments on ultrasonic crop density measurement. *Journal of Sound and Vibration*, 266(3):655–665, 2003.

[12] P. Reyns, B. Missotten, H. Ramon, and J. De Baerdemaeker. A review of combine sensors for precision farming. *Precision Agriculture*, 3(2):169–182, 2002.

[13] W. Saeys, B. Lenaerts, G. Craessaerts, and J. De Baerdemaeker. Estimation of the crop density of small grains using lidar sensors. *Biosystems Engineering*, 102(1):22–30, 2009.

[14] Lars Thylén and Donal P.L. Murphy. The control of errors in momentary yield data from combine harvesters. *Journal of Agricultural Engineering Research*, 64(4):271–278, aug 1996.

A.3   Article 3: Computer based Control of the Separation Process in a Combine Harvester

Title: Computer based Control of the Separation Process in a
                         Combine Harvester
Publication type: Conference Paper
Conference: EurAgEng VDI-MEG Conference, Hannover, Germany
Date: November 2017
Authors: Dan Hermann
                         Flemming Schøler
                         Morten Leth Bilde
                         Nils Axel Andersen
                         Ole Ravn

Computer based Control of the Separation Process in a Combine Harvester

D. Hermann*,** F. Schøler** M.L. Bilde** N.A. Andersen* O. Ravn*

* *Automation and Control Group, Dept. of Electrical Engineering, Technical University Denmark, Lyngby, Denmark*
** *AGCO A/S, Research and Advanced Engineering, Randers, Denmark*

Abstract

This paper addresses the design of a control system for a rotary threshing and separation system in a combine harvester. Utilising a distributed control architecture containing all observable crop flow parameters, the rotor speed is adjusted to maintain acceptable separation loss and grain damage using distributed impact sensors and a grain quality sensor (GQS). The GQS settling time for rotor speed changes is significantly reduced using a model based observer facilitating faster adjustment for grain losses in varying conditions.

1 Introduction

During a busy harvest it is desirable to utilise the full capacity of the combine harvester by operating at high throughput whilst maintaining an acceptable grain loss and grain quality. Hence the rotor speed in the threshing and separation system should be adjusted to separate grains from the chaff and straw particles with least possible loss and grain damage. In modern combine harvesters the default machine settings are pre-set in the control computer for each crop type and in some cases adjusted by the operator during harvest after manual inspection of the residue, whereupon site specific conditions are often ignored. Advances within sensor technologies and material flow models have procured a potential for automatic control of the machine settings, that is faster and more precise than a human operator. A sensor for grain quality was shown in [10], an acoustic impact type sensor strip for loss detection was presented in [1], an online separation loss monitoring algorithm in [8] and an online throughput prediction method in [6]. Section 2 presents a novel overall distributed control architecture and a novel rotor speed control scheme for the separation process. In Section 3 the design and implementation of the control system is described. Section 4 and Section 5 presents simulation and field test results.

2 Control Architecture

The threshing, separation and cleaning processes are assigned to numerous optimisation parameters for throughput, loss and quality, where many are even conflicting, see Fig. 1. In order to optimise the overall process it is vital to
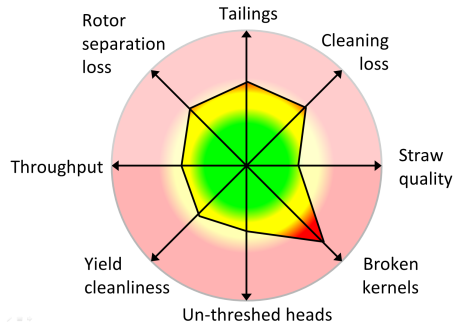
Figure 1: Overall optimisation problem for throughput, loss and quality parameters.
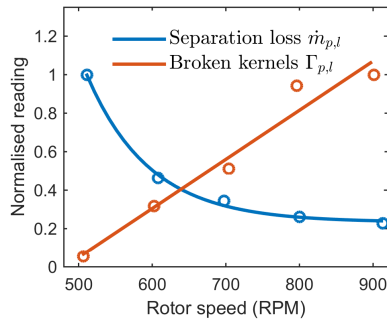
Figure 2: Acquired field samples of rotor separation loss and broken kernels.

understand the underlying interdependencies [2, 4, 5, 9] in the multiple-input-multiple-output (MIMO) system as most actuator adjustments affect multiple parameters. The overall optimisation problem can be formulated as one common cost function for all process parameters. However, in order to simplify the controller complexity a hierarchical architecture is chosen with distributed

control schemes for each actuator, where the control loop can be designed using standard methodologies for single-input-single-output (SISO) systems. This result in a shorter design and implementation phase as well as it reduces time for parameter tuning. For each actuator the dominant opposed process parameters are used to describe a cost function related to the overall optimisation goal. However some parameters are not directly available using state of the art process sensors, such as un-threshed heads or straw quality. The speed of the threshing and separation rotor is the dominating effect on the opposed parameters separation loss and grain damage; see field test samples in Fig. 2. An acoustic impact type sensor strip [1] with four membranes is used to measure the grain loss. Several sensor strips are placed strategically along the separation rotor to obtain the best possible measurement of the separation loss. The GQS is located in the top of the clean grain elevator measuring the relationship of broken kernels and materials other than grain (MOG) in the clean grain throughput. The windows size of the GQS captures approximately 100 grain kernels for each sample in small grain, i.e. a large number of images is required provide an accurate observation of grain damage significantly below 1%.

3 Rotor Speed Control Scheme

The objective for the rotor speed controller is to optimise the distributed cost function for separations loss and grain damage, i.e. balance the two opposed parameters. The closed-loop implementation is shown in Fig. 3. Here the estimate of the broken kernels $\hat{\Gamma}_{p,b}$ is subtracted from the separation loss $\dot{m}_{p,l}$ normalised with the yield sensor reading $\dot{m}_y$. A model based observer is designed to estimate grain damage $\hat{\Gamma}_{p,b}$ using GQS reading $\Gamma_{p,b}$ and rotor speed ω_r, see Fig. 4. A graphical user interface allows the operator to provide weights within a preselected range for grain loss $u_{p,l}$ and grain damage $u_{\Gamma,b}$.
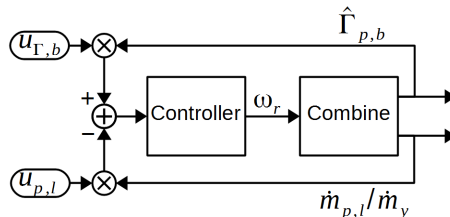

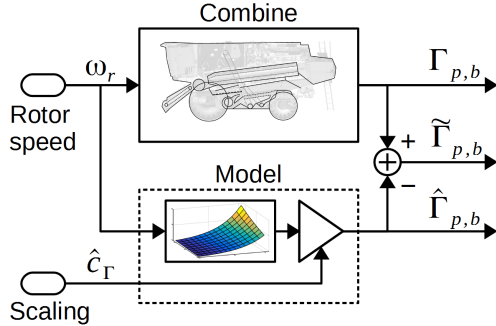Figure 3: Closed-loop control scheme.

Figure 4: Grain damage observer.

3.1 Model generation

The static grain damage model is obtained from multiple rotor speed actuator curves, similar to Fig. 1b, obtained from material samples or averaged GQS readings over several minutes for each rotor speed set point, [5]. The obtained data points are then fitted to the model describing the static grain damage from rotor speed, given by $\Gamma_{p,b} = c_\Gamma \exp(p_\Gamma \omega_p)$.

3.2 Observer design

The Luenberger observers state-space vector $x = [c_\Gamma, \ \omega_p]^T$ is given by the model scaling parameter c_Γ and ω_p, the filtered state of the input vector $u = \omega_r$. The state ω_p is filtered with the time constant τ_p characterising the threshing and separation system dynamics. The continuous time state-space model is given by

$$\dot{x} = f(x) = \begin{bmatrix} \dot{c}_\Gamma \\ \dot{\omega}_p \end{bmatrix} = \begin{bmatrix} \sigma_c^2 \\ a_p \omega_p + b_p \omega_r \end{bmatrix} \quad \text{and} \quad \Gamma_{p,g} = y = h(x) = c_\Gamma \exp(p_r \omega_p)$$

for the zero-mean white noise variance σ_c^2, threshing and separation system dynamics a_p and b_p as well as the grain damage loss model parameter p_Γ. The GQS has a varying sample time T_{GQS} as it relies on a material flow in the clean grain elevator, correct paddle sample synchronisation and image processing time. For each GQS measurement update, the estimate is updated using $\hat{x}(k+1) = F\hat{x}(k) + Gu(k) + K(y - \hat{y})$, else the estimate is predicted according to $\hat{x}(k+1) = F\hat{x}(k) + Gu(k)$.

4 Simulation Results

The observer and closed-loop control system is tested by means of simulation, using a virtual combine [3, 5, 7]. The virtual combine facilitates simulation of all actuators inputs (u), states (x) and crop flow sensor readings (y). Fig. 5 shows an open-loop (a) and closed-loop (b) simulation in soybeans for observer and controller verification respectively. In Fig. 5a the first plot row shows the
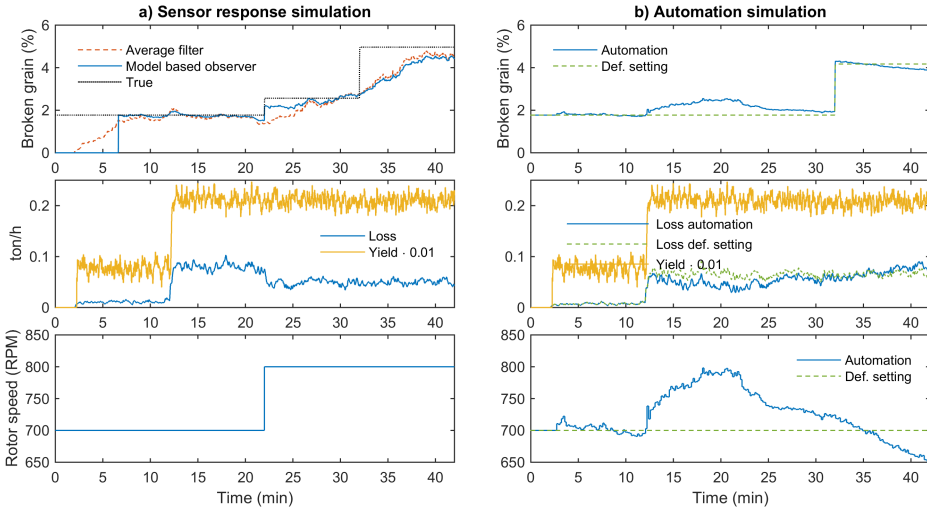
Figure 5: Simulation of separation process with loss and grain damage sensors. Fig. 5a shows a simulation of the two observers for broken grain in open-loop. Fig. 5b shows a simulation with the closed-loop rotor speed controller.

estimated and true percentage of broken kernels. Second plot the estimated separation loss $\dot{m}_{p,l}$ and yield sensor reading $\dot{m}_y$, and third plot the rotor speed ω_r. The combine enters crop after 2 min and all estimates are initialised after 7 min. After 12 min the throughput increases and causes a separation loss increase. Rotor speed is increased after 22 min, reducing separation loss and increasing grain damage. Notice the rapid response from the model based observer compared to the average filter. After 32 min a change (disturbance) in the field conditions increases the grain damage significantly. Fig. 5b shows a similar sequence, except the operator optimisation focus ($u_{\Gamma,b}$ and $u_{p,l}$) is adjusted after 22 min. The controller increases the rotor speed as the separation

loss increase with throughput after 12 min. After 22 min the operator user input changes focus towards separation loss, causing the rotor speed to increase. When the disturbance in field conditions causes increased grain damage after 32 min. the rotor speed is reduced to maintain the control balance.

5 Field Test Results

In Fig. 6 field test sequence from barley is shown with same row division as in Fig. 5.
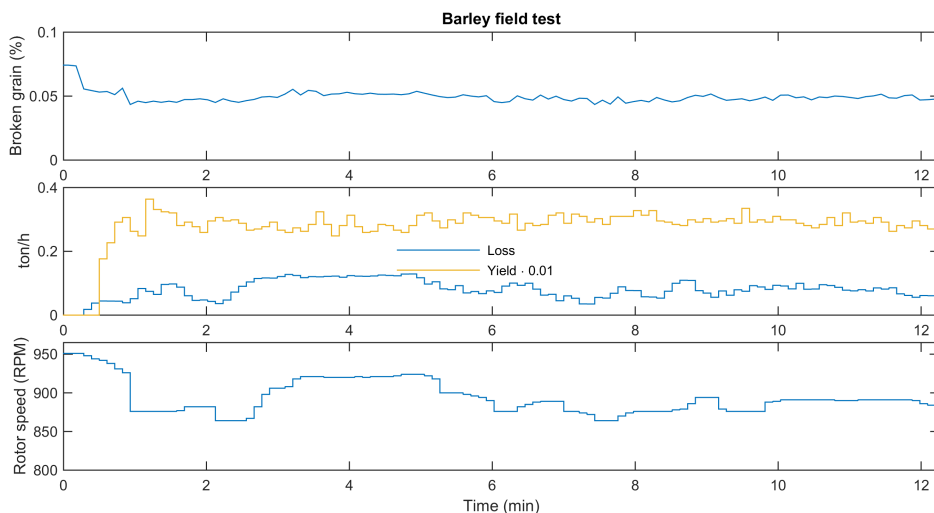
Figure 6: Field test results for rotor speed controller for barley.

In Fig. 6 the combine enters barley after 20 sec, with a high initial rotor speed which is rapidly decreased. The combine is operating in consistent yield density but varying separation loss. A increase in separation loss is observed between two and six minutes of operation, where the rotor speed is temporarily increased to reduce separation loss, causing a minor increase in broken kernels.

6 Conclusion

The paper described the distributed control architecture derived from the observable optimisation objectives. The rotor speed control scheme was presented explaining the interaction from separation loss and grain damage as well as operator interaction. Model generation and observer design was presented in order to reduce the settling for the GQS grain damage observation. Simulation showed a reduction of the maximum separation loss and grain damage. Results from full scale field tests verified the actuator response to varying crop conditions. The automatic adjustment of the grain damage and separation loss balance indicates a significant improvement of the overall threshing and separation system performance.

Acknowledgement

References

[1] N. Butts and M. Bremer. Material and distribution sensor (mads) for combine material flow. In *Landtechnik AgEng Proceedings*, pages 591–597, 2017.

[2] G. Craessaerts, W. Saeys, B. Missotten, and J. De Baerdemaeker. A genetic input selection methodology for identification of the cleaning process on a combine harvester, part i: Selection of relevant input variables for identification of the sieve losses. *Biosystems Engineering, Biosyst. Eng, Biosyst Eng, Biosystems Eng*, 98(2):166–175, 2007.

[3] A. Eggerl, H. Bösch, A. Bruns, and S. Wöbcke. Model-based development of control algorithms for optimizing combine prococess. In *VDI-MEG Kolloquium Möhdrescher*, volume 40, 2010.

[4] T. Freye. *Untersuchungen zur Trennung von Korn-Spreu-Gemischen durch die Reinigungsanlage des Mhdreschers*. Ph.d. thesis, Universitt Hohenheim, 1980.

[5] D. Hermann, M. L. Bilde, N. A. Andersen, and O. Ravn. A framework for semi-automated generation of a virtual combine harvester. *IFAC-papersonline*, 49(16):55–60, 2016.

[6] D. Hermann, M. L. Bilde, N. A. Andersen, and O. Ravn. On-the-go throughput prediction in a combine harbester using sensor fusion. *Proceedings of the 2017 Ieee Conference on Control Technology and Applications*, pages 67–72, 2017.

[7] K. Maertens and J. De Baerdemaeker. Design of a virtual combine harvester. *Mathematics and Computers in Simulation*, 65(1-2):49–57, 2004.

[8] K. Maertens, H. Ramon, and J. De Baerdemaeker. An on-the-go monitoring algorithm for separation processes in combine harvesters. *Computers and Electronics in Agriculture*, 43(3):197–207, 2004.

[9] P. Miu. *Combine Harvesters Theory, Modeling, and Design.* CRC Press, 2016.

[10] C. Wallays, W. Saeys, and J. De Baerdemaeker. Material other than grain and broken grain sensor for combine harvesters. In *Landtechnik AgEng Proceedings*, pages 373–378, 2007.

A.4 Article 4: Design of Laboratory Environment for Development of Cleaning System

Title:	Design of Laboratory Environment for Development of Cleaning System
Publication type:	Conference Paper
Conference:	EurAgEng VDI-MEG Conference, Hannover, Germany
Date:	November 2017
Authors:	Dan Hermann
	Flemming Schøler
	Morten Leth Bilde
	Nils Axel Andersen
	Ole Ravn

Design of Laboratory Environment for Development of Cleaning System Automation

D. Hermann[⋆,⋆⋆] **F. Schøler**[⋆⋆] **M.L. Bilde**[⋆⋆] **N.A. Andersen**[⋆] **O. Ravn**[⋆]

[⋆] *Automation and Control Group, Dept. of Electrical Engineering, Technical University Denmark, Lyngby, Denmark*
[⋆⋆] *AGCO A/S, Research and Advanced Engineering, Randers, Denmark*

Abstract

This paper addresses the design of a laboratory environment for research and development activities used for automating the cleaning process in a combine harvester. The aim is to facilitate closed-loop automation test runs with extended duration. By utilising individual MOG and grain feeding units as well as recirculating the biomass material any combination of these occurring in an actual field can be simulated in the laboratory.

1 Introduction

Development of a closed-loop control system for fan speed and sieve openings in a combine harvester cleaning system requires extensive test with material collection for system modelling as well as sensor and control scheme verification. Acquiring material samples during actual field tests are often subject to large variations due to varying local field conditions causing low repeatability. Additionally it is not possible to control the cleaning throughput of material other than grain (MOG) during field experiments, which is the dominant variable for grain loss.

Previous laboratory setups had limited total test time either due to length of the conveyor belt using manual material distribution or due to reservoir capacity using automated feeding.

It was shown by [7] that it was possible to build a MOG feeding system with a high repeatability ($R^2 = 0.99$). Later [6] showed that the cleaning loss could be continuously measured as an absolute quantity by collecting all the residue flow continuously and post cleaning a sub-flow in a cyclone separator.

By complementing field data collection with laboratory data collection one avoids the dependency on machine availability and limited harvest windows as well as variations from whether, crop and local field conditions. The laboratory provides a solid basis for elementary verification with a large number

of material samples and high repeatability, which is difficult to acquire during field experiments. Performance evaluation and control scheme comparison is advantageously conducted in the laboratory, where after the final verification and robustness to varying biological parameters should be conducted in the field.

This paper will present the design of a system able to continuously feed grain and MOG material to a cleaning system. An analysis of the required excitation variables and measurement variables is given in Section 2. Design of the material feeding unit, material recirculation, test stand and sampling is described in Section 3. Results for feeding accuracy as well as a comparison between laboratory and field data is provided in Section 4.

2 Analysis

2.1 Cleaning System Optimisation Goals

The cleaning process is a complex process with tightly coupled interdependencies. Hence, it is important to sample the grain and MOG components of the residue (grain loss), tailings and clean grain material flows. The material samples are used to investigate actuator, material and sensor interdependencies for model generation and performance evaluation [4].

2.2 System Excitation

The MOG throughput and moisture content are the dominant non-controllable extrinsic parameters affecting the separation performance in the cleaning system [5, 1, 3, 2]. The continuous feeding unit should reproduce the variations in local crop conditions to provide any combination of MOG and grain within the nominal range for the cleaning system. However on-line excitation of the moisture content in grain and MOG is not practical, hence all material must be affected prior to any test.

2.3 Design of Experiments

Design of experiments is crucial in the evaluation process of different control methodologies and for parameter tuning. Hence the possibility to repeat sequences with equivalent excitation of total throughput and material composition provide a solid foundation for performance evaluation. The continuous flow test facilities will primarily be used for these categories

- **Single run:** cleaning system performance evaluation and modelling

- **Continuous run:** long duration runs for closed-loop automation testing

For single test runs the grain and MOG reservoirs should contain sufficient biomass to complete a 2 minute test. For long automation test runs it is not practical to increase the reservoir size accordingly, hence the biomass material will be re-circulate to extend the test duration.

3 Laboratory Design

The aim is to design laboratory test facilities that allow control of total material throughput and MOG ratio in a controllable environment with high repeatability.

3.1 Cleaning System

The cleaning system is mounted in a frame facilitating lateral and longitudinal excitation using a single pivot point in the front end and two vertical actuated points in the left and right rear end. The test stand is additionally equipped with a yield sensor, moisture sensor, grain quality sensor, infra-red tailings volume sensor as well as impact type sensors for loss, tailings and upper sieve distribution.

3.2 Biomass Feeding

The largest single challenge in the overall laboratory setup is to provide continuous MOG feeding, as the MOG material is challenging to handle and easily can build up in lumps at various locations causing material blockage. However [7] showed good performance with a novel concept for MOG feeding, where the MOG in the feeding unit was constantly kept in motion and the provided throughput depends on the speed of the feeding chain conveyor and the opening to a scraper conveyor. A somewhat similar concept is utilised in design of the MOG feeder, Fig. 1. A constant relationship between the conveyor speed and the MOG feeding rate can be maintained when the MOG feeding buffer level is kept within a specified range. The grain feeding unit is designed as a large grain tank with a funnel shaped bottom where the material layer is kept at a constant height. The grain throughput is proportional to the conveyor belt speed. The grain material is delivered on top of the MOG layer before the final conveyor belt is feeding material into the cleaning system.
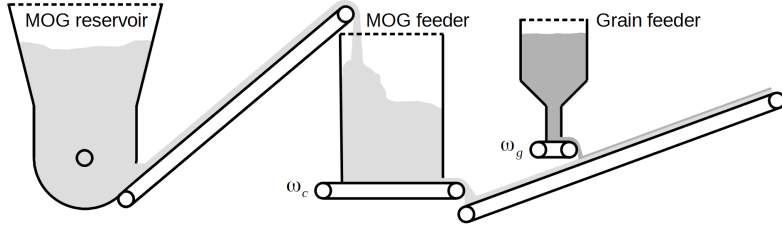
Figure 1: Feeding system for grain and MOG biomass.

3.3   Material Recirculation

A material re-circulating system is designed in order to extend the run time for automation testing, see Fig. 2. The MOG reservoir, MOG feeder and grain feeder are the individual units forming the overall biomass feeding system in Fig. 1. The re-circulation system consists of the residue collection unit located after the cleaning system as well as the MOG and grain return conveyor belts that transport the material back to the MOG and grain reservoirs respectively. When running single tests, the continuous mode can be used to clean the material by feeding the material grain or MOG reservoirs individually through the cleaning system at a low throughput where a high separation performance obtained. Fine cut straw is used to simulate the MOG material instead of collecting actual MOG consisting of chaff and straw pieces, as these are not available in the required quantities for laboratory testing.

Figure 2: Overall continuous laboratory material flow with material recirculation.

3.4 Material Sampling

When the cleaning system has reached steady-state in single run mode material samples are acquired from the residue, tailings and clean grain material flows. The sampling system is designed so material samples can be acquired in continuous mode during automation tests as well, in order to compare performance improvements for the automation system.
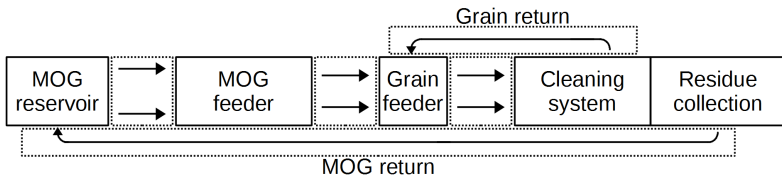
4 Results

The MOG and grain feeding units are evaluated by sampling material on the conveyor belts just before the cleaning system with sample lengths of 1m. The results are shown in Fig. 3, where a coefficient of determination of $R^2 = 0.99$ and $R^2 = 1.00$ are obtained for the MOG and grain feeder respectively. The accuracy is considered satisfactory.

In order the verify that the laboratory environment represents actual field experiments, the aim is to see the similar trends from actuators to material flow and from material flow to sensor readings. It is not expected to obtain an exact match of the measured material flows between field and laboratory experiments, as these are known to vary significantly from field to field due to various non-observable biological parameters. In Fig. 4 an example for comparison of grain
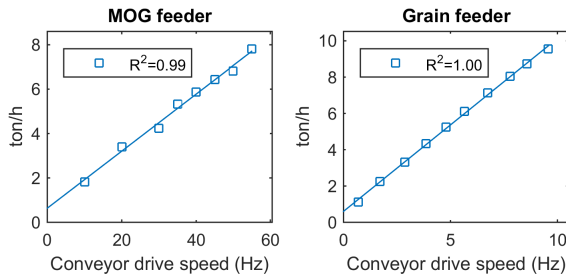
Figure 3: Evaluation of feeding system for grain and MOG biomass.

loss, tailings grain and tailings MOG material flows are shown as a dependency of fan speed at a similar throughput. Each point represents a 10 s material sample. It is vital that the three dominant phases of packed bed, fluidised and air borne described by [3] are obtainable. The packed bed occurs at low fan speeds where the grain kernels are travelling on top of a MOG mat on the upper sieve
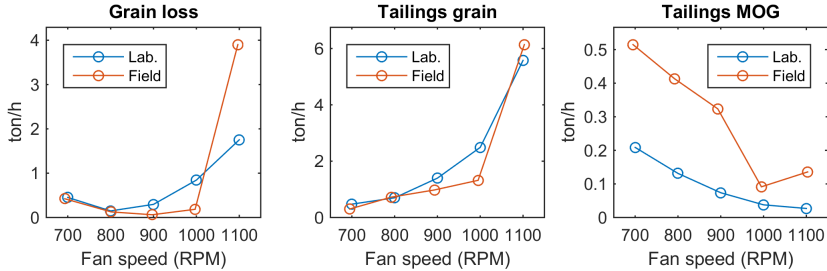
Figure 4: Comparison of field and laboratory test results.

(sloughing loss), fluidised where the grain loss is lowest and the air borne phase where the kernels become air borne, hence not segregated though the upper sieve (blowing loss). The three phases are present in both the field and laboratory data. For the tailings grain and MOG throughput an exponential increase and a roughly linear decrease dependency to fan speed are represented respectively in both the field and laboratory data.

5 Conclusion

An analysis of the laboratory set-up required for closed-loop automation test was conducted, showing the need to run short tests for performance evaluation, modelling and sensor evaluation as well as long duration runs for closed-loop automation testing and verification.

The overall design of the biomass feeding system and cleaning system test stand with material sampling and re-circulation was described. The biomass feeding showed a reasonable good accuracy with a coefficient of determination at $R^2 = 0.99$ and $R^2 = 1.00$ for MOG and grain respectively.

Evaluation of trends for grain loss, tailings grain and tailings MOG dependency on fan speed showed good resemblance between acquired material samples from field and laboratory.

The continuous cleaning system laboratory facilities are expected to provide a significant advantage in the design and verification process for state of the art automated cleaning systems as well as future generations to come.

Acknowledgement

References

[1] G. Craessaerts, W. Saeys, B. Missotten, and J. De Baerdemaeker. A genetic input selection methodology for identification of the cleaning process on a combine harvester, part i: Selection of relevant input variables for identification of the sieve losses. *Biosystems Engineering, Biosyst. Eng, Biosyst Eng, Biosystems Eng*, 98(2):166–175, 2007.

[2] L. Fliege. *Einfluss der Hangneigung auf die Leistungsfhigkeit von Reinigungsanlagen im Mhdrescher.* Ph.d. thesis, Universitt Hohenheim, 2010.

[3] T. Freye. *Untersuchungen zur Trennung von Korn-Spreu-Gemischen durch die Reinigungsanlage des Mhdreschers.* Ph.d. thesis, Universitt Hohenheim, 1980.

[4] D. Hermann, M. L. Bilde, N. A. Andersen, and O. Ravn. A framework for semi-automated generation of a virtual combine harvester. *IFAC-papersonline*, 49(16):55–60, 2016.

[5] P. Miu. *Combine Harvesters Theory, Modeling, and Design.* CRC Press, 2016.

[6] M. Schwarz, S. Häberle, and S. Böttinger. Kornverlusterfassung an getreidevorreinigern. *Landtechnik*, 67(1):42–46, 2012.

[7] M. Schwarz, W. Schulz, J. Baumgarten, and S. Böttionger. Chaff feeding concept for laboratory tests of combine harvester cleaning units. *Landtechnik Agricultural Engineering*, 65(5):376–379, 2010.

A.5 Article 5: Model-based Cleaning Fan Speed Control in a Combine Harvester, Part I: Identification and Optimisation

Title:	Model-based Cleaning Fan Speed Control in a Combine Harvester, Part I: Identification and Optimisation
Publication type:	Journal Paper
Journal:	Elsevier, Biosystem Engineering
Date:	March 2018
Authors:	Dan Hermann
	Morten Leth Bilde
	Nils Axel Andersen
	Ole Ravn

Model-based Control of Cleaning Fan Speed in a Combine Harvester
Part I: Identification and Optimisation

D. Hermann⋆,⋆⋆ M.L. Bilde⋆⋆ N.A. Andersen⋆ O. Ravn⋆

⋆ *Automation and Control Group, Dept. of Electrical Engineering, Technical University Denmark, Lyngby, Denmark*
⋆⋆ *AGCO A/S, Research and Advanced Engineering, Randers, Denmark*

Abstract

The cleaning system fan speed in combine harvesters have traditionally been adjusted by manual inspection of grain loss in the field residue and tailings composition, which requires an experienced operator in order to maintain high performance. During operation the operator normally has grain loss sensors and a single tailings sensor for reference in the cabin which only provide an indication of the actual throughputs. In order to facilitate automatic adjustment of the fan speed a higher degree of transparency to the material throughputs and process understanding are required.

This article addresses the modelling process for the cleaning system and the design of a closed-loop fan speed control system in a combine harvester cleaning system using the tailings throughput. The aim is to generate a mathematical model of the material flow in the cleaning system that can be utilised for closed-loop fan speed control in conjunction with traditional sensor technologies. A material flow model is generated using material samples from laboratory test stands, which showed a dominating effect on grain loss from the material-other-than grain throughput and the longitudinal inclination angle. By means of simulation and optimisation it was possible to identify a regime characterising the fluidised phase of the cleaning system using the tailings throughput.

1 Introduction

Combine harvesters are harvesting various crop types under varying environmental conditions all over the world. The cleaning process should be adjusted continuously in order to optimise yield and crop quality. However actuator settings are often not accommodated due to lack of operator experience or information about the harvesting process. Hence there is a large potential to

automate the adjustment of the cleaning system actuators in order to increase the general efficiency of the combine harvester and reduce operator fatigue. However these processes are assigned to numerous uncontrollable biological variables where many of the optimisation parameters are even conflicting. Like loss, throughput, tailings and grain cleanliness.

The modelling of material flow in combine harvesters started with low order regression models primarily intended for performance evaluation of threshing and separation systems [40, 42, 26], as well as cleaning systems [30, 37]. The primary focus was to model separation distribution curves and material flow interdependencies to a single input variable, such as throughput, moisture content or inclination angle. However in order to implement a closed-loop control system it is necessary to obtain models that describe the observable variables that are desirable to control as well as the impact from dominating disturbances.

A new hill-side cleaning system test stand with automated feeding of grain and Material-Other-than-Grain (MOG) biomass as well as recirculation of residue biomass facilitates a large increase in the number of material samples possible to acquire as well as it facilitates closed-loop automation testing in the laboratory environment [23], which has previously not been possible. Advances within sensor technologies [16, 1, 2, 10, 8] and the development virtual combines [15, 29, 21] have provided an increased transparency into the process parameters along with the ability to simulate closed-loop control systems.

The last two decades the modelling effort has focused on model generation for material throughput estimation [3, 27], separation loss [28], cleaning loss [10], yield cleanliness [10] and grain damage [16, 22]. Which greatly has contributed to the overall understanding of the material flow in the combine harvester and facilitated the required observability to enable automatic adjustment the process actuators.

The aim is to obtain a total material flow model in order to increase the general process knowledge as well as facilitate Hardware-In-the-Loop (HIL) simulations and estimation of non-observable process variables. The model inputs are material flows, biological parameters and actuator settings, and the outputs will be internal material flows, material residue flows and sensor readings. The experimental setup and data acquisition is shown in Section 2.1 with an analysis of the interdependencies in Section 2.2. Based the acquired data the model structure and generation process of the material flow models is outlined in Section 2.3. In Section 2.4 the material flow models are used to obtain an analytical model of the tailings composition characterising the process regime of the cleaning system providing low grain loss. This facilitates a novel fan speed control system where the fan speed is controlled using the tailings grain

composition.

Table 1: List of variables.

Variable	Unit	Description
d_c	mm	Upper sieve spacing
d_s	mm	Lower sieve spacing
$\dot{m}_{c,c}$	ton/h	Cleaning MOG throughput
$\dot{m}_{c,g}$	ton/h	Cleaning grain throughput
$\dot{m}_{c,l}$	ton/h	Cleaning grain loss
$\dot{m}_{c,r}$	ton/h	Cleaning MOG residue
$\dot{m}_f$	ton/h	Total throughput
$\dot{m}_{p,c}$	ton/h	Threshing and separation MOG sep. throughput
$\dot{m}_{p,g}$	ton/h	Threshing and separation grain sep. throughput
$\dot{m}_{p,l}$	ton/h	Threshing and separation grain loss
$\dot{m}_{p,r}$	ton/h	Threshing and separation MOG residue
$\dot{m}_{t,c}$	ton/h	Tailings MOG throughput
$\dot{m}_{t,g}$	ton/h	Tailings grain throughput
$\dot{m}_{y,c}$	ton/h	Clean grain MOG throughput (cleanliness)
$\dot{m}_{y,g}$	ton/h	Clean grain throughput
ω_f	RPM	Fan speed
ϕ	^{o}	Chassis longitudinal inclination angle (pitch)
θ	^{o}	Chassis lateral inclination angle (roll)
v	m/s	Combine forward speed sensor
$y_{c,l}$		Cleaning grain loss sensor
$y_{t,g}$		Tailings grain throughput sensor
$y_{t,v}$	V	Tailings volume sensor
$y_{y,g}$		Yield (clean grain throughput) sensor
$y_{\Gamma,c}$	%	Cleanliness (clean grain throughput) sensor

Nomenclature

2 Material and Methods

The combine harvester crop processing consists of three main modules, the threshing, separation and cleaning processes. The threshing process separates

the grain kernels from the ears/pods of the straw and the separation process segregates the remaining kernels from the straw material prior to leaving the combine as residue material. This yield a mixed material flow of grain and MOG to be separated in the cleaning system, see Figure 1. The MOG segregation from
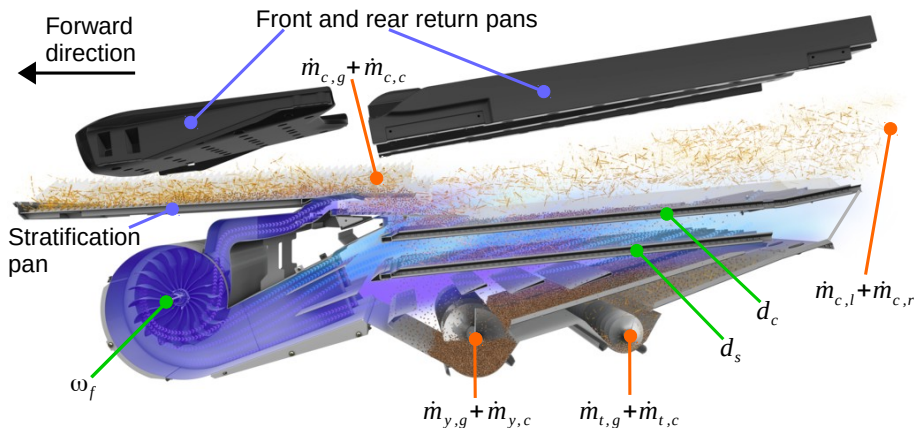
Figure 1: Cleaning system cross section with material flows.

the threshing and separation system depends primarily on the total throughput, rotor speed, concave clearance and straw humidity [24]. The purpose of the cleaning process is to keep the low-density MOG particles airborne thus the high-density kernels can penetrate the sieves and be collected in the grain bin. The cleaning process in Figure 2, is characterised by the *flight phase* where the kernels are air borne when fan speed it too high, the *fluidised phase* where all MOG material is airborne, and the *packed phase* where the MOG material is travelling of the upper sieve significantly reducing the grain segregation when fan speed is too low[18].

State-of-the-art cleaning systems utilise a two sieve construction, where ideally the function of the upper sieve is to segregate all kernels and lower sieve purpose is to avoid segregation of MOG to the clean grain product. The tailings throughput is the material segregating the upper sieve but not the lower sieve which is returned either directly into the cleaning system or the threshing system, creating an internal loop.

The combination of fan speed and sieve settings to maintain the fluidised phase depends largely on the MOG throughput in the cleaning system, how-
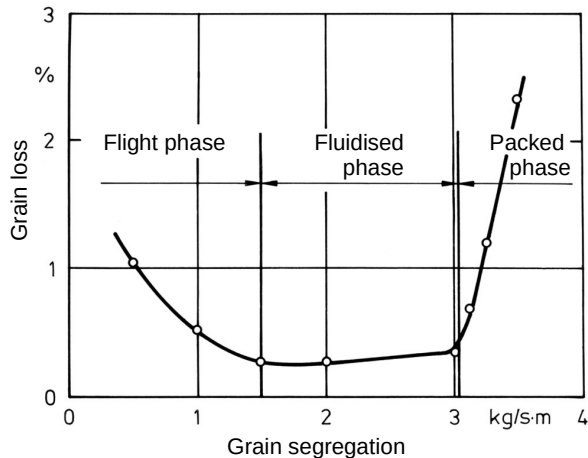
Figure 2: Cleaning sieve segregation model [18]

.

ever no sensor technologies are available for a direct measurement of the MOG throughput delivered to the cleaning system and traditional cleaning loss sensor are know to only provide a indication of the actual loss [13, 34]. However the tailings throughput is known to provide essential information concerning the cleaning separation process as it can be considered the residual material of the cleaning process. For the same reason many combines provide a physical window to the tailings return in the cabin for the operator. Using an impact sensor and a proximity volume sensor an estimate of the tailings composition and throughput can be obtained. These are used in combination with a reference signal from a model based set-point estimator to maintain the fluidised phase of the cleaning system.

A cost function including to tailings grain, tailings volume and grain loss readings are used by [39, 41, 32], i.e. reducing the tailing throughput components is a dedicated goal equally to the grain loss. The proposed method uses a predetermined model-based reference for the tailings grain composition, which is optimised for the cleaning system to operate in the fluidised phase in order to reduce grain loss.

For test purposes a laboratory cleaning system test stand is available as well as a mobile combine harvester, both facilitating material sampling of grain

and MOG components of residue, tailings and clean grain material flows. The model is generated using the framework described in [21] using a combination of material samples and sensor data obtained both from laboratory and field tests.

2.1   Experimental Setup and Data Collection

In order to map the material flow interdependencies in the cleaning system it is vital to obtain data sets with sufficient excitation of all actuators as well as capturing the relevant material flows. It is convenient to acquire large amounts of sensor data on an actual combine in the field, however all sensors except the yield sensor provide a relative sensor reading depending on the disturbances originating from spatial and temporal varying non-observable biological parameters, i.e. local field conditions. In order to fully understand the relationship from the actuator (input) to the actual material flow (state) as well as the relationship from material flow (state) to the sensor reading (observation) it is required to obtain material flow samples from residue, augers or elevators in the combine harvester. However acquiring samples in the field is time consuming and the composition of the fed material is not controllable. Utilising laboratory test stands facilitate high repeatability and controllability of the throughput into the system.

2.1.1   Cleaning System Test stand

The experimental setup is a full scale cleaning system mounted in a frame facilitating excitation of lateral and longitudinal inclination angles using a single pivot point in the front end and two vertical actuated points in the left and right rear end. The test stand is equipped with a yield sensor, grain moisture sensor, grain quality sensor, infra-red tailings volume sensor as well as impact sensors for loss, tailings and upper sieve distribution. A automatic feeding system provides full scale feeding of MOG and grain biomass to the cleaning system, which facilitate recreation of actual variations from the field in the laboratory [23]. A MOG biomass feeding unit is used, where the MOG in the feeding unit was constantly kept in motion [36] and the provided throughput depends on the speed of the feeding chain conveyor (ω_c) and the opening to a scraper conveyor, see Figure 3. A constant relationship between the conveyor speed and the MOG feeding rate can be maintained when the MOG feeding buffer level is kept within a specified range. The grain feeding unit is designed as a large grain tank with a funnel shaped bottom where the material layer is kept at a constant height.

Table 2: Design of experiments excitation and sample parameters.

Configurable	Sampled
Fan speed (ω_f)	Grain loss ($\dot{m}_{c,l}$)
Upper sieve (d_c)	MOG residue ($\dot{m}_{c,r}$)
Lower sieve (d_s)	Tailings grain ($\dot{m}_{t,g}$)
Grain throughput ($\dot{m}_{c,g}$)	Tailings MOG ($\dot{m}_{t,c}$)
MOG throughput ($\dot{m}_{c,c}$)	Clean grain ($\dot{m}_{y,g}$)
Longitudinal inclination angle (ϕ)	MOG in clean grain ($\dot{m}_{y,c}$)
Lateral inclination angle (θ)	
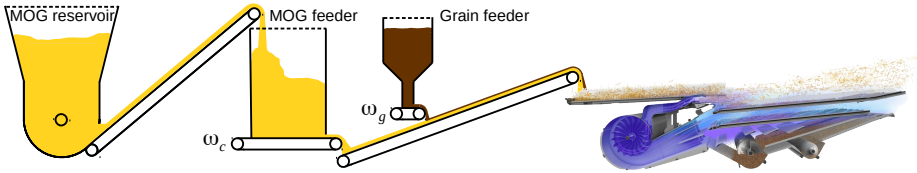
Figure 3: Laboratory cleaning system test stand with continuous feeding.

The grain throughput is proportional to the conveyor belt speed (ω_g). The grain material is delivered on top of the MOG layer before the final conveyor belt is feeding material into the cleaning system.

2.1.2 Design of Experiments

A series of designed experiments were conducted in the laboratory test stand using variable rates of grain and MOG to span both the range of total throughput and MOG ratio delivered under various conditions from the threshing and separation system. The variable biomass throughput was combined with excitation of fan speed as well as the upper and lower sieve opening, see excitation variables and sampled variables in Table 2. The data were collected from individual test runs, where a 10 s material sample was acquired after the cleaning system entered steady-state. The tailings flow was not returned to the cleaning system during the test. Material samples were acquired from residue, tailings and clean grain flows, which are subsequently cleaned in a post-process to obtain individual measures of the grain and MOG components. Chopped straw is utilised for MOG it is difficult to obtain sufficient quantities from field collection.

2.2 Data Analysis

Several hundred data points has been collected in the cleaning system test stand to generate material flow models and verify sensor performance in wheat. Additionally a number of actuator curves has been acquired from field test data, which primarily are used for verification. From the obtained data sets it is desirable to investigate the interdependencies from actuators settings (inputs) to the material flows (states), and from the material flows to sensor readings (observations). The obtained data sets are applicable for verification of controllability and observability of the combine harvester in general, hence it will form the basics for deciding the structure of the control system.

2.2.1 Actuator and Throughput Impact

A normalised relative grain array (RGA) [38] is shown in Table 3, which presents the interdependencies from actuators setting and cleaning system throughputs to the material cleaning loss ($\dot{m}_{c,l}$) and tailings throughputs ($\dot{m}_{t,g}$ and $\dot{m}_{t,c}$). The RGA is normalised with the range of the actuator and material flow, i.e. the indices are given by

$$g_{ij} = \frac{\sum_{k=1}^{n}(\mathbf{u_i}[k] - \bar{\mathbf{u}}_\mathbf{i})(\mathbf{x_i}[k] - \bar{\mathbf{x}}_\mathbf{i})}{\sum_{k=1}^{n}(\mathbf{u_i}[k] - \bar{\mathbf{u}}_\mathbf{i})^2} \cdot \frac{max(\mathbf{u_j}) - min(\mathbf{u_j})}{max(\mathbf{x_i}) - min(\mathbf{x_i})}. \tag{1}$$

Note the cross-correlation has a linear basis, whereas several of the relationships are known to be non-linear, hence the cross-correlation can vary considerable depending on the crop conditions and actuator excitation. Especially the relationship from fan speed ω_f to cleaning loss $\dot{m}_{c,l}$ is known to be non-monotonic.

Table 3: Normalised RGA for the cleaning system material throughputs.

	$\dot{m}_{c,l}$	$\dot{m}_{t,g}$	$\dot{m}_{t,c}$	$\dot{m}_{y,c}$
ω_f	0.18	0.48	−0.31	−0.99
d_c	−0.13	−0.09	0.19	0.49
d_s	−0.03	−0.18	−0.00	0.28
$\dot{m}_{c,g}$	0.07	0.09	0.25	0.00
$\dot{m}_{c,c}$	0.22	0.13	0.36	−0.04

The actuator impact is tightly coupled for all material flows desirable to control, thus each actuator has an effect on all material flows in the cleaning

system, however the material flows desirable to control generally have a dominating influence from two of the three actuators d_c, d_s or ω_f. The fan speed (ω_f) has the largest actuator impact on grain loss, tailings grain throughput and cleanliness, where the upper sieve spacing d_c clearly has a high impact on the cleaning loss $\dot{m}_{c,l}$ and tailings MOG throughput $\dot{m}_{t,c}$, and the lower sieve d_s has the highest effect on tailings grain throughput $\dot{m}_{t,g}$. The lower sieve has the lowest effect on the cleanliness, however this does greatly vary with the conditions. In the laboratory the MOG consist of chopped straw only, where it often contains large straw pieces and weed particles in the field. Thus the lower sieve is the primary actuator to adjust in order to reduce MOG particles in the clean grain throughput. Looking at the cleaning grain ($\dot{m}_{c,g}$) and MOG ($\dot{m}_{c,c}$) throughputs, the MOG clearly has a significantly higher negative effect of the performance, where loss and tailing components increases with the MOG load.

Hence to control the cleaning loss it is desirable to adjust fan speed or upper sieve opening, where tailings grain can be controlled from fan speed and lower sieve opening, and the tailings MOG component from fan speed and upper sieve opening [38].

The dominating effects from each actuator on the grain loss, tailings and cleanliness is roughly known by the experienced operator. Thus Table 3 represents the general actuator effect, where the models can be used to determine whether e.g. the fan speed, upper or lower sieve should be changed to accommodate a desired change in the tailings grain throughput. From the underlying data-set from Table 3 is it desirable to utilise non-linear models for observer design and actuator set-point estimation to reduce grain loss and increase cleanliness.

The impact on the cleaning loss and tailing throughputs is shown in Figure 4 for a five point fan speed curve from 700 RPM to 1100 RPM. The data points originate from the data-set used to obtain the results in Table 3. The curvature for the cleaning loss $\dot{m}_{c,l}$ is similar to that of the three phases shown in Figure 2, except that the fan speed on the horizontal axes is shown in Figure 4 where Figure 2 shows the grain segregation, which generally decreases for an increasing fan speed. The trend of the tailings grain throughput ($\dot{m}_{t,g}$) clearly follows the cleaning loss ($\dot{m}_{c,l}$) in the high fan speed range (ω_f) corresponding to the flight phase. The fan speed (ω_f) affects the tailings MOG throughput ($\dot{m}_{t,c}$) in the opposite direction causing a higher throughput in the low fan speed range, corresponding to the packed phase, however the slope of the tailings MOG throughput is not as steep af the cleaning loss. The aim is to utilise the two tailing throughput components to obtain the desirable balance characterising the fluidised phase, indicated on Figure 4 where the fan speed $\omega_r^\star$ yield the

minimum grain loss.
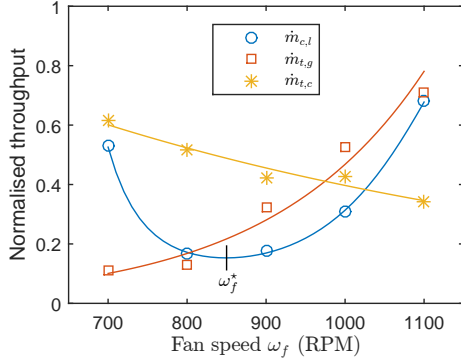
Figure 4: Fan speed dependency curve for cleaning loss and tailings return throughputs.

The loss and tailing throughputs in Figure 4 were obtained with a MOG load of 12 ton/h. In Figure 5 the grain loss $\dot{m}_{c,l}$, tailings grain $\dot{m}_{t,g}$ and tailings MOG $\dot{m}_{t,c}$ throughputs are shown for three different throughputs at respectively 6, 9 and 12 ton/h. The fluidised phase is only visible at the highest throughput of 12
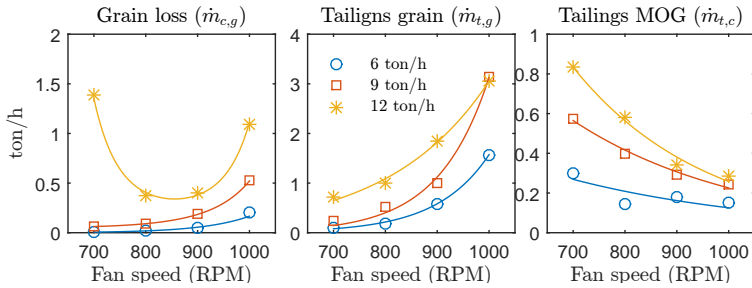
Figure 5: Fan speed curves with different MOG ($\dot{m}_{c,g}$) throughputs.

ton/h, which further complicates the detection of $\omega_f^\star$ as the grain loss originating from the packed phase varies drastically between the two highest throughputs. In theory $\omega_f^\star$ is located at the lowest fan speed when the packed phase is not present. However, uneven feeding can easily cause temporary throughput vari-

ations between the shown trends for 9 and 12 ton/h, thus in order to increase robustness the fan speed should be set some margin above $\omega_f^\star$ when the packed phase is not present. The rate of change for the grain loss when the packed phase occurs is not of same magnitude as the tailings throughputs, however both the grain and MOG throughputs are monotonic and increases with grain loss for the flight and packed phases respectively.

2.2.2 Inclination Impact

In order to obtain high performance from the cleaning system it is vital to adjust the fan speed to operate in the fluidised phase, where the MOG is airborne and the grain is segregated through the sieves. This process is very sensitive to the effect from lateral (θ) and longitudinal (ϕ) inclination which previously has been addressed in [37, 17, 7], however the effect from the fan speed and sieve openings was not modelled. Both longitudinal and lateral inclination variations in on the cleaning system has a significant effect of the cleaning losses, however the largest effect originate from the lateral inclination [17, 7].

For lateral inclination (θ) adjustment of fan speed and sieve openings has as negligible effect compared to the inflicted increase in grain loss originating from the lateral inclination. The effect from the lateral inclination has in practice been solved by adding additional actuation, e.g. lateral sieve oscillation [14], levelling cleaning sieves [35], redistribution of material from separation system till the grain pans using actuated rotor flaps [6], levelling the whole machine on the front axle [5], or passively by redistributing the material using curved return pans [4].

The fan speed is known to potentially reduce the effect from longitudinal inclination (ϕ) using feed-forward from the longitudinal inclination angle to the fan speed. In Figure 6 the cleaning loss is mapped with excitation of fan speed (ω_r) and longitudinal inclination angle (ϕ), where the lower (down-hill) and upper (up-hill) limit for the lateral inclination angle (ϕ) are $-6.1°$ (down hill) and $6.1°$ (up hill) respectively. All data-set were obtained with identical grain and MOG throughput.

The loss mesh is fitted to the measured data points marked with blue circles. It is clear that an acceptable loss can be maintained using linear feed-forward of from the lateral inclination angle to the fan speed,

$$\omega_f = f_\phi(\bar{\omega}_f, \phi) = \bar{\omega}_f + c\phi, \tag{2}$$

where $\bar{\omega}_f$ is the initial fan speed set-point from the operator or a control system and c the feed-forward rate from the longitudinal inclination angle, which is
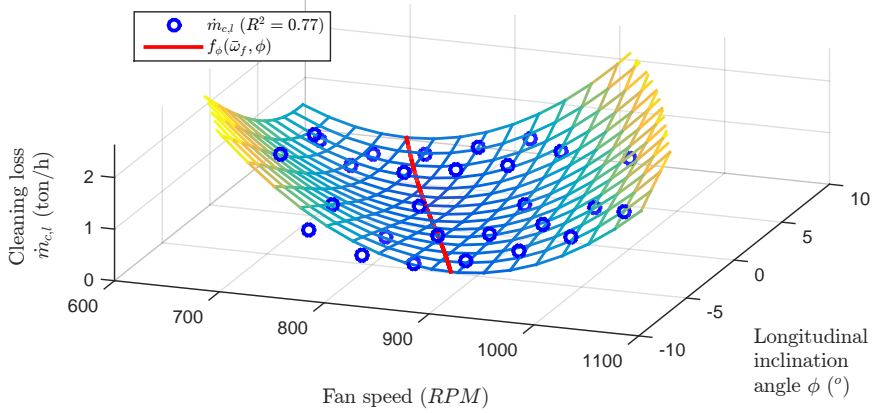
Figure 6: Cleaning grain loss for fan speed (ω_f) versus chassis lateral inclination angle (ϕ).

found by solving the optimisation problem

$$\underset{\bar{\omega}_f, c}{\arg\min} \quad f_{c,l}(\omega_f = f_\phi(\bar{\omega}_f, \phi), \phi) \quad \forall \quad \omega_f \in \mathbb{N}[\omega_{f,min} : \omega_{f,max}]. \tag{3}$$

The largest contribution to grain loss exist in the corners either with low fan speed and negative longitudinal inclination, or with high fan speed and positive longitudinal inclination, which can be linked to the packed and flight cleaning phases in Figure 2. The combination of low fan speed and the necessity to transport the MOG material in a steeper angle of $\phi = -6.1°$ against gravity causes a significant increase in grain loss. The opposite effect occurs at high fan speeds with the contribution in increased material conveying capability from gravity with the longitudinal inclination angle of $\phi = 6.1°$.

The closed-loop fan speed control system will in time reach a fan speed setting in the fluidised phase for varying longitudinal inclination, however by utilising the known effect from the longitudinal inclination angle to grain loss the control system can adjust the fan speed before the effect is observable on grain loss or tailings sensors, thus additionally reduce the cleaning grain loss.

2.3 Plant Model

The developed models are used for building virtual combine simulation tools, control system optimisation as well as observer design for throughput estimation in a closed-loop control system. All states are modelled as throughput in ton/h or percent. The model should have a flexible modular based structure where individually obtained datasets from threshing and separation system, and cleaning system can be combined, or a new sensor can be added from a dataset obtained later. As acquisition of material samples in both laboratory and field are time consuming and are known to provide a large number of outliers as well as being sensitive to disturbances from non-observable biological parameters, the chosen methodology should facilitate detection of outliers, verification of known material flow relationships and actuator interdependencies.

The material flow model of the combine harvesters is divided into four modules processing or transporting biomass: threshing and separation system, grain pans, cleaning system and return system, see Figure 7. All the material flow models are given at a single point of delivery indicated by the lines between modules.
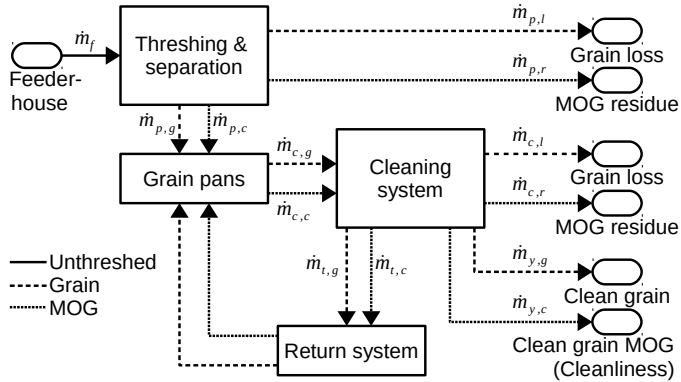
Figure 7: Combine material flow model block diagram.

A Weiner model structure is chosen where the dynamics are modelled by first order moving average filters and the non-linear interdependencies can be individually modelled for each material flow or sensor [31], see Figure 8. The acquired data from material samples are representing the various non-linear steady-state trends of the combine harvester, where dynamics are captured from
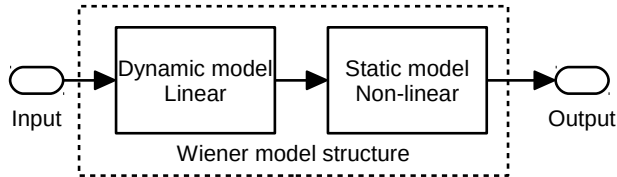
Figure 8: Wiener model structure

the sensor readings. The identification of dynamic parameters is treated in [21], where the remainder of this section will focus on identification of the static models only.

In literature polynomial based grey-box models were used to model steady-state material flow characteristics by [39, 32, 41] and Fuzzy logic by [9, 33, 11, 12]. In general various methods are available for modelling the non-linear interdependencies, e.g. grey-box model variants of polynomials, black-box approaches as non-linear Fuzzy modelling and non-parametric as K-Nearest Neighbours (KNN). The black-box approaches such as non-linear Fuzzy modelling has an intuitive representation of the process by charactering the process in to a number different regimes (discrete states) [31], however the models are generated using hidden states which are very difficult to troubleshoot and has a tendency of over-fitting for a low number of measurements. The KNN utilises a weighted average of the nearest observation in a measurement database, hence it does not require a fitting procedure as well as it is flexible to any non-linear trend, however KNN are generally outperformed by polynomial based models for low number of samples [19].

A polynomial based model structure was chosen as it facilitate a number of statistical tools for evaluation of model uncertainties and statistical parameters of the acquired data sets. Additionally it allows to update parameters fully or partially online [41, 22], if the data-set fulfils some predetermined criteria depending on the model structure, actuator excitation and sensor readings. In the model generation process it is necessary to ensure a number of constraints, where some originates in the polynomial structure and some by inequality constraint in the formulated optimisation problem. The material flow is modelled using relative gain function $f(p, x)$, which yield the ratio of the input flow u going to the output flow y, for the vector $\mathbf{x}$, containing actuator settings, material flows, disturbances and sensor readings,

$$y = f(\mathbf{p}, \mathbf{x})u. \tag{4}$$

149

This model structure ensures zero output flow when there is zero input flow. The general feasible constraints are listed with a physical description and a mathematical interpretation in Table 4, similar to the representation given in [28]. The general actuator and material flow interdependencies, also refereed to

Table 4: Definition of material flow model constraints and mathematical interpolation.

	Physical material flow constraint	Mathematical interpolation
1a	Negative material flows not possible	$f(\mathbf{p}, \mathbf{x}) \geq 0$
1b	Output flows cannot exceed input flows	$f(\mathbf{p}, \mathbf{x}) \leq 1$
2a	Output increases monotonically with input	$\frac{\partial f(\mathbf{p}, \mathbf{x}) u}{\partial u} \geq 0$
2b	Output decreases monotonically with input	$\frac{\partial f(\mathbf{p}, \mathbf{x}) u}{\partial u} \leq 0$
3a	Output flow increase more rapidly than increasing input	$\frac{\partial^2 f(\mathbf{p}, \mathbf{x})}{\partial^2 u} \geq 0$
3b	Output flow increase more rapidly than decreasing input	$\frac{\partial^2 f(\mathbf{p}, \mathbf{x})}{\partial^2 u} \leq 0$

as operator experience, can then be included in the polynomial models using constraints in the optimisation problem.

2.3.1 Modelled Material Flows

Given the material flows of grain ($\dot{m}_{p,g}$) and MOG ($\dot{m}_{p,c}$) from the threshing and separations system, the four materials flows desirable to control are modelled by

$$\dot{m}_{c,l} = \Gamma_{c,l}\dot{m}_{c,g} = f_{c,l}(\mathbf{p_{c,l}}, \mathbf{\Theta_c})\dot{m}_{c,g} \tag{5}$$

$$\dot{m}_{t,g} = \Gamma_{t,g}\dot{m}_{c,g} = f_{t,g}(\mathbf{p_{t,g}}, \mathbf{\Theta_c})\dot{m}_{c,g} \tag{6}$$

$$\dot{m}_{t,c} = \Gamma_{t,c}\dot{m}_{c,c} = f_{t,c}(\mathbf{p_{t,c}}, \mathbf{\Theta_c})\dot{m}_{c,c} \tag{7}$$

$$\dot{m}_{y,c} = \Gamma_{y,c}\dot{m}_{c,c} = f_{y,c}(\mathbf{p_{y,c}}, \mathbf{\Theta_c})\dot{m}_{c,c}, \tag{8}$$

where the model input vector containing actuator settings, material throughputs and various disturbances are given by

$$\mathbf{\Theta_c} = \begin{pmatrix} \omega_f & d_c & d_s & \dot{m}_{c,g} & \dot{m}_{c,c} & \phi & \theta & \rho_g & \rho_c & \dots \end{pmatrix}^T. \tag{9}$$

The function $f_{c,l}$ describes the relative grain loss from the total grain throughput in the cleaning shoe $\dot{m}_{c,g}$ in Eq. (5). In the same manner the tailings ratio

of grain and MOG are given in Eq. (6) and Eq. (7). The clean grain MOG throughput (cleanliness) is given by Eq. (8).

The remaining materials flows $\dot{m}_{y,g}$ and $\dot{m}_{c,r}$ are computed as the residuals from the steady-state material flows constraints

$$\dot{m}_{c,g} \quad = \dot{m}_{t,g} + \dot{m}_{p,g} = \dot{m}_{t,g} + \dot{m}_{y,g} + \dot{m}_{c,l} \tag{10}$$

$$\dot{m}_{c,c} \quad = \dot{m}_{t,c} + \dot{m}_{p,c} = \dot{m}_{t,c} + \dot{m}_{y,c} + \dot{m}_{c,r}. \tag{11}$$

The static material flow models are given by a polynomial, a polynomial in an exponential function, and polynomial in a logistic sigmoid function,

$$f(\mathbf{p}, \mathbf{\Theta_c}) = \mathbf{p}X(\mathbf{\Theta_c}) \tag{12}$$

$$f(\mathbf{p}, \mathbf{\Theta_c}) = \exp(\mathbf{p}X(\mathbf{\Theta_c})) \tag{13}$$

$$f(\mathbf{p}, \mathbf{\Theta_c}) = \frac{1}{1 + \exp(\mathbf{p}X(\mathbf{\Theta_c}))} \tag{14}$$

with the parameters vector $\mathbf{p}$ and design matrix X being a function of $\mathbf{\Theta_c}$. The steady-steady model fits are then obtained by solving the optimisation problem,

$$\arg\min_{\mathbf{p}} ||\mathbf{Y} - f(\mathbf{p}, \mathbf{\Theta_c})||, \tag{15}$$

where Y is the relative material flow given by $\mathbf{Y}_{c,g}^{c,l} = \dot{\mathbf{m}}_{\mathbf{c,l}}/\dot{\mathbf{m}}_{\mathbf{c,g}}$, $\mathbf{Y}_{c,g}^{t,g} = \dot{\mathbf{m}}_{\mathbf{t,g}}/\dot{\mathbf{m}}_{\mathbf{c,g}}$, $\mathbf{Y}_{c,c}^{t,c} = \dot{\mathbf{m}}_{\mathbf{t,c}}/\dot{\mathbf{m}}_{\mathbf{c,c}}$ and $\mathbf{Y}_{c,c}^{y,c} = \dot{\mathbf{m}}_{\mathbf{y,c}}/\dot{\mathbf{m}}_{\mathbf{c,c}}$ The obtained model parameters have to fulfil the material flow constraints 1a and 1b in Table 4, generally describing that the output flow are non-negative and cannot exceed the input material flow,

$$0 < f_{c,l}(\mathbf{p}_{c,l}, \mathbf{\Theta_c}) < 1 \tag{16}$$

$$0 < f_{t,g}(\mathbf{p}_{t,g}, \mathbf{\Theta_c}) < 1 \tag{17}$$

$$0 < f_{c,l}(\mathbf{p}_{c,l}, \mathbf{\Theta_c}) + f_{t,g}(\mathbf{p}_{t,g}, \mathbf{\Theta_c}) < 1 \tag{18}$$

$$0 < f_{t,c}(\mathbf{p}_{t,c}, \mathbf{\Theta_c}) < 1 \tag{19}$$

$$0 < f_{y,c}(\mathbf{p}_{y,c}, \mathbf{\Theta_c}) < 1 \tag{20}$$

$$0 < f_{t,c}(\mathbf{p}_{t,c}, \mathbf{\Theta_c}) + f_{y,c}(\mathbf{p}_{y,c}, \mathbf{\Theta_c}) < 1. \tag{21}$$

In [11] a method flow was presented to include operator experience in the Fuzzy model in order to create a general rule base for the interaction between actuators and material, which is similar to the formulated constraints formulated in constraint 2b, 2b, 3a and 3b in Table 4. For the static material flow models in

Table 5: Model constraints.

-	$f_{c,l}$	$f_{t,c}$	$f_{t,g}$	$f_{t,c}\dot{m}_{c,c}$	$f_{t,g}\dot{m}_{c,g}$
$\frac{\partial f}{\partial \omega_f}$		<0	>0		
$\frac{\partial f}{\partial d_c}$	<0	>0	<0		
$\frac{\partial f}{\partial d_s}$			<0		
$\frac{\partial f}{\partial \dot{m}_{c,g}}$	>0				
$\frac{\partial f}{\partial \dot{m}_{c,c}}$	>0			>0	>0

Eq. (5-8) the rule base of operator experience in Table 5 is applied as constraints for the model parametrisation using the partial derivative for the actuators ω_f, d_c, d_s as well as the material throughputs $\dot{m}_{c,g}$ and $\dot{m}_{c,c}$.

The model order is selected manually using the *forward selection* method [19] of the model structures given in Eq. (12-14). The bias/variance trade-off is validated by means of *k-fold cross validation* [25].

2.3.2 Model Visualisation

In Figure 9 a matrix mesh plot for the static model behaviour is shown for excitation of cleaning MOG throughput ($\dot{m}_{c,c}$), fan speed (ω_f) and sieve openings (d_c and d_s). The column plot shows the relative tailings grain ratio $\Gamma_{t,g}$, tailings MOG ratio $\Gamma_{t,c}$ and cleaning grain loss ratio $\Gamma_{c,l}$, where each plot is shown as a function of the MOG throughput $\dot{m}_{c,c}$ and fan speed ω_f. The dependency from the upper d_c and lower d_s sieve openings are shown for three different combinations in the row plots.

The tailings grain ratio show a clear exponential increase with fan speed as the dominant effect. The ratio of kernels blown into the tailings increases with the MOG throughput where the grain separation is pushed towards the rear end of the sieves. Clearly the lower sieve has a larger effect on the tailings grain ratio than the upper sieve, matching the initial analysis in Table 3.

The dominant factor for the tailings MOG ratio is the cleaning MOG throughputs $\dot{m}_{c,c}$. An exponential decrease of the tailings MOG throughput for a decreasing fan speed matches state where the cleaning system approaches a collapse, i.e. the packed phase [18] where the MOG material is no longer air borne, causing a significant increase in grain losses at high MOG loads. The ratio ($\Gamma_{t,g}$) of the cleaning MOG ($\dot{m}_{c,c}$) entering the tailings does decrease for and increase

in the cleaning MOG throughput ($\dot{m}_{t,c}$). However the actual tailings MOG throughput ($\dot{m}_{t,c} = \Gamma_{t,g}\dot{m}_{c,c}$) does increase with the cleaning MOG throughput ($\dot{m}_{t,c}$) according to the constraint in Table 5, though it is not obvious from the mesh plot.
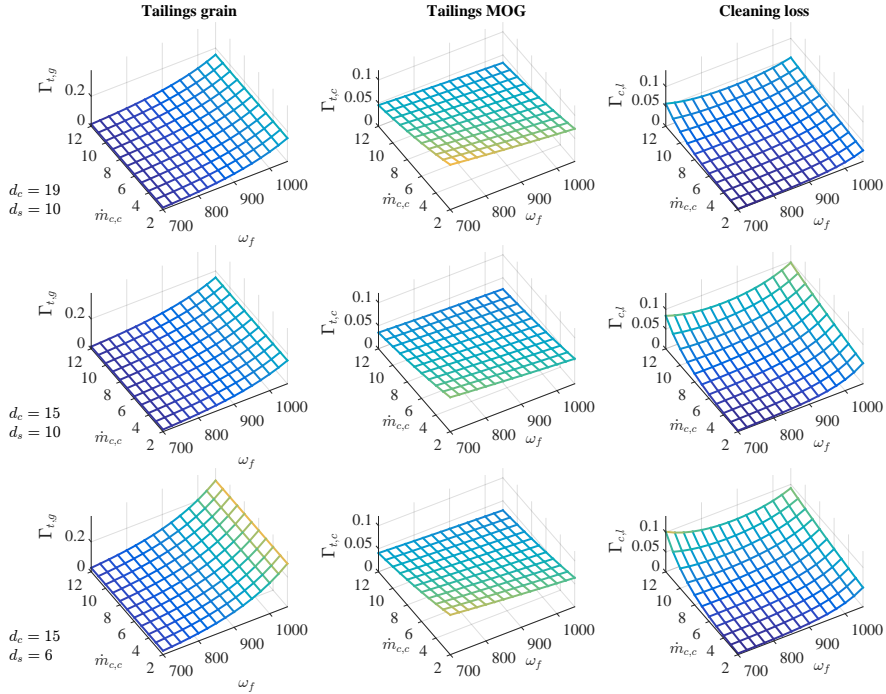
Figure 9: Model matrix plot for tailings grain ratio $\Gamma_{t,g}$, tailings MOG ratio $\Gamma_{t,c}$, and grain loss $\Gamma_{c,l}$ for excitation of cleaning MOG throughput $\dot{m}_{c,c}$, fan speed ω_r and the sieve openings d_c and d_s

.

The most right column shows the cleaning loss. A clear dependency from both fan speed and cleaning MOG throughput is observed. At low MOG loads the fan speed only causes grain loss in the airborne phase within the nominal fan speed range. At high MOG loads the air pressure for from the low range of the fan speed is insufficient to maintain the fluidised phase, where the MOG is

air borne and the kernels are segregated through the sieves. This phase where the upper sieve is partly covered by MOG or fully in the case of a collapsed, causes a significant decrease in segregation performance whereas the kernels are transported in the MOG material mat to the end of the upper sieve. From a sensor perspective this is the most challenging phase to measure for impact loss sensors, as the kernels are encapsulated in the MOG material mat, hence reducing the number of impacts on the sensor membrane. Is it clear that the fan speed facilitating operation in the fluidised phase increases with the cleaning MOG throughput.

2.4 Grain Loss Identification

In order to minimise the cleaning grain loss by automatically adjusting the fan speed the intuitive choice would be to utilise of the reading directly from the cleaning grain loss sensor or cleaning MOG load which is the most dominant parameter for grain loss, see Table 3. However the impact loss sensors are known to only provide an indication of the actual loss [20, 13] and MOG throughput sensors are not commercially available [34]. The composition of the tailings throughput is known to provide essential information concerning the cleaning separation process, for the same reason many combines provide a window of the tailings return in the cabin for the operator.

The aim is to obtain a mathematical function describing a regime characterising the fluidised phase for the cleaning system using the tailing throughput. Here the largest challenge is to obtain an observation that is to independent of the dominating effect from the cleaning MOG throughput. Using laboratory data and simulation the cleaning system feed-rate of grain and MOG material can be excited in order to obtain a reference signal of tailings composition for fan speed control using existing tailings sensor technologies.

2.4.1 Closed-loop Cleaning System

The material samples acquired for modelling of the grain loss and tailings ratio are acquired without returning the tailings material. In order close the tailings return loop the steady-state constraints in Eq. (10-11) are used as the mathematical representation of the actual cleaning system. By means of simulation the closed-loop performance is found by iterating the material flow models in Eq. (5-8) till the simulated states reaches steady-state, see Algorithm 1. In the algorithm all material flows for tailings ($\dot{m}_{t,g}$ and $\dot{m}_{t,c}$), residue ($\dot{m}_{c,l}$ and $\dot{m}_{c,r}$) and clean grain throughput ($\dot{m}_{y,g}$ and $\dot{m}_{y,c}$) are initialised as zero. The material

flow of grain ($\dot{m}_{c,g}$) and MOG ($\dot{m}_{c,c}$) are initialised as the throughput delivered to the cleaning system ($\dot{m}_{p,g}$ and $\dot{m}_{p,c}$) from the threshing and separation system. The simulation is iterated in steps where the modelled material flows are updated according to Eq. (5-8) and the remaining material flows of the clean grain ($\dot{m}_{y,g}$) and residue MOG ($\dot{m}_{c,r}$) throughput are updated as residual flows according to Eq. (10-11).

Algorithm 1 Closed tailings return loop simulation

---

    procedure $f_{CLT}(\dot{m}_{p,g}, \dot{m}_{p,c}, \mathbf{\Theta_c}, \omega_f)$
        k=1   ▷ Initialise discrete time index
        $\dot{m}_{c,g}[k] = \dot{m}_{t,g}, \dot{m}_{c,c}[k] = \dot{m}_{p,c}$ ▷ Initialise cleaning feed-rate
        $\dot{m}_{t,g}[k] = 0, \dot{m}_{t,c}[k] = 0$ ▷ Initialise tailings throughput
        $\dot{m}_{c,l}[k] = 0, \dot{m}_{c,r}[k] = 0$ ▷ Initialise grain loss and MOG residue
        $\dot{m}_{y,g}[k] = 0, \dot{m}_{y,r}[k] = 0$ ▷ Initialise clean grain throughputs
        $\dot{\mathbf{m}} = (\dot{m}_{c,g} \quad \dot{m}_{c,c} \quad \dot{m}_{t,g} \quad \dot{m}_{t,c} \quad \dot{m}_{c,l} \quad \dot{m}_{c,r} \quad \dot{m}_{y,g} \quad \dot{m}_{y,c})^T$ ▷ Define $\dot{\mathbf{m}}$
        while $|\dot{\mathbf{m}}[k] - \dot{\mathbf{m}}(k-1)| > \lambda$ **do**
            $k = k + 1$
            $\dot{m}_{t,g}[k] = \Gamma_{t,g}(\mathbf{p_{t,g}}, \mathbf{\Theta_c})\dot{m}_{c,g}[k]$ ▷ Update modelled flows
            $\dot{m}_{t,c}[k] = \Gamma_{t,c}(\mathbf{p_{t,c}}, \mathbf{\Theta_c})\dot{m}_{c,c}[k]$
            $\dot{m}_{c,l}[k] = \Gamma_{c,l}(\mathbf{p_{c,l}}, \mathbf{\Theta_c})\dot{m}_{c,g}[k]$
            $\dot{m}_{y,c}[k] = \Gamma_{y,c}(\mathbf{p_{y,c}}, \mathbf{\Theta_c})\dot{m}_{c,c}[k]$
            $\dot{m}_{y,g}[k] = \dot{m}_{c,g}[k] - \dot{m}_{t,g}[k] - \dot{m}_{c,l}[k]$ ▷ Update residual flows
            $\dot{m}_{c,r}[k] = \dot{m}_{c,c}[k] - \dot{m}_{t,c}[k] - \dot{m}_{y,c}[k]$
            $\dot{m}_{c,g}[k+1] = \dot{m}_{c,g}[k] + \dot{m}_{t,g}[k]$ ▷ Update cleaning load
            $\dot{m}_{c,c}[k+1] = \dot{m}_{c,c}[k] + \dot{m}_{t,c}[k]$
        end while
        $\dot{\mathbf{m}}_{\mathbf{CLT}} = \dot{\mathbf{m}}$
    end procedure

2.4.2 Identification of the Fluidised Phase

To obtain the fan speed $\omega_f^\star$ characterising operation in the fluidised phase, the optimisation problem is formulated using Algorithm 1,

$$\omega_f^\star = \arg\min_{\omega_f} \; f_{CLT}(\dot{m}_{p,g}, \dot{m}_{p,c}, \mathbf{\Theta_c}, \omega_f) \quad \forall \quad \omega_f \in \mathbb{N}[\omega_{f,min} : \omega_{f,max}], \quad (22)$$

where the simulated fan speed ranges from $\omega_{f,min}$ to $\omega_{f,max}$. This closed-loop description provides cleaning loss using the open-loop cleaning loss model in

Eq. (5) combined with the return material flow models Eq. (6-7), subject to the constraints in Eq. (10-11).

From the obtained data sets the fan speed tailings return loop is closed using Algorithm 1 where the fan speed $(\omega_f^\star)$ and tailing throughputs $(\dot{m}_{t,g}^\star$ and $\dot{m}_{t,c}^\star)$ related to the minimum cleaning loss using Eq. (22) are obtained as visualised on Figure 4. The tailings grain composition characterising the fluidised phase is then modelled using a polynomial based function,

$$\Gamma_t^\star = \frac{\dot{m}_{t,g}^\star}{\dot{m}_{t,g}^\star + \dot{m}_{t,c}^\star} \approx \hat{\Gamma}_t^\star = f_t^\star(\mathbf{p_t}^\star, \Theta_c). \tag{23}$$

The computed optimum $\Gamma_t^\star$ and predicted $\hat{\Gamma}_t^\star$ tailings grain composition are show in Figure 10 with a coefficient of determination at $R^2 = 0.88$. The high R^2 value shows the prediction of the desirable fan speed setting without knowledge of the actual cleaning MOG load $\dot{m}_{c,c}$, as this information is mapped to actuator settings and estimated material flows.

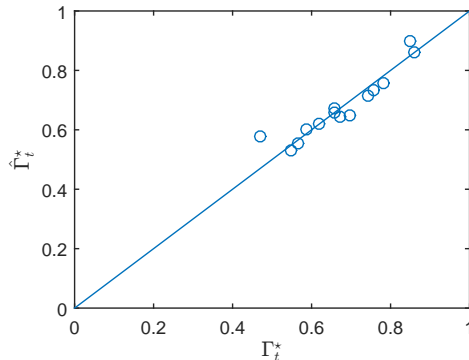Figure 10: Estimated tailings grain composition $\Gamma_t^\star$ set-point for the fan speed controller to maintain operation in the fluidised phase.

3 Conclusion

This article described the material flow model generation for the cleaning system in a combine harvester with focus on the tailings material flow in order to control the fan speed. The main goal was to obtain a model of the cleaning system

that can be used control the fan speed using the tailings grain throughput components of grain and MOG.

Several hundred data points were acquired exciting grain throughput, MOG throughput, fan speed, upper and lower sieves as well as the longitudinal inclination angle. The interdependency analysis showed that the MOG throughput and the longitudinal inclination angle to be the dominating effects causing grain loss. It was shown that a linear feed-forward model from the longitudinal inclination angle to the fan speed could reduce the grain loss significantly compared to a static fan speed.

The modular model structure was outlined with a description of the specific modelled material flow rates. It was shown how the prior knowledge of material flow interdependencies could be included in the static models using inequality constraints.

Using a method combining simulation and optimisation a set-point reference estimate was obtained of the tailings grain composition that identifies the fluidised phase in the cleaning system, which facilitates a novel closed-loop fan speed controller using traditional tailings throughput sensors.

References

[1] M. Sanjeev Arulampalam, Simon Maskell, Neil Gordon, and Tim Clapp. A tutorial on particle filters for online nonlinear/non-Gaussian Bayesian tracking. *IEEE Transactions on Signal Processing*, 50(2):174–188, 2002.

[2] J. Baumgarten, W. Behnke, and N. Diekhans. Sensor for kernel-detection in the retrun for improved adjustment of a combine harvester. *Vdi-berichte*, 1798:181–186, 2003.

[3] V.D. Berner and W.H. Grobler. Gesteuerte adaptive regelung einer mh-drescherreinigungsanlage. *Landtechnik*, 36(36):73–78, 1986.

[4] M.L. Bilde and T. Revsbeck. Optimized material flow and cleaning capacity with ew return pan system in a combine harvester. In *Landtechnik AgEng Proceedings*, pages 105–110, 2017.

[5] J.C. Boone. Leveling system for hillside combines.

[6] B. Bormann and R. Middelberg. Performance enhancement in combine harvesters through auto crop flow control. In *Landtechnik AgEng Proceedings*, 2015.

[7] Stefan Böttinger and Lars Fliege. Working performance of cleaning units of combine harvesters on sloped fields. *Landtechnik*, 67(1):34–36, 2012.

[8] N. Butts and M. Bremer. Material and distribution sensor (mads) for combine material flow. In *Landtechnik AgEng Proceedings*, pages 591–597, 2017.

[9] J. Chen, S. Zheng, L. Shijie, and Y. Zheng. Research of predictive system for feed quantity of combine based on fuzzy neural network. *Proceedings - 2011 8th International Conference on Fuzzy Systems and Knowledge Discovery, FSKD 2011*, pages 863–867, 2011.

[10] G. Craessaerts, W. Saeys, B. Missotten, and J. De Baerdemaeker. A genetic input selection methodology for identification of the cleaning process on a combine harvester, part i: Selection of relevant input variables for identification of the sieve losses. *Biosystems Engineering, Biosyst. Eng, Biosyst Eng, Biosystems Eng*, 98(2):166–175, 2007.

[11] Geert Craessaerts, Josse de Baerdemaeker, Bart Missotten, and Wouter Saeys. Fuzzy control of the cleaning process on a combine harvester. *Biosystems Engineering*, 106(2):103–111, 2010.

[12] Geert Craessaerts, Wouter Saeys, Bart Missotten, and Josse De Baerdemaeker. Identification of the cleaning process on combine harvesters. Part I: A fuzzy model for prediction of the material other than grain (MOG) content in the grain bin. *Biosystems Engineering*, 101(1):42–49, 2008.

[13] J. De Baerdemaeker and W. Saeys. Advanced control of combine harvesters. *IFAC Proceedings Volumes*, 46(18):1 – 5, 2013. 4th IFAC Conference on Modelling and Control in Agriculture, Horticulture and Post Harvest Industry.

[14] F. Duquesne and T. Somers. Grain cleaning system for a combine harvester.

[15] A. Eggerl, H. Bösch, A. Bruns, and S. Wöbcke. Model-based development of control algorithms for optimizing combine prococess. In *VDI-MEG Kolloquium Möhdrescher*, volume 40, 2010.

[16] M. Escher and T. Krause. Grain quality camera. *Machine Control and Guidance Proceedings*, pages 8–15, 2014.

[17] L. Fliege. *Einfluss der Hangneigung auf die Leistungsfhigkeit von Reinigungsanlagen im Mhdrescher*. Ph.d. thesis, Universitt Hohenheim, 2010.

[18] T. Freye. *Untersuchungen zur Trennung von Korn-Spreu-Gemischen durch die Reinigungsanlage des Mhdreschers.* Ph.d. thesis, Universitt Hohenheim, 1980.

[19] J. Friedman, T. Hastie, and R. Tibshirani. *The elements of statistical learning.* Springer New york, 2001.

[20] T. Herlitzius, R. Hübner, A. Gönther, and C. Korn. Sensor study to identify process characteristics of crop and air flow in a combine harvester. In *Landtechnik AgEng Proceedings*, pages 583–590, 2017.

[21] D. Hermann, M. L. Bilde, N. A. Andersen, and O. Ravn. A framework for semi-automated generation of a virtual combine harvester. *IFAC-papersonline*, 49(16):55–60, 2016.

[22] D. Hermann, F. Schöler, M. L. Bilde, N. A. Andersen, and O. Ravn. Computer based control of the separation process in a combine harvester. In *Landtechnik AgEng Proceedings*, pages 599–604, 2017.

[23] D. Hermann, F. Schöler, M. L. Bilde, N. A. Andersen, and O. Ravn. Design of laboratory environment for development of cleaning system automation. In *Landtechnik AgEng Proceedings*, pages 485–490, 2017.

[24] R Hubner and G Bernhardt. More authentic field tests of combine harvesters by consideration of straw moisture. *VDI-berichte*, 1798:187–192, 2003.

[25] G. James, D. Witten, T. Hastie, and R. Tibshirani. *An Introduction to Statistical Learning.* Springer New York, 2013.

[26] H.D. Kutzbach. Approaches for mathematical modelling of grain separation. *International Conference on Crop Harvesting and Processing*, 2003(701):9–11, 2003.

[27] K. Maertens and J. De Baerdemaeker. Flow rate based prediction of threshing process in combine harvesters. *Applied Engineering in Agriculture*, 19(4):383–388, 2003.

[28] K. Maertens, P. Calmeyn, H. D. Kutzbach, and J. De Baerdemaeker. Throughput-loss relation in conventional combine harvesters - a comparison between stationary and mobile units. In *Landtechnik AgEng Proceedings*, pages 591–597, 2003.

[29] K. Maertens and J. De Baerdemaeker. Design of a virtual combine harvester. *Mathematics and Computers in Simulation*, 65(1-2):49–57, 2004.

[30] P. I. Miu. Stochastic modeling of separation process on combine cleaning shoe. *International Conference on Crop Harvesting and Processing*, 2003(701):9–11, 2003.

[31] Oliver. Nelles. *Nonlinear system identification : From classical approaches to neural networks and fuzzy models*. Springer, 2001.

[32] Sebastian Neu, Henner Voecking, and Andreas Wilken. Online modellbildung verfahrenstechnischer prozesse. *Vdi-berichte*, 2173:417–423, 2012.

[33] Mahmoud Omid, Majid Lashgari, Hossein Mobli, Reza Alimardani, Saeid Mohtasebi, and Reza Hesamifard. Design of fuzzy logic control system incorporating human expert knowledge for combine harvester. *Expert Systems With Applications*, 37(10):7080–7085, 2010.

[34] P. Reyns, B. Missotten, H. Ramon, and J. De Baerdemaeker. A review of combine sensors for precision farming. *Precision Agriculture*, 3(2):169–182, 2002.

[35] J.E. Ricketts, B.J. Wagner, and T. Cannegieter. Distribution leveling for an agricultural combine.

[36] M. Schwarz, W. Schulz, J. Baumgarten, and S. Böttionger. Chaff feeding concept for laboratory tests of combine harvester cleaning units. *Landtechnik Agricultural Engineering*, 65(5):376–379, 2010.

[37] J.B. Simpson. Effect of front-rear slope on combine-shoe performance. *American Society of Agricultural Engineers - Transactions*, 9(1):1–3, 1966.

[38] Sigurd Skogestad and Ian Postlethwaite. *Multivariable feedback control: analysis and design*, volume 2. Wiley, 2007.

[39] S. Terörde and S. Neu. Online modelling of harvesting process. *Machine Control and Guidance Proceedings*, pages 55–61, 2014.

[40] J.R. Trollope. A mathematical model of the threshing process in a conventional combine-thresher. *Journal of Agricultural Engineering Research*, 27(2):119–130, 1982.

[41] H. Vöcking, C. Heitmann, and A. Wilken. Automatic adjustments of combine harvesters. In *Landtechnik AgEng Proceedings*, pages 99–104, 2017.

[42] P. Wacker. Einflussgrössen auf die arbeitsqualitöt von axial- und tangentialdreschwerken (parameters that influence the quality work of axial and tangential threshing units). *Agrartechnik*, 40(3):102–104, 1990.

A.6   Article 6: Model-based Cleaning Fan Speed Control in a Combine Harvester, Part II: Design and Verification

Title:	Model-based Cleaning Fan Speed Control
	in a Combine Harvester,
	Part II: Design and Verification
Publication type:	Journal Paper
Journal:	Elsevier, Biosystem Engineering
Date:	March 2018
Authors:	Dan Hermann
	Morten Leth Bilde
	Nils Axel Andersen
	Ole Ravn

Model-based Control of Cleaning Fan Speed in a Combine Harvester
Part II: Design and Verification

D. Hermann⋆,⋆⋆ M.L. Bilde⋆⋆ N.A. Andersen⋆ O. Ravn⋆

⋆ *Automation and Control Group, Dept. of Electrical Engineering, Technical University Denmark, Lyngby, Denmark*
⋆⋆ *AGCO A/S, Research and Advanced Engineering, Randers, Denmark*

Abstract

During a busy harvest it is desirable to utilise the full capacity of the combine harvester by maintaining a high throughput and an acceptable grain loss. The fan speed has traditionally been adjustment using loss and tailings sensor readings on the operator terminal, where some manufactures additionally provide a physical window to the tailings return flow in the cabin as this is known to represent the performance of the separations process in the cleaning system. However there are no adequate models available in literature to describe this effect between tailings and grain loss.

Material flow models were generated using material sample data from laboratory test stands, which were used to identify the fluidised phase using a mathematical model of the tailings grain composition. However the tailings grain composition is not directly observable using traditional tailings sensors. Using sensor fusion combining a tailings impact sensor and a tailings volume sensor the tailings grain ratio can be estimated, which facilitate closed-loop control of the fan speed for operation in the fluidised phase. The fan speed control scheme is implemented and tested by means of simulation using a virtual combine, in a laboratory cleaning system test stand and during full scale field test, showing a significant reduction of grain loss in varying conditions compared to a static fan speed.

1   Introduction

In modern combines the machine settings are pre-set in the control computer for each crop type. Some operators adjust the machine settings during harvest after manual inspection of the residue, whereupon site specific conditions often are ignored. Some manufactures provide simple automation for hill-side conditions

based on feed-forward control from the chassis longitudinal inclination angle, however these systems does not adjust due to varying biological variables such as MOG load, crop moisture content etc. Impact sensors used for loss sensing only provide an indication of the actual loss due to inadequate spatial representation of the total loss at the physical sampling position. Thus a control system cannot fully rely the cleaning grain loss sensors alone [6, 9, 4].

Advances within sensor and computer technologies have procured a potential for automatic control of the cleaning fan speed, faster and more precise than a human operator. This will release the operator to increase focus on other tasks and facilitate operation by an unskilled operator. An estimate of the tailings composition can be obtained using sensor fusion from inexpensive tailings sensor technologies, which is applied in conjunction with cleaning system material flow models to obtain the fan speed setting characterising the low grain loss regime, i.e. the fluidised phase. Furthermore a new cleaning system test stand with automated feeding of grain and MOG biomass as well as recirculation of residue biomass facilitates closed-loop automation testing in the laboratory [12].

A fan speed control system was presented by [2], using differential air pressure sensors located under the upper sieve. An model was utilised to predict the MOG load in the cleaning system to set the fan speed. However the reading from the differential air pressure sensors is a combination of the MOG-load and the actual air pressure, which depends on environmental conditions. Thus additional knowledge is required from other sensors and/or models to calibrate the MOG-load estimate. In order to improve the robustness to varying field conditions [4] added an yield cleanliness estimate [5] and sieve impact loss sensor to the system. Fuzzy logic was applied to obtain relative MOG-load estimate, which were demonstrated in a field with slopes.

A general optimisation approach was presented by [18, 19, 15] where a model was continuously updated by periodically exciting each individual actuator to a predetermined setting outside the normal area of operation using predefined excitation set points for each actuator. The models representing material flow from actuator inputs used a cost function with individual throughput weights to obtain the optimal actuator settings.

It was shown that the tailings grain composition can be used to described the fluidised phase on the cleaning process. This facilitate a novel fan speed control system where the fan speed is controlled using the tailings grain composition obtained by means of sensor fusion from an impact type sensor characterising the tailings grain throughput and a volumetric sensor reading used to estimate the tailings MOG throughput. The experimental setup is shown in Section 2.1. Identification and evaluation of an impact type tailings grain throughput

sensor and a novel tailings volume sensor was shown in Section 2.2. The tailings throughput estimate and the closed-loop fan speed control system are presented in Section 2.3. Finally the control loop is validated by means simulation, in the laboratory continuous cleaning system and during field test in Section 3, showing a significant grain loss reduction.

2 Material and Methods

It was shown in [10] that the tailings grain composition and throughput could be used to describe the fluidised phase of the cleaning system, however no single sensor is available to provide a reading of the individual components. The sensors are evaluated individually using material samples obtained from laboratory test stands. The obtained sensor models are the used to estimate the tailings grain ($\dot{m}_{t,g}$) and MOG ($\dot{m}_{t,c}$) throughputs.

Test and verification can be conducted for the closed-loop control system using a virtual combine [11] (simulation), the continuous cleaning system laboratory environment [12] or during full scale field test with a combine harvester. The evaluation procedure for each of these environments have different impact on ease of change of the closed-loop control system, the individual test time consumption and test availability, see Figure 1.
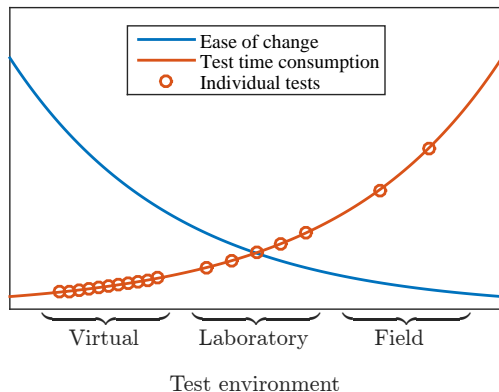

Figure 1: Controller development scheme and test activities.

The individual test time consumption is clearly lowest for the virtual tests

and largest for the full scale field tests which rely on harvest seasons and weather conditions. The laboratory tests has the advantage of all year availability and being close to a real world representation. However it is also time consuming to build laboratory facilities as well as a substantial activities are required for data acquisition to build the virtual combine simulation environment. The preliminary tuning and sensitivity to a sub-set of biological parameters can advantageously be verified in a virtual test environment using standardised unit tests as this facilitate full transparency to the true material flow states and has full repeatability, see Table 1.

Table 1: Relative mapping of pros and cons for test environments.

	Virtual	Laboratory	Field
Repeatability	✓	✓	✗
Real world	✗	✓	✓
Trouble shooting	✓	✓	✓

However it is not realistic to cover all real world harvesting scenarios and characteristics from noise and disturbances occurring during field test. In the laboratory environment the full scale cleaning system with full scale material feed-rate and sensor setup facilitates a near real world representation of field test experiments, however it does not cover the range of disturbances from biological parameters present during full scale field test. With the possibility to acquire material samples in a repeatable environment the laboratory though offers the best option for performance comparison considering controller evaluation and parameter tuning. The final validation has to be conducted during field test where the full range of biological disturbances can be applied to the system. The virtual and laboratory environments cannot fully replace the need of full scale field tests, however these are useful to expand test activities and obtain transparency to the process in order to reduce both the development and test periods.

The final goal will be to increase the performance of the cleaning system, i.e. primarily to reduce grain loss which is possible to measure continuously or sample using all three test environments. However during field test a true loss reference is not always available, instead the known effect from an increase in throughput changing the forward speed or the effect from excitation of the longitudinal inclination angle when driving up- and down-hill are useful indicators together with the grain loss sensor.

2.1 Experimental Setup

The virtual test environment described in [11] facilitates excitation of feed-rate with grain and MOG composition and inclination angles. The model structure allows transparency to all material flows in ton/h or percent as well as all process sensor readings on the combine harvester are available.

A material re-circulating system is designed in order to extend the run time for automation testing [12], see the block diagram in Figure 2. The MOG reservoir, MOG feeder [17] and grain feeder are the individual units forming the overall biomass feeding system. The re-circulation system consists of the residue collection unit located after the cleaning system as well as the MOG and grain return conveyor belts that transport the material back to the MOG and grain reservoirs respectively. Fine cut straw is used to simulate the MOG material instead of collecting actual MOG consisting of chaff and straw pieces, as these are not available in the required quantities for laboratory testing.
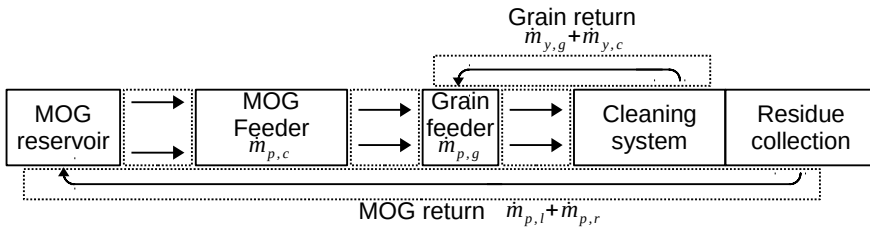

Figure 2: Laboratory cleaning system test stand with continuous feeding and material re-circulation.

The field test experiments can be conducted with various equipment facilitating sampling of the total grain loss from pans under the swath, from individual samples from threshing and separation system or cleaning system, or from elevators and augers similar to the method used by [1]. However the samples only provide a snapshot of the overall performance, hence large scale experiments with numerous samples are required for a final field test validation.

2.2 Process Sensors

The material flow in the tailings return system is a mixture of grain and MOG, where the individual throughputs are obtained from process sensors located in the material flow. A configuration using two sensors measuring tailings throughput utilised. An impact sensor [3] is located at the end of the lower sieve in

the tailings return pan and an infra red triangulation based proximity sensor is located in the paddle head of the tailings return system.

A novel acoustic sensor strip with four membranes is utilised [3], instead of utilising traditional single membrane piezo impact sensors. The acoustic sensor is a low cost unit with four individual plastic membranes connected to microphones on a common electronics board using the rubber tubes. The impact sensor strip provides a more accurate reading covering the full width of the sieve with a total of four membranes. Due to the large difference in density of grain and MOG, which primarily consists of chaff, the impact sensor has a high sensitivity to grain and a low sensitivity to MOG.

The tailings grain sensor trend is found using designed experiments in the laboratory cleaning system test stand. In Figure 3 the raw data points are shown for the given grain throughput $(\dot{m}_{t,g})$ and average of the corresponding sensor reading $(y_{t,g})$, similar to [1] using a piezo sensor in a comparable location. The sensor was then evaluated from the sampled tailings material throughputs
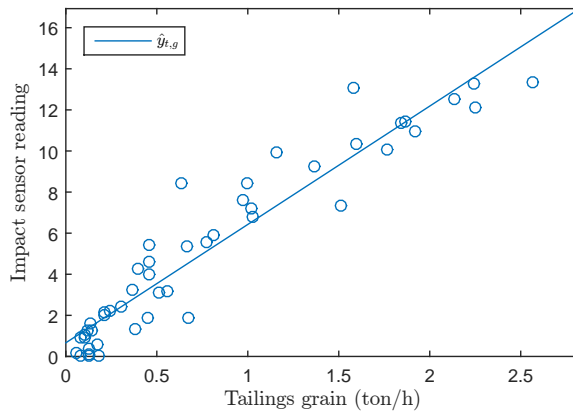

Figure 3: Tailings impact sensor.

of grain, and the data correlated with the average sensor reading during the equivalent period using the affine sensor model

$$y_{t,g} = q_{t,g1} + q_{t,g2}\dot{m}_{t,g}. \tag{1}$$

providing a coefficient of determination at $R^2 = 0.90$ for the estimate $\hat{\dot{m}}_{t,g}$.

The tailings return system utilise an auger to elevate the tailings material where a paddle is mounted on top of the auger to spread the material on the

return pans before re-entering the cleaning system. Traditionally one of the two paddles has been spring loaded where an inductive sensor measured the phase shift between the two paddles due to material load. However the spring loaded paddle is known to reduce capacity and can block in some crop conditions. Instead an infra red proximity sensor is used the measure the material flow in the channel between the return system paddle housing and the chassis side wall of the cleaning shoe, see Figure 4. When the material is delivered from the paddle the velocity vector causes the material to travel along the outer side wall. Here the sensor is located on the opposite side to measure the thickness of the material layer, corresponding the tailings volume.
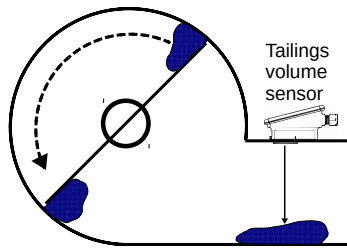

Figure 4: Tailings volume sensor measurement principle.

In Figure 5 the trend for the volume sensor is shown using a combination of 4 grain throughputs and 6 MOG throughputs. The MOG trend is indicated with a line connecting the individual samples points for the 4 grain throughputs. The plots shows a non-linear trend for the tailings volume, with highest sensitivity in the lower end of the scale for both material components.

The volume sensor reading $y_{t,v}$ is modelled using the non-linear model

$$
\begin{aligned}
y_{t,v} &= f_{t,v}(\mathbf{q_{t,v}}, \hat{\dot{m}}_{c,g}, \hat{\dot{m}}_{c,c}) \\
&\Updownarrow \\
y_{t,v} &= q_{t,v1} + q_{t,v2} \left(1 - \exp(q_{t,v3}\dot{m}_{c,g} + q_{t,v4}\dot{m}_{c,g}^3 + q_{t,v5}\dot{m}_{c,c} + q_{t,v6}\dot{m}_{c,c}^3)\right),
\end{aligned}
\tag{2}
$$

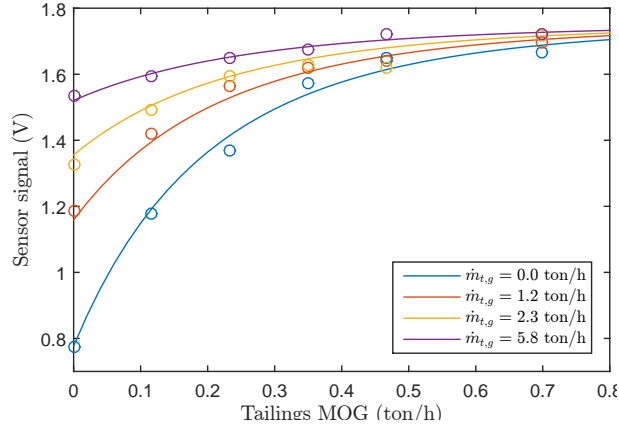which provide a fit with a coefficient of determination at $R^2 = 0.99$.

Figure 5: Tailings volume sensor.

2.3 Controller Design

It was shown in [10] that the tailings grain composition (Γ_t) can be used to identify the fluidised phase of the cleaning system, however it is not directly observable from the combine process sensors. In order to obtain an estimate of Γ_t, the tailings grain ($\dot{m}_{t,g}$) and MOG ($\dot{m}_{t,c}$) throughputs are estimated from the sensor observations of $y_{t,g}$ and $y_{t,v}$.

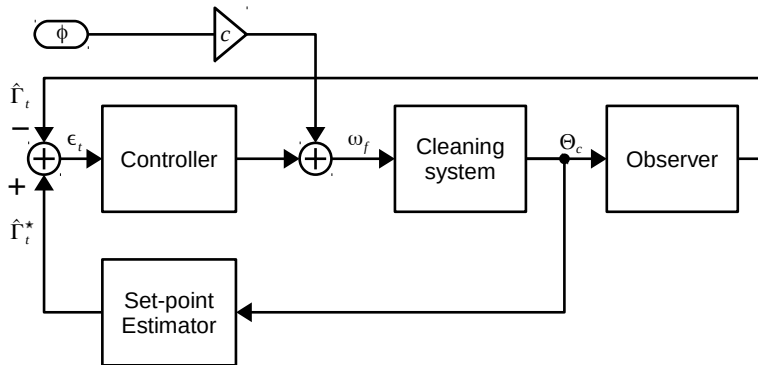The fan speed closed-loop control is shown in Figure 6. The actuator settings

Figure 6: Closed-loop fan speed controller.

and sensors readings ($\mathbf{\Theta_c}$) are used in the set-point estimate to compute the reference tailings grain composition $\hat{\Gamma}_t^\star$ characterising the fluidised phase. The control error for the fan speed control input is then given by

$$\epsilon_t = \hat{\Gamma}_t^\star - \hat{\Gamma}_t = \hat{\Gamma}_t^\star - \frac{\hat{\dot{m}}_{t,g}}{\hat{\dot{m}}_{t,g} + \hat{\dot{m}}_{t,c}}. \tag{3}$$

The aim is to observe the tailings grain ratio with a reasonable accuracy in order to facilitate closed-loop control of the fan speed using an estimate based on the affine and non-linear models in Eq. (1) and Eq. (2).

The state vector $\mathbf{x} = (\dot{m}_{t,g} \quad \dot{m}_{t,c})^T$ is contains tailings grain ($\dot{m}_{t,g}$) and MOG ($\dot{m}_{t,c}$) throughputs, and output vector $\mathbf{y} = (y_{t,g} \quad y_{t,v})^T$ contains of the observations from the tailings grain ($y_{t,g}$) and tailings volume ($y_{t,v}$) process sensors. The estimated observations are given by

$$\hat{\mathbf{y}} = h(\hat{\mathbf{x}}) = \begin{pmatrix} p_{t,g1} + p_{t,g2}\hat{\dot{m}}_{t,g} \\ f_{t,v}(\mathbf{p_{t,v}}, \hat{\dot{m}}_{c,g}, \hat{\dot{m}}_{c,c}) \end{pmatrix}. \tag{4}$$

The tailings throughputs $\hat{\mathbf{x}}$ then are estimated using the update equation

$$\hat{\mathbf{x}}(k) = K(\mathbf{y}(k) - \hat{\mathbf{y}}(k)) = K(\mathbf{y}(k) - h(\hat{\mathbf{x}}(k))), \tag{5}$$

for the discrete time index k.

It was shown in [10] that an acceptable grain loss can be maintained during longitudinal inclination using a linear feed-forward term to the fan speed,

$$\omega_f = f_\phi(\bar{\omega}_f, \phi) = \bar{\omega}_f + c\phi, \tag{6}$$

where $\bar{\omega}_f$ is the fan speed set-point from the control system at flat land conditions and c the feed-forward rate from the longitudinal inclination angle. The closed-loop control system should reach a similar fan speed as induced in Eq. (6), however by using feed-forward the response will be significantly faster, greatly reducing grain loss in hilly terrain.

The tailings throughput estimate is validated in Figure 7 with a reasonably good coefficient of determination at $R^2 = 0.79$.
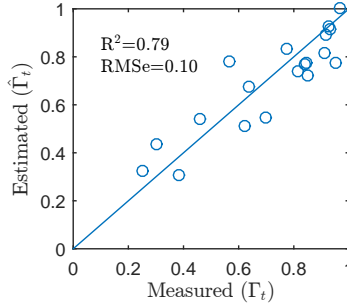
Figure 7: Estimated tailings throughput.

3   Results and Discussion

The cleaning process is sensitive to a number of temporal and spatial varying biological parameters. It is not realistic to acquire samples of the performance during field test of throughput relationships and actuator settings in all conceivable conditions. However it is important to verify the controller response to the dominating effects from MOG throughput, slopes and crop moisture content. As field test is time consuming it is desirable to move as many activities as possible from the field to the laboratory and virtual environments, where controller performance can be verified in a controlled environment. The final validation will always be conducted during full scale field tests by exposing the control system to as many conditions as possible in order to verify the performance.

3.1   Simulation Test Results

The performance evaluation is simulated using a virtual combine [14, 7, 11], where the data acquisition, modelling and identification for the virtual combine is described in [11].

The closed-loop control system should adjust the fan speed in any condition to maintain the fluidised phase for the cleaning process, i.e. operate in the low grain loss regime [8]. By means of simulation the controller can conveniently be compared to multiple static fan speed settings to verify the performance enhancement for a designed sequence exciting sieve actuators, throughputs and disturbances.

The evaluation sequence is designed to excite the longitudinal inclination angle, total throughput, MOG composition and sieve actuators to verify the performance from the closed-loop control system under varying conditions, see Figure 8.

The first plot show the cleaning MOG feed-rate $\dot{m}_{c,c}$, upper sieve spacing d_c, lower sieve spacing d_s and longitudinal inclination angle ϕ for all sequences. Second plot shows the cleaning loss $\dot{m}_{c,l}$ for the individual test sequences. All static fan speeds are marked with dashed lines and the fan speed from the closed-loop control system with a black solid line, which is applicable for the remaining plots. Third plot shows the cleanliness of the clean grain throughput $\dot{m}_{y,c}/(\dot{m}_{y,c} + \dot{m}_{y,g})$, fourth plot the tailings grain composition Γ_t and fifth plot the fan speed ω_f.

The excitation test sequence consists of 8 steps each with a duration of 360 s. Initially the down-hill ($\phi = -6.0°$) and up-hill ($\phi = 6.0°$) longitudinal inclination angles were excited at a cleaning MOG feed-rate of $\dot{m}_{c,c} = 12$ ton/h. During the excitation of the longitudinal inclination angle in the first two periods the fan speed controller increase running down-hill and increases running up-hill, which was shown to reduce grain loss in the trend plot shown in [10]. The feed-forward term from the longitudinal inclination angle in Eq. (6) was not enable in the simulation in order to verify the correct response from the tailings grain ratio. The following three steps gradually decreases $m_{c,c}$ from 12 to 9 and then 6 ton/h in flat land conditions ($\phi = 0°$). It is clear that the fan speed causing the highest grain loss at $\dot{m}_{c,c} = 12$ ton/h is $\omega_f = 700$ RPM, i.e. operating in the packed phase. When the MOG feed-rate decreases to $\dot{m}_{c,c} = 6$ ton/h the highest grain loss originate from at $\omega_r = 950$ RPM, i.e. flight phase. The closed-loop control system maintains the flourished phase for varying of MOG load resulting in low grain loss. In the sixth step the lower sieve d_s is closed from 10 mm till 6 mm and in step seven both sieves are opened till $d_c = 21$ mm and $d_c = 14$ mm. In the eight and last step the MOG throughput is again increases from 6 till 12 ton/h.
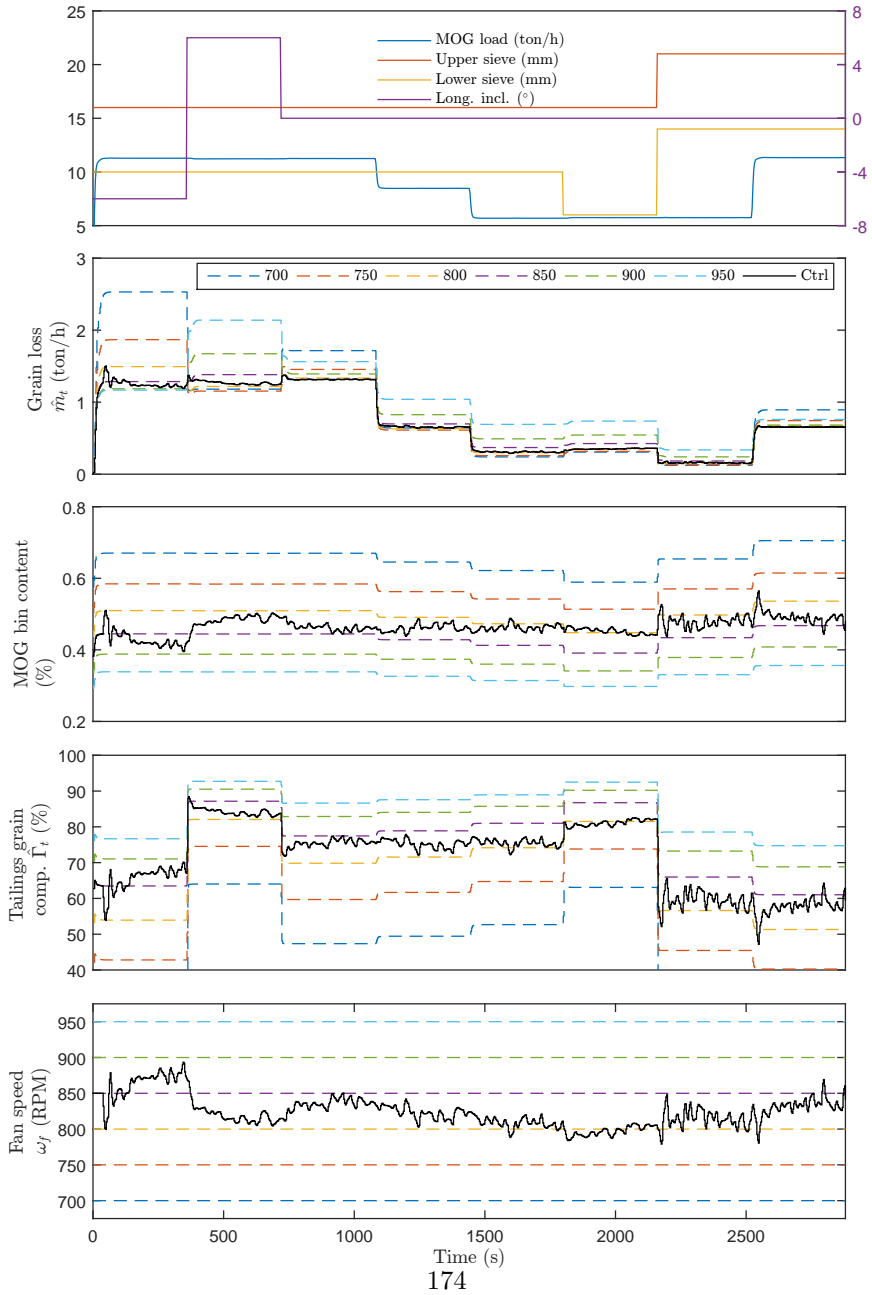
Figure 8: Performance evaluation with multiple fan speed.

The fan speed controller is generally in the lower end of the grain loss range compared to the static fan speed during the excitation steps of longitudinal inclination angle, MOG throughput and sieve openings. For all eight excitation steps the controller adjust the fan speed in the direction reducing the grain loss only using the two tailings sensor readings in order to maintain operation in the fluidised phase. The average grain loss $\dot{m}_{c,l}$ for all eight excitation steps is shown in Figure 9, where the lowest grain loss using static fan speed is obtained at 800 RPM. The closed-loop fan speed controller reduces this grain loss with a narrow margin, however it is most important that the controller did maintain operation 800 RPM in the region near $\omega_f^\star$, where $\omega_f^\star$ varies depending on crop conditions.
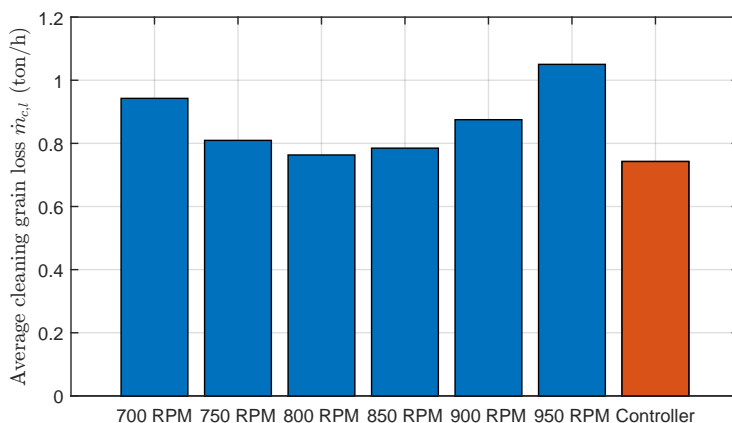
Figure 9: Grain loss statistics for virtual combine fan speed controller test.

3.2   Laboratory Test Results

After the verification of the closed-loop performance of the control system by means of simulation it is desirable to conduct a reduced test sequences with an actual combine during full scale field test. However actual field test is time consuming, subject to weather conditions, local crop harvest windows and uncontrollable crop conditions, which often does not facilitate repeatable results nor sufficient excitation of crop flow. The laboratory allows to repeat sequences with equivalent excitation of total throughput and material composition, which

provide a solid foundation for performance evaluation even for smaller performance enhancements of the control system.

The aim is to evaluate the performance of the closed-loop fan speed controller to changes in throughput, where previous material sample measurements of grain loss are used for reference to validate the fan speed controller performance.

A test sequence with increasing throughput ($\dot{m}_{p,g}$ and $\dot{m}_{p,c}$) is shown in Figure 10. First plot shows the increasing grain and MOG throughputs ($\dot{m}_{p,g}$
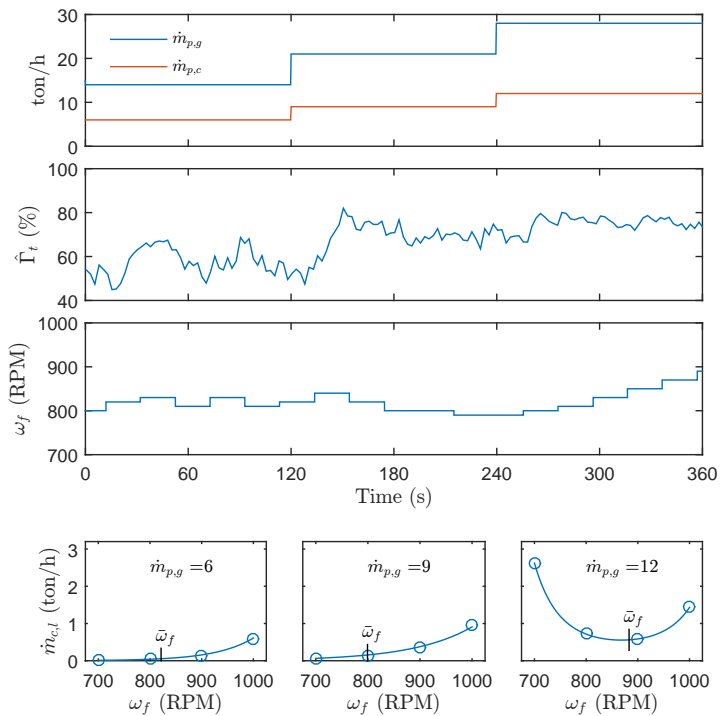
Figure 10: Closed-loop fan speed controller laboratory test with increasing throughput.

and $\dot{m}_{p,c}$), second plot the estimated tailings grain composition ($\hat{\Gamma}_g$) and third plot fan speed (ω_f). The last row shows the sampled grain loss ($\dot{m}_{c,l}$) for a four point fan speed curve with identical throughput and sieve openings for the three throughput stairs. The average fan speed from for the last 60 s in each

throughput stair with the controller enabled is marked $\bar{\omega}_f$.

The material throughput is increased in three stairs of 120 s, at 6, 9 and 12 ton/h of MOG. Each step in the cleaning throughput after 120 s and 240 s cleanly causes a step in the estimated tailings grain ration ($\hat{\Gamma}_t$). The fan speed varies in the range from 800 to 840 RPM during the first two periods causing a relative low grain loss, however decreasing the fan speed would marginally decrease the grain loss. For uneven feeding in actual field conditions further reducing the fan speed can easily result in periodical operation in the packed phase (collapse), causing substantial grain losses. In the third period with the highest throughput the fan speed is increased in the area of ∼880 RPM in the fluidised phase causing low grain loss.

In Figure 11 the estimated grain loss from the trend curves in Figure 10 is shown. The controller obtains a lower grain loss compared to the static fan speeds with a narrow margin. However, most important the primary aim of operation in the fluidised phase is achieved.
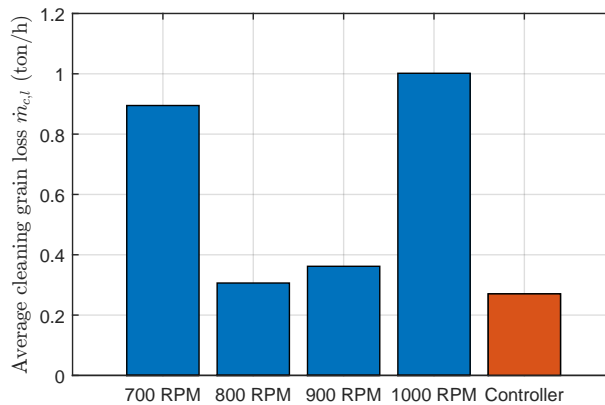

Figure 11: Grain loss statistics for laboratory fan speed controller test.

3.3 Field Test Results

In order to evaluate the closed-loop controller it is desirable to excite the dominant controllable parameters known to cause grain loss, i.e. cleaning MOG load, moisture content and field slopes. Field test results from a field with slopes and flat field with varying MOG throughput by changing forward speed will be presented.

Ideally it would be desirable to collect all residue material from the cleaning system and perform post-cleaning to obtain the true loss, however it is not practical. It was shown by [16] that the cleaning loss could be continuously measured as an absolute quantity by collecting all the residue flow and continuously post clean a sub-flow in a cyclone separator which would be a good solution for this field test verification. However such measurement equipment is not available. Material samples only provide a snapshot hence it does not show the full picture of the loss during a whole test sequence in varying conditions. Though standard grain loss sensors only provide a relative reading it is considered acceptable for comparison between two adjacent rows in the same field for preliminary verification.

3.3.1 Slope Field

In a test field two rows next to each other were chosen to induce a comparable effect from the longitudinal inclination angle (ϕ) on the cleaning system running with the control loop enabled and disabled respectively. The grain moisture content was $\rho_g = 18\%$. Prior to the test the fan speed was adjusted manually by the operator to a low grain loss by means of visual inspection of the residue in the field.

The test result is shown in Figure 12 with the automation enabled in the left column and disabled in the right column. First row shows the averaged loss sensor reading ($y_{c,l}$), second row the longitudinal inclination angle (ϕ) and last row the fan speed (ω_f).

The combine initially runs on flat land for approximately 30 s, then uphill for 80 s and downhill for 40 s. The operator adjusted the fan speed to 800 RPM, which is static for the sequence with automation disabled. The fan speed controller initially reaches stead-state at 780 RPM on flat land, close to the setpoint from the operator. The cleaning loss is generally lower with the controller enabled during the whole sequence, however it is most significant during the first 80 s. A relative constant ratio of the tailings grain composition is maintained during the whole sequence with automation enabled by adjusting the fan
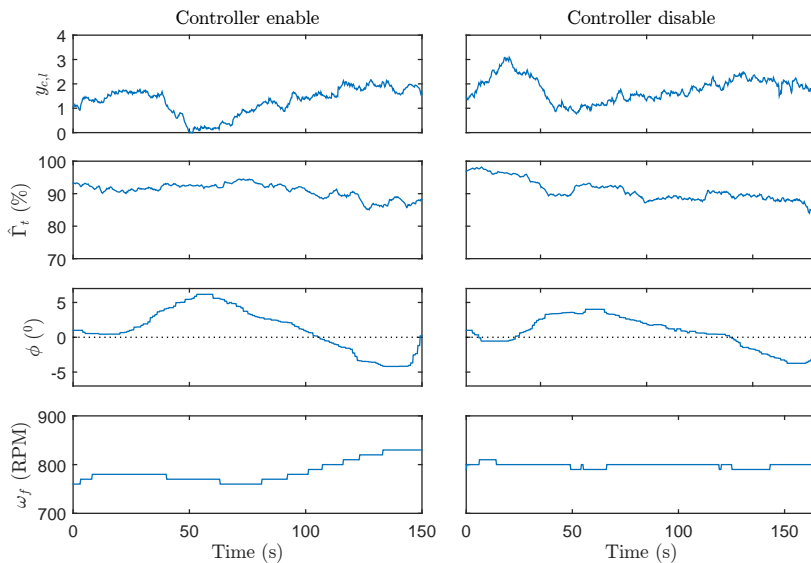
Figure 12: Field test in hilly terrain.

speed. The slope curvature is clearly very similar to both sequences, however the maximum obtained angle is slightly higher when automation is enabled. In order to quantify the effect from the inclination the longitudinal inclination index is given by $\phi_\angle = \|\phi\|$. The statistics in Table 2 shows an average grain loss reduction of 34% from the loss sensor reading, taking into account that the inclination index $\phi_\angle$ is significantly larger for the sequence with automation enabled.

Table 2: Evaluation parameters for field tests on sloped field.

Parameter	Enable	Disable
Grain loss ($y_{c,l}$)	1.30	1.79
Min inclination	$-7.7°$	$-7.0°$
Max inclination	$8.9°$	$5.0°$
Inclination index ($\phi_\angle$)	1.18	0.53

179

3.3.2 Cleaning MOG Load

A field test sequence with three increasing stairs of total throughput (forward speed) is shown in Figure 13 in very dry conditions with grain moisture content of $\rho_g = 9\%$. The row plot division is similar to Figure 12 except for plot three which shows the yield sensor reading $(y_{y,g})$, the tailings grain $(y_{y,g})$ and MOG $(y_{y,c})$ throughput estimates.
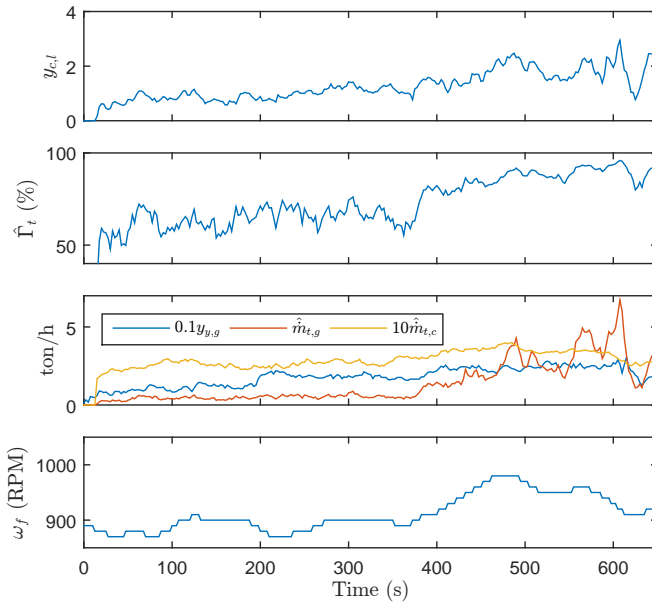
Figure 13: Closed-loop fan speed controller field test in hard threshing wheat.

The sequence is selected as the wheat heads were hard to thresh, thus a high rotor speed and narrow concave clearance were used, consequently the separated MOG throughput was high and contained a high ratio of straw pieces which are challenging to separate for the cleaning system [13]. Additionally the MOG contained large amounts of scattered weed creating a non-uniform MOG biomass which is a contrast to the consistent MOG composition used in the laboratory test stand.

The tailings grain composition is significantly lower than it was been ob-

served in Figure 12, thus the fan speed roughly 100 RPM higher due to increased MOG load in the cleaning system. The throughput ($y_{y,g}$) increased after 190 s however it does not cause a significant increase in grain loss nor the individual tailing throughputs, thus the controller does not change to fan speed. After 380 s the throughput ($y_{y,g}$) increases again, causing an increase in the grain loss reading and both estimated tailings throughputs. This causes an increase in fan speed with the increasing MOG load, verifying the controller response for the given sequence.

3.3.3 Discussion

The achieved results from the test using the virtual combine and the laboratory showed that the fan speed controller could obtain a performance level comparable to the best static setting from an experienced operator. This requires that the operator actually does check for grain losses, understand the system interaction and apply changes as well as having the ability to discriminate the cleaning grain losses from the separation grain loss in the residue. During field test the controller preliminary verified the expected behaviour when exposed to varying longitudinal inclination angles and cleaning MOG load where the actual grain loss with a high plausibility was reduced substantially. The actual gain of the fan speed controller is difficult to quantify in general as it depend entirely on the disturbances that the cleaning system is exposed to. Any quantified performance enhancements will be tied to the local crop conditions. The operators primary focus is on feeding of the header, thus the fan speed is not adjusted dynamically to inclination or throughput changes despite the operated knows the impact on the cleaning grain loss. Thus it must be assumed that the fan speed controller in general can reduce the cleaning grain loss considerably.

4 Conclusion

This article described the design of a novel closed-loop fan speed control system and the evaluation procedure using a virtual combine, laboratory test stands and full scale field tests. The main goal was to reduce the cleaning grain loss by automatically adjusting the fan speed.

It was shown that the two individual components of tailings grain and MOG could be estimated using sensor fusion with an impact sensor and proximity based volumetric sensor located in the mixed tailings materiel flow. The individual evaluation of the sensors showed a high coefficient of determination for

the grain and MOG material flow components.

The fan speed controller was tested using a virtual combine showing that it maintained the fluidised phase, i.e. a low grain loss. The controller adjusted the fan speed to compensate for disturbances originating from the longitudinal inclination angle, MOG throughput and sieve openings.

The results from the simulation was confirmed in the continuous cleaning system test stand where the fluidised phase was maintained and grain loss was lower than the best static fan speed setting.

The fan speed controller was preliminary validated in two different field conditions. First the fan speed controller was evaluated in a field with slopes and high moisture content (18%), where the grain loss reading was reduced by 34% with the fan speed controller enabled for two comparable sequences. Second field test showed the controller in dry conditions with 9% grain moisture content and a MOG composition containing large straw pieces and scattered weed lumps which reduces the cleaning system performance significantly. Here the controller successfully adjusted to an increasing throughput in challenging conditions.

References

[1] J. Baumgarten, W. Behnke, and N. Diekhans. Sensor for kernel-detection in the retrun for improved adjustment of a combine harvester. *Vdi-berichte*, 1798:181–186, 2003.

[2] V.D. Berner and W.H. Grobler. Gesteuerte adaptive regelung einer mhdrescherreinigungsanlage. *Landtechnik*, 36(36):73–78, 1986.

[3] N. Butts and M. Bremer. Material and distribution sensor (mads) for combine material flow. In *Landtechnik AgEng Proceedings*, pages 591–597, 2017.

[4] Geert Craessaerts, Josse de Baerdemaeker, Bart Missotten, and Wouter Saeys. Fuzzy control of the cleaning process on a combine harvester. *Biosystems Engineering*, 106(2):103–111, 2010.

[5] Geert Craessaerts, Wouter Saeys, Bart Missotten, and Josse De Baerdemaeker. A genetic input selection methodology for identification of the cleaning process on a combine harvester, part ii: Selection of relevant input variables for identification of material other than grain (mog) content in the grain bin. *Biosystems Engineering*, 98(3):297–303, 2007.

[6] J. De Baerdemaeker and W. Saeys. Advanced control of combine harvesters. *IFAC Proceedings Volumes*, 46(18):1 – 5, 2013. 4th IFAC Conference on Modelling and Control in Agriculture, Horticulture and Post Harvest Industry.

[7] A. Eggerl, H. Bösch, A. Bruns, and S. Wöbcke. Model-based development of control algorithms for optimizing combine prococess. In *VDI-MEG Kolloquium Möhdrescher*, volume 40, 2010.

[8] T. Freye. *Untersuchungen zur Trennung von Korn-Spreu-Gemischen durch die Reinigungsanlage des Mhdreschers.* Ph.d. thesis, Universitt Hohenheim, 1980.

[9] T. Herlitzius, R. Hübner, A. Gönther, and C. Korn. Sensor study to identify process characteristics of crop and air flow in a combine harvester. In *Landtechnik AgEng Proceedings*, pages 583–590, 2017.

[10] D. Hermann, M. L. Bilde, N. A. Andersen, and O. Ravn. Model-based control of cleaning fan speed in a combine harvester - part i: Identification and optimisation.

[11] D. Hermann, M. L. Bilde, N. A. Andersen, and O. Ravn. A framework for semi-automated generation of a virtual combine harvester. *IFAC-papersonline*, 49(16):55–60, 2016.

[12] D. Hermann, F. Schöler, M. L. Bilde, N. A. Andersen, and O. Ravn. Design of laboratory environment for development of cleaning system automation. In *Landtechnik AgEng Proceedings*, pages 485–490, 2017.

[13] C. Korn and T. Herlitzius. Coupled cfd-dem simulation of separation process in combine harvester cleaning devies. *Landtechnik*, 72(5):247–261, 2017.

[14] K. Maertens and J. De Baerdemaeker. Design of a virtual combine harvester. *Mathematics and Computers in Simulation*, 65(1-2):49–57, 2004.

[15] Sebastian Neu, Henner Voecking, and Andreas Wilken. Online modellbildung verfahrenstechnischer prozesse. *Vdi-berichte*, 2173:417–423, 2012.

[16] M. Schwarz, S. Häberle, and S. Böttinger. Kornverlusterfassung an getreidevorreinigern. *Landtechnik*, 67(1):42–46, 2012.

[17] M. Schwarz, W. Schulz, J. Baumgarten, and S. Böttionger. Chaff feeding concept for laboratory tests of combine harvester cleaning units. *Landtechnik Agricultural Engineering*, 65(5):376–379, 2010.

[18] S. Terörde and S. Neu. Online modelling of harvesting process. *Machine Control and Guidance Proceedings*, pages 55–61, 2014.

[19] H. Vöcking, C. Heitmann, and A. Wilken. Automatic adjustments of combine harvesters. In *Landtechnik AgEng Proceedings*, pages 99–104, 2017.

A.7 Patent A: Volume Sensor for Combine Harvester Tailings Return System

Title:	Volume Sensor for Combine Harvester Tailings Return System,
Regions:	EU and USA
Date:	October 2017
Authors:	Dan Hermann
	Morten Leth Bilde

Volume Sensor for Combine Harvester Tailings Return System.

Inventors: Dan Hermann and Morten Leth Bilde

1   Field of Invention

The invention relates to combine harvesters and particularly to tailings return systems used therein, wherein the tailings return system serves to collect tailings screened out from a crop material stream by a grain cleaning system, and return the tailings to a location in the combine harvester upstream of the grain cleaning system for reprocessing.

2   Background

The use of combine harvesters, hereinafter referred to as combines, in the agriculture industry is well established, and so too are the principals upon which they operate. In general combines comprise a header for cutting and/or gathering a crop as the machine is driven across a crop field. The crop stream passes through threshing apparatus and separating apparatus. Residue straw is ejected from the rear of the machine either in a deposited windrow for subsequent baling or chopped and spread. The portion of crop material, typically made up of grain and material other than grain (MOG) such as chaff and unthreshed seed heads, is conveyed to a grain cleaning system which utilises sieves together with a cleaning airstream. Clean grain passing through the sieves is conveyed to an on-board grain tank. Lighter material including chaff and straw is blown out of the rear of the cleaning system by the cleaning airstream. Material that is screened out by the sieves is referred to as tailings and these typically comprise a high proportion of unthreshed heads.

A tailings return system is provided to collect the tailings and return them to a location upstream in the crop processing apparatus. In some combines the tailings are returned to the threshing apparatus, whereas in other machines the tailings are returned to a grain pan upstream of the grain cleaning system but downstream of the threshing and separating apparatus. In the latter case, the tailings return system may include a secondary threshing device for processing the tailings before being returned.

186

During operation the settings of the various processing apparatus may be changed to adapt to changing harvesting conditions and/or desired harvest outcomes. For example, the speed of the fan that generates the cleaning airstream may be changed to optimise cleaning without excessive grain loss. In another example, the sieve openings may be adjusted. Selecting the various settings was traditionally done manually by the operator based on observations and experience. However, in recent years, technology has evolved to provide for automatic-setting systems that monitor the status of the crop flow at various locations in the combine and automatically adjust the settings accordingly.

It is recognised that the total volume of material in the tailings return system is an important input parameter for automatic setting combines and it is known to provide one or more sensors to provide this information during operation. US-6,115,115 discloses a tailings return system fitted with a laser-based volume sensor that measures the height of the tailings material stream inside the paddle conveyor. However, the laser sensor employed requires more than one unit to decipher the irregular and inconsistent profile present inside the paddle conveyor.

3   Summary of Invention

According to an aspect of the invention there is provided a combine harvester comprising a frame having a pair of side walls, a grain cleaning system located between the side walls, and a tailings return system arranged to collect tailings ejected by the cleaning system, wherein the tailing return system comprises a conveyance channel located outboard of the side walls, an ejection channel connected between a downstream end of the conveyance channel and an opening in one of said side walls at a location upstream of the cleaning system, and a proximity sensor mounted to the ejection channel and configured to sense a thickness of a material layer present therein.

The ejection channel is typically devoid of any moving mechanical components and so the signal produced by the proximity sensor is cleaner and a more reliable representation of the tailings volume. The proximity sensor can be conveniently mounted on an exterior surface of the ejection channel against a window provided in a wall.

The proximity sensor is preferably an infrared proximity sensor.

In a preferred arrangement the tailings return system further comprises an impellor housed upstream of the ejection channel. The impellor comprises a plurality of paddles operable to rotate and project a tailings stream toward

and through the ejection channel. In such an arrangement the paddles fling the tailings stream into and through the ejection channel. The impellor is preferably housed inside the downstream end of the conveyance channel.

The tailings return system may comprise a screw conveyor extending inside of the conveyance channel, wherein the impellor and screw conveyor are mounted upon a common shaft. Therefore, the screw conveyor is operable to deliver the tailings stream direct to the impellor.

The combine may further comprise threshing and separating apparatus, wherein the side wall opening is located downstream of the threshing and separating apparatus. In this arrangement the tailings may be delivered onto a grain pans, or a preparation pan, immediately upstream of the cleaning system. A secondary threshing unit is preferably provided by the tailings return unit to thresh the tailings before returning into the combine.

In an alternative arrangement, the tailings may be delivered upstream of the (primary) threshing apparatus so as to avoid the need for a secondary threshing unit and to utilise the threshing apparatus to re-thresh the tailings.

4 Brief Description of the Drawings

Further advantages of the invention will become apparent from reading the following description of specific embodiments with reference to the appended drawings in which:

- Figure 1 is a side view of a combine harvester revealing, in schematic form, a grain cleaning system and a tailings return system in accordance with the invention;

- Figure 2 is a schematic vertical sectional view of part of the tailings return system shown in Fig. 1;

- Figure 3 is a schematic sectional view taken along the line III-III of Fig. 2; and,

- Figure 4 is an exploded perspective view of a proximity sensor utilised in an embodiment of the invention.

5 Detailed Description of Specific Embodiments

Relative terms such as forward, rearward, transverse, lateral, longitudinal and sideways will be made with reference to the normal forward direction of travel

of the combine 10 and indicated by arrow F. The terms vertical and horizontal will be made with reference to the level ground 101 upon which the combine 10 is disposed. In other words the Cartesian axes of longitudinal, transverse, and vertical are made in relation to the frame 12 of combine 10 and are not affected by any slope in the ground. The terms upstream and downstream are made with reference of the general direction of crop flow along the material conveyance systems described.

Figure 1 illustrates in schematic form the main components of a crop processing system of a combine harvester 10 and will be used to explain the flow of material below. The crop processing system is shown in solid lines whilst the outline profile of harvester 10 is shown in ghost form.

Combine harvester 10, hereinafter referred to as combine, includes a frame 12 supported on front wheels 14 and rear steerable wheels 16 which engage the ground 101. A drivers cab 18 is also supported on the frame 12 and houses a drivers station from where a driver controls the combine 10.

A cutting header 20 is detachably supported on the front of a feederhouse 22 which is pivotable about a transverse axis x to lift and lower the header 20 in a conventional manner.

The combine 10 is driven in a forward direction (arrow F) across a field of standing crop 102 in a known manner. The header 20 serves to cut and gather the standing crop material before conveying such as a crop material stream into feederhouse 22. An elevator 24, normally in the form of a chain and slat elevator as shown, is housed within the feederhouse 22 and serves to convey the crop material stream upwardly and rearwardly from the header 20 to the crop processor designated generally at 26. At this stage the crop material stream is unprocessed.

Threshing and separating apparatus 26 includes a pair of axial flow threshing and separating rotors 28 fed by a tangential flow, crop material impelling, feed beater 30.

The feed beater 30 rotates on a transverse axis and comprises crop engaging vanes (not shown) which convey the crop material stream under the beater and into rotor housings 32 which each house one of said rotors 28. It should be appreciated that only the left-hand rotor 28 and housing 32 is shown in Figure 1 whereas the right-hand equivalent is hidden from view.

Axial flow rotors 20 serves to thresh the crop stream in a front region, separate the grain therefrom in a rear region, and eject the straw residue through an outlet 34 in the housing 32 at the rear of the machine either directly onto the ground in a windrow 104 as shown, or via a straw chopper (not shown).

A part-cylindrical grate 36 provided in the underside of each rotor housing

189

32 allows the separated material to fall by gravity onto either a return pan 38 located below a rear section of the processor 26, or directly onto a preparation pan 40 located below a front section of the processor 26. In reality the separated material falling through the grate 36 is typically a mix of grain and material other than grain (MOG) which may include chaff, unthreshed seed head and some straw.

The twin rotor axial flow processor 26 shown is one example of known system providing threshing and separating apparatus employed in combines today. Other known, and well established, types of crop processors include single rotor axial flow processors, tangential flow/straw walker (or conventional) processors, and hybrid processors.

The return pan 38 and preparation pan 40 together serve as a material conveyance system arranged to convey the separated crop material to a grain cleaning shoe designated generally at 42.

The grain-MOG mix falls from the preparation pan 40 into the cleaning shoe 42 where the cascading mix is subjected to a cleaning airstream generated by fan 48, before falling onto the front of upper sieve or chaffer 50.

Chaffer 50 comprises adjustable louvres supported on a frame which is driven in fore-and-aft oscillating manner. The material which settles on the chaffer 50 is conveyed in a generally rearward direction and the heavier smaller grain-rich material passes between the louvres onto an underlying lower sieve 52, whereas the lighter larger material passes to the end of the chaffer and out of the rear of the machine at 54. A rear section of chaffer 50a is usually independently adjustable and is configurable to allow un-threshed seed heads to pass therethrough into a tailing collection channel 56.

Lower sieve 52 is also driven in an oscillating manner to convey the collected grain-MOG mix rearwardly wherein the material falling therethrough is collected by a clean grain auger 60 for conveyance to an elevator (not shown) for onward conveyance to a grain tank 62. Tailings that are screened out by the lower sieve 52 fall off the rear edge thereof and into the tailing collection channel 56.

A tailings return system 70 is provided to collect the tailings from the tailings collection channel 56 and convey, or return the tailings to the preparation pan 40. The tailings return system 70 comprises a tailings collection auger 58 which resides in a trough at the base of the tailings collection channel 56, the auger 58 being operable to deliver the tailings to one side of the combine (the left-hand side in the illustrated embodiment) and into an inlet of a tailings conveyor 72 which is external the left-hand side wall 12.

With reference to Fig. 2, the tailings conveyor 72 comprises a screw con-

veyor 74 located inside a tailings conveyance channel 75, the screw conveyor 74 being operable to convey the tailings from the collection auger 58 upwardly and forwardly (in the direction of arrow T) through the conveyance channel 75 into an impellor housing or drum 76 located at a downstream end of the conveyance channel 75.

An impellor 78 is housed within the impellor housing 76 and comprises a pair of paddles mounted to a shaft 80 which is common with the screw conveyor 74. The impellor 78 is operable to rotate and project a tailings stream toward and through an ejection channel 82 as best seen in Fig. 3.

The tailings conveyor 72 is mounted externally of, and extends parallel to, the side wall 12 which can be considered as part of frame 12. Although the illustrated embodiment includes a screw conveyor, alternative conveyors can be employed without deviating from the scope of the invention. For example, the screw conveyor 74 can be replaced with a paddle-type conveyor as is known in the art.

Turning back to Fig. 3, the paddles of impellor 78 rotate with shaft 80 and serve to propel the tailings stream tangentially from the impellor housing 76 into the ejection channel 82. The ejection channel 82 provides a conduit through an opening 84 provided in the side wall 12 above the preparation pan 40. The tailings stream is projected onto the preparation pan 40, through the ejection channel 82, by the impellor 78.

Although described as being located proximate to the preparation pan 40, the opening 84 in the side wall 12 can be located in alternative positions depending upon where the tailings are to be returned. In the illustrated embodiment a secondary threshing unit is provided in the tailings return system 70 to thresh the tailings before the stream is returned to the preparation pan 40. In an alternative embodiment, the re-threshing is carried out by the threshing apparatus 26 and the tailings are returned through an opening proximate, but upstream of, the threshing/separating rotors 28.

Turning back to Fig. 3, the tailings stream is fluid and accumulates in transit upon an inside surface 82 of the ejection channel 82 as represented by area A before being conveyed with momentum through the opening 84. The invention involves the recognition that the height B of the accumulated tailings material upon the inside of ejection channel 82 is proportional to the volume flow rate of the tailings being conveyed through the tailings return system 70 at any one time. In accordance with an aspect of the present invention, a proximity sensor 90 is mounted to the ejection channel 82.

The active component 90 of proximity sensor 90 is of the infra-red type such as that manufactured by Sharp (trade mark), model GP2Y0A41SK0F, having

a measuring range of approximately 4-16cm. The sensor 90 is mounted on an exterior surface 82 of the ejection channel 82 against a window 86 provided in the wall thereof.

Fig. 4 shows an exploded view of a sensor 90 which includes a box-type housing 92 and a mounting device 94 which is secured to the exterior surface 82 of the ejection channel 82. The active sensor component 90 is mounted upon a circuit board 95 which is secured inside the housing 92, and is connected to an ECU 100 via a conduit 96.

The proximity sensor 90 is configured to sense the distance C between the sensor 90 and the top of material layer A and communicate a representative signal to the ECU 100. The ECU 100 is then operable to calculate the material volume flow from said signal.

Although described as employing a screw auger and an impellor to convey the tailings stream through the ejection channel, the tailings return system may use alternative means to propel the tailings such as a blower which creates a pressurised airstream.

In summary there is provided a combine harvester tailings return system which includes a tailings conveyor and an ejection channel for depositing tailings upstream of a cleaning system. A proximity sensor is mounted to the ejection channel and is configured to sense the height of a layer of tailings during transit through the returns system.

It should be emphasized that the above-described embodiments of the present disclosure are merely possible examples of implementation, merely set forth for a clear understanding of the principles of the disclosure. Many variations and modifications may be made to the above-described embodiments of the disclosure without departing substantially from the spirit and principles of the disclosure.

6 Claims

1. A combine harvester comprising a frame having a pair of side walls, a grain cleaning system located between the side walls, and a tailings return system arranged to collect tailings ejected by the cleaning system, wherein the tailing return system comprises a conveyance channel located outboard of the side walls, an ejection channel connected between a downstream end of the conveyance channel and an opening in one of said side walls at a location upstream of the cleaning system, and a proximity sensor mounted to the ejection channel and configured to sense a thickness of a material layer present therein.

2. A combine harvester according to Claim 1, wherein the proximity sensor is mounted on an exterior surface of the ejection channel against a window provided in a wall of the ejection channel.

3. A combine harvester according to Claim 1 or 2, wherein the proximity sensor is an infrared proximity sensor.

4. A combine harvester according to any preceding claim, wherein the tailings return system further comprises an impellor housed upstream of the ejection channel, wherein the impellor comprises a plurality of paddles operable to rotate and project a tailings stream toward and through the ejection channel.

5. A combine harvester according to Claim 4, wherein the impellor is housed inside the downstream end of the conveyance channel.

6. A combine harvester according to Claim 5, wherein the tailings return system comprises a screw conveyor extending inside of the conveyance channel, and wherein the impellor and screw conveyor are mounted upon a common shaft.

7. A combine harvester according to any preceding claim, further comprising threshing and separating apparatus, wherein said opening is located downstream of the threshing and separating apparatus.

8. A combine harvester according to any preceding claim, wherein the tailings return system comprises a secondary threshing unit for threshing a tailings stream conveyed therethrough.

7 Volume Sensor for Combine Harvester Tailings Return System

A combine harvester tailings return system (70) includes a tailings conveyor (72) and an ejection channel (82) for depositing tailings upstream of a cleaning system (42). A proximity sensor (90) is mounted to the ejection channel (82) and is configured to sense the height (B) of a layer of tailings during transit through the returns system.
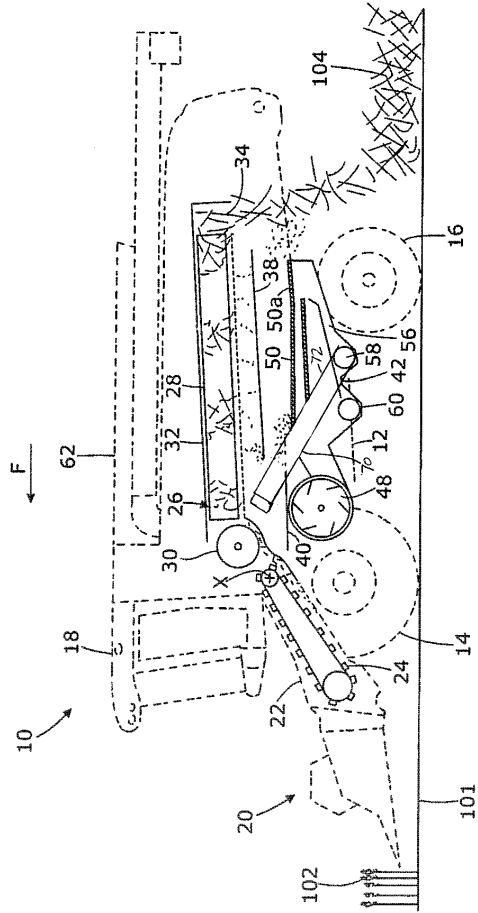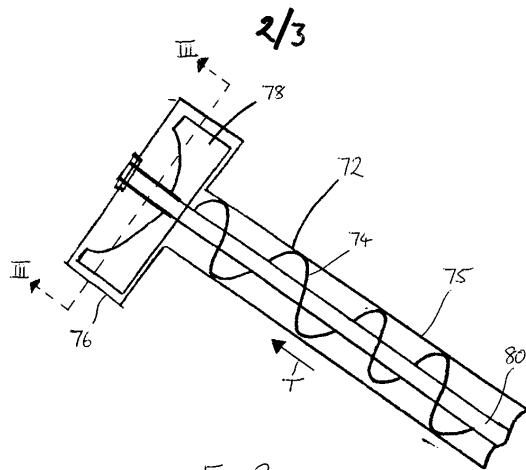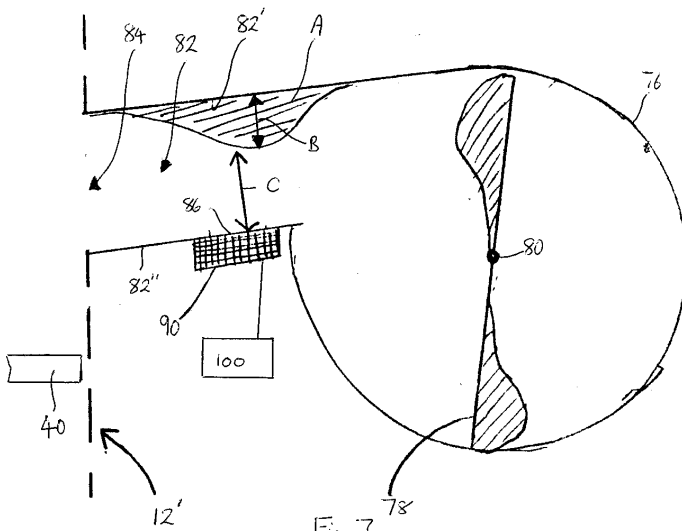
Fig. 1

Fig 2

Fig 3
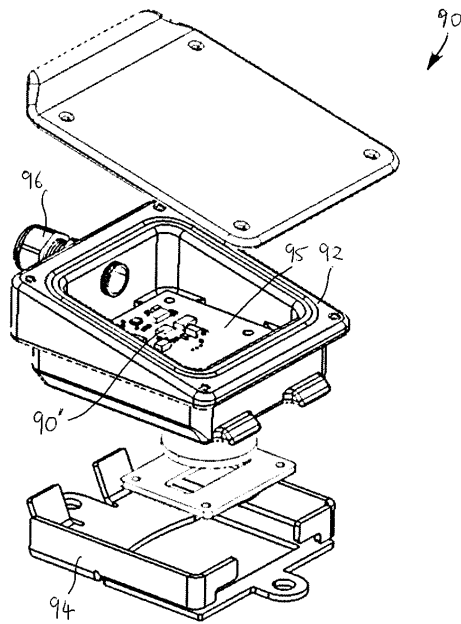
Fig. 4

Bibliography

[1]   AGCO. Annual report. Technical report, 2013.

[2]   Selcuk Arslan. A grain flow model to simulate grain yield sensor response. *Sensors*, 8(2):952–962, 2008.

[3]   D. C. Baruah and B. S. Panesar. Energy requirement model for a combine harvester, part I: Development of component models. *Biosystems Engineering*, 90(1):9–25, 2005.

[4]   J. Baumgarten, W. Behnke, and N. Diekhans. Sensor for kernel-detection in the retrun for improved adjustment of a combine harvester. *Vdi-berichte*, 1798:181–186, 2003.

[5]   Konstantin Beckmann, M. Schwarz, S. Böttinger, R. Bölling, L. Frerichs, and M. Eberhorn. Experimental determination of the segregation process using computer tomography. *Landtechnik*, 71(4):131–138, 2016.

[6]   V.D. Berner and W.H. Grobler. Gesteuerte adaptive regelung einer mäh-drescherreinigungsanlage. *Landtechnik*, 36(36):73–78, 1986.

[7]   M.L. Bilde and T. Revsbeck. Optimized material flow and cleaning capacity with ew return pan system in a combine harvester. In *Landtechnik AgEng Proceedings*, pages 105–110, 2017.

[8]   M. Blanke, M. Kinnaert, J. Lunze, and M. Staroswiecki. *Diagnosis and fault-tolerant control*. Springer Verlag, 2003.

[9]   J.C. Boone. Leveling system for hillside combines.

[10]   B. Bormann and R. Middelberg. Performance enhancement in combine har-
       vesters through auto crop flow control. In *Landtechnik AgEng Proceedings*,
       2015.

[11]   S. Böttinger and A. Timofeev. Conveying and pre-separation on the grain
       pan of combine harvesters. *Landtechnik*, 65(5):380–382, 2010.

[12]   Stefan Böttinger. Electronics in combine harvesters. *Landtechnik – Agricul-
       tural Engineering*, 63(1):22–23, 2008.

[13]   Stefan Böttinger and Lars Fliege. Working performance of cleaning units of
       combine harvesters on sloped fields. *Landtechnik*, 67(1):34–36, 2012.

[14]   B. Broholm and A. Morrison. Combine harvester concave adjustment sys-
       tem. In *Landtechnik AgEng Proceedings*, pages 111–116, 2017.

[15]   P. R. Brown and R. R. Rhinehart. Automated steady-state identification in
       multivariable systems. *Hydrocarbon Processing*, 79(9):79–83, 2000.

[16]   C. Bussmann, J. Baumgarten, and J. Bussmann. Performance stabilization of
       the separation and cleaning process in a standard combine harvester working
       on slopes. In *Landtechnik AgEng Proceedings*, 2015.

[17]   N. Butts and M. Bremer. Material and distribution sensor (mads) for com-
       bine material flow. In *Landtechnik AgEng Proceedings*, pages 591–597,
       2017.

[18]   J. Chen, S. Zheng, L. Shijie, and Y. Zheng. Research of predictive system for
       feed quantity of combine based on fuzzy neural network. *Proceedings - 2011
       8th International Conference on Fuzzy Systems and Knowledge Discovery,
       FSKD 2011*, pages 863–867, 2011.

[19]   T. Coen, J. Anthonis, and J. De Baerdemaeker. Cruise control using model
       predictive control with constraints. *Computers and Electronics in Agricul-
       ture*, 63(2):227–236, 2008.

[20]   T. Coen, B. Missotten, and J. De Baerdemaeker. Feed rate control on a
       combine harvester. *Vdi-berichte*, 2001:379–385, 2007.

[21]   T. Coen, A. Vanrenterghem, W. Saeys, and J. De Baerdemaeker. Autopi-
       lot for a combine harvester. *Computers and Electronics in Agriculture*,
       63(1):57–64, 2008.

[22] Tom Coen, Josse De Baerdemaeker, and Wouter Saeys. A stochastic mpc approach to controlling biological variable processes. *IFAC Proceedings Volumes (IFAC-PapersOnline)*, 3, 2010.

[23] Tom Coen, Johan Paduart, Jan Anthonis, Johan Schoukens, and Josse De Baerdemaeker. Nonlinear system identification on a combine harvester. *Proceedings of the American Control Conference*, 2006:1657189, 3074–3079, 2006.

[24] G. Craessaerts, W. Saeys, B. Missotten, and J. De Baerdemaeker. A genetic input selection methodology for identification of the cleaning process on a combine harvester, part i: Selection of relevant input variables for identification of the sieve losses. *Biosystems Engineering, Biosyst. Eng, Biosyst Eng, Biosystems Eng*, 98(2):166–175, 2007.

[25] Geert Craessaerts, Josse de Baerdemaeker, Bart Missotten, and Wouter Saeys. Fuzzy control of the cleaning process on a combine harvester. *Biosystems Engineering*, 106(2):103–111, 2010.

[26] Geert Craessaerts, Wouter Saeys, Bart Missotten, and Josse De Baerdemaeker. A genetic input selection methodology for identification of the cleaning process on a combine harvester, part ii: Selection of relevant input variables for identification of material other than grain (mog) content in the grain bin. *Biosystems Engineering*, 98(3):297–303, 2007.

[27] Geert Craessaerts, Wouter Saeys, Bart Missotten, and Josse De Baerdemaeker. Identification of the cleaning process on combine harvesters. Part I: A fuzzy model for prediction of the material other than grain (MOG) content in the grain bin. *Biosystems Engineering*, 101(1):42–49, 2008.

[28] Geert Craessaerts, Wouter Saeys, Bart Missotten, and Josse De Baerdemaeker. Identification of the cleaning process on combine harvesters, Part II: A fuzzy model for prediction of the sieve losses. *Biosystems Engineering*, 106(2):97–102, 2010.

[29] A. Dahany. *Verbesserung der Leistungsfähigkeit luftdurchströmter Schwingsieve bei der Korn-Spreu-Trennung im Mähdrescher durch Optimierung der Luftverteilung.* Ph.d. thesis, Universität Hohenheim, 1994.

[30] J. De Baerdemaeker and W. Saeys. Advanced control of combine harvesters. *IFAC Proceedings Volumes*, 46(18):1 – 5, 2013. 4th IFAC Conference on

Modelling and Control in Agriculture, Horticulture and Post Harvest Industry.

[31] F. M. Dekking, C. Kraaikamp, H. P. Lopuhaä, and L. E. Meester. *A Modern Introduction to Probability and Statistics: Understanding Why and How*. Springer Texts in Statistics. Springer, 2005.

[32] F. Duquesne and T. Somers. Grain cleaning system for a combine harvester.

[33] A. Eggerl. *Optimization of combine processes using expert knowledge and methods of artificial intelligence.* Ph.d. thesis, Universität Hohenheim, 2017.

[34] A. Eggerl, H. Bösch, A. Bruns, and S. Wöbcke. Model-based development of control algorithms for optimizing combine prococess. In *VDI-MEG Kolloquium Möhdrescher*, volume 40, 2010.

[35] M. Escher and T. Krause. Grain quality camera. *Machine Control and Guidance Proceedings*, pages 8–15, 2014.

[36] L. Fliege. *Einfluss der Hangneigung auf die Leistungsfähigkeit von Reinigungsanlagen im Mähdrescher.* Ph.d. thesis, Universität Hohenheim, 2010.

[37] Food and Agriculture Orginization. World agriculture: Towards 2015/2030. Technical report, of the United Nations, 2002.

[38] T. Freye. *Untersuchungen zur Trennung von Korn-Spreu-Gemischen durch die Reinigungsanlage des Mähdreschers.* Ph.d. thesis, Universität Hohenheim, 1980.

[39] J. Friedman, T. Hastie, and R. Tibshirani. *The elements of statistical learning*. Springer New york, 2001.

[40] C. A. Glasbey and M. B. McGechan. Threshing loss stochastic variability on combine harvesters. *Journal of Agricultural Engineering Research*, 28(2):163–174, 1983.

[41] Monson H Hayes. *Statistical digital signal processing and modeling*. John Wiley & Sons, 2009.

[42] Elbert Hendricks, Ole Jannerup, and Paul Haase Sørensen. *Linear Systems Control: deterministic and stochastic methods*. Springer, 2008.

[43] Elbert Hendricks, Ole Erik Jannerup, and Paul Haase Sørenson. *Linear Systems Control: Deterministic and Stochastic Methods*. Springer Verlag, 2008.

[44] T. Herlitzius, R. Hübner, A. Gönther, and C. Korn. Sensor study to identify process characteristics of crop and air flow in a combine harvester. In *Landtechnik AgEng Proceedings*, pages 583–590, 2017.

[45] D. Hermann, F. Schöler, M. L. Bilde, N. A. Andersen, and O. Ravn. Computer based control of the separation process in a combine harvester. In *Landtechnik AgEng Proceedings*, pages 599–604, 2017.

[46] R Hubner and G Bernhardt. More authentic field tests of combine harvesters by consideration of straw moisture. *VDI-berichte*, 1798:187–192, 2003.

[47] G. James, D. Witten, T. Hastie, and R. Tibshirani. *An Introduction to Statistical Learning*. Springer New York, 2013.

[48] Steven M Kay. *Fundamentals of Statistical signal processing, Volume 2: Detection theory*. Prentice Hall PTR, 1998.

[49] Jeffrey D. Kelly and John D. Hedengren. A steady-state detection (ssd) algorithm to detect non-stationary drifts in processes. *Journal of Process Control*, 23(3):326–331, 2013.

[50] C. Korn and T. Herlitzius. Coupled cfd-dem simulation of separation process in combine harvester cleaning devies. *Landtechnik*, 72(5):247–261, 2017.

[51] Christian Korn, Ralf Hübner, Thomas Herlitzius, Frank Rüdiger, and Jochen Fröhlich. Numerische untersuchung der luftströmung in der reinigungseinrichtung von mähdreschern. *Landtechnik*, 68(2):83–88, 2013.

[52] H.D. Kutzbach. Combine cleaning shoe - development basics and tendencies. *Landtechnik – Agricultural Engineering*, 56(6):392–393, 2001.

[53] H.D. Kutzbach. Combine harvester cleaning systems. *Landtechnik*, 56(6):392–393, 2001.

[54] H.D. Kutzbach. Approaches for mathematical modelling of grain separation. *International Conference on Crop Harvesting and Processing*, 2003(701):9–11, 2003.

[55] Bart Lenaerts, Thomas Aertsen, Engelbert Tijskens, Bart De Ketelaere, Herman Ramon, Josse De Baerdemaeker, and Wouter Saeys. Simulation of grain-straw separation by discrete element modeling with bendable straw particles. *Computers and Electronics in Agriculture*, 101:24–33, 2014.

[56] Bart Lenaerts, Bart Missotten, Josse De Baerdemaeker, and Wouter Saeys. LiDaR sensing to monitor straw output quality of a combine harvester. *Computers and Electronics in Agriculture*, 85:40–44, 2012.

[57] Hongchang Li, Yaoming Li, Fang Gao, Zhan Zhao, and Lizhang Xu. CFD-DEM simulation of material motion in air-and-screen cleaning device. *Computers and Electronics in Agriculture*, 88:111–119, 2012.

[58] Zhenwei Liang, Yaoming Li, Lizhang Xu, Zhan Zhao, and Zhong Tang. Optimum design of an array structure for the grain loss sensor to upgrade its resolution for harvesting rice in a combine harvester. *Biosystems Engineering*, 157:24 – 34, 2017.

[59] Zhenwei Liang, Yaoming Li, and Zhan Zhao. Monitoring method and sensor for grain separation loss on axial flow combine harvester. *Nongye Gongcheng Xuebao/Transactions of the Chinese Society of Agricultural Engineering*, 30(3):18–26, 2014.

[60] Xiaojuan Liu and Xinbing Huang. Design of front end circuits in cleaning grain loss monitoring and control system for electric combine harvester. *Advanced Materials Research*, 317-319(2):1295–1299, 2011.

[61] Luenberger. Observers for multivariable systems. *Ieee Transactions on Automatic Control*, AC-11(2):190–197, 190–197, 1966.

[62] K. Maertens and J. De Baerdemaeker. Flow rate based prediction of threshing process in combine harvesters. *Applied Engineering in Agriculture*, 19(4):383–388, 2003.

[63] K. Maertens, P. Calmeyn, H. D. Kutzbach, and J. De Baerdemaeker. Throughput-loss relation in conventional combine harvesters - a comparison between stationary and mobile units. In *Landtechnik AgEng Proceedings*, pages 591–597, 2003.

[64] K. Maertens and J. De Baerdemaeker. Design of a virtual combine harvester. *Mathematics and Computers in Simulation*, 65(1-2):49–57, 2004.

[65] K. Maertens, J. De Baerdemaeker, and H. Ramon. Modelbased signal processing of a combine harvester. In *Proceedings of the 25th International Conference on Noise and Vibration Engineering, ISMA*, pages 1641–1646, 2000.

[66] K. Maertens, H. Ramon, and J. De Baerdemaeker. An on-the-go monitoring algorithm for separation processes in combine harvesters. *Computers and Electronics in Agriculture*, 43(3):197–207, 2004.

[67] K. Maertens, M. Reyniers, and J. De Baerdemaeker. Design and application of a dynamic separation model for combine harvesters. *Loboratory of Agro-Machinery and Processing*, 2001.

[68] K. Maertens, P. Reyns, J. De Clippel, and J. De Baerdemaeker. First experiments on ultrasonic crop density measurement. *Journal of Sound and Vibration*, 266(3):655–665, 2003.

[69] K.H. Mertins and D.W. Kmoch. Subsystems for automated combines. *Vdiberichte*, 1636(1636):325–330, 2001.

[70] P. Miu. Kinematic model of material movement through an axial threshing unit, 1 2002.

[71] P. Miu. *Combine Harvesters Theory, Modeling, and Design*. CRC Press, 2016.

[72] P. I. Miu. Stochastic modeling of separation process on combine cleaning shoe. *International Conference on Crop Harvesting and Processing*, 2003(701):9–11, 2003.

[73] P. I. Miu. Applied modeling theory of material separation in combine harvesters. *Asae Annual International Meeting 2004*, pages 2–11, 2004.

[74] Petre Miu, Folker Beck, and H.-D Kutzbach. Simulation des gesamt- mähdreschers. *Landtechnik*, 54(2):90–97, 2 1999.

[75] Petre Miu, P Wacker, and H.-D Kutzbach. A comprehensive simulation model of threshing and separating process in axial units part i. further model development. In *EurAgEng Conference*, 1 1998.

[76] Petre Miu, P Wacker, and H.-D Kutzbach. A comprehensive simulation model of threshing and separating process in axial units part ii. model validation. In *EurAgEng Conference*, 1 1998.

[77] Petre I. Miu and Heinz Dieter Kutzbach. Mathematical model of material kinematics in an axial threshing unit. *Computers and Electronics in Agriculture*, 58(2):93–99, 2007.

[78] Petre I. Miu and Heinz Dieter Kutzbach. Modeling and simulation of grain threshing and separation in axial threshing units. Part II. Application to tangential feeding. *Computers and Electronics in Agriculture*, 60(1):105–109, 2008.

[79] Petre I. Miu and Heinz Dieter Kutzbach. Modeling and simulation of grain threshing and separation in threshing units-Part I. *Computers and Electronics in Agriculture*, 60(1):96–104, 2008.

[80] Md Abdul Momin, Kazuya Yamamoto, Munenori Miyamoto, Naoshi Kondo, and Tony Grift. Machine vision based soybean quality evaluation. *Computers and Electronics in Agriculture*, 140(Supplement C):452 – 460, 2017.

[81] Ryszard Myhan and Ewelina Jachimczyk. Grain separation in a straw walker unit of a combine harvester: Process model. *Biosystems Engineering*, 145:93–107, 2016.

[82] Oliver. Nelles. *Nonlinear system identification : From classical approaches to neural networks and fuzzy models*. Springer, 2001.

[83] Sebastian Neu, Henner Voecking, and Andreas Wilken. Online modellbildung verfahrenstechnischer prozesse. *Vdi-berichte*, 2173:417–423, 2012.

[84] J. Ni, H. Mao, and P. Li. Design of intelligent grain cleaning losses monitor based on array piezocrystals. *Nongye Jixie Xuebao/transactions of the Chinese Society of Agricultural Machinery*, 41:175–177, 08 2010.

[85] E. O. Nyborg and H. R McColly. Grain-combine loss characteristics. *Transactions of the Asae*, 12(6):0727–0732, 1969.

[86] Mahmoud Omid, Majid Lashgari, Hossein Mobli, Reza Alimardani, Saeid Mohtasebi, and Reza Hesamifard. Design of fuzzy logic control system incorporating human expert knowledge for combine harvester. *Expert Systems With Applications*, 37(10):7080–7085, 2010.

[87] W. Peter. Maize grain damage during harvest. *Landtechnik – Agricultural Engineering*, 60(2):84–85, 2005.

[88] K. Pfahler. *Einfluss der Hangneigung auf die Verfahrenstechnik am Beispiel des Anbaus von Getreide und Körnermais – eine Grundlage für die Bewertung hängiger Flurstücke.* Ph.d. thesis, Technische Universität München, 1985.

[89] P R Philips. Cereal Harvesting. *Journal of Agriculture Engineering Reseach*, 19(1974):415–433, 1974.

[90] P Reitz and HD Kutzbach. Investigations on a particular yield mapping system for combine harvesters. *Computers and Electronics in Agriculture*, 14(2-3):137–150, 1996.

[91] P. Reyns, B. Missotten, H. Ramon, and J. De Baerdemaeker. A review of combine sensors for precision farming. *Precision Agriculture*, 3(2):169–182, 2002.

[92] J.E. Ricketts, B.J. Wagner, and T. Cannegieter. Distribution leveling for an agricultural combine.

[93] W. Saeys, B. Lenaerts, G. Craessaerts, and J. De Baerdemaeker. Estimation of the crop density of small grains using lidar sensors. *Biosystems Engineering*, 102(1):22–30, 2009.

[94] M. Schreiber and H.D. Kutzbach. Modelling separation characteristics in combine cleaning shoes. *Landtechnik – Agricultural Engineering*, 58(4):236–237, 2003.

[95] M. Schwarz, S. Häberle, and S. Böttinger. Kornverlusterfassung an getreidevorreinigern. *Landtechnik*, 67(1):42–46, 2012.

[96] M. Schwarz, W. Schulz, J. Baumgarten, and S. Böttionger. Chaff feeding concept for laboratory tests of combine harvester cleaning units. *Landtechnik – Agricultural Engineering*, 65(5):376–379, 2010.

[97] J.B. Simpson. Effect of front-rear slope on combine-shoe performance. *American Society of Agricultural Engineers - Transactions*, 9(1):1–3, 1966.

[98] Sigurd Skogestad and Ian Postlethwaite. *Multivariable feedback control: analysis and design*, volume 2. Wiley, 2007.

[99] C. Tarcolea, T. Casandroiu, and G. Voicu. Stochastic models for simulating seed separation process on sieves. *Agriculturae Conspectus Scientificus*, 36:293–306, 2008.

[100] S. Terörde and S. Neu. Online modelling of harvesting process. *Machine Control and Guidance Proceedings*, pages 55–61, 2014.

[101] Lars Thylén and Donal P.L. Murphy. The control of errors in momentary yield data from combine harvesters. *Journal of Agricultural Engineering Research*, 64(4):271–278, aug 1996.

[102] J.R. Trollope. A mathematical model of the threshing process in a conventional combine-thresher. *Journal of Agricultural Engineering Research*, 27(2):119–130, 1982.

[103] M. W. Veal, S. A. Shearer, and J. P. Fulton. Development and performance assessment of a grain combine feeder house-based mass flow sensing device. *Transactions of the Asabe*, 53(2):339–348, 2010.

[104] Michel Verhaegen and Vincent Verdult. *Filtering and system identification: a least squares approach*. Cambridge University Press, 2007.

[105] H. Vöcking, C. Heitmann, and A. Wilken. Automatic adjustments of combine harvesters. In *Landtechnik AgEng Proceedings*, pages 99–104, 2017.

[106] G. Voicu, T. Casandroiu, and G. Stan. Using the dimensional analysis for a mathematical model to predict the seeds losses at the cleaning system of the cereals harvesting combines. *UPB Scientific Bulletin, Series D: Mechanical Engineering*, 69(4):29–39, 2007.

[107] G. Voicu, T. Casandroiu, and G. Stan. Using the dimensional analysis for a mathematical model to predict the seeds losses at the cleaning system of the cereals harvesting combines. *Upb Scientific Bulletin, Series D: Mechanical Engineering*, 69(4):29–39, 2007.

[108] P. Wacker. Einflussgrössen auf die arbeitsqualitöt von axial- und tangentialdreschwerken (parameters that influence the quality work of axial and tangential threshing units). *Agrartechnik*, 40(3):102–104, 1990.

[109] C. Wallays, W. Saeys, and J. De Baerdemaeker. Material other than grain and broken grain sensor for combine harvesters. In *Landtechnik AgEng Proceedings*, pages 373–378, 2007.

[110] Carmen Wallays, Bart Missotten, Josse De Baerdemaeker, and Wouter Saeys. Hyperspectral waveband selection for on-line measurement of grain cleanness. *Biosystems Engineering*, 104(1):1–7, 2009.

[111] Zhou Wan, Yijin Huang, Xin Xiong, and Jiande Wu. Research of measurement system of straw moisture content based on microwave. *Proceedings - 2010 International Conference on Digital Manufacturing and Automation, Icdma 2010*, 2:5701379, 178–181, 2010.

[112] Zhan Zhao, Yaoming Li, Jin Chen, and Jiaojiao Xu. Grain separation loss monitoring system in combine harvester. *Computers and Electronics in Agriculture*, 76(2):183–188, 2011.